EFFECTS OF PLASTICIZERS ON EXTRUSION OF PVC : AN EXPERIMENTAL & NUMERICAL STUDY

by

Arindam Datta

Dissertation submitted to the Faculty of the

Virginia Polytechnic Institute and State University

in partial fulfillment of the requirements for the degree of

DOCTOR OF PHILOSOPHY

in

Chemical Engineering

APPROVED:

Dr. Donald G. Baird, Chairman

Dr. Garth L. Wilkes

Dr. William E. Conger

Dr. Junuthula N. Reddy

Dr. Mark E. Davis

April 14, 1989

Blacksburg, Virginia

EFFECTS OF PLASTICIZERS ON EXTRUSION OF PVC :

AN EXPERIMENTAL & NUMERICAL STUDY

by

Arindam Datta

Dr. Donald G. Baird, Chairman

Chemical Engineering

(ABSTRACT)

Plasticizers are often interchanged with the idea that they will not affect the processing behavior of Polyvinyl Chloride (PVC). However, when the plasticizer type is changed, various complaints are made by the processors that the material no longer processes the same. This research was concerned with the effect of three different plasticizers on the plasticating extrusion behavior of PVC. Di-isodecyl pthalate (DIDP), di-hexyl pthalate (DHP) and 2-ethyl hexyl pthalate (DOP) are the three plasticizers used in this study. First some differences in the extrusion performance of the three differently plasticized PVC compounds were identified. In particular, it was observed that pressure build-up, flow rate and power requirement were affected by the plasticizer type with the DIDP plasticized materials generating higher pressures and requiring more power than the other two plasticized materials. The differences in extrusion characteristics have been observed for two different dies (1/8 and 1/16 inch diameter) attached to the extruder. The differences were most significant between the DIDP and the DHP plasticized mixes.

Factors which could influence the processing behavior of plasticized PVC include viscosity, compaction, thermal conductivity, specific heat, and friction coefficient. It was found that all other properties other than the viscosity were unaffected by the plasticizer type. On the other hand, viscosities were significantly affected by the plasticizer type with the DIDP plasticized materials displaying higher values between 160 and 190 °C. The difference in viscosity was larger between the DIDP and DHP plasticized materials than between DIDP and DOP plasticized materials. The differences in viscosity between DIDP and DOP plasticized

materials tend to diminish considerably at 190 °C. Two flow regions characterized by different degrees of fusion above and below 165 °C were identified for the plasticized PVC compounds. Plasticized PVC exhibited yield stresses with the DIDP plasticized materials having higher values. The yield stresses were responsible for the significant difference in viscosity at lower shear rates. The yield stress was a more dominant feature at temperatures below 160 °C and this fact was made use of in modeling the solids conveying zone as a fluid with yield stress. Correlation was established between the viscosities and the extrusion behavior of the plasticized PVC compounds. It was observed that the DIDP plasticized mixes had higher viscosities, fused earlier in the screw channel, gave rise to higher pressures, required more power and in general exhibited higher flow rates at the same screw speed.

The finite element method was used for the numerical simulations. Based on the experimental results, the numerical modeling of the melt zone was performed in order to predict the differences in the extrusion characteristics. The melt zones were modeled as a temperature dependent power law fluid having two different viscosity expressions above and below 165 °C. The numerical predictions for pressures and flow rates in the extruder with the 1/8 inch diameter die were in good agreement with the experimental results. For the case of the 1/16 inch diameter die attached to the extruder, the numerical and experimental flow rates were in good agreement but the pressure predictions, although indicating the correct trends, were off by 15 to 20 % from the experimental results. In general the differences in the physical properties, viz. viscosities, were used to predict the differences in the pressure build-ups and flow rates. Also the solid conveying zone was modeled using a Herschel Bulkley model. It was possible to match the experimental and numerical results for the solids conveying zone by using an average density value for the entire solids conveying zone, but more work needs to be done in order to establish greater validity and applicability of this model.

Acknowledgements

The author wishes to express his sincere appreciation to Prof. Donald G. Baird for his support, guidance, and criticism throughout the course of this study. He would also like to thank Prof. Garth L. Wilkes for his interest and suggestions concerning the various aspects of this study. In addition, he would like to thank Professors Mark E. Davis, William E. Conger, and J. N. Reddy for serving on his advisory committee.

The author extends special thanks to Dr. Norman Eiss, , , , Dr. S. Kim, and Dr. S. Ray for assisting him actively and providing him with valuable suggestions for the experimental and numerical work. The use of Dr. Glasser's laboratory for part of the experimental work is appreciated. He would like to acknowledge the advice and cooperation of , , Dr. Ravi Ramanathan, Dr. D. S. Done, , , , and other members of Prof. Baird's research group. He extends his appreciation to and in the workshop and to , , , and in the office. The author would also like to take this opportunity to express his gratitude to Exxon corporation and CIT Institute of Materials Science and Engineering for funding this research, and to Cornell University for allowing him access to their supercomputing facilities.

The author extends his deepest appreciation to his parents and family for their love, support, and patience. Finally, he would like to express his heartfelt gratitude to , whose help, encouragement, and friendship were important to the successful completion of this dissertation.

Table of Contents

1.0 INTRODUCTION **1**

2.0 LITERATURE REVIEW **4**

2.1 MORPHOLOGY AND STRUCTURE 6

2.2 EFFECTS OF PLASTICIZERS ON PVC MORPHOLOGY 13

2.3 RHEOLOGY 19

2.4 FRICTION COEFFICIENTS 55

2.5 EXTRUSION 56

2.5.1 Single Screw Extruder 57

2.5.2 Melting Mechanism 59

2.5.3 Extrusion of PVC 61

2.5.4 Modelling The Extruder 69

2.5.5 Numerical Methods 74

2.6 CONCLUSIONS OF THE LITERATURE REVIEW AND THE PROPOSED RESEARCH ... 80

3.0 EXPERIMENTAL APPARATUS AND PROCEDURE **85**

3.1 MATERIALS 85

3.1.1 Sample preparation 86
3.2 APPARATUS 87
3.2.1 Extruder Experiments 88
3.2.2 Scanning Electron Microscopy (SEM) 89
3.2.3 Capillary Rheometry 90
3.2.4 Capillary Rheometer to Measure Density 91
3.2.5 Rotary Rheometry 92
3.2.6 Differential Scanning Calorimetry 94
3.2.7 Thermal Diffusivity Measurement 95
3.2.8 Measurement of Friction Coefficients 97

4.0 FINITE ELEMENT FORMULATION 101
4.1 INTRODUCTION 101
4.2 FORMULATION OF THE CONTINUOUS PROBLEM 103
4.3 CONSTITUTIVE EQUATION 106
4.4 MESH GENERATION 109
4.5 PENALTY FUNCTION APPROXIMATION 111
4.6 DISCRETIZATION OF THE CONTINUOUS PROBLEM 112
4.7 EVALUATION OF THE MATRIX COEFFICIENTS 116
4.8 BOUNDARY CONDITIONS 116
4.9 SOLUTION PROCEDURE 118

5.0 RESULTS AND DISCUSSIONS 120
5.1 EFFECTS OF PLASTICIZERS ON PHYSICAL PROPERTIES 121
5.1.1 Viscosity Measurements 121
5.1.2 Compaction 129
5.1.3 Yield Stress Measurements 147
5.1.4 Determination of Thermal Properties 173

5.1.5 Friction measurements 191
5.2 EXTRUSION STUDIES 195
5.2.1 Studies on the Effect of Plasticizers on Extrusion Characteristics 196
5.2.2 Studies of the Melting Mechanism 202
5.2.3 Dry Extruder Runs 232
5.3 NUMERICAL RESULTS 233
5.3.1 Testing of Various Empiricisms in the GNF Constitutive Models. 234
5.3.2 Predictions of Isothermal Solids Conveying Model 241
5.3.3 Prediction of the Melt Zones 253

6.0 CONCLUSIONS AND RECOMMENDATIONS 321
6.1 Conclusions : Experimental Study 321
6.2 Conclusions : Numerical Study 324
6.3 Recommendations 326

Appendix A. APPENDIX A - EXISTING SOLIDS CONVEYING MODEL 328

REFERENCES 332

Vita 337

List of Illustrations

Figure 2. 1. Schematic internal structure of PVC Particles [15]. 8

Figure 2. 2. Internal structure of suspension PVC with loose packing [6]. 9

Figure 2. 3. Schematic concept of a fringed micelle [1]. 12

Figure 2. 4. Schematic diagram of fusion of primary particles [7]. 14

Figure 2. 5. Schematic Brabender torque curves [14] 22

Figure 2. 6. Fusion curves for simple and commercial compoundds [14]. 23

Figure 2. 7. Simple compound processed to 120 °C in a Brabender [15]. 24

Figure 2. 8. Simple compound processed to 140 °C in a Brabender [15]. 25

Figure 2. 9. Simple compound processed to 210 °C in a Brabender [15]. 26

Figure 2. 10. Viscosity vs. shear rate for a PVC compound starting at different shear rates [36]. 30

Figure 2. 11. Comparison of melt viscosities at 200 ° C for different molecular weigt PVC [25]. 32

Figure 2. 12. Relationship between constant shear rate viscosity and reciprocal absolute temperature for PVC sample with mol. wt. of 60000 33

Figure 2. 13. Flow curves of low mol.wt. (20000) PVC samples at different temperatures [27]. 36

Figure 2. 14. Flow profiles of Polystyrene and PVC at different temps. [29]. 38

Figure 2. 15. Variation of extrudate quality with extrusion temperature and shear rate (schematic) [14]. 40

Figure 2. 16. Superposition of melt flow data for plasticized PVC at different extrusion temperatures [12] 42

Figure 2. 17. Flow curves of filled and unfilled molded samples using a capillary of radius = 0.03792 cm [32] 44

Figure 2. 18. Plasti-corder dry blending test results [37]. 46

Figure 2. 19. Viscosity vs. shear rate data of DOP plasticized PVC at different temperatures [40]. 48

Figure 2. 20. Primary normal stress difference coefficient vs. shear rate at different temperatures [40]. 49

Figure 2. 21. Comparison of fusion for PVC compounds with and without wax and hav CaSt as a lubricant [78]. 53

Figure 2. 22. Schematic drawing of plasticating extruder. 58

Figure 2. 23. Geometry of the "unwound" rectangular channel [48]. 60

Figure 2. 24. Cross-section of screw channel [51]. 62

Figure 2. 25. Cross-sections obtained from "cooling" experiments with rigid PVC [49]. 64

Figure 2. 26. Definition of terminologies used in solids conveying. 70

Figure 3. 1. Schematic of Laser Flash Diffusivity Apparatus 96

Figure 5. 1. Viscosity Shear Rate Data for PVC dry blends at 190 ° C 123

Figure 5. 2. Viscosity Shear Rate Data for PVC dry blends at 180 ° C 124

Figure 5. 3. Viscosity Shear Rate Data for PVC dry blends at 170 ° C 125

Figure 5. 4. Viscosity Shear Rate Data for PVC dry blends at 160 ° C 126

Figure 5. 5. Viscosity Shear Rate Data for PVC dry blends at 150 ° C 127

Figure 5. 6. Viscosity Shear Rate Data for PVC Pellets at 190 ° C 130

Figure 5. 7. Viscosity Shear Rate Data for PVC Pellets at 180 ° C 131

Figure 5. 8. Viscosity Shear Rate Data for PVC Pellets at 170 ° C 132

Figure 5. 9. Viscosity Shear Rate Data for PVC Pellets at 160 ° C 133

Figure 5. 10. Viscosity Shear Rate Data for PVC Pellets at 150 ° C 134

Figure 5. 11. Density of Plasticized PVC Pellets at 150 ° C 136

Figure 5. 12. Density of Plasticized PVC Pellets at 170 ° C 137

Figure 5. 13. Density of Plasticized PVC Pellets at 190 ° C 138

Figure 5. 14. Density of DIDP Plasticized PVC Dry Blends at different temperatures. . . . 140

Figure 5. 15. Density of DHP Plasticized PVC Dry Blends at different temperatures. 141

Figure 5. 16. Density of DOP Plasticized PVC Dry Blends at different temperatures. 142

Figure 5. 17. Flow Energetics (Arrhenius Plots) for DIDP Dry Blend 144

Figure 5. 18. Flow Energetics (Arrhenius Plots) for DHP Dry Blend 145
Figure 5. 19. Strain Sweep Experiment of DIDP Dry Blends at 140 C 150
Figure 5. 20. Strain Sweep Experiment of DIDP Dry Blends at 150 C 151
Figure 5. 21. Strain Sweep Experiment of DIDP Dry Blends at 160 C 152
Figure 5. 22. Dynamic Response of PVC Dry Blends at 130 C 154
Figure 5. 23. Dynamic Response of DIDP Dry Blends at 140 C 155
Figure 5. 24. Dynamic Response of DIDP Dry Blends at 150 C 156
Figure 5. 25. Dynamic Response of DIDP Dry Blends at 160 C 157
Figure 5. 26. Dynamic Response of DIDP Dry Blends at 170 C 158
Figure 5. 27. Dynamic Response of DHP Dry Blends at 140 C 159
Figure 5. 28. Dynamic Response of DHP Dry Blends at 150 C 160
Figure 5. 29. Dynamic Response of DIDP Dry Blends at 160 C 161
Figure 5. 30. Dynamic Response of DHP Dry Blends at 170 C 162
Figure 5. 31. Complex Viscosity vs Storage Modulus Plots for DIDP Dry Blends. 164
Figure 5. 32. Complex Viscosity vs Storage Modulus Plots for DHP Dry Blends. 165
Figure 5. 33. Fitting various models to the DIDP dry blend shear stress-shear rate data at 140 ° C 168
Figure 5. 34. Fitting various models to the DHP dry blend shear stress-shear rate data at 140 ° C 169
Figure 5. 35. Comparisons of Steady Shear & Dynamic data for DIDP dry blend at 150 ° C 170
Figure 5. 36. Comparisons of Steady Shear & Dynamic data for DIDP dry blend at 160 ° C 171
Figure 5. 37. Comparisons of Steady Shear & Dynamic data for DIDP dry blend at 170 ° C 172
Figure 5. 38. DSC Scans for Rigid PVC 175
Figure 5. 39. DSC Scans for DIDP plasticized Dry Blended PVC 176
Figure 5. 40. DSC Scans for DHP plasticized Dry Blended PVC 177
Figure 5. 41. DSC Scans for DIDP plasticized PVC Pellets 178
Figure 5. 42. DSC Scans for DHP plasticized PVC Pellets 179
Figure 5. 43. Specific Heats of plasticized PVC Dry Blends 182

Figure 5. 44. Specific Heats of plasticized PVC Pellets 184
Figure 5. 45. Specific Heats of Extrudates of Dry Blended PVC samples. 185
Figure 5. 46. Thermal Diffusivities of DIDP Plasticized PVC Dry Blend. 188
Figure 5. 47. Thermal Diffusivities of DHP Plasticized PVC Dry Blend. 189
Figure 5. 48. Thermal Diffusivities of DOP Plasticized PVC Dry Blend. 190
Figure 5. 49. Friction Coefficients vs Temperature of Dry Blended DIDP Samples 193
Figure 5. 50. Friction Coefficients vs Temperature of Dry Blended DHP Samples 194
Figure 5. 51. Polymer Coils showing the change from solid to melt form occurring in the extruder. 203
Figure 5. 52. Fusion Study of DIDP dry blend by SEM (1/8 inch dia. die) at turns 9 & 10. 211
Figure 5. 53. Fusion Study of DIDP dry blend by SEM (1/8 inch dia. die) at turn 12 1/4 . 212
Figure 5. 54. Fusion Study of DIDP dry blend by SEM (1/8 inch dia. die) at turn 12 3/4 . 213
Figure 5. 55. Fusion Study of DIDP dry blend by SEM (1/8 inch dia. die) at turn 15. 214
Figure 5. 56. Fusion Study of DHP dry blend by SEM (1/8 inch dia. die) at turns 9 and 12. 215
Figure 5. 57. Fusion Study of DHP dry blend by SEM (1/8 inch dia. die) at turn 13. 216
Figure 5. 58. Fusion Study of DHP dry blend by SEM (1/8 inch dia. die) at turn 14. 217
Figure 5. 59. Fusion Study of DHP dry blend by SEM (1/8 inch dia. die) at turn 17. 218
Figure 5. 60. Fusion Study of DIDP dry blend by SEM (1/16 inch dia. die) at turn 9 1/2 . 219
Figure 5. 61. Fusion Study of DIDP dry blend by SEM (1/16 inch dia. die) at turn 10. ... 220
Figure 5. 62. Fusion Study of DIDP dry blend by SEM (1/16 inch dia. die) at turn 10. ... 221
Figure 5. 63. Fusion Study of DIDP dry blend by SEM (1/16 inch dia. die) at turn 12. ... 222
Figure 5. 64. Fusion Study of DIDP dry blend by SEM (1/16 inch dia. die) at turn 14. ... 223
Figure 5. 65. Fusion Study of DIDP dry blend by SEM (1/16 inch dia. die) at turn 16. ... 224
Figure 5. 66. Fusion Study of DHP dry blend by SEM (1/16 inch dia. die) at turn 9. 226
Figure 5. 67. Fusion Study of DHP dry blend by SEM (1/16 inch dia. die) at turn 10. ... 227
Figure 5. 68. Fusion Study of DHP dry blend by SEM (1/16 inch dia. die) at turn 11 1/2 . 228
Figure 5. 69. Fusion Study of DHP dry blend by SEM (1/16 inch dia. die) at turn 11 1/2 . 229
Figure 5. 70. Fusion Study of DHP dry blend by SEM (1/16 inch dia. die) at turn 14. ... 230
Figure 5. 71. Fusion Study of DHP dry blend by SEM (1/16 inch dia. die) at turn 16. ... 231

Figure 5. 72. Dimensions of Extruder Channel and Approximate Mesh for 2-D Solids Conveying Simulation. 245

Figure 5. 73. Numerical predictions of Down Channel Velocity versus Channel Depth at different Exit Press. at 121cm (15 RPM) 247

Figure 5. 74. Numerical predictions of Down Channel Velocity versus Channel Depth at different Exit Press. at 141cm (15 RPM) 248

Figure 5. 75. Numerical predictions of Down Channel Velocity versus Channel Depth at different Exit Press. at 121cm (35 RPM) 249

Figure 5. 76. Numerical predictions of Down Channel Velocity versus Channel Depth at different Exit Press. at 141cm (35 RPM) 250

Figure 5. 77. Numerical predictions of Down Channel Velocity versus Channel Depth at different Screw Turns (1/8 inch die). 258

Figure 5. 78. Numerical predictions of Temperature versus Channel Depth at different Screw Turns with 1/8 inch die. 259

Figure 5. 79. Velcity, Pressure & Temperature Contours for DIDP dry Blend with 1/8 inch die at 35 RPM. 260

Figure 5. 80. Numerical predictions of Temperature versus Channel Depth at different Screw Turns with 1/16 inch die. 262

Figure 5. 81. Velocity, Pressure & Temperature Contours for DIDP dry Blend with 1/16 inch die at 35 RPM. 263

List of Tables

Table 2. 1. Terminologies used for PVC structures [76] 7

Table 3. 1. Viscosity Comparison of Two Separately Prepared Dry Blended Sample ...99

Table 3. 2. Specifications of the single screw extruder 100

Table 5. 1. Viscosity Shear Rate data of DIDP dry blend 265

Table 5. 2. Viscosity Shear Rate data of DHP plasticized PVC dry blend 267

Table 5. 3. Viscosity Shear Rate data of DOP plasticized PVC dry blend 269

Table 5. 4. Viscosity Shear Rate data of DIDP plasticized PVC pellets 271

Table 5. 5. Viscosity Shear Rate data of DHP plasticized PVC pellets 273

Table 5. 6. Viscosity Shear Rate data of DOP plasticized PVC pellets 275

Table 5. 7. Power law parameters for Plasticized PVC Dry Blends 277

Table 5. 8. Power law parameters for Plasticized PVC Pellets 278

Table 5. 9. Viscosity comparison of dry-blended PVC 279

Table 5. 10. Viscosity comparison of pelletized PVC 280

Table 5. 11. Viscosity as a function of shear rate and temperature 281

Table 5. 12. Dynamic Data of DIDP Dry Blend at T = 140°C 282

Table 5. 13. Dynamic Data of DIDP Dry Blend at T = 150°C 283

Table 5. 14. Dynamic Data of DIDP Dry Blend at T = 160°C 284

Table 5. 15. Dynamic Data of DIDP Dry Blend at T = 170°C 285

Table 5. 16. Dynamic Data of DHP Dry Blend at T = 140°C 286

Table 5. 17. Dynamic Data of DHP Dry Blend at T = 150°C 287

Table 5. 18. Dynamic Data of DHP Dry Blend at T = 160°C 288

Table 5. 19. Dynamic Data of DHP Dry Blend at T = 170°C 289
Table 5. 20. Yield stresses of PVC dry blends 290
Table 5. 21. Herschel Bulkley & Bingham Fluid Parameters for the dry blends 291
Table 5. 22. Specific Heats of Plasticized PVC Dry Blends 292
Table 5. 23. Specific Heat of Plasticized PVC pellets 293
Table 5. 24. Specific Heats of Plasticized PVC Dry Blend Extrudates 294
Table 5. 25. Thermal Diffusivities of Dry Blends 295
Table 5. 26. Friction Coefficient of Dry Blended DIDP 296
Table 5. 27. Friction Coefficient of Dry Blended DHP 297
Table 5. 28. Results of Extruder Runs 298
Table 5. 29. Results of Extruder Runs 299
Table 5. 30. Results of Extruder Runs 300
Table 5. 31. Results of Extruder Runs 301
Table 5. 32. Results of Extruder Runs 302
Table 5. 33. Results of Extruder Runs 303
Table 5. 34. Results of Extruder Runs 304
Table 5. 35. Results of Extruder Runs 305
Table 5. 36. Results of Extruder Runs 306
Table 5. 37. Results of Extruder Runs 307
Table 5. 38. Results of Extruder Runs 308
Table 5. 39. Results of Extruder Runs 309
Table 5. 40. Results of Dry Extruder Runs 310
Table 5. 41. Results of Dry Extruder Runs 311
Table 5. 42. Results of Dry Extruder Runs 312
Table 5. 43. Density of Extrudates from Dry Extruder Runs 313
Table 5. 44. Comparisons of Tempertaure Predictions from Fidap and Finite difference methods for Power Law fluid from Ref. [98]. 314
Table 5. 45. Testing of HB Model 315

Table 5. 46. Fitting of Finite Difference Solids Conveying Model for a Tapered Channel to the Experimental Data from Dry Extruder Runs 315

Table 5. 47. 2-D Modeling of Solids Conveying in Tapered Extruder Channel using HB model 316

Table 5. 48. 3-D Solids Conveying Model in Tapered Extruder Channels using HB Models (includes cross channel flow) 316

Table 5. 49. Approximate Density Values Required to Match 3-D Numerical Simulation Results and Experimental Results of Dry Extruder ru 317

Table 5. 50. Comparison of Numerical and Experimental Results for DIDP Dry Blend usin 1/8 inch Diameter die. 317

Table 5. 51. Comparison of Numerical and Experimental Results for DHP Dry Blend usin 1/8 inch Diameter die. 318

Table 5. 52. Comparison of Numerical and Experimental Results for DIDP Dry Blend usin 1/16 inch Diameter die. 319

Table 5. 53. Comparison of Numerical and Experimental Results for DHP Dry Blend usin 1/16 inch Diameter die. 320

1.0 INTRODUCTION

Polyvinyl Chloride (PVC) has been one of the largest used thermoplastics in the world for several decades. It is amenable to extensive modifications in its properties by the incorporation of additives. This fact makes it possible to find a large range of PVC products encompassing numerous applications. Although it has been put to use in diverse applications in the form of films, pipes, rods and wire coatings, to mention a few, its morphology and physical properties are still not very well understood. We find many researchers engaged in the study of various aspects of PVC relating to its structure, rheology and processability.

PVC is rarely processed all by itself but as mentioned above, it is generally mixed with processing aids, plasticizers, heat stabilizers, lubricants, etc. Plasticating extrusion is one of the most important processing techniques for PVC. In plasticating extrusion the polymer is mixed with additives and fed to the extruder feed hopper in the shape of pellets, powders, beads or other solid forms. These particulate solids flow under gravity into the screw channel formed within the rotating screw and the fixed barrel. They are conveyed and compressed by a drag induced mechanism towards the extruder exit. At the exit of the extruder, the polymer comes out of the die in the form of a melt. The transition from solid to melt occurs in the melting zone, where both the solid and polymer melt coexist. The polymer, in addition of getting melted, is homogenized and pumped out at high pressure. The energy required to

melt the polymer comes not only from the heated extruder barrel but also from the frictional heating in the solids and viscous dissipation in the melt. The different processes described here are dependent on screw geometry, processing conditions and the properties of the polymer which can be modified by the compounding of the various additives.

Of all the additives, the ones which are used in greatest quantities are the plasticizers. The addition of the plasticizers are known to affect the performance of PVC in extrusion but it is somewhat unclear as to the manifestation of this effect. An understanding of the plasticizer's effect on extrusion can lead to better performance in terms of throughput, energy requirements, product quality and physical properties.

The objective of this research project is to determine the effect of three different plasticizers on the characteristic properties of PVC related to extrusion and on the extrusion performance of these plasticized PVC's in single screw extruders. Determination of physical properties such as viscosity, thermal diffusivity, and specific heat can reflect the effect of the plasticizer type and content. The three plasticzers of interest are a) DIDP (Di-isodecyl pthalate), b) DHP (dihexyl pthalate) and c) DOP (2- ethyl hexyl pthalate). Furthermore, it is the objective to simulate the extrusion of plasticized PVC using finite element methods to predict any observed differences in extrusion between different plasticized mixes. The differences could be in pressure profiles and temperature progression along the extruder or on the material flow rates. Of specific interest to this research is whether the plasticizer type introduces any changes in the melting mechanism of the polymer in the extruder. The simulation efforts will involve modeling of the solids conveying zone and the two melt zones. The latter zones are where the compacted polymer under the action of shear and heat gradually transforms itself into a melt, gets homogenized, and builds up pressure before being pumped out of the die.

The prediction and simulation of plasticized PVC requires the determination of rheological, thermal and frictional properties of PVC as a function of plasticizer type and quantity. These property variations are manifestations of the changes in the melt viscosity and elasticity, thermal behavior and transitions or frictional characteristics or a combination

of all of these. These in turn may affect the variation in the performance of PVC in the extruder. Further, it is known that the behavior of PVC at the processing temperatures to be employed in this research is not that of a pure melt [13-15,24-29,30,34,40 -43]. Particle fusion and compaction plays a dominant role in the processing of PVC and in the development of physical properties in the processed material [21,22,65,66]. In the fusion process, interdiffusion and penetration of the amorphous regions of the supermolecular structures present in PVC lead to a clearing of the PVC with melt-like properties. Particle breakdown does not occur during solids conveying and original resin grain boundaries are retained. Even the melt pool initially contains the original particulate structure but the particulate boundaries are completely destroyed in the later flights of the screw. The effect of the particular plasticizers on the fusion and morphological progression of PVC in the single screw extruder will also be investigated. Of particular interest will be the causes of the differences in the effect of plasticizer on the melting mechanism and on the formation of different zones in the extruder. These differences along with the property variations will be used for the simulation input and modelling in the computer.

To the best of the author's knowledge a comparative study of the effect on extrusion of the three different plasticizers used in this research has not been studied. Also their effect on the melting mechanism and fusion has not been investigated.

In the next chapter the literature will be reviewed to understand the work already done. Emphasis will be concentrated on the work on fusion behavior and rheological properties of PVC and attention also will be focused on its morphology. The various mechanisms in the different zones of the extruder will be examined and different methods used to model them will be studied. The published work on the behavior of PVC in single screw extruder and the efforts at numerical predictions of this behavior will also be considered and analyzed.

2.0 LITERATURE REVIEW

The literature on PVC is vast but most of it may not be of relevance to the objectives of this research. A critical analysis of the development concerning the rheology and the processing aspects of PVC will be presented in this chapter.

Understanding the morphology of PVC is important for explaining the rheological properties, which are not necessarily similar to those of other pure melt. The PVC morphology will be briefly reviewed in section 2.1. The structure of both rigid and plasticized PVC will be considered. The action of plasticizers on PVC structure will also be discussed.

Section 2.3 will deal with the rheological aspects of PVC. It was mentioned in chapter 1 that fusion plays an important role in the melt flow of PVC. First, the work on this aspect will be covered. Next, the effect of molecular weight on viscosity measured in capillary rheometers will be covered. This will be followed by a review of phenomena like die swell and melt fracture. The effect of plasticizers on rheological properties of PVC will be considered and wherever possible distinction between rigid and plasticized PVC will be made. Work on measurements of rheological properties in small strain dynamic oscillatory flow and in extensional flow have been reviewed. The data from the former experiments show that PVC displays yield stress at lower temperautre as well as at high temperatures, where it is proc-

essed. The last topic in this section will deal with the effect of various additives on the fusion process.

Section 2.4 will provide a review of the work done on measurements of friction coefficients of PVC.

One of the objectives of this research is to simulate the extrusion of plasticized PVC in a single screw extruder. Thus an understanding of the mechanism of the single screw extruder is essential. Section 2.5 will review the literature dealing with the examination of the mechanisms and the development of the mathematical models for the different zones. The various numerical methods used to solve the governing equations for the single screw extruders will considered. It has been mentioned in chapter 1 that fusion plays a dominant role in the processing of PVC in the extruder and this possibly differentiates the behavior of certain PVC formulations from other polymers possessing sharp melting points. The research done on extrusion of PVC in single screw extruders will be described and the different melting behaviors will be considered.

In section 2.6 the findings of the published work will be summarized and the areas where investigation needs to be conducted to achieve the objectives of this research will be specified. The objectives of the research will be proposed in this section.

In the review the efforts will be directed towards finding out if the effects of the three specific plasticizers have been studied with respect to properties related to extrusion. These, if present, can be used directly as input for simulation purposes. If the data on the three plasticizers are not available, it would be of interest to observe the trends arising out of the action of other plasticizers on PVC. These facts will allow us to cross check the data generated in this research.

2.1 MORPHOLOGY AND STRUCTURE

In order to comprehend the rheological and processing properties of PVC, it is necessary to have an understanding about the morphology and structure of the polymer. A number of reviews [1,2,3,4] summarize the findings on the structure of PVC.

In this section the structure of as-polymerized PVC will be examined and the nature of the crystallinity present in PVC and its effect on microstructure will be discussed. The melt flow units of PVC are supermolecular structures and their morphology will also introduced at the end of the section.

PVC is generally produced by the suspension polymerization process and is composed of particulate products with diameter ranging between 100 to 200 μm. These particles themselves are made up of agglomerates of smaller particles. In addition to the suspension method, PVC is commercially produced by bulk and emulsion polymerization techniques The bulk polymerized material, like the suspension material, consists of agglomerates of primary particles with a dimension of 1 μm. The suspension PVC differs from the bulk PVC in that the particles are covered with a skin, contain a more porous structure and are about 1 μm in diameter.

There has been a wide range of terminologies to describe the particles and the domains that exist in PVC and this has led to confusion among various researchers. Fig. 2.1 is a schematic diagram of one of the ways in which the PVC particulate structure has been presented in the literature [3]. After the second international symposium on PVC at Lyon in 1976, a generalized nomenclature was adopted as per Table 1.1 [5,76]. The purpose of this was to clear any ambiguity and thus bring consistency to the system of nomenclature.

Since the majority of the PVC is produced by the suspension method it will be useful to look into its structure. Fig. 2.2 is a typical picture of a suspension resin particle with a loose packing. Each particle is an aggregate of several irregular smaller particles formed during polymerization. By changing the conditions of polymerization, resins with different particle

Table 2. 1. Terminologies used for PVC structures [76]

Term	Approximate size in typical PVC	Origin or description
Grain	100 μm	Free flowing at room temperature
Agglomerate	10 μm	Formed during polymerization by merging of primary particles
Primary Particles	1 μm	Formed from single polymerization site at conversions of 10-50%
Domain	100 nm	Presence not clearly proven, possibly formed by mechanical working within or from primary particles
Microdomain	10 nm	Crystallite or nodule ?

agglomeration distribution can be obtained. Krzewki and Sieglaff [6] have categorized the particles into five groups depending on the degree of agglomeration. By a combination of the density gradient technique and the silicon oil absorption technique, the particles were graded according to their porosity into different levels of heterogeneity. These characteristic differences among the particles, which were also confirmed by microscopy, were thought to affect the processing of the PVC leading to differences in their fusion behavior [3,6,74]. This fact will be emphasized in greater detail in section 2.3 and 2.4.3.

PVC is a semicrystalline material. However, its crystallinity is difficult to measure and varies with the conditions under which it is produced. It has a broad range of melting points and running repetitive thermal cycles produce crystals that melt at progressively higher temperatures. The crystalline melting point varies from 212 °C to 273 °C [1], but these are obviously not equilibrium melting points. As PVC does degrade at these high temperatures, it is processed at temperatures below its melting point. Reference [1] contains the different re-

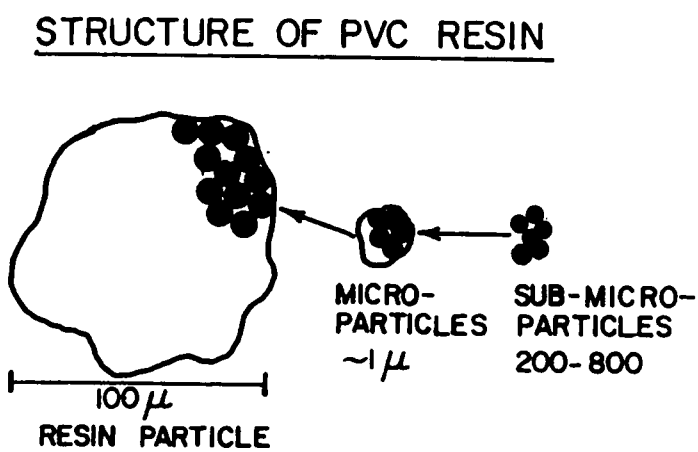

Figure 2. 1. Schematic internal structure of PVC Particles [15].

Figure 2. 2. Internal structure of suspension PVC with loose packing [6].

ported melting points and shows how they are affected by annealing , heating rate and recrystallization.

Commercial PVC has a relatively low crystallinity content of 5 to 15 %. The amount of branching content or the nature of the tacticity of the material, among other things, can be the cause of the low crystallinity content. It is a material without long branching and normally during synthesis has the most probable weight distribution [4] leading to a low polydispersity. PVC has been known to possess branching with short chain branching being predominant [2]. The exact number of branches has been a matter of controversy, but it is now believed that the number of short chains are three per thousand carbon atoms and the number of long chains are one per thousand carbon atoms. By decreasing the polymerization temperature, branching can be reduced. The low branching content does not cause much problem with the crystallization of PVC.

Another important factor affecting crystallinity is tacticity. PVC has about 55 % syndiotacticity when polymerized between 40 and 70 °C but the syndiotacticity will rise if the polymerization temperature is lowered [1,2]. The syndiotacticity order may vary between 5 and 7 but can increase to 12 if polymerized at lower temperatures and has been shown to explain certain differences in the mechanical properties of PVC [2]. The low crystalline syndiotactic PVC has orthorhombic unit cells which have been have assigned dimensions of a=10.24 °A, b=5.24 °A and c=5.08 °A [1,2]. The order along the chain axis is poor and is attributed to the short syndiotactic order. It has been shown that the incorporation of isotactic straight chains into the orthorombic crystallite structure accounted for a rather short sequence length of syndiotactic units and less order along the chain axis [2].

It had been postulated that crystallites act as cross linking points in an amorphous PVC network with the cross linking units having the dimension of approximately 100 °A. The crystallites are connected in a 3-D network by tie molecules. This has been referred to in [1] and [2] as fringed micelle structure with thin sheaf like crystallite connected by disordered segments as shown in Fig. 2.3. These ordered domains are 50 to 100 °A wide and measure about 100 to 150 °A in length [2]. The fact that the domains have small lengths agrees well

with the concept of short syndiotactic units having lower order along the chain axis. In [1], structures different from fringed micelle have been referred to. In one of these structures the crystallites resemble thin platelets forming lamellae with folded chains. Gale and coworkers [12] observed the existence of 100 to 200 °A particulate structures or domains which were nodular in form. As they did not obtain sharp SAXS peak, Gale et al. contended that density differences between the domain, which presumably contained the crystallites, and their surroundings were small. Some more references will be made to the different structures which arise in plasticized PVC in the next section.

In melt flow of PVC, the above-mentioned domains of submicron dimensions are not the flow units. Berens and Folt [13,14] were the first to establish the existence of large supermolecular structures that govern the flow of PVC and give rise to certain peculiar properties associated with its flow. These are dual valued flow activation energies or reduced viscosity at low temperatures and are a consequence of the existence of particulates which retain some crystallinity even in the melt state. A particulate flow mechanism arise because of these supermolecular entities called primary particles. They measure about 1 μm although some researchers [8] report values as low as 0.1 μm. Their presence has been established by examining the fractured surfaces of PVC samples under electron microscopes.

As the temperature of PVC is raised above 170 or 180 °C, the primary particle boundaries start to interdiffuse. Summers [7] contended that material within the primary particles were held together by a 3-D network. At low temperatures, the interaction between primary particles is low. But as the temperature increases, the interaction increases by interdiffusion of the chains within the primary particles. The particle boundaries disappear to form a melt which has a fibrillar structure. When they recrystallize, a new structure develops linking the primary particles together by newly formed crystallites as shown in Fig. 2.4. Terdelius and Ranby [2] described the mechanism of fusion of primary particles subjected to shear and temperature. They postulated that at any time with respect to shear field and temperature there existed a stable number of crystallites connected by amorphous regions. The increase of shear or decrease of temperature stabilizes these particular structural arrangements

Figure 2. 3. Schematic concept of a fringed micelle [1].

known as primary particles. In the case of melting of crystallites, loosening of the entanglements leads to interdiffusion and formation of new structures whose stability is determined by the amount of shear and the new thermal conditions. The old configuration does not determine the properties and characteristics of PVC. Faulkner [74] also reported the presence of primary particles composed of 100 °A microdomain. At temperatures above 210 °C when the fusion has progressed sufficiently and the primary particle boundaries are not distinguishable, he still observed large fibrillar structures. But the microdomains still persist. In section 2.3 the effect of particulate structures on rheology will be analyzed in greater detail.

2.2 EFFECTS OF PLASTICIZERS ON PVC MORPHOLOGY

In the previous section the discussion has been concerned with structure of suspension PVC, the microstructure of PVC and the presence of large supermolecular structure in PVC melt flow. In this section the mechanics of plasticization and how it specifically influences the structure of PVC will be examined. The efficiency of a plasticizer can be defined in various terms ranging from the depression of glass temperature, Tg, to its ability to modify the moduli values. To account for the effect of plasticizers, Sears and Derby [9] outline some of the theories and mechanisms. These theories are generally applicable to any plasticized material.

The lubricant theory states that plasticizers act to facilitate the relative movement of the resin particles. This theory is rarely used as the sole theory of plasticization, but it can be applicable at high temperatures in the elastomeric region where the plasticizer effect is related to the coefficient of friction. In the gel theory, some of the plasticizers mask or break the attachments which make up the rigid gel. Additional plasticizers swell the gel and increase the flexibility of the resin molecules. The free volume theory centers around the cre-

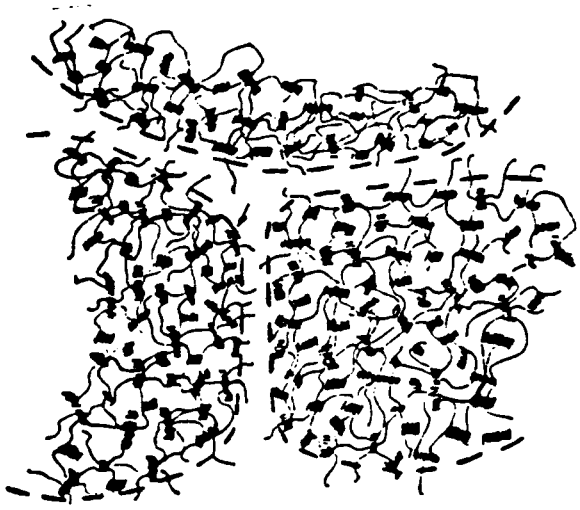

Primary particles in a low temperature melt (162°C).

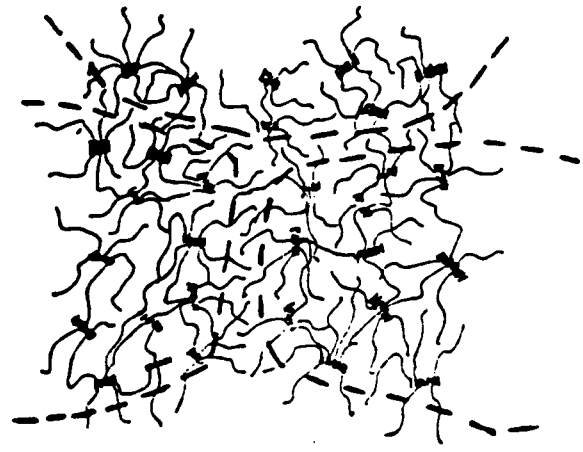

Primary particles, partially melted and interacting in a 177°C melt.

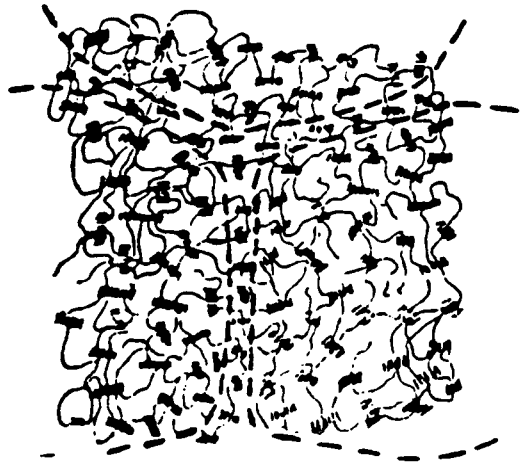

Primary particles after coolong and recrystallization from a 177°C melt.

Figure 2. 4. Schematic diagram of fusion of primary particles [7].

ation of free volume through the movements of the chains and deals mainly with lowering of the glass temperature, Tg [10]. In all the three above-mentioned theories, plasticizers affect the resins by attaching themselves to the resins by forces which are not very strong. The forces which bind the solvent molecules to each other and the forces which hold the polymer molecules together are not very different in magnitude. This results in a dynamic equilibrium between solvation and desolvation, and the plasticizer molecules continuously exchange their positions of attachments to the gel. This is called the mechanistic theory of plasticization [9].

When a plasticizer is added to the resin, its incorporation is associated with the following general steps. It gets adsorbed in the resin pores and then solvates and swells the surface of the resin. It penetrates the particle, swells the amorphous region and aids in the disassociation of the polar and hydrogen bonds, thereby essentially dissolving select parts of the chain. It can thus affect the destruction of the supermolecular structure. Finally it helps to reestablish the formation of a new supermolecular structure. The addition of plasticizers to PVC are postulated to follow the same pattern, however, Sears and Derby [8] do not report on the effect of plasticizers on the microdomains or the primary particles in the PVC.

The compatibility of various plasticizers with the resins can be used as an indicator of this efficiency. For PVC and other polymers, this compatibility has been measured by diverse methods like solubility parameter or Flory-Higgins interaction parameter, to mention a few. These methods are based on the solvation of the resin by the plasticizer. These respective compatibility measurement values can be used to predict their compatibility. For instance, it has been shown that the interaction parameter has a limiting value of 0.55, and values above this lead to incompatibility between the resin and the plasticizer. For PVC the corresponding value of the interaction parameter was 0.4 instead of 0.55. This parameter is a function of temperature and concentration and lower values indicate good compatibility [1,8].

The exact nature of the plasticizer interaction with the PVC network has been subjected to examination by X-ray diffraction and electron microscopy. The works of Geil and coworkers [12,74] and more recently the studies in [1] merit some critical consideration. The SAXS technique was used to study the structure of plasticized PVC with different levels of DOP [12].

The plasticizer was mixed with the PVC by milling in the roll mill. It was observed as a general trend that the peak intensity increased and the scattering angle of the maximum moved to a smaller angle with increasing plasticizer content. It was also observed that for processing conditions like high temperature milling the peak intensities increased. The unplasticized sample showed no domain structures by means of SAXS as mentioned in the last section [12]. As the plasticizer content was raised from 20 to 60 % the size of the interdomain spacings increased and the domains became more distinct. This was sought to be explained by the fact that the plasticizer only affected the amorphous region and additional plasticizer at higher concentration went to the already plasticized material. The interlamellaer or interdomain distance, as indicated by the Bragg spacings, from the intensity peaks were between 100 to 150 °A. The structure as seen under the electron microscope was nodular and sometimes the sizes of these nodules varied with the increase in the plasticizer content. A comparison between SAXS and electron microscopy was not easily deduced because of the lack of a highly ordered lattice or packing of spheres required for interpretable scattering pattern. The correlation was also difficult because poor reproducibility of the data from the microscopy. Nodules observed under EM were for most parts considerably larger than what was anticipated from the SAXS patterns. The authors in [12] were not very clear in their findings as to whether the plasticizer affected both the nodular and the internodular regions or only the latter. Later Summers [7] showed that these spacings corresponding to the nodular structure in the plasticized PVC were the interdomain spacing. By differentiating between the different regions as shown by the differences in their densities, he was able to conclude that these spacings, arising out of the swelling of the amorphous regions, were the interdomain distances measured from the SAXS peak in [12].

A reason for the poor reproducibility of the freeze fracture data from the electron microscope was the fracture process itself. Geil and coworkers [74] improved the ability to observe the PVC structure by staining and etching ultra-thin sections of PVC embedded in Epoxy. They looked at the effects of plasticizers like DOP, diallyl pthalate (DAP) and ethyl vinyl acetate copolymer (EVAC). They were milled with PVC in a two roll mill. The conclusions from both

etched and stained samples were the same and clearly showed the presence of 100 to 200 °A microdomains. The sharper boundaries from etched samples and sharper contrast between bright and dark regions from the stained samples allowed the authors to study the effects of plasticizers without ambiguity which had not been possible in [12]. Addition of plasticizers increased the microdomain spacings with little, if any, penetrating the microdomains whose sizes were unaffected. This agreed with the results of the SAXS measurements in [12]. Also observed were 0.1 to 0.2 μm domains that did not break down during milling. The distribution of plasticizers was not very homogeneous at low temperatures and two glass transitions were observed. As the temperature was raised above 180 °C, the amount of unplasticized material was seen to decrease. This preceding observation and the fall in distinctness of the microdomains because of fusion gave a more homogeneous plasticizer distribution. At temperatures above 180 °C both the primary particles and the microdomains supposedly fused simultaneously for the plasticized PVC. For unplasticized PVC, Faulkner [73] had observed that primary particles fused at 190 °C but the microdomains persisted until 215 °C. The question how the action of plasticizers brought about faster fusion for the primary particles or the microdomains has not been answered satisfactorily in [74].

Yorkgitis [1] studied the effect of some benzyl pthalate plasticizers on the SAXS and WAXS patterns. In this report some of the possible models of plasticized PVC were discussed. In the first model the chain entanglements form the physical crosslinks and the action of the plasticizer reduces the number of these crosslinks and increases the molecular weight between the crosslinks. It was thought unlikely that entanglements of this kind can give rise to discrete peaks by SAXS. Plasticized PVC in the next three models can be held together by different combinations of lamellar crystallites and micelles. The network points can come out of either crystallites, or micelles, or a combination of these two. A number of crystallizable segments can incorporate themselves into micelle or into adjustable reentry lamellae. The SAXS peaks can come from the lamellae spacings or the micelle spacings. Sometimes the SAXS peaks are dual valued signifying contribution from both the sources. With the addition of plasticizers the number of crosslinks may remain the same, but a smaller number of chains

will be included in them. These disconnected chains can recrystallize to form new crosslinks in such a manner that the SAXS spacings remained invariant. The last model described the crystallites as dispersed in pockets where a regular structure exists. The pockets are randomly distributed in the amorphous region. In this model the addition of the plasticizer increases the molecular weight between the crosslinks but leaves the spacings in the pockets unchanged.

In sections 2.1 and 2.2 briefly the morphology of rigid and plasticized PVC have been reviewed. The microstructure and the macrostructure of rigid PVC have been studied in detail and the presence of domains of different sizes have been established [1,12,74]. The crystallinity content is low and the crystallites can be found in certain structural configurations like fringed micelle or thin lamellae [1,2]. The existence of primary particles as flow units at low temperatures has also been established [13,14,73]. The conclusions about the structure of plasticized PVC are varied. Some studies have been reported on the effect of plasticizers on the microstructure [1,12,74] but there seems to be a lack of consistency with regards to how exactly this interaction takes place. There is no reference as to the way in which plasticizers can effect the structure or the size of the primary particles and if this is reflected in the fusion process of PVC. In processes like extrusion, the behavior of primary particles can be affected by the plasticizers. In section 2.5.3 some morphological studies on PVC in single screw extruders will bw discussed but it can be mentioned here that the effect of plasticizers on the morphological developments in single screw extruders have not come to the author's attention.

In the next section the rheology of PVC will be discussed.

2.3 RHEOLOGY

Comprehending the rheological properties of PVC has been complicated because at temperatures at which it is processed the material fuses rather than melts. In the begining of this section the fusion of PVC will be examined. Next, the effect of molecular weight on viscosity measured in capillary rheometer will be reported. Phenomena like die swell and melt fracture will be considered. The effects of plasticizers on rheological properties will be assessed. Work on rheological measurements in extensional flow and small strain dynamic oscillatory flow will be reported. The yield stress phenomenon of PVC will be discussed. PVC is always processed with additives like lubricants, stabilizers, processing aids, etc. The last section will deal with the effects of various additives on the PVC melt flow.

Till the late 1960's researchers were trying to explain the flow of PVC in the same way as that of a normal homogeneous polymer melt. During the latter part of that decade Berens and Folt [13,14] published their findings showing that particulate flow characterized by slippage was the flow mechanism at low temperatures and high shear rates. At the higher temperatures and lower shear rates, the flow mechanism was dominated by molecular deformation where the different chain segments had enough time to change their conformation and relax the stresses that had built up because of imposition of external forces.

Comparing the flows between differently sized suspension and emulsion polymerized PVC in capillary rheometers, and looking at various fractured surfaces under the electron microscope Berens and Folt, arrived at some general conclusions. The emulsion PVC sized about 1000 to 4000 °A maintained its particle identity even when extruded at high temperatures of 190 °C. The suspension PVC was broken down from a larger agglomerate to primary particles measuring approximately 1 μm, and at higher temperatures of 190 °C the particles started getting bridged by a fibrular structure. In emulsion PVC, the absence of bridging or interparticle fusion led to particle slippage, which was responsible for reduced viscosity and elasticity. It was shown how viscous and elastic properties depended on molecular weight

and particle size, which were independently controlled. For a fixed molecular weight, viscosity and elasticity decreased with particle size especially at high shear rates. At lower shear rates an increase in viscosity was observed with increase in molecular weight. But at higher shear rates viscosities were more dependent on particle size. The dominant effect of molecular weight at lower shear rates and that of particle size at higher shear rates underline the difference of the two prevailing mechanisms of flow. It was postulated that as the shear rate was increased, a yield value was crossed before appreciable particle slippage occurred. Below this critical shear rate the flow was relatively slow allowing time for molecular deformation within the flow units. In spite of slippage at higher shear rates the flow was thought to be a superposition of molecular deformation on the particle slippage. The elasticity measurements were done by comparing the die swell values which were only in the order of 10 %. These values were rather low and basing decisions on these might seem questionable. However their relative values predicted the trends in the elasticity behavior. As the temperatures were raised the differences in the die swell and the viscosity between the two resins diminished. At about 200 °C the transition from particulate flow to melt flow took place.

The mechanism of fusion and its progression during processing was studied by Krzewki and Collins. [15,44]. The study was conducted by examining what the authors thought to be changes in the elasticity of PVC by following the changes in the particulate structure from breakdown to fusion. The change in the so called melt elasticity was characterized by measuring the entrance pressure loss in a very short capillary of diameter 1.6 mm and L/D of 0.24 [15]. The pressure difference from a material extruded in this short capillary at 140 °C and a shear rate of 6 (1/s) was used to quantify the elasticity. The flow existing in the entrance region to a capillary is more extensional in nature than shear flow. Thus the variations in the entrance pressure drop for a small L/D capillary do not characterize a change in the elasticity but is a measure of the material being to force to stretch as in entrance flow. As the PVC gets more fused or the particle boundaries interdiffuse, a network is formed. Higher degree of fusion causes higher resistance to flow in the short capillary. Thus pressure drop in short capillary although indicating the degree of fusion does not reflect on the elasticity build up.

It reflects the resistance to extensional flow owing to the formation of an interdiffusing network of primary particles. Using a temperature programmed Brabender with sigma mixing blades, PVC mixes of different fusion were prepared by thorough fluxing. The torque developed in the Brabender is a measure of degree of the fusion as a result of shear and heat. The degree of shear uniformity of these mixes is not known and the fusion can be affected by additional shearing after the fluxing process is completed [35]. Fig. 2.5 is a schematic of Brabender torque curves as a function of temperature for a simple compound containing stabilizer and lubricant and a fully formulated commercial compound, respectively. The Brabender method to prepare samples to study fusion has been used extensively. Fig. 2.6 shows typical fusion curves obtained by plotting the entry pressure from a zero length capillary for materials sampled at different Brabender temperatures. Since this method is inexact, the fusion curves had been supplemented by electron microscopy.

For the simple compound, the torque reached a minimum at about 140 °C as the particles broke down. There was no inter-particle diffusion at this stage and the low entrance pressure indicated the absence of interparticle strength. As the temperature was raised, the interparticle strength started to develop and reached a maximum around 190 to 200 °C. This kind of measurement was indirect and the samples from different fused states were observed under the microscope. Figures 2.7, 2.8 and 2.9 show the particle distribution at three different temperatures of 120, 140 and 210 °C, respectively. At a temperature of 120 °C, the 1 μm particles were clearly seen; at 140 °C the destruction of the primary particles was complete and domains of the size 700 to 2000 °A remained. At 210 °C the structure was that of a totally fused homogeneous material. At the intermediate temperatures of 160 to 180 °C, the 700 to 2000 °A particles still remained but the particle interface became less defined. As it proceeded, this sintering or interdiffusion made the particles loose their identity and at 210 °C the three dimensional network of PVC was complete. The elastic response is strongly composition dependent and thus the commercial compound, although showing the same characteristics, achieved a significantly lower melt elasticity.

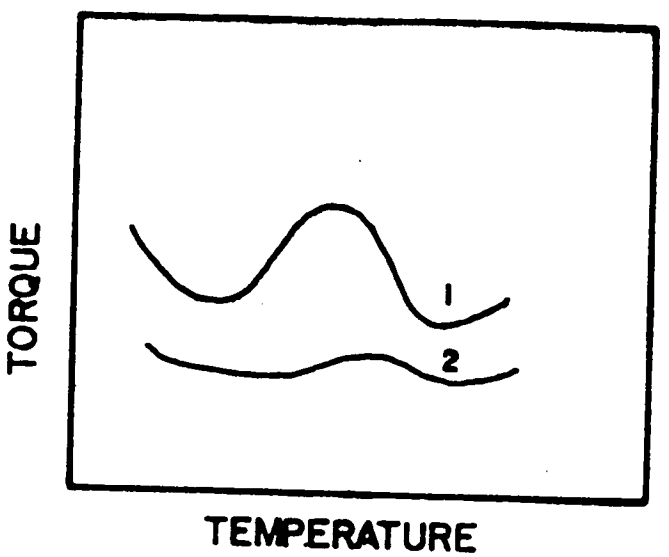

Figure 2. 5. Schematic Brabender torque curves [14]: 1 - simple compound, 2 - commercial compound

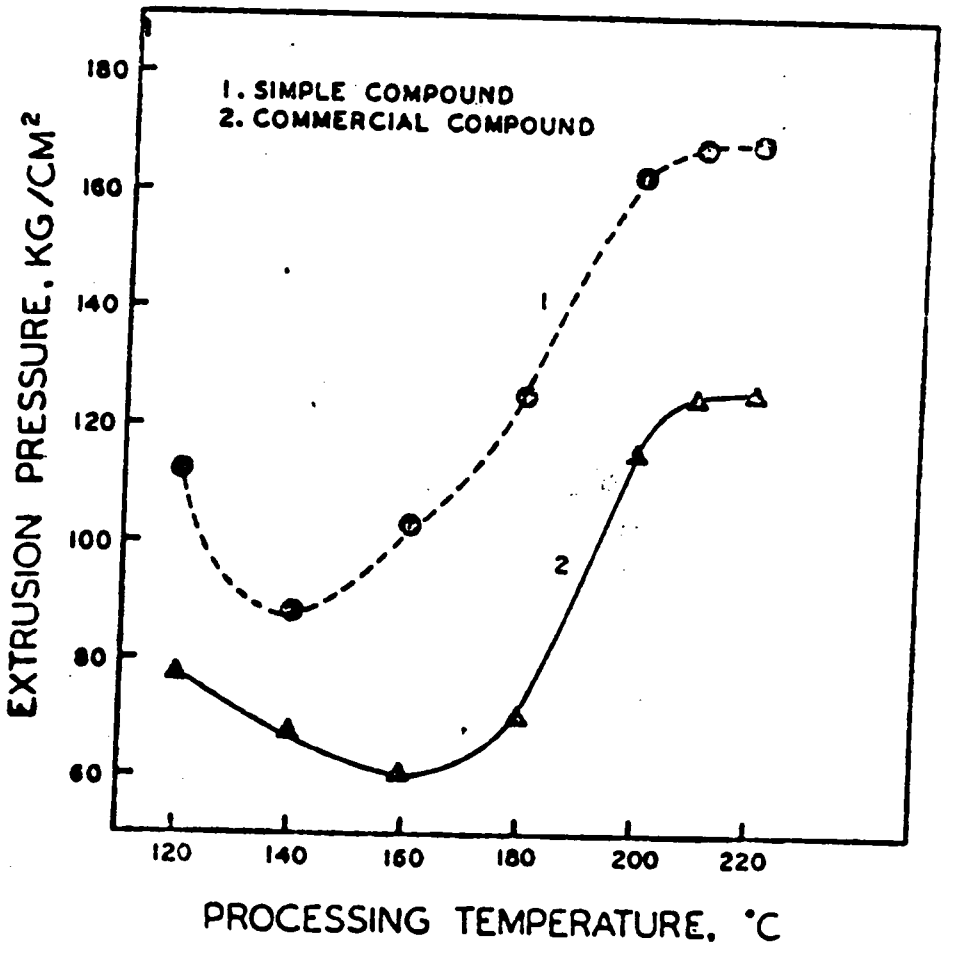

Figure 2. 6. Fusion curves for simple and commercial compoundds [14].

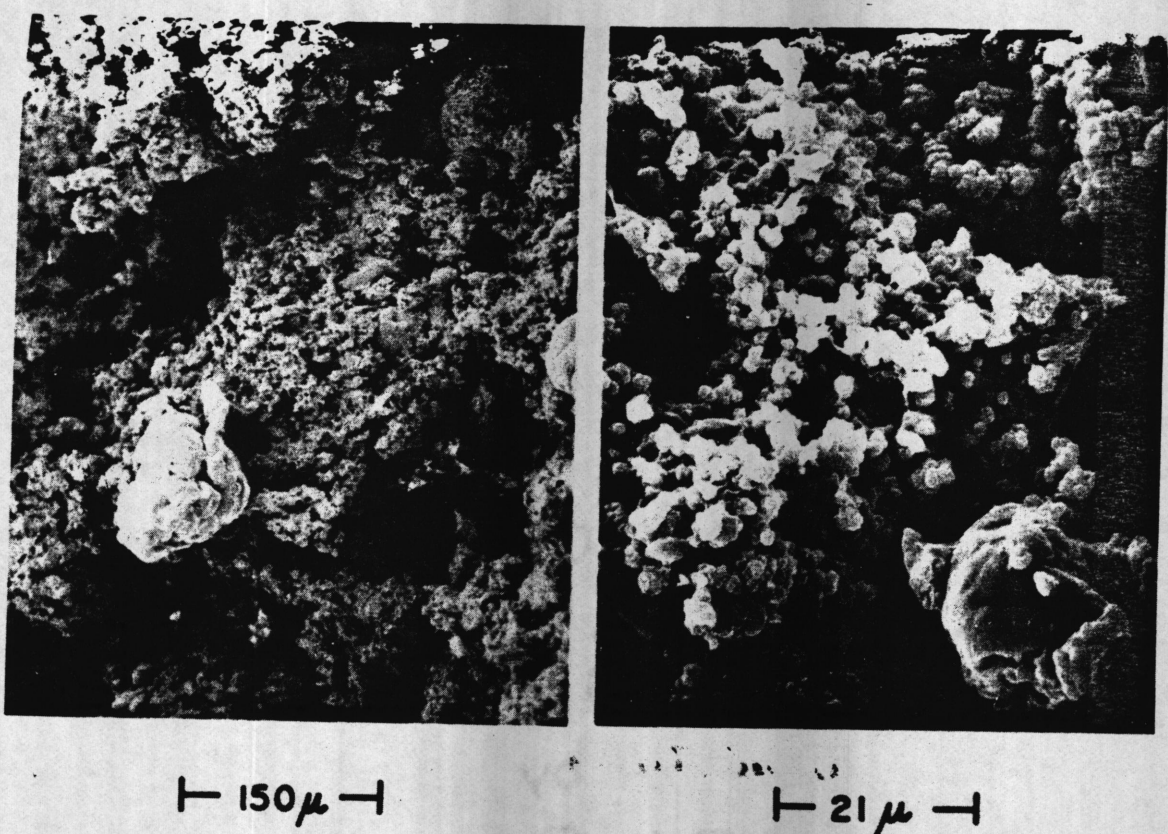

Figure 2. 7. Simple compound processed to 120 °C in a Brabender [15].

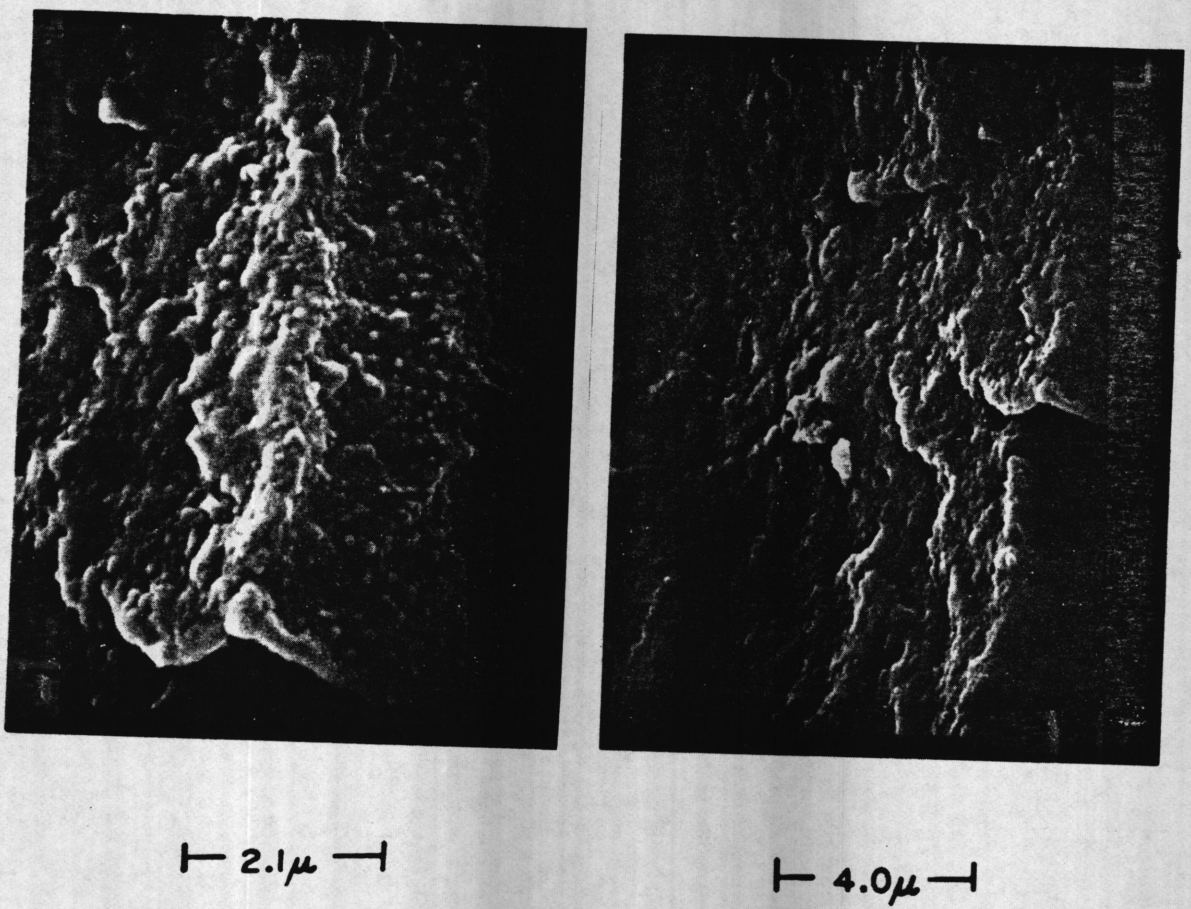

Figure 2. 8. Simple compound processed to 140 °C in a Brabender [15].

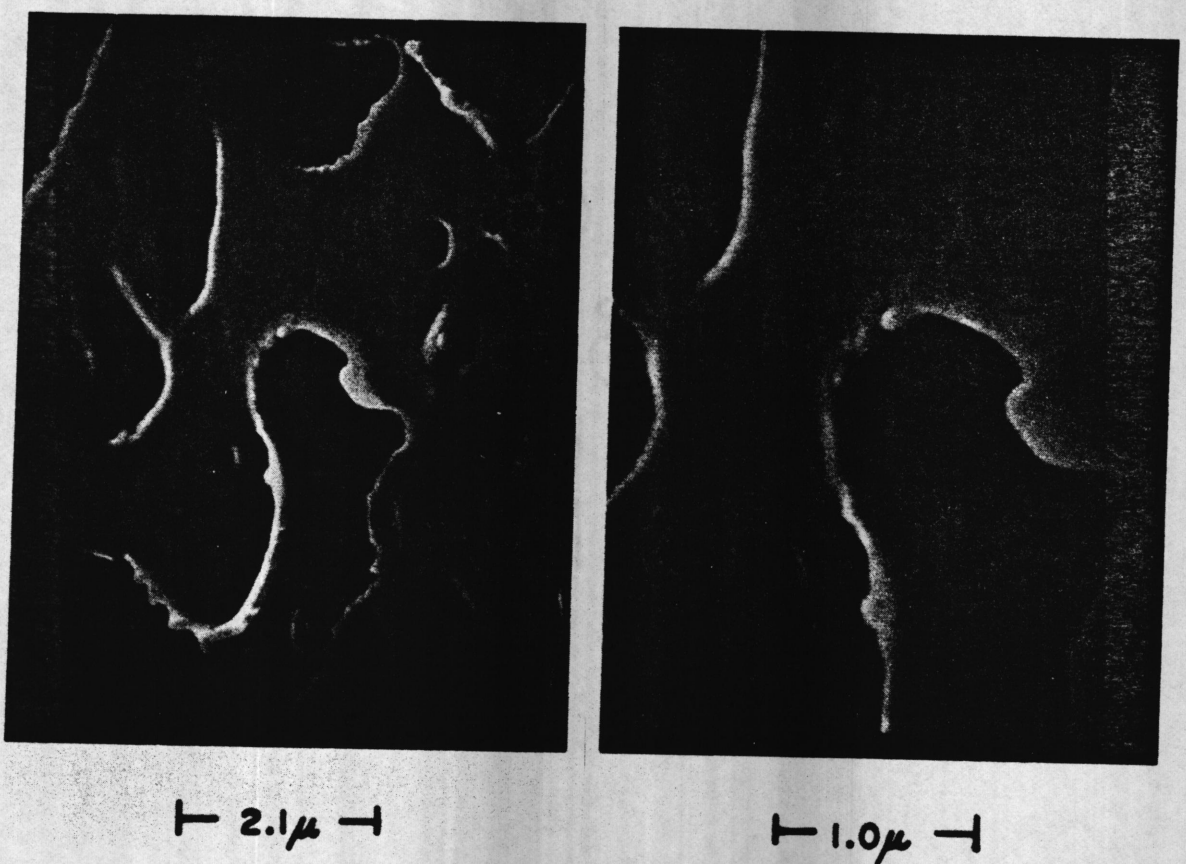

Figure 2. 9. Simple compound processed to 210 °C in a Brabender [15].

Similar experiments were conducted by Faulkner [74] who observed the same trends. In addition, he observed that the initial breakdown of the 100 μm domains and densification of the resulting primary particles lead to a maxima in the torque before the fusion peak. At higher temperatures of about 215 °C, another maxima in the torque was cited. It was initially suggested this possibly was due to the breakdown of the 100 °A crystalline microdomains but the presence of microdomains as observed from electron micropscope pictures proved otherwise. He also tried to explain how the particle sizes and temperatures affected the positions of the torque peaks.

It was shown that several different paths could lead to fusion [15]. By the first method, the particles were broken down to submicron level and interdiffusion among these formed fused material. In the second method, the breaking down occurred till micron level and these were compacted and internally fused. In the third mechanism, there is no particle breakdown, but compaction with time and temperature caused the resin particles to diffuse internally and form a fused material. In commercial processes it is most likely that a combination of all three mechanisms exists.

The mechanism of fusion has been explained from structural consideration by Summers [7]. At low temperatures, the material within a primary particle is held together by a 3-D network which prevents interaction with other primary particles, and they flow independently of each other. As the temperature is raised the crystallites melt and interactions between the primary particles increase through their amorphous regions. In a more recent paper, Summers et al. [18] postulated the rationale behind measuring the entrance pressure loss as a measurement of fusion in terms of measuring the force to deform or fracture the 3D network. They showed that higher molecular weight PVC developed higher fusion by their increased number of tie molecules. A lower number of tie molecules in the lower molecular weight PVC prevented the formation of a more effective network to link the crystallites. . A network is made during the polymerization process. This network can be broken by the action of milling or extrusion and leads to a lower elasticity during grinding.

A number of researchers have looked into similar techniques to study the fusion process as described in [15,74] with some modifications [16-23]. Some of their findings are discussed here. It has been shown in [19] that the pressure drops in zero length capillary were not always readily related to changes in the microstructure. It was shown that formation of fibrils signifying flow and the corresponding disappearance of the primary particles occurred not at the fusion peak but after it [74]. Different tests have been suggested to determine the different stages in the fusion process. The first minima in the fusion curve has been associated with the starting of the breakdown of the primary particles. The formation of a continuous phase with the additives and the primary particles coincided with the ductile to brittle transition region in the impact test. The end of the primary particle breakdown and the formation of a continuous network can be deduced from the maxima in the yield stress with temperature [19]. Individually not any one of these methods are capable of supplying all the information on particle breakdown and fusion. These methods are complementary and should be used in conjunction with each other.

Different samples of PVC from the Brabender were swollen in Acetone and then studied under an optical microscope [16]. This method was proved to be useful until the maximum torque in the Brabender is reached. As the fusion increased, the acetone was unable to swell appreciably any further and electron microscopy had to be used. A method developed by Hattori et al.[17] of embedding PVC in methyl methacrylate has proved to be useful in obtaining information on 1 μm primary particles. They showed the existence of 100 to 300 °A fibrils in the primary particles by this technique and followed their presence during the fusion process. These fibrils were present even at high temperatures after considerable fusion had taken place. The presence of 100 to 200 °A microdomain has been discussed in section 2.1 and 2.2 and it had been mentioned that Faulkner [73] observed that these continued to exist at temperatures 20 °C higher than the temperatures at which the primary particle boundaries interdiffused completely.

A certain amount of caution needs to be exercised when processing PVC, as its thermal and shear history has a strong influence on its flow properties. At lower temperatures, re-

peated working of PVC has been known to increase its viscosity because of progressively increasing fusion[11,36]. Reproducibility of the flow curves is dependent on thermal and shear history. Fig. 2.10 shows the effect of starting the viscosity measurements from different shear rates [36]. The amount of time for which the material was maintained at 190 °C made a difference to the viscosity value. The error bars have not been indicated for the data but still at lower shear rates the absence of potential for compaction might have caused less interdiffusion of the primary particles. This possibly was the cause of the differences in the viscosities. This figure could be taken as an indicator of the difficulty involved in reporting an unique viscocity-shear rate data owing to fusion. Thus two differently processed materials - one in Brabender and one in the roll mill might not give rise to similar properties though processed under similar conditions.

Processing with or without shear in a Brabender and Hydraulic press, respectively, gave similar fusion curves [21, 22]. Fusion was accelerated when shear was present but the final interparticle strength as deduced from pressure drop in 'zero length' capillary was lower. It is interesting to note that even without shear, i.e. in the press, the fusion curves reached a minimum before building up to a steady state value. The crystallites constrain large scale movements and were thought to give rise to elasticity, and an explanation of the fusion curve was attempted on the basis of the amount of crystallites. The amount of crystallites was calculated from the molecular weight between entanglements. Initially the crystallinity as measured by this method fell rapidly but it later levelled out. The authors postulated that in the early stages of the process crystallites melted allowing for a decrease in elastic energy as the chains moved past one another. As the process continued these chains formed new crystallites in the previously unoccupied grain boundaries. This was connected mathematically to the growth of the 'neck volume' between the diffusing polymer particles to form new crystallites. The mathematical model was able to explain the initial fall and the subsequent rise of the degree of fusion. However it was unable to predict the final plateau reached as the fusion is completed.

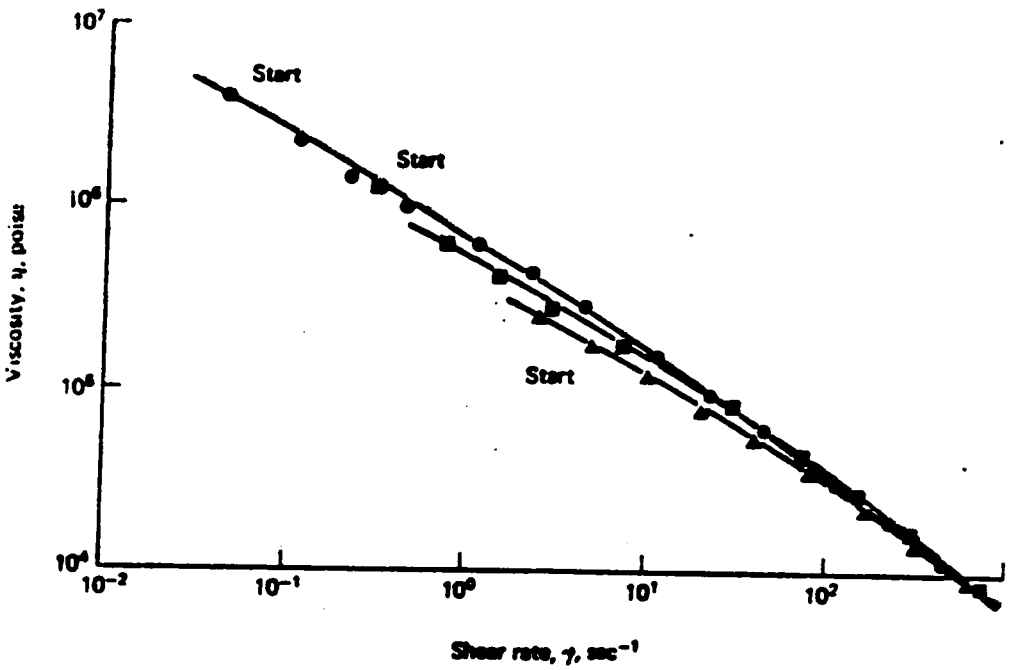

Figure 2. 10. Viscosity vs. shear rate for a PVC compound starting at different shear rates [36].

The decrease in entrance pressure loss without fusion and without shearing as reported above [21, 22] could be explained by the findings of Smith [20]. He experimented with suspension and emulsion polymerized PVC which were subjected to non-shearing processing in a hydraulic press. The emulsion resin consisted of an agglomeration of individual primary particles but was not porous like the suspension resin. The samples from each process at different time were tested for degree of fusion by measurement of entrance pressure in zero length capillary. In the suspension PVC, the non-shearing process did not lead to particle breakdown. The internal fusion of the porous grains led to a fall in the elasticity. For the emulsion PVC, the absence of internal porous structure meant no internal fusion could have occurred and hence no loss of elasticity was to be found.

The transition in the melt flow behavior of PVC from its loss of particulate identity at higher temperatures led to a flow having two activation energies in the range of 160 to 230 °C. This was true for measurements made at both constant shear stress and constant shear rate. These dual valued Arrhenius plots were observed earlier for PVC blended with various additives such as low molecular weight polymers, esters, plasticizers etc. [24]. It was left to Collins and co-workers [25-27] and Pezzin [28] to establish a link between this fact and the flow mechanism. The effect of molecular weight, shear rate and temperature have also been investigated in [25-27]. As seen in Fig. 2.11 the molecular weight of PVC influences the extent of temperature dependence of viscosity. The flow activation energy decreased with increasing molecular weight but the critical transition temperature increased with increasing molecular weight. The high and low activation energies were 18.8 and 35.5 Kcal/mole, respectively, for a molecular weight of 60,000, but these dropped to 15.2 and 22.5 Kcal/mole, respectively, as the molecular weight increased to 207,000. The transition temperature went up from 165 °C at 60,000 to 217 °C at 105,000 [25]. At higher shear rates the activation energies decreased and the differences between the high and low temperature activation energies diminished as shown in Fig. 2.12. It was also demonstrated that activation energy calculated at constant shear stress was also dual valued and unlike the constant shear rate, the dependence value increased with molecular weight.

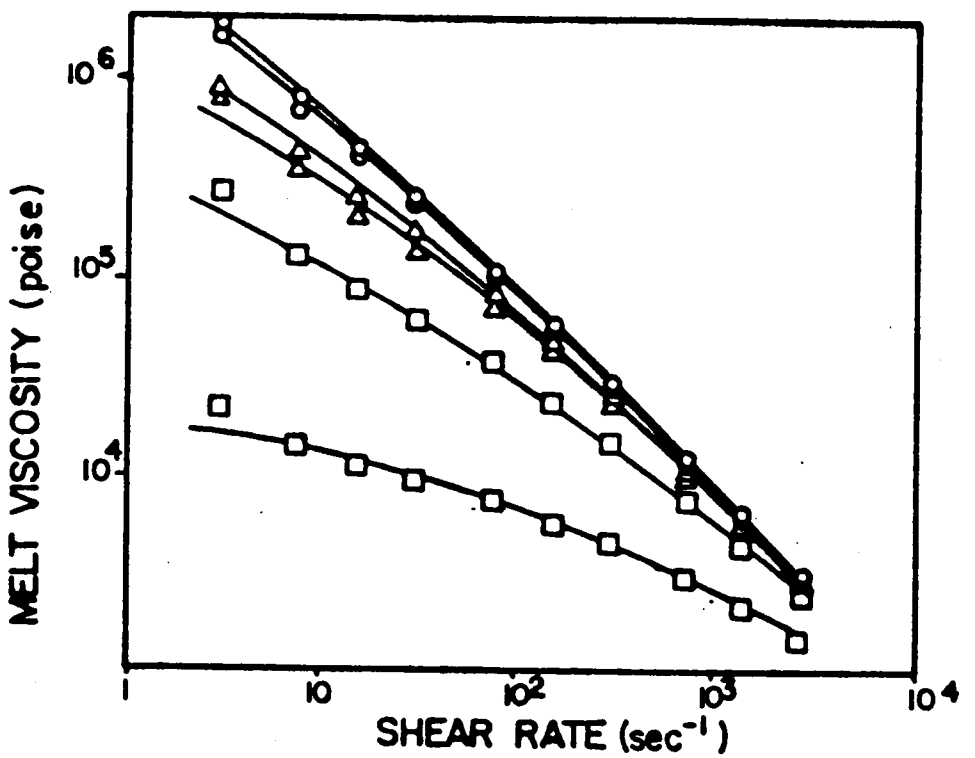

Figure 2. 11. Comparison of melt viscosities at 200 ° C for different molecular weigt PVC [25].: Top Curve mol.wt. = 459100, Bottom Curve mol.wt. 60000

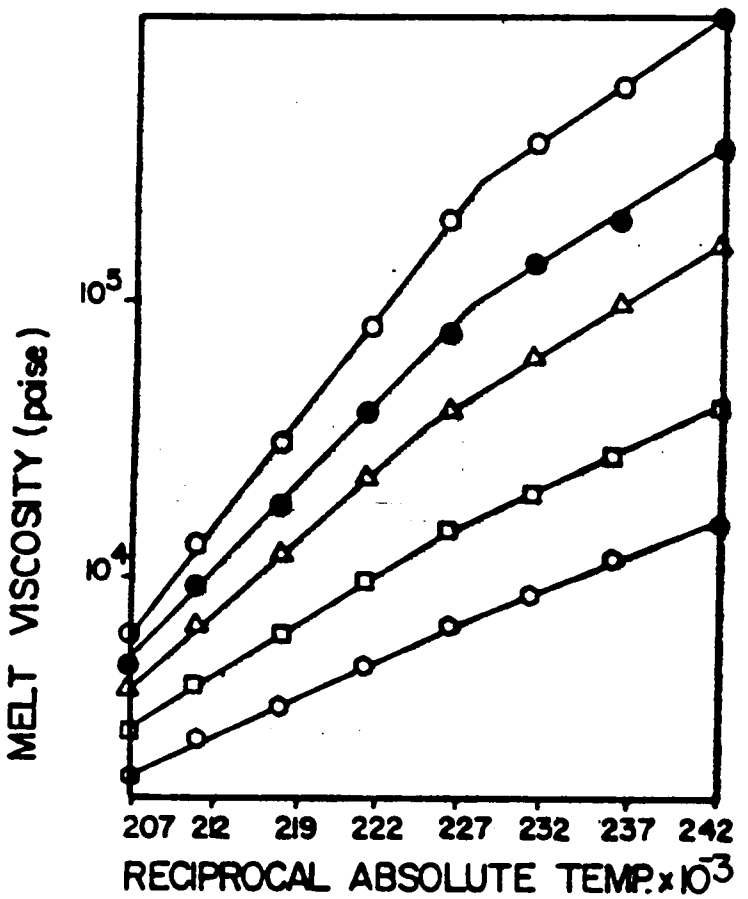

Figure 2. 12. **Relationship between constant shear rate viscosity and reciprocal absolute temperature for PVC sample with mol. wt. of 60000: ○ 10 1/s, ⊙ 40 1/s, △ 100 1/s, □ 400 1/s, ⬡ 1000 1/s**

Attempts have been made to link the zero shear viscosity η_0 to molecular weight . While most homogeneous polymers follow the empirical relation

$$\eta_0 = K \ Mw^{3.4} \qquad (2.1)$$

the exponent for PVC was found to be higher than 3.4. The exponent was 8.2 at 150 °C, 7.8 at 170 °C and 4.5 at 190 °C [28]. The marked dependence on temperature was a departure from ideal behavior and was attributed to association arising out of the presence of crystallites at these temperatures, the flow units being supermolecular particulates [13]. At high temperatures above the crystalline melting point there is a possibility that this exponent might approach that of other normal amorphous polymers. It was seen from the results in [26], the exponential dependence of viscosity on molecular weight was 3.4 for values of viscosity measured at a higher shear rate of 10 (1/s). Again from evidence based on blends of PVC samples having very different molecular weights, the authors in the same reference report a large deviation from equation (1) [26]. The degree of difference between the blends depended on whether the blends were produced by tumbling or milling, i.e. if they had a different shear and thermal history. The differences between the observations made in [26] and [28] could have been due to dispersity in the blends or due to previous history. This difference in the dependence of zero shear viscosity on molecular weight is another indication of why it has been difficult to compare the results of various research data from different sources.

Experiments were carried out to investigate the effect of polymerization conditions and hence the chain structure on the viscosity of PVC melts [27]. As has been mentioned earlier, Tp, the temperature of polymerization, affects not only the molecular weight but also tacticity and crystallinity [1,2]. Between polymerization temperatures of 40 and 70 °C no difference was observed in the flow behavior in a capillary rheometer. But for a Tp of 5 °C, the increased syndiotacticity gave a nearly ten-fold increase in viscosity, even at low shear rates. It was observed that a zero shear viscosity, η_0, was approached only for low molecular weight PVC samples, a high temperature of 210 °C and a shear rate of 5 (1/s) as shown in Fig. 2.13. Again

for large molecular weight material, the zero shear viscosity was not obtained at temperatures around 210 °C. The deviation was higher for higher molecular weights and the exponential dependence of viscosity varied substantially from the value of 3.4. For larger syndiotacticity the zero shear viscosity was never attained. Even the attainment of the zero shear viscosity can be questioned from the fact that at low shear rates, the loads measured in the capillary rheometer are small and therefore their accuracy is prone to questioning.

Munstedt [29] reported a comparative study of PVC melt flow behavior with respect to the other two common polymers, like polyethylene and polystyrene. He showed that the viscosity of PVC possessed a stronger temperature dependence than polystyrene. As has been mentioned before, a zero shear viscosity was approached for PVC at about 210 °C [27]. For PS the corresponding temperature was 180 °C and a true zero shear viscosity was attained. For high molecular weight PS, the levelling off of the viscosity took place at a temperature of 10°C higher. A reduced viscosity based on a particular stress, τ_o, and temperature, To, was calculated to compare the viscosity of the PS and the PVC. Arrhenius plots were prepared. The activation energy of the polystyrene was single valued and independent of the shear rate but those for the PVC, as found by others in [25] to [28] were shear dependent and dual valued. There was an anomaly in the activation energy of PVC in that the values were lower for higher temperatures as opposed to previous results from others. This might be due to the choice of To and τ_o which were not specified and could be affected by the choice of reference temperature as the flow mechanism changes.

This report [29] also dealt with the phenomenon of slip and die swell. The variation of shear rate at constant shear stress with the use of different die diameters was observed and attributed correctly to slip flow. The difference in shear rates disappeared at high temperatures which coincided with the temperature at which particulate flow ceased to exist. Berens and Folt [14] also observed the disappearance of slip flow at higher temperatures. Fig. 2.14 shows the profile of PS and PVC at different temperatures photographed in a die. At temperatures above 210°C, both the profiles were parabolic. With the help of some dyes it was shown that at lower temperatures PVC did not stick to the wall and had a flatter profile. At

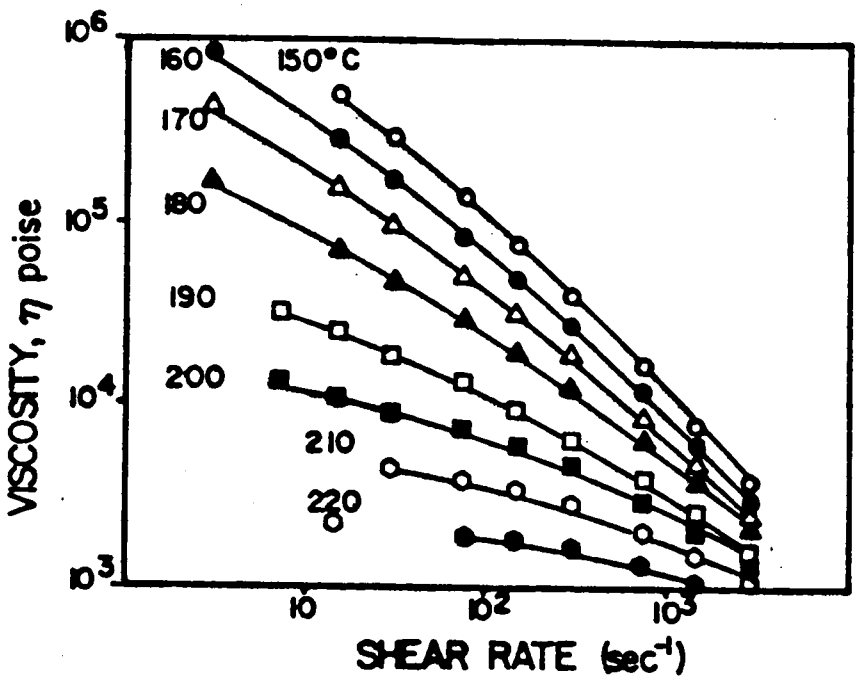

Figure 2. 13. Flow curves of low mol.wt. (20000) PVC samples at different temperatures [27].

all temperatures, PS showed parabolic profile which agreed with a no slip boundary condition.

Die swell for rigid PVC extrudates from the capillary rheometer has been measured by many researchers [13,14,29,30,32]. The die swells in PVC show a similarity to other polymers in that they increase with shear rates, decrease with molecular weights and decrease with an increase in capillary length. The die swell characteristics differ from other polymers in two respects. Firstly, unlike others the die swell increase with temperature, and secondly, their values exhibit only about a maximum of 25 %. In general the values of the die swell were of even lower magnitude. The reported die swell from [13] and [14] decreased with increase in particle size and passed through a minimum as shear rate was increased. While the decrease with particle size was expected because of slippage, the other phenomenon was not explained. The explanation was obviously complicated by the low values of die swell. A reasonable explanation of the low die swell has been given by Munstedt [29]. He attributed it to the existence of crystalline crosslinks in PVC at lower temperatures. Extrudate swelling depends on the ability of the polymer melt to recover from the imposed axial elastic strain. Higher entanglements and higher strain values lead to higher swelling at the capillary exit [48]. For PVC, the reduced stretch in the entry region from the presence of the restraining cross links lead to smaller recovery and smaller die swell. At higher temperatures for the amorphous melts faster strain recovery causes a decrease in swelling [29]. For PVC the disappearance of crosslinks at high temperatures leads to higher die swell as the material is less restrained. It is seen that at high temperatures the die swell reaches a limiting value for any molecular weight. Further investigation was supposedly limited by the onset of degradation.

Two types of surface irregularities have been reported for PVC in the literature [14, 30, 35,]. At the high shear rates melt fracture involves gross distortion of the surface. It is characterized by a flow instability as demonstrated by a break in the shear stress shear rate curves and is said to arise because of instability at the entrance of the die [48]. Fracture also occurs at low shear rates and has a sharkskin type scaly appearance whose initiation sites could be the die exit [48]. Berens and Folt [14] constructed a map for the 'smooth extrusion

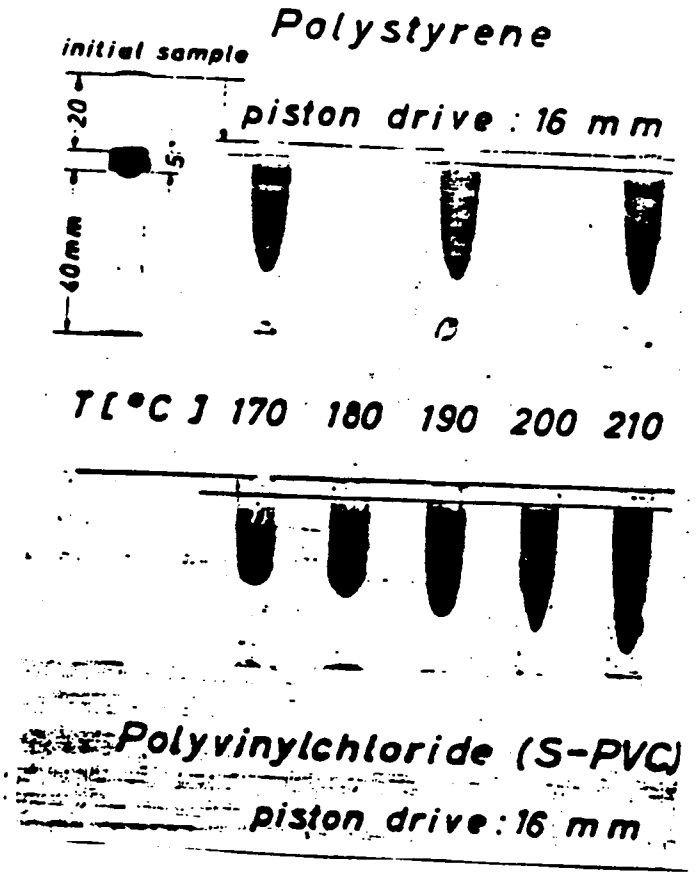

Figure 2. 14. Flow profiles of Polystyrene and PVC at different temps. [29].

area' on a temperature-shear rate plot as shown schematically in Fig. 2.15. The boundary of this region changed with molecular weight and particle size. The type of fracture was governed by molecular deformation at low shear rates and by slippage at higher shear rates. This map is limited by the lack of flexibility in the molecular weight distribution and a variation in the particle size.

A detailed study on melt fracture was conducted by Rudin [35]. Working with 50% benzyl pthalate plasticized PVC Rudin attributed melt fracture to a mechanism similar to that in die swell. He postulated that it was an elastic effect arising out of strain recovery of entanglements as the polymer comes out of the die. He derived a mathematical expression for the degree of distortion as compared to that arising from shorter capillaries and linked it to the experimental observations. The distortion decreased with an increase in the L/D ratio of the die and decreased with increased extrusion temperature. Increase in temperature decreased relaxation time and diminished the severity of the extrudate appearance. The decreased severity was also obtained for samples prepared by milling the polymer at a lower temperature. It showed the importance of sample preparation history especially when extruded at temperatures at or below sample preparation temperatures. But the author did not give a reasonable explanation for this in terms of particle fusion and also did not investigate the effect when extrusion temperature exceeded sample preparation temperature.

The flow behavior of PVC is affected by the addition of plasticizers. They do affect fusion time and fusion temperature [37,38]. It has been shown that the addition of plasticizers decrease the viscosity and affect melt flow of PVC but the mechanism of their action had not been explained [8,30, 31,33]. Initial rheological studies [30, 31] dealt with trying to find an expression for viscosity as a function of shear rate, concentration and temperature. Detailed studies concerning the relative influence of different plasticizers on viscosity, die swell and fracture have not been reported.

Plasticized and rigid PVC demonstrate similar rheological behavior but the magnitude of the responses vary. By depressing the Tg, the plasticizers allow the PVC to be processed more easily. It was observed that plasticizer does decrease viscosity especially at lower

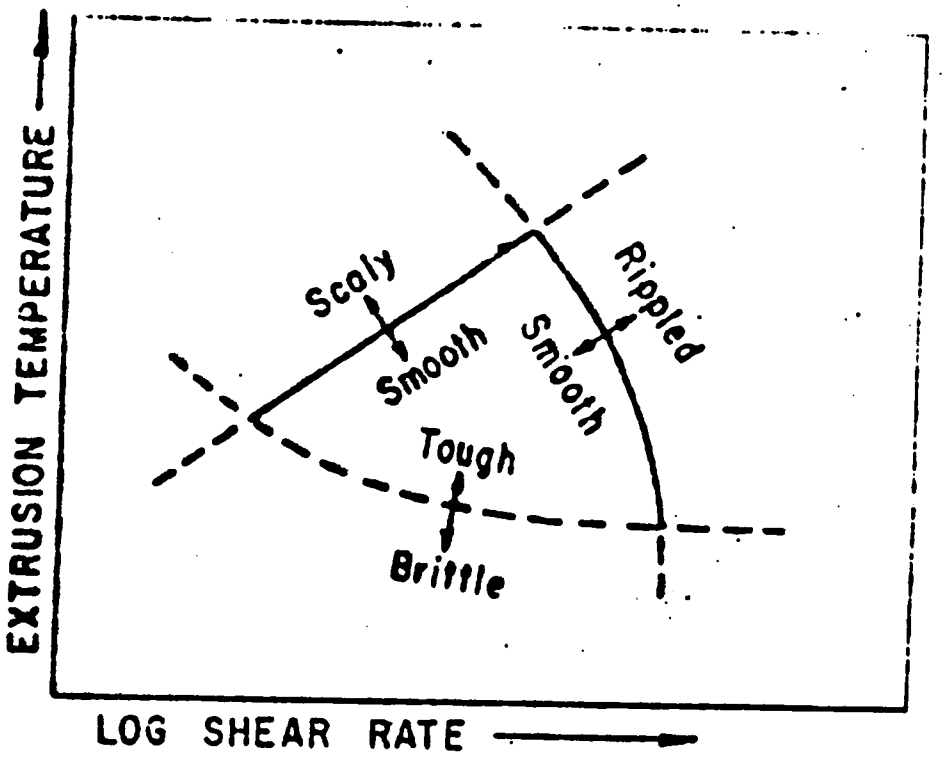

Figure 2. 15. Variation of extrudate quality with extrusion temperature and shear rate (schematic) [14].

shear rates [8,30,31]. In the same way as in rigid formulations, plasticized formulations showed breaks in the flow curves, that signified the onset of melt fracture [31]. Thermal and shear history had a profound effect on their properties and processing of both rigid and plasticized PVC. Attempts have been made to produce master flow curves at a particular reference temperature by horizontally and vertical shifting of the flow curves at different temperatures [12]. This was done for a particular plasticizer content of 40 % as shown in Fig. 2.16. The error ranges for the individual flow curves were nor reported. The shift factors for changes in the scale were missing. At high shear rates they superposed well but at low shear rates they did not as seen in Fig. 2.16 [12]. At low shear rates particulate flow prevailed and was dependent on temperature. At high shear rates good superposition implied the breakdown of particulate flow and the existence of a more homogeneous flow. Though the presentation of the data could have been better it still probably brought to focus the fact that a more homogeneous flow is possible for plasticized PVC at high temperatures and high shear rates. Activation energy was still dual valued and the similarity between plasticized and unplasticized PVC led to the conclusion that similar flow mechanisms were effective [12]. For plasticizer level between 10 to 40 % for a DOP plasticized PVC the magnitude of the activation energies did not alter much from those of rigid PVC samples but the flow transition temperature decreased slightly with increasing plasticizer content. These transition temperatures were lower than those of the unplasticized PVC.

Tse [32] conducted experiments in capillary rheometer with plasticized PVC containing fillers like clay and calcium carbonate. Samples were prepared by different methods like dry blending, milling in a roll mill at 150 °C, or were compression molded at 170 °C. The results of the filled samples were compared to the unfilled samples. For the filled samples below 170 °C, the particulate nature of PVC prevailed and the molded samples showed higher viscosities than the milled or the dry blended samples. The flow curves of the three samples having different thermal histories merged at 170 °C implying that above this temperature molecular deformation is the common flow mechanism. In general the molded unfilled samples had lower viscosities than the molded filled samples and the difference decreased with increasing

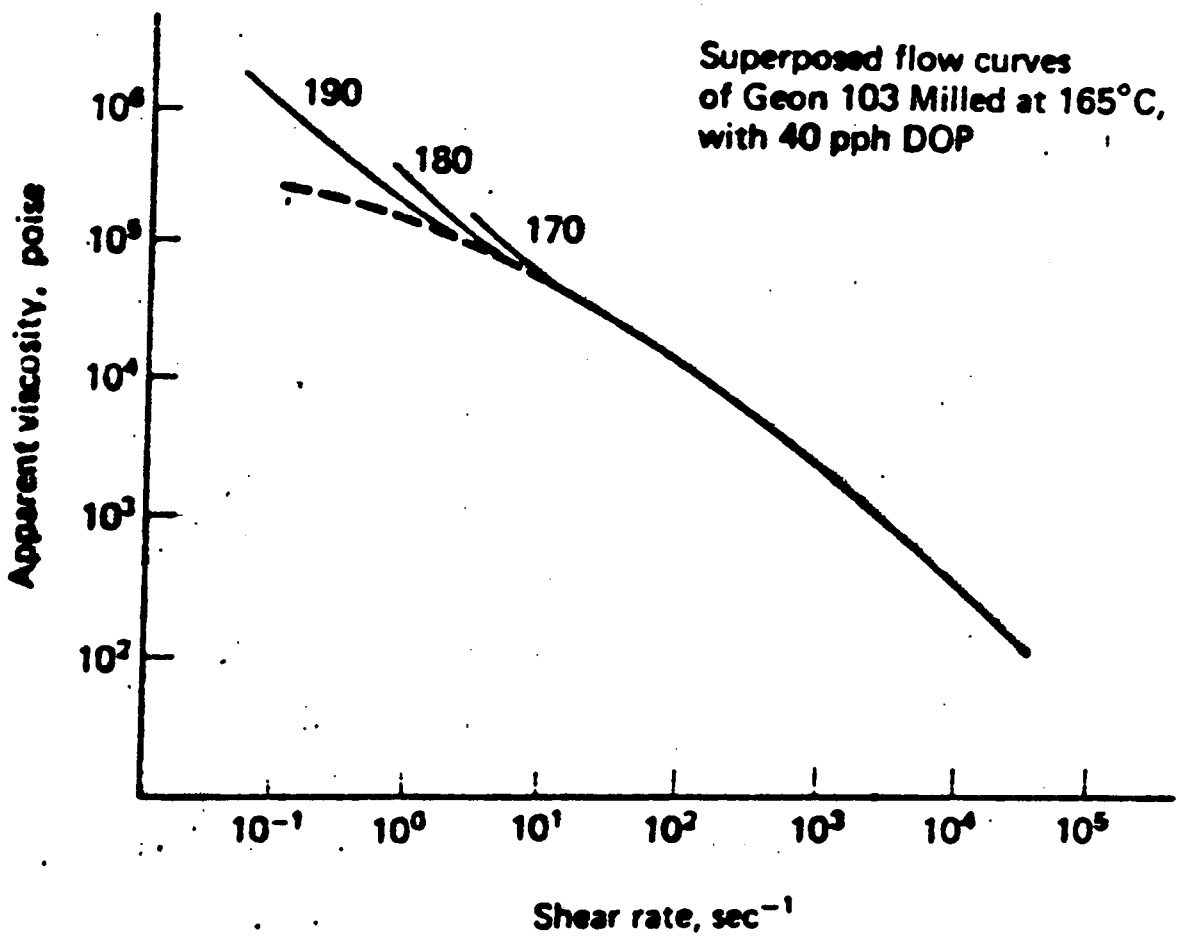

Figure 2. 16. Superposition of melt flow data for plasticized PVC at different extrusion temperatures [12]

temperatures and increasing shear rates as in Fig. 2.17. The author did not compare the two other materials with or without fillers and different thermal history. Here again temperature-shear rate superposition agreed well for viscosity values at higher shear rates but substantial deviation was noticed for lower shear rates. In this report shift factors were reported temperature shear rate superposition curves. It seemed that the unfilled sample gave a better master curve but less scatter might be due to a fewer number of data points. The activation energy was dual valued for the filled samples and decreased with increase in both shear rates and shear stress. The presence of fillers generally increased the activation energies. The die swell for the molded samples were higher than for the milled and dry blended samples, but as in rigid PVC the differences merged at 200 °C. Above 200 °C they became independent of the shear rates. The unfilled samples showed lower die swell as compared to the filled samples and the trend was opposite to their viscosity behavior. Generally, both the viscosity and the die swell behave similarly and no explanation was given for this opposing trend. The difference in die swell diminished at 200 °C but the differences were larger at 185 °C than at 170 °C and no attempt was made to explain this irregularity.

Extensional flow characteristics of rigid PVC was studied in an extensional rheometer at different temperatures [34]. PVC was mixed with lubricants and stabilizers and extruded in a Brabender extruder. These extruded samples were tested in the extensional rheometer at different temperatures. Steady state extensional viscosities were calculated for a constant shear stress of 24 Kpa. As in the shear flow case PVC exhibits a flow transition at 185 °C, as seen from Arrhenius plots. The activation energy and extensional viscosity increased with higher material preparation temperatures signifying destruction of the structures responsible for particulate flow. The material preparation temperature affected the extensional flow more at lower than at higher temperatures. This led to a higher difference in activation energies from the two regions as the material extrusion temperature was increased. At temperatures below 185 °C where particulate flow existed, the extensions were low and the stress strain relations were linear. As the temperatures were raised to the melt flow region, the decreasing crystallinity made the PVC flow similar to true melts. This was especially valid for PVC pre-

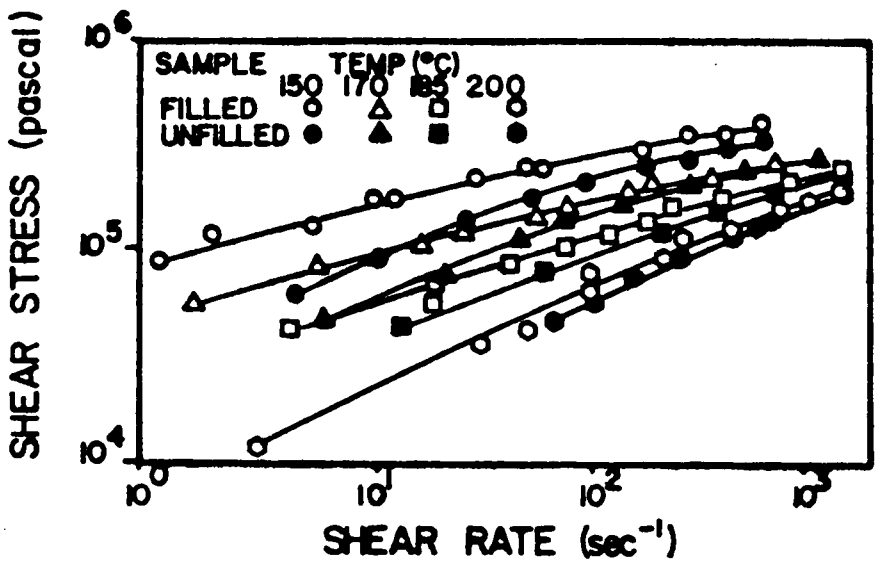

Figure 2. 17. Flow curves of filled and unfilled molded samples using a capillary of radius = 0.03792 cm [32]

pared by Brabender extruder at higher temperatures. It should be noted that there is an absence of extensional flow data in the literature. The data collected in ref. [34] were from samples that were prepared by extrusion and not milled or dry blended. It could be suggested that in the later two cases there is not enough thermal and shear history to obliterate the particulate nature of PVC, prevent slip flow and make it flow in the extensional rheometer. The importance of thermal history was clearly demonstrated from the melt behavior of PVC prepared by extrusion at higher temperatures. Samples prepared at low temperatures when tested in extensional rheometer gave almost linear stress strain curves. Samples prepared at high temperatures because of higher degree of fusion behaved more like true melt of linear polymer.

The amount and type of plasticizer have significant effect on dry blending as reported in various studies [37-39]. Fig. 2.18 shows a typical dry blending curve in which the measured amperage from a Brabender is used to study the addition of plasticizers to PVC. After the PVC has attained a predetermined temperature by mixing in the Brabender, the plasticizers are added. They get adsorbed in the pores, solvate the surface and increase the torque requirement. The solvating powers of the plasticizers determine how fast the amperage goes through the maximum. As the plasticizer penetrates deeper, the material becomes more free flowing and the torque falls to a minimum, signifying that dry time has been reached. It has been seen that differences in dry blending time and temperature necessitate the change in dry blending conditions with change in plasticizer. This is because a too dry or too wet PVC will result in poorer processing [37]. It was seen that high molecular weight resin dries faster and porosity does not affect drying times for low to medium plasticizer content. Tables have been prepared to show the variation of dry times with benzyl pthalates drying faster than alkyl pthalates [37,38]. Studies showed that partial replacements of alkyl pthalate by benzyl pthalate improved the dry blending time of the former [39]. The faster drying plasticizers have also been shown to fuse faster in the Brabender. Additives were shown to improve the drying times of very slow drying plasticizers like polymeric ones.

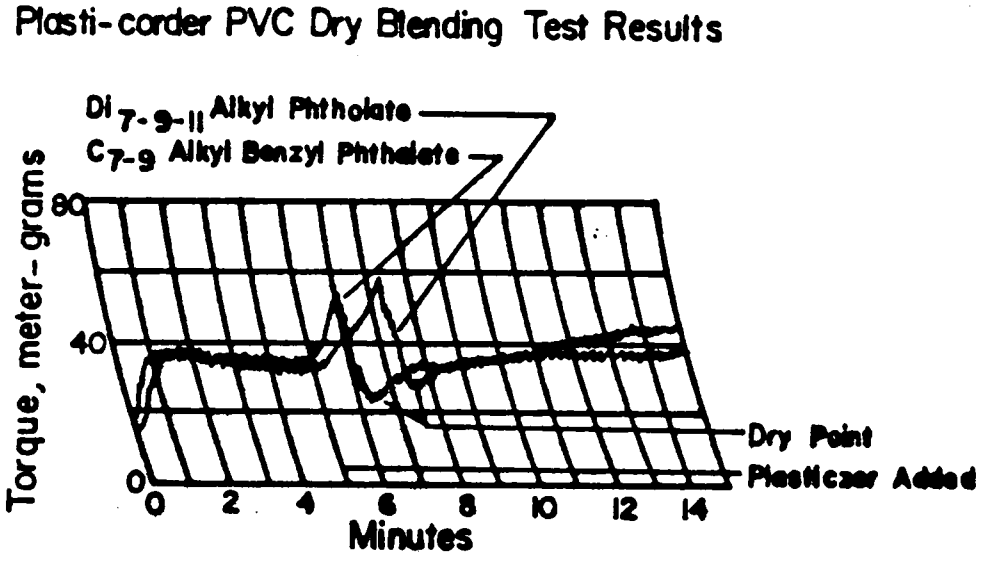

Figure 2. 18. Plasti-corder dry blending test results [37].

Both rigid and plasticized PVC have been studied in rotational rheometers under steady shear conditions and in the dynamic mode [40 - 43]. Over the years, Utraki [40, 41, 43] has done a systematic investigation of PVC using this kind of rheometer. Since PVC degrades at high temperatures during long exposure, preheating of the samples was done in order for the stresses to relax faster. The time for degradation at each temperature was measured and experiments were carefully controlled and repeated several times. Utraki used a cone and plate device (dia = 2.5 cm and cone angle = 4 °). The temperature of measurement was between 228 and 242 °C for rigid PVC and between 195 and 230 °C for plasticized PVC, depending on the plasticizer level. The plasticizer level was varied from 0 to 60 % . Under steady shear conditions at these high temperatures he was able to obtain zero shear viscosity values. As the plasticizer level increased this region shifted to higher shear rates than for rigid PVC [41]. He also obtained the normal stress difference coefficient as a function of the shear rate. This and the viscosity as a function of shear rate for a 40 % DOP plasticized PVC are shown in Figures 2.19 and 2.20. The activation energies were calculated from the dual valued Arrhenius plots of zero shear viscosity and zero-shear normal stress difference coefficient. At higher temperatures the activation energy values from normal stress difference coefficients were five times larger than those obtained from shear viscosities.

Utraki also reported the storage modulus, loss modulus and complex viscosity, η^*, from experiments carried out in the dynamic mode [43,88]. The behavior of the storage modulus, G,′ and loss modulus, G″, deviates from those of a normal polymer because of a presence of a yield stress. The yield stress was calculated and shown to be zero above 210 °C. Furthermore above this temperature the variation of moduli were similar to those of other normal polymers.

Studies were conducted on a 50/50 blend made out of two PVC samples having molecular weights of 56,000 and 123,000 respectively [42]. Experiments were also conducted on the two individual PVC samples. The experimental conditions or precautions taken during the experiments were not detailed as in [39] and [40]. Temperature-shear rate superposition of G′ and G″ was attempted in order to extend the lower end of the shear rate region to values that

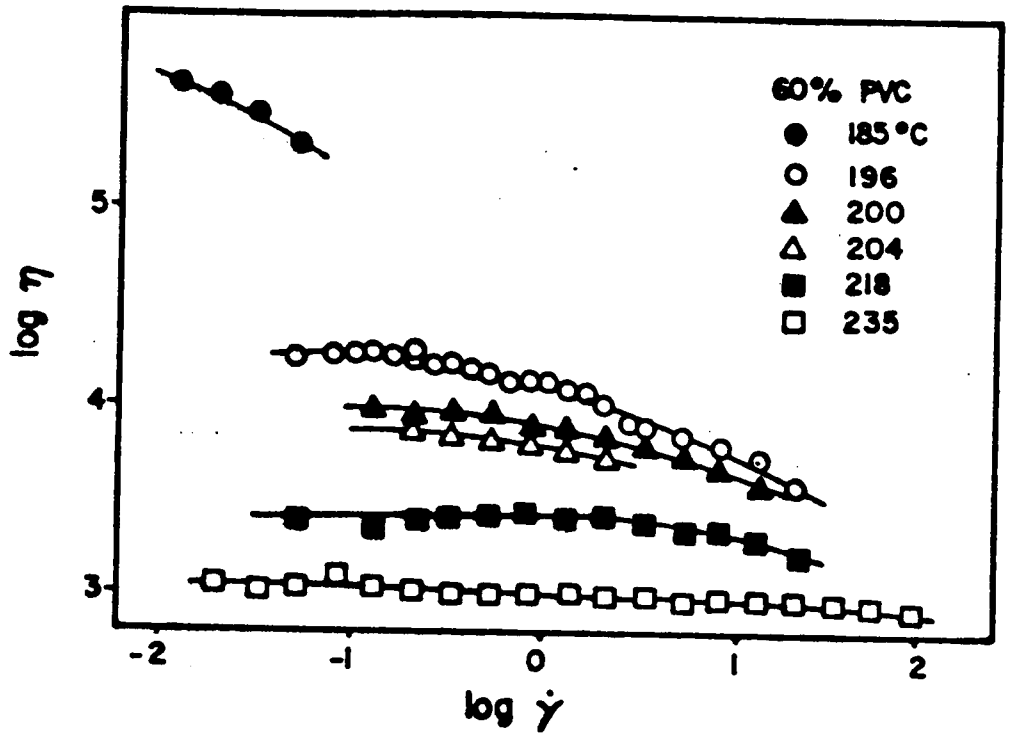

Figure 2. 19. Viscosity vs. shear rate data of DOP plasticized PVC at different temperatures [40].

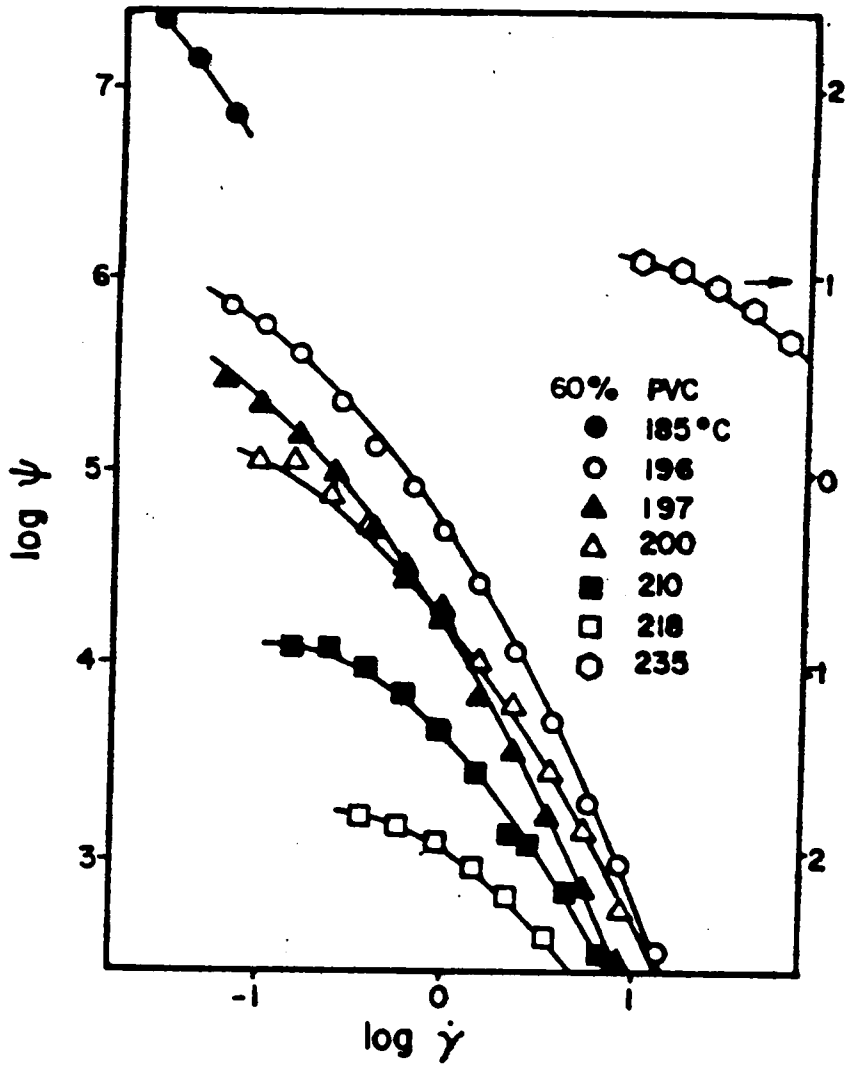

Figure 2. 20. Primary normal stress difference coefficient vs. shear rate at different temperatures [40].

were not possible to measure by the instrument used. Rigid PVC did not show a Newtonian behavior at 190 °C for a low shear rate corresponding to $10^{(-4)}$ rad/s. This can be explained by referring to the previous study [43] where it was shown that a yield stress existed at 190 °C and thus prevented the attainment of Newtonian behavior. η^* in the Arrhenius plots showed two transitions. The higher one corresponded to the upper limit of the particulate flow and the lower one was tentatively related to sample preparation history which was milling and then molding in these experiments. It was postulated that the dynamic mechanical measurements were more sensitive than those made in the capillary rheometer for sensing the differences in the thermal history but this was not substantiated. The lower transition temperature for the high molecular weight PVC did not correspond to the material preparation temperature and this seemed to become less prominent at higher frequencies. The cause for this discrepancy on the trend was not explained.

It has been mentioned in the last two paragraphs that PVC displays yield stress behavior even at temperatures above 190 ° C [43,88]. As mentioned previously, this is observed from the viscosity - shear rate curves not attaining zero shear viscosity at low shear rates but instead becoming steeper as the shear rates drop. The presence of yield stress is not considered unnatural considering the presence of crystallites at 190 ° C or higher [73]. The yield stress of a liquid is defined as the critical stress which has to be exceeded in order to produce a shearing flow. Thus yield stress marks a transition and demarcates the material elastic and viscous responses. For applied stresses below the yield stress, the material may be expected to follow Hooke's law and for stresses above the yield stress, it follows the viscous flow models like Newtonian or power law models [86].

Usually two methods are commonly cited in the literature for measurement of yield stress. A graph of log (shear stress) against log (shear rate), obtained by means of cone and plate or parallel plate attachments in a RMS, shows a linear portion which is parallel to the shear rate axis at low shear rates and this may be extrapolated to give a yield stress [86]. This same result could be achieved by plotting viscosity vs shear stress. The shear stress where the viscosity starts to rise asymptotically is assigned the yield stress value [70]. In the second

method, the (shear stress)$^{1/2}$ is plotted against (shear rate)$^{1/2}$ or (modified shear rate)$^{1/2}$ and the intercept with the ordinate is the measure of the yield stress [87]. The second method has been mainly used for polymer solutions. Depending on whether shear rate or modified shear rate (modified by the viscosity ratios of the disperse or the continuous phase) is being used to calculate the yield stress, the method is known as Caisson or Modified Caisson method.

In ref. [88], the dynamic data for rigid PVC has been used to fit the modified Caisson equation without sufficient explanation as to why a method suitable for polymer solutions or filled systems should be used for rigid PVC. Again the shear stress values in the Caisson's plots were to be substituted from G",the loss modulus, or G* which is equal to $\sqrt{G'^2 + G''^2}$. G' is the storage modulus. But finally , the author chose G" to substitute for the shear stress because he felt that G" generated a reasonable value for the yield stresses at different temperatures. He observed that the G* data was rendered meaningless by a rapid increase in the values of G' at low temperature and low shear rates - the temperature and shear rates where yield stresses are more easily detected. At higher temperatures, the G* (or some times G') and shear stress values can match but it is difficult to predict the relation between these quantities or G" and shear stress at lower temperatures. The choice of G" to be used in place of shear stress in Caisson plots seemed quite arbitrary. His decision to determine the yield stress measurements based on the loss modulus, G", at low temperatures where rigid PVC is more likely to behave as solids can possibly be questioned. So though PVC displays yield stress behavior, its determination may not have been proper. There has been no published data for yield stress of plasticized PVC.

In actual practice, PVC is never processed by itself and is always processed in combination with other ingredients. A review of the PVC rheology will be incomplete without mentioning the effects of various lubricants, processing aids and stabilizers. Numerous papers have been published but only some of them will be discussed here [14, 44-47,78]. It should be pointed out that additives used in PVC do not act independently of each other. Processing aids initiate early fusion but lubricants delay it. Therefore a good balance between the additives is a mandatory requirement.

Lubricants can be classified as external or internal. The internal lubricant reduces the amount of heat build-up within the compound when subject to shearing. The external lubricant reduces the heat build up between the metallic part of the equipment and the polymer. This terminology can be misleading because in the presence or absence of certain compounds, a particular lubricant can behave differently. This kind of behavior makes the understanding of lubricant behavior very difficult. In their experiments Krzewki and Collins [44,78] studied the effect of lubricants on fusion by measuring the entrance pressure in a 'zero length' capillary. A relative degree of fusion was obtained by relating the pressure drop to the degree of fusion at the start and at final fusion. These values were assigned zero and hundred percent, respectively. This indirect method was supplemented by electron microscopy. From a relative fusion curve in Fig. 2.21. it was seen that calcium stearate (CaSt) behaved differently with or without wax. It was suggested that in the absence of wax at lower temperatures increasing amounts of CaSt acted as external lubricant and thus delayed fusion. At higher temperatures, the internal lubrication of CaSt started to play a dominant role and the opposite effect was observed. With wax, CaSt acted as an internal lubricant and increased fusion. The dramatic difference of the action of CaSt can be seen in Fig. 2.21. Tests were carried out to see the effect of processing aids like MMA which has a high compatibility with PVC. By getting adsorbed faster, they distribute evenly and were seen to increase the torque significantly, thereby increasing the particle breakdown rate. The fusion in these PVC formulations started early and they became compacted to a greater density. The processing aid might have aided in forming a network across the domain boundaries [44]. The exactness of this mechanism can be questioned and the action might be very different with the addition of another compound.

There have been other studies concerned with the effect of carbon chain length of different fatty acids on lubrication efficiency [40, 45]. In experiments with a Brabender, it was shown that an increase in the number of carbon atoms delayed fusion. This effect was more pronounced at lower shear rates and at lower temperatures. But at higher shear rates and temperatures the capacity of the fatty acid to delay fusion was insignificant.

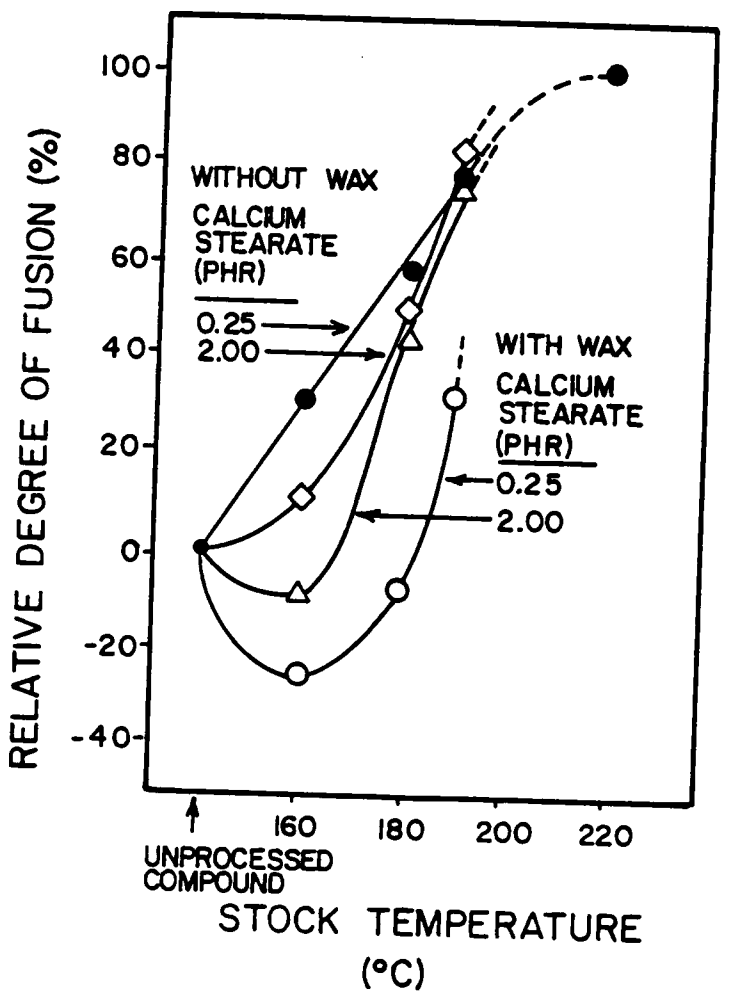

Figure 2. 21. Comparison of fusion for PVC compounds with and without wax and having CaSt as a lubricant [78].

By studying their effect on fusion, Haritz had grouped lubricants into two groups [47]. Group A contained soaps or their metallic derivatives. Group B contained non soap fatty acids, polyolefines, paraffin wax and mineral oils. Individual fusion times for each member of both groups were obtained. The effect of different combinations of lubricants on the fusion time was observed. It was found out that when lubricants of the opposing groups were combined, the retardation time was more than the sum of their individual fusion times. When the lubricants came from the same group, no retardation in fusion time was observed. No logical explanation of this interesting phenomenon was attempted since the nature of the synergism remained unclear.

In this section the rheology of rigid and plasticized PVC have been reviewed. Melt flow of PVC is not like that of other pure amorphous melts. Instead, particulate flow governs the properties of PVC melts. The degree of fusion of these particulates under heat and pressure determine the flow characteristics of PVC. This particulate effect manifests itself in dual valued flow activation curves in shear flow [13,14,30,31,36] extensional flow [34] and dynamic oscillatory flow [40 - 43]. The particulate flow mechanism is responsible for smaller die swell in PVC compare to PS or PE [14, 29, 30, 32]. The particulate nature is also the reason for the strong influence of previous thermal and shear history [36] of PVC on its properties. Differences exist regarding the nature of the transition from particulate flow to a flow mechanism similar to that of a pure melt. At higher temperatures, the existence of primary particles are no longer observed. But from section 2.1 it is known that some crystallinity still exists [73]. It is difficult to accept that above the transition temperature, which is usually above 180 °C, the flow is that of a pure melt. The failure to attain zero shear viscosity at temperatures above 200°C [26,27] is a possible indicator of the absence of true melt flow at these temperatures. Again the presence of yield stress explains the above observations at lower shear rates.

In the next section, the determiation of friction coefficients for rigid PVC will be analyzed.

2.4 FRICTION COEFFICIENTS

The existing solids conveying model requires the determination of friction coefficients between the polymer and the materials of the screw and the barrel. Friction is the tangential resistance developed between two solid surfaces when they slide over each other. The ratio of the tangential to the normal force, existing between the surfaces, is the coefficient of friction. It is independent of the contact area and depends only on the normal force. Adhesion occurs between the two contacting surfaces and frictional resistance is generated when the adhered junctions get sheared during the sliding motion. The second cause of fricion arises when the asperities of one surface plough or groove into the asperities of the other surface. The nature of the fricional forces between the polymer and the metal surface seems to be dominated by abrasive wear rather than by adhesion[49]. After repeated use, a polymer coating forms on the rubbed surface and the friction coefficients are higher than the initial friction coefficients between the polymer and the unused metal surface [80,93,94]. But the measurement of friction coefficient is further complicated by local heating and pressure buildup between the contacting surfaces, alteration of surface topography arising out of deformation and wear, and viscoelastic response of of polymer particulate system under deformation.

Friction coefficients of various polymers on syeel surfaces have been reported [80,93,94] and rigid PVC is one of them. Schneider [80] reported the variation of PVC friction coefficients with temperature and the friction coefficients rose till about 100 ° C. He did not report any data beyond this temperature. He found out that surface roughness was not a factor in determining friction coefficients and they reached an equilibriam value after a certain numer of repeated rubbing between the surfaces. Also sliding velocities had no effect on friction coefficients but the coefficients decreased with increase in normal forces. The variation of the friction coefficients with normal forces was in contrast to the earlier assertion that the coefficients are independent of normal forces. Eiss et al. [93,94] observed all the above characteristics except

the variation of the friction coefficients with normal force and also examined the effect of molecular weight and glass transition of PVC on the friction coefficients. They also showed with the help of coated and uncoated surfaces that deformation and wear rather than adhesion are the main factors governing friction. The wear rate which influences the amount of polymer deposited depends on TG and the molecular weight. The wear rate also depends on the surface roughness and the sliding speed. Below TG, chain rupture becomes the predominant mechanism of debris formation and low molecular weight PVC formed more debris. Above TG, chain slippage can occur due to greater mobility and the influence of molecular weight on wear rate becomes insignificant. Schneider had found no effect of sliding velocity and surface roughness on friction coefficients. Although Eiss et al.[93,94] largely corroborated the same facts, they found that beyond a certain critical value of surface roughness the coefficients depended on the texture of the surface and the sliding velocity. In fact a slight sliding velocity effect was noticed at all values of surface roughness but at higher velocities the differences were small. The friction coefficients were linked to the wear rates. The friction coefficients varied with temperature but the values were lower than those of Schneider.

In the next section, the extrusion process and the modelling of the different zones in the extruder and their numerical solutions will be discussed.

2.5 EXTRUSION

This section deals with the review of the literature of the processing of polymers in plasticating extruders. First a description of the single screw extruder with its various zones will be discussed. The processes occurring in these zones are quite complex and special experimental technique is required to gain an insight into them. This technique involves pulling out the screw with the material solidified on it and observing the changes which take place as the granular or the powdered solid polymer turns into a melt. Different polymers can have

different mechanisms by which they melt in the extruder. Thus each polymer needs to be separately studied for analyzing the exact mechanism. Studies relating to morphology, melting mechanism and fusion of PVC in single screw extruders will be reviewed . The theoretical development and the consequent mathematical modelling of the individual zones will be discussed. Lastly, some of the works concerning numerical modelling and solutions for the entire extruder will be reviewed.

2.5.1 Single Screw Extruder

PVC and other polymers are processed in plasticating extruders, where the material is fed in the form of particulate solids or powders but comes out of the die as a molten plastic. The material in the extruder moves through the helical conduit formed between the screw, the screw flights and the barrel. The forward movement is brought about by a drag induced mechanism, which compresses, conveys, and melts the polymer as it moves down the extruder. Additionally, the polymer gets thoroughly mixed and pressurized.

The plasticating extruder contains three functional zones as shown in Fig. 2.22. The first zone is the solid conveying zone in which the solid polymer is compacted and conveyed. In the second zone heat conducted from the hot barrel and the heat generated by viscous dissipation gradually melt the polymer. This zone occupies a major portion of the extruder, and the solid polymer and the melted polymer coexist in this zone. The final section is the melt conveying zone where a uniform melt is generated and conveyed to the die. A more careful analysis reveals the existence of two more zones. They are the zone below the feed hopper and the delay zone. The latter originates where the first traces of the melt appear at the end of the solid conveying zone and continues until the melt film grows to a certain thickness to begin the formation of a melt pool in the melting zone.

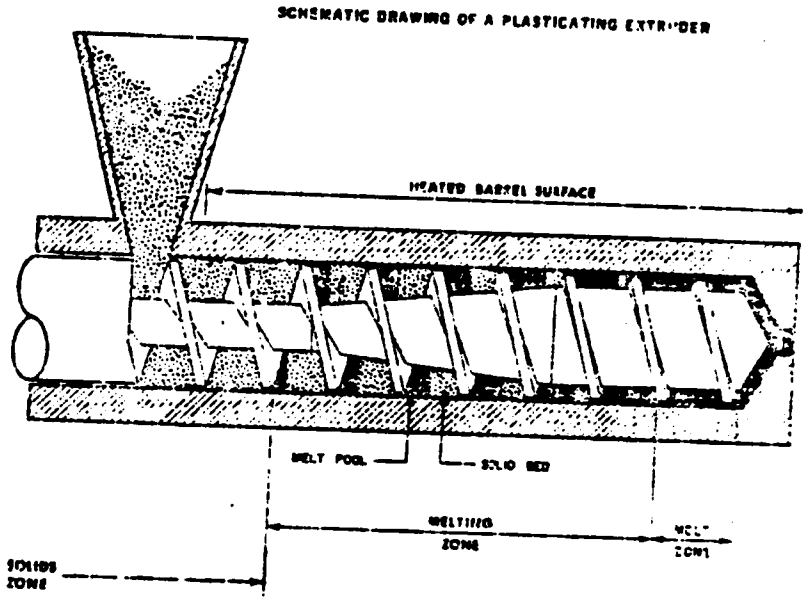

Figure 2. 22. Schematic drawing of plasticating extruder.

2.5.2 Melting Mechanism

In order to analyze the mechanism of the flow in the various zones of the extruder, the extruder conduit is unwound into a rectangular channel covered by a moving upper plate that slides over the material in the channel with a constant velocity at an angle to the down channel direction. Instead of a rotating screw in a hollow barrel, the reverse is assumed. These two configurations have been shown to be equivalent [49]. Fig. 2.23 shows the geometry of the unwound channel.

The mechanism of the plasticating extruder is complex and cannot be understood, visualized or modeled without the aid of experimental investigations. The technique to study the melting mechanism was developed by Maddock [50] and has formed the basis for investigating the extrusion process in later years. Tadmor et al. [48, 49] described this process in detail and used it to study the melting mechanism for various polymers like LDPE, HDPE, PVC, Nylon etc. This technique involved stopping the screw after steady state has been reached, and then cooling the system until the polymer solidified on the screw. The screw was then pulled out and the solidified polymer unwound from it. To visualize the process a small amount of colored dye or polymer is added as a tracer. By visually examining the unwound helical coil of the plastic at the cross sections perpendicular to the flow direction, important information about the melting process was obtained. This procedure to study the melting mechanism has been called 'cooling experiment'. Tadmor et al. established a general qualitative mechanism for the melting process which is described in the next paragraph.

The polymer, in the form of powder or pellets, enters the screw channel from the feed hopper and gets compressed and dragged by the motion of the moving barrel surface. The frictional forces exerted at the screw and barrel walls raise the temperature of the solid bed. This frictional heating and the heat from the barrel raise the temperature of the polymer beyond its melting or softening point . This results in the formation of a thin film in the area adjoining the barrel and marks the end of the solid conveying zone. The thin film experiences

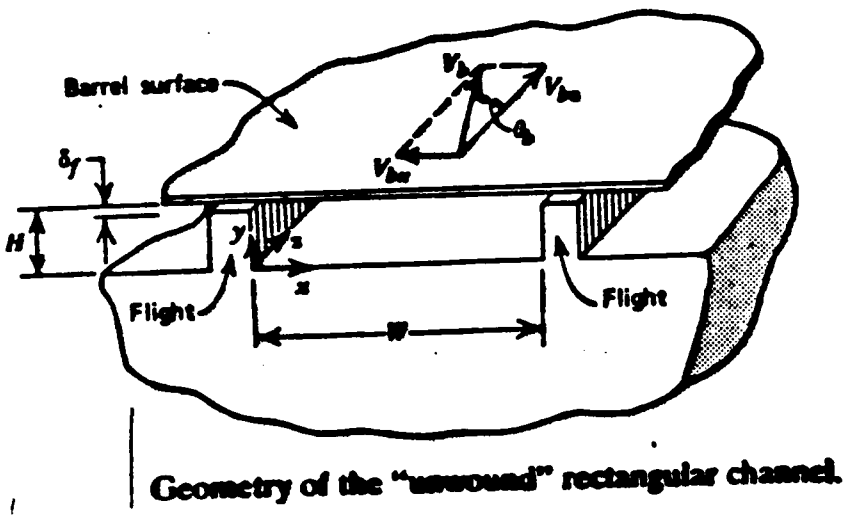

Figure 2. 23. Geometry of the "unwound" rectangular channel [48].

high shear because of the relative motion of the barrel and the screw leading to high viscous dissipation. The thermal energy from viscous dissipation and from the heated barrel cause further melting of the solid bed and the melt film width thickens beyond the flight clearance. The advancing flights then start to scrape the molten polymer from the region adjacent to the barrel and drag the molten polymer into a melt pool in the rear of the channel. This pool is formed in front of the advancing flights. As more melt enters the pool, it grows in size and the solid bed width decreases. In the melt pool a circulatory flow is set up because of the relative motion of the barrel and the screw. The rising pressure in the melt pool forces the solid to segregate at the trailing edge. The solid bed moves as a compacted plug besides the melt pool and gradually decreases in size. It has been assumed to possess a constant down channel velocity. The melting of solids was assumed to take place at the interface between the molten polymer film and the solid bed. It was also assumed that the solid bed moves at a constant velocity to this interface. The disappearance of the solid bed signals the end of the melting zone. A schematic of the melting zone is shown in Fig. 2.24. As the solid bed approaches the end of the melt conveying zone, it frequently breaks up and the gaps are filled by the melt [49, 51]. Alternatively, the melt gets under the solid bed and completely encompasses it [75]. This breaking up of the bed often leads to pressure fluctuations at the die. After all the polymer has melted, it gets more homogenized and is pumped out of the die.

2.5.3 Extrusion of PVC

The general melting mechanisms of PVC have not always conformed to the mechanism described above. Tadmor et al. [51] conducted cooling experiments with rigid PVC in a 2.5 inch diameter extruder having a L/D ratio of 26. The results are shown in Fig. 2.25. Here the melt pool collected at the pushing flight in accordance with the melting mechanism described in the last paragraph. The solid bed did not break up in the melting zone and the authors felt

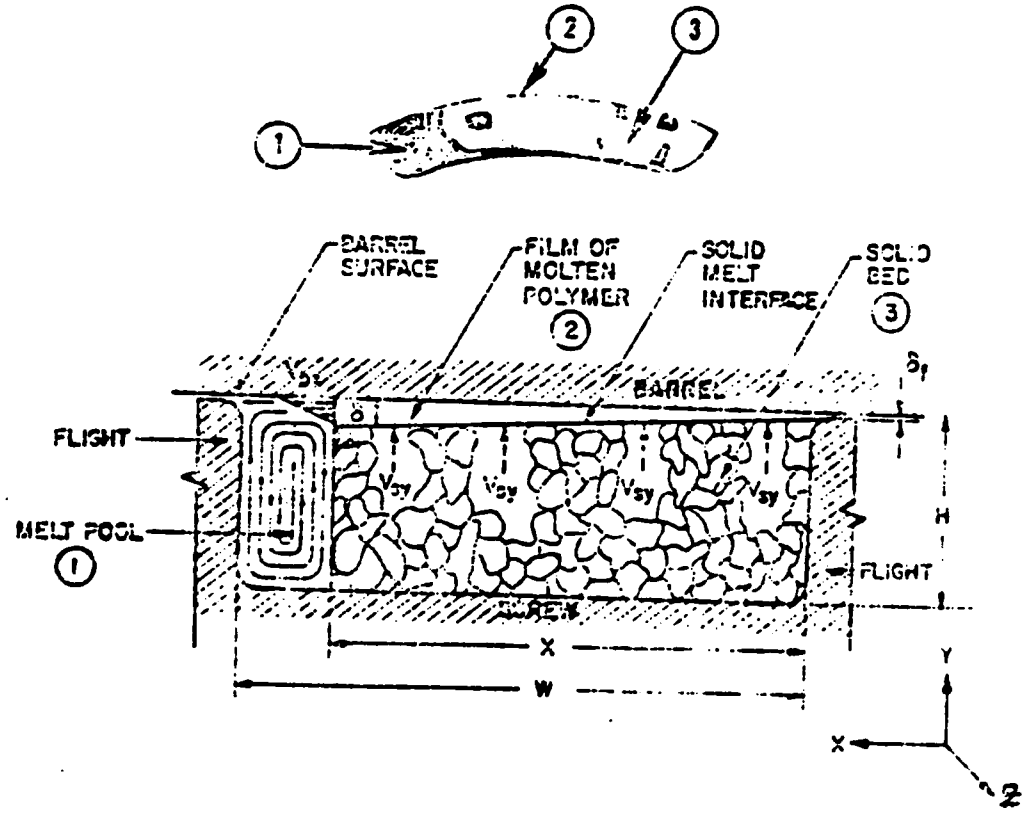

Figure 2. 24. Cross-section of screw channel [51].

that smaller particle size gave rise to a sturdier bed. As mentioned in section 2.3, the PVC particles fuse under the action of temperature and pressure. Gale [52] tried to explain the behavior in the melting zone in terms of particle fusion and showed the existence of a different mechanism from the one reported by Tadmor et al. in [51].

Gale [52] and Klenk [53] observed that under certain conditions PVC melts instead of accumulating at the leading edge collected at the trailing edge. Klenk [53] reported that after initial compaction, the non-wetting non-plasticized compacted PVC powder leaked between the barrel surface and the flights and got fused into a melt under the action of shear and heat. As the material progressed along the screw, the process continued to build up a pool of melt at the trailing edge. The rate of fusion was low and at the die exit some solid materials remained which needed more extreme conditions to improve the fusion quality.

This non-wetting characteristic of rigid PVC was further studied by Gale [52], who demonstrated that depending on the type of lubricant, either of the two mechanisms were possible. The two different mechanisms were 'rear channel fusion model' as reported by Tadmor et al. [49, 51] or 'forward channel fusion model' as observed by Klenk [53]. When glycerol monostearate (GMS) was used as a lubricant, it gave rise to melt collecting at the rear of the channel. The PVC was compressed and sintered and then started to fuse near the barrel and towards the rear of the channel and was scraped to a melt pool at the leading flight. The sintered material was slowly eroded and when examined under the microscope the fused bed appeared sheared as demonstrated by the elongation of the particles. The particles adjacent to the barrel showed evidence of this shear towards the pushing flight especially where it was sharply drawn out. But the area adjacent to the screw showed no signs of shear. Two sections parallel to the downstream directions were cut. One was adjacent to the leading edge and the other adjacent to the trailing edge. The section close to the leading edge or the melt pool was sheared more than the one away from it. The shearing action was towards the down channel direction. When the lubricant was changed from GMS to stearic acid, the friction supposedly dropped. This caused a decrease in the magnitude of both the shear and the fusion rate leading to an incomplete fusion as was also observed by Klenk in [53]. The melt

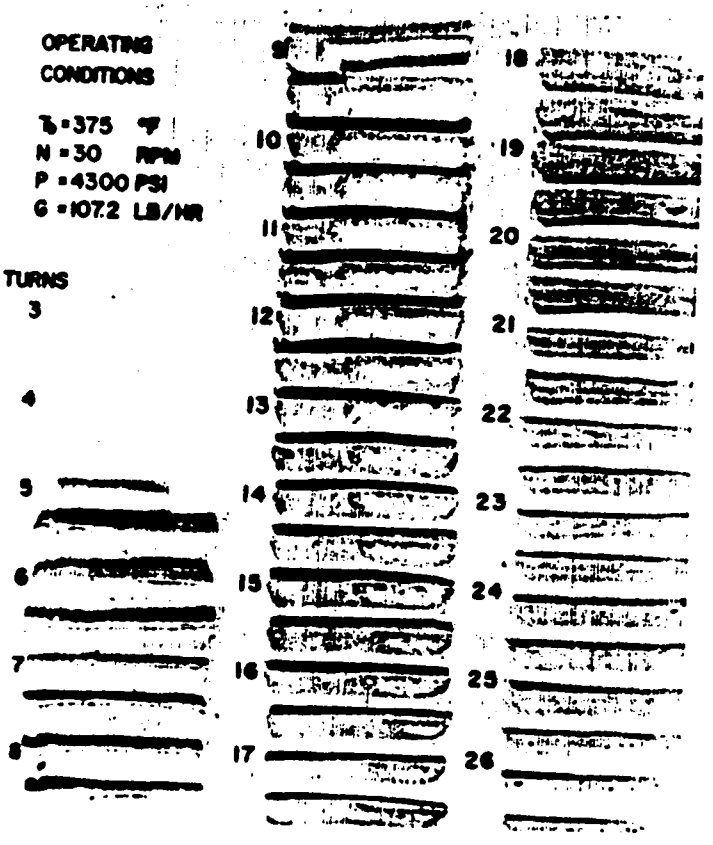

Figure 2. 25. Cross-sections obtained from "cooling" experiments with rigid PVC [49]. Barrel diameter 2.5 inch, L/D ratio of screw extruder channel = 26.5

collected at the trailing edge and contained unfused particles. The solid compaction seemed weak and some unfused solids got carried away by the melt. There appeared to be an additional transition zone between the sintered solid and the melt and this zone supplied the unfused material to the melt. Inspection of cross and down channel cross sections apparently gave no clear indications about the mechanism and it was suggested that it was possibly similar to the one earlier reported by Klenk. It was also thought that the melt initially accumulated at the rear but then flowed around the sintered bed to the trailing edge. The author dismissed the phenomenon as undesirable as it gave a poorly fused end product.

The cooling experiment was used to study the morphological progression of PVC in single screw extruders by Fahey [66] and Kulas and Thorshaug [65]. Fahey [66] studied the melt pool width and the fusion development along a single screw extruder for suspension and bulk polymerized PVC. The degree of fusion was obtained by measuring the pressure drop in a zero L/D capillary [15] for the material removed from the screw. The melt pool width was reported relative to the channel width and the degree of fusion was measured by the capillary entrance pressure method. For the suspension resin , as the material progressed along the screw, intergrain diffusion occurred blurring particle boundaries, but no particle breakdown was observed. By the end of the compression section the particles were highly fused but the original particle boundaries were still evident. This evidence of primary particles started to disappear as the melt started to form. The primary particles, which were clustered together, started to knit and after the melt pool had spread across the entire channel the fractured surface showed less evidence of primary particles and resembled fibrillar structures much larger than the primary particles. Their exact dimensions were not reported. Fusion continued to develop even after the melt filled up the entire channel. Compared to the suspension resin, the bulk polymerized PVC fused at a higher rate but its melt pool growth rate was slower. The fusion of the suspension PVC was thought to be impeded by the skin formed during polymerization. No explanation was offered for the difference in the melt pool width.

Kulas and Thorshaug [65] conducted a similar study. They studied the melt pool width and the fractured surfaces along the screw for two suspension PVC samples and one bulk

polymerized PVC samples. All the samples were unplasticized. The bulk PVC (sample A) and one of the suspension PVC's (sample C) were loosely agglomerated and porous while the other suspension PVC (sample B) was tightly agglomerated with diffuse interfaces and possessed low porosity. Initially the melt pool growth rate of all three samples was the same because of the same heating from the barrel. In the tapered section, owing to compression and shear the loosely agglomerated materials like sample A and sample C generated additional internal frictional heat because of their larger surface areas. It was proposed that this was a supplemental heat source to the material in addition to the two usual sources of thermal energy for melting. The usual sources of energy are heat from the barrel and heat from viscous dissipation. Also this being an internal source the heat generated was more uniformly distributed. Beyond a certain shear or screw speed, this internal heat source caused the loosely agglomerated samples to fuse faster than for sample B. This was possibly also the reason for the melt pool to grow faster for the suspension PVC than for the bulk PVC in the experiments of Fahey [66]. For sample B the melt pool collected at the front end of the channel at all screw speeds. For samples A and C, at low speed, the melting mechanism was similar to sample B. At the high speed of 80 rpm, for these samples the melt pool changed its position from the trailing flight in the feed section to the pushing flight at the end of the compression section and metering section. The internal frictional heat generation was high enough to lower the viscosity and change the mechanism similar to that of lower viscosity materials like PE or plasticized PVC. When all the three samples were pelletized, the differences in their structure were obliterated and the differences in their melting behavior disappeared.

Payne et al. [37,67] studied the effect of plasticizers on the extrusion of PVC. In their initial study [67] the effects of partial replacement of general purpose pthalates by benzyl pthalates on production rate and surface qualities of the extrudates were studied. Both the production rate and the surface appearance improved. In a later study the effect of resin molecular weight and plasticizers were examined in greater detail [37]. It was observed medium molecular weight resin (I.V. of 0.9 to 1.0) with porosities above 0.2 gm/ml gave the

best processing characteristics with regard to output and surface appearance. The plasticizer affected the production rate and the back pressure development. The fusion time of different plasticizers was determined by standard ASTM tests. It was found that the faster fusing plasticizer from the ASTM tests gave rise to higher back pressure and output rate in the extruder. It was postulated that by decreasing the time to melt, the faster fusing plasticizers had more time for homogenizing and shearing out irregularities like gels on the surface and thus improve the surface appearance. A ranking of the different plasticizers placed DOP, DINP, DIDP in decreasing order of fusion at 50 % plasticizer level. The study did not report the effect of plasticizers on rheological and thermal properties or the morphological development along the screw. Alternately, the study did not investigate the cause for the differences in the behavior of PVC because of different plasticizers.

A similar study by Pazur [69] demonstrated the effect of different plasticizers on the visual gel ratings of PVC extrudates. Gels are non-fused PVC resin grains present on the surface of extruded products. A pigment like carbon black is mixed with PVC feed and the unfused particles in the extrudate cannot absorb the pigment. If held against light, the gels show up. Gel values are reported as gels per square centimeter. It gives an indication about the fusion quality in the extrudates. A higher gel rating indicates poorer quality. Different plasticizers affect the gel rating of the extrudates differently. It was initially thought that lower plasticizer content in the gels, which resulted from less porous grains, caused higher gel rating. But studies with IR spectroscopy proved otherwise with lack of porosity being the reason for poor fusion. High compression ratio and larger residence time resulted in lower gel level, but the difference in the plasicizer effects was not properly explained and no attempt was made to link it to the variation in their fusion rates with different plasticizers.

Recently Summers and coworkers [68] have reported the effect of extrusion temperature and extrusion rate on smoothness of extrudates from a slit die. They observed that powdered compounds, which were not subjected to high shear or temperature, resulted in a rougher surface when extruded at lower temperatures. This was because of larger melt flow units arising out of incomplete breakdown of larger grains. For cubed or pelletized samples, the

smaller primary particles formed during pelletizing gave a smoother extrudate surface during extrusion at lower temperatures . But at high temperatures for the cubed samples, the formation of larger flow units by fusion gave rise to surface roughness. Extrusion did affect the surface roughness with higher rates causing higher roughness, the effect being more prominent for higher molecular weight PVC at high temperatures. The authors also noted that if the die temperature was below the melt temperature, surface roughness appeared and the authors postulated that it could have been due to the recrystallization of primary particles to large fused agglomerates. It was apparent that previous thermal and shear history were important factors in determining the surface roughness for the extrudates.

There seems to be an absence of single or unique melting behavior of PVC in the single screw extruders. The Tadmor model of melt accumulating at the pushing flight has been observed for both rigid and plasticized PVC [49, 51]. Studies have also reported a different mechanism in which the melt pool collected at the trailing edge [52, 53]. It has also been reported that depending on the screw speed and the structure of the PVC, i.e. whether it is tightly agglomerated or loosely porous, the melt could collect at either the leading edge or the trailing edge [65]. The effect of plasticizers on fusion time has been investigated [37, 67]. This could have been a consequence of the effect of plasticizers on the melting mechanism. No studies relating the melting mechanism to the type of plasticizers have been reported.

In the following section the modelling of the different zones of the extruder will be discussed. It should be noted that although there are variations in the melting mechanism, the mathematical models that have been developed are for most part applicable to the model of Tadmor and coworkers [49, 51, 56, 57]. Improvements to this model have been suggested by other researchers [59, 60, 71]. Some of them will be discussed in the next section. The flow of both rigid and plasticized PVC has been modelled using the Tadmor model [49, 51, 56, 59, 60, 61]. The observed deviations from the Tadmor model in the melting of PVC has not been incorporated in any model.

2.5.4 Modelling The Extruder

The different processes in the extruder have been described in the beginning of section 2.4. Following the results of the cooling experiments, the mechanisms in the different zones have been studied. In this section the formulation of the governing equations to model these mechanisms in single screw extruders [49, 51, 54, 55] are presented. Several attempts have been made to formulate, model and solve the equations with each new modification attempting to improve upon the past endeavors. A comprehensive review of the theory and solutions of the governing equations are found in references [49] and [77]. A brief overview of the modelling of the solids conveying, melting and melt conveying zones will be presented here.

A realistic analysis of the flow in the solids conveying zone was first attempted by Darnel and Mol [79]. They perceived a dependence of the direction of the drag, exerted by the barrel on the solid, on the velocity of the solid in the screw channel. This dependence was related through the definition of the angle ϕ, which is the angle between the direction of the force exerted by the moving plate on the solids and the direction of the motion of the moving plate as shown in Fig. 2.26 [48]. A expression was obtained for the flow rate in terms of screw geometry, operating speed and frictional drag terms. The last terms were expressed in terms of ϕ and θ, which is the angle at which the plate is dragged across the screw channel. By doing a force and a torque balance they were able to relate the flow rate and pressure rise in a homogeneous, isotropic and isothermal plug flow of solid. The pressure rose exponentially in the down channel direction and the solid velocity in the zone was constant.

Tadmor and Klein [49] incorporated the effect of flight width on the area available for solids conveying. Later, Tadmor and Broyer [54] significantly improved upon the model by incorporating the effect of tapered channel, non-isotropic pressure, changes in the bulk density as a function of pressure and different friction coefficients at the barrel and the screw. The torque and the force balances were modified from those reported by Darnel and Mol [79]. Because of consideration of additional forces arising out of the screw taper. The force on the

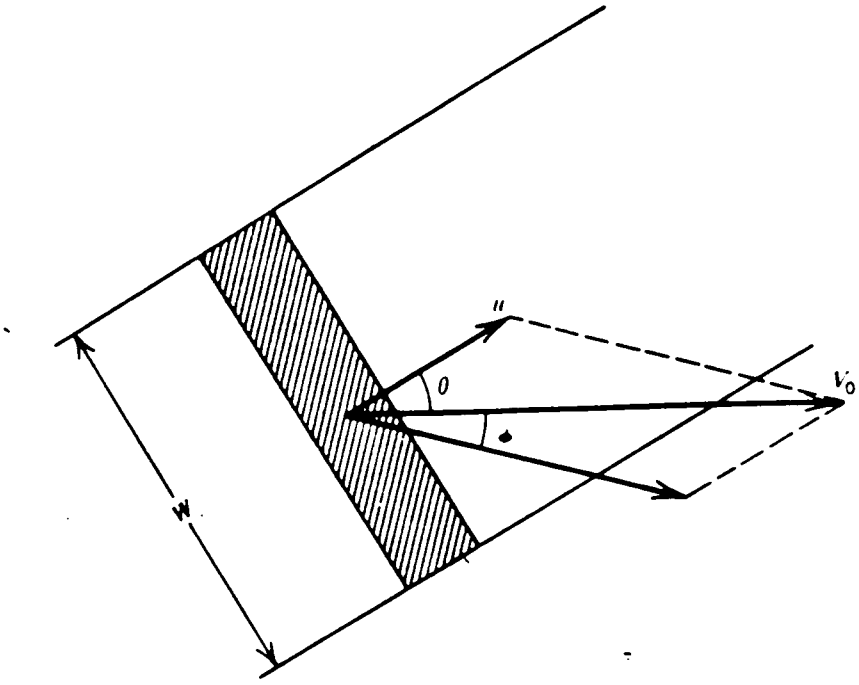

$$\tan \phi = \frac{u \sin \theta}{V_0 - u \cos \theta}$$

Figure 2. 26. Definition of terminologies used in solids conveying. Vo is the barrel velocity, u is the solid velocity & W is channel width.

barrel and on the screw root and the flights were still proportional to the down channel pressure but the dependence was different on different surfaces. The incorporation of these additional functions obviously changed the form of the flow rate and pressure relation and called for a numerical solution to obtain the values for pressures and solid bed velocities. Flow rates were found to increase with decreasing friction at the screw surface and increasing friction at the barrel surface. Pressure rise was found to be higher for tapered channels but its value was limited by the maximum flow rate at that channel depth. Also pressure rise in the non-isotropic case was found to be lower. In a later paper the same authors developed a non-isothermal solid conveying model, which accounted for the temperature rise due to friction in the solid bed [55]. The model proposed in [54] had limited applicability and could be used only when the pressure rise was small. As the solid bed moves down the channel, its temperature rises because of the friction between the barrel and the solid polymer plug. The frictional coefficients also changed with temperature. The thermal energy equation was reduced to a one dimensional heat conduction problem, with suitable assumptions, and solved in conjunction with those in ref. [54]. In the solids conveying zone, the temperature rise followed the exponential pressure rise in this zone. The pressure rise was limited by the temperature of the solid bed. This was because when the temperature reached the melting point of the solid, the solid conveying zone was terminated.

Owing to the works of Tadmor and coworkers [54,55], the pressure rise and the flow rates in the solids conveying zones have been more accurately modelled than was done by Darnel and Mol [50]. Factors to improve the model include non-isotropic pressure distribution, non-isothermal flow conditions and flow in tapered channels.

The melting mechanism has been modeled by Tadmor et al. [49, 51, 56, 58]. Their pioneering efforts have progressively improved the melting zone model incorporating fewer simplifying assumptions to reduce the discrepancy between the temperature and pressure values predicted by the models and those from the experiments. The modelling of the two phase system proved to be more difficult because of difficulty in analyzing the exact mechanism. Basing their development on the mechanism in which the melt collected at the rear

of the channel, Tadmor [56] proposed a model to calculate the length of the melting zone. He assumed a pure drag flow of incompressible Newtonian flow in the melt film adjacent to the barrel, constant solid bed velocities, flow in a rectangular channel, constant properties and sharp melting points of the polymer. By doing a thermal balance across the interface and linking it to the flow in the solid bed, he was able to calculate the decreasing solid bed width and the rate of melting in both tapered and parallel channels. This model suffered two major shortcomings. Firstly, the assumption of linear velocity profile owing to pure drag flow was not valid because of temperature dependent non- Newtonian flow in the film. Secondly, the effect of convective heat transfer arising out of melt removal was not incorporated in the thermal balance in the melt film .

Tadmor et al. [51] attempted to incorporate features to eliminate both the above sources of error in their later model. A temperature dependent power law model was assumed for the flow in the melt film. They then assumed a linear temperature profile across the film. In order to circumvent the complexities, the temperature dependence of the viscosity was converted to a dependence of viscosity on distance via the assumed temperature profile. The temperature and the velocity profile depended on the difference in the velocities between the barrel and the solid velocities. The coupled energy and momentum equations were solved. These results were used to modify the rate of heat transfer at the solid melt interface and the rate of melt flow in the film. New expressions for the solid bed profile and film thickness were obtained. All these new expressions would reduce to the ones for the simpler Newtonian case in [56]. The same procedure was repeated for an assumed non-linear temperature profile in the melt film. It resulted in more complex solutions but was reported in the same form as the two previous ones. The solid bed thickness predicted from these models was compared to cooling experiments with LDPE, HDPE, rigid PVC, Polypropylene, etc. and a significantly better fit was observed than in the simple case reported in ref. [56]. There was some discrepancy between the prediction of the theories and the experimental results towards the latter part of the screw where the solid bed broke up and the melting mechanism changed. In general when this did not take place the agreement was good between the theoretical and

predicted values of the solid bed thickness. Tadmor and Klein [49] further improved the model by incorporating the effect of channel curvature.

The disagreements between experimental and predicted values in the solid bed thickness profile led Donnovan [59,60] to suggest certain modifications. He derived equations to calculate the change in temperature in the solid bed and also altered the assumption of constant solid bed velocity. This was done by defining a factor called solid bed acceleration Parameter (SBAP). For rigid polymers with no solid bed acceleration, it has a value of one and is zero for soft thermoplastics. By comparing the theoretical and experimental data for various polymers , the SBAP values were ascertained. He successfully employed this technique to improve the predictions for the solid bed thickness for a number of polymers with different screw diameters. He did an integral mass balance to calculate the flow rate in the melt pool. Using this flow rate and the SBAP parameter, he improved upon the pressure predictions. The solid bed velocity and width were affected by the SBAP and they in turn affected the pressure profiles. In the region where the solid bed broke, the predictions from this method were not accurate. Also, a certain SBAP value did not always give the best fit for both pressure and solid bed profiles. SBAP was supposedly dependent on polymer rigidity but no experimental determination of this was presented and determination of its value was empirical.

The difficulty in obtaining an experimental or theoretical value for the SBAP led Fukase et al. [71] to attempt other techniques to model the changing solid bed velocity. They were able to show both experimentally and mathematically that for certain polymers, the solid bed decreased both in width and thickness at the same rate. The shear stress distribution in a simple one dimensional flow was linked to non-isothermal and non-Newtonian flow in the melt film by a shear rate and temperature dependent viscosity. The temperature distribution in the diminishing solid bed was used to predict the solid bed velocity in the down channel direction and the melting velocity of the solid bed. The agreement between the predicted and the experimental solid bed thickness and width was better than that found by Tadmor et al. [49, 51] or Donnovan [59, 60]. The pressure predictions were better but the temperature predictions were slightly offset because the delay zone was not modeled. The works of Donnovan [60,61]

and Fukase et al. [71] are but few of the efforts that have been undertaken to improve the modelling in the melting zone. The solutions to these have been made easier to obtain due to the ease of numerical solution using computers.

The flow in the melt conveying zone is governed by cross channel and down channel velocity. Equations for velocity and pressure gradients in both these directions have been solved for isothermal Newtonian flow in [49] as a first approximation. It was found that flow rate was composed of contributions from both drag and pressure flow and the velocity profile depended on the relative contribution from them. Improvements to the model which takes into account the non-Newtonian, non- isothermal flow allowing for channel curvature have also been reported in references [49] or [77].

2.5.5 Numerical Methods

The reasonable objective of a mathematical model for a single screw extruder is to be able to predict temperature, pressure and the amount of unmelted solid, if any, at the die exit. Since pressure, temperature and amount of unmelted solid at the die exit depend on the history of the polymer in the whole extruder, the final predictions require the determination and calculation of these variables at axial increments along the screw channel. Again, the total power requirement at each axial position can be obtained and the cumulative power requirement at the end of the screw should give the extruder power requirement. Barrel and screw temperatures, melt temperatures, channel cross section, shear rates etc. gradually change along the screw. The computations start at the hopper end and are performed in small increments down the channel until the end of the screw. No quantitative melt modeling can give meaningful results without accurate input data. The input data must contain information about extruder geometry, operating conditions and physical properties of the polymer. The information on the extruder geometry includes the length and diameter of the screw, flight widths, flight clearances and channel depths. The processing conditions include the screw speed,

barrel temperatures and flow rates. Polymer properties include shear rate-viscosity data, thermal data, friction coefficients and density values. The following paragraphs briefly review some of the attempts at numerical modelling of the entire extruder . These have been based on the theoretical development of the mechanism in the different extruder zones, as described previously in this section.

Tadmor and Klein [61] were among the first to obtain a temperature and pressure profile for all the zones in the extruder by solving the governing equations in each zone as developed in references [49] and [51 to 53]. It is not clear whether the solid conveying zone was modelled as per Darnel and Mol's theory [53] as the computation required the friction coefficients as a function of temperature, and doubts were expressed about their values. It appeared that by keeping this zone small, large errors were avoided by calculating the rate of pressure rise in the solid conveying zone to be the same as in the first few inches of the melting zone. The areas occupied by the solid and the melt were calculated for two phase flow in the melting zone. Knowing the dimensions of the melt filled part of the channel, the temperatures and pressures in it along the screw were obtained by a finite difference iterative solution procedure. The authors simplified the calculations towards the end of the melting zone, where the solid bed broke up. They based the pressure prediction on the assumption that the entire channel was filled with the melt. The temperature was obtained as a time averaged value of the two conditions consisting of a completely filled channel and a channel cross section retaining the solid bed. The flow in the melt conveying zone and melting zone was based on a power law fluid. For most of their experiments some unmelted material remained at the die exit and this amount was used to predict the temperature fluctuations at the die exit. Temperature and pressure profiles were compared for HDPE, LDPE, rigid and plasticized PVC and in some of these the measured pressures were lower than the predicted pressures. The discrepancy in the temperature profiles in the beginning of the melting zone was attributed to the position of the measuring thermocouples in the tapered section. The differences in the temperature fluctuations at the die were generally small and the larger differences were attributed to the breaking up of the solid bed. This showed that the assumptions of time averaged value

for temperature did not lead to a correct prediction. Some physical data were taken from other sources and might not have been suitable for the materials tested because of the strong dependence of PVC properties on previous thermal and shear history. The channel curvature was not taken into account and the authors also did not specify how the zone boundaries were demarcated for computation purposes.

Agur and Vlachopoulas [62] developed a model to predict the flow rate, temperature and pressure profile along the extruder channel and in the die, and to predict the die swell. The basic formulation was similar to that given by Tadmor and Klein [61], with certain deviations. The flow and the pressure rise in the solid conveying zone was modelled on Darnel and Mol's theory [50] modified by consideration of the channel taper but the non-isotropic and non-isothermal conditions were not included. The initial pressure distribution in the solid conveying zone was calculated from pressure distribution at the base of the hopper. The melting zone model was essentially the same as that developed by Tadmor et al. [49,51]. They neglected the convective heat transfer in the melt film [51] but incorporated a shear rate dependent viscosity for the flow in the film. This was done from a linear regression of the capillary rheometer data linking the viscosity to the temperature and the magnitude of the shear rate tensor. The final forms of the melting rate and the solid bed thickness resembled the simpler Newtonian model [56] more closely than the more complicated power law model with convective heat transfer in the melt film in [49] and [51]. In the melt pool, the melt conveying zone and in the die the equations of mass, momentum and energy were solved using an implicit finite difference method. It was different from the Tadmor's model in that by retaining the convective term in the energy equation, the temperature profile in the downstream direction was also calculated. The operating variables, the screw geometry, and the specification of the properties as input to the model led to prediction of power, temperature and pressure profile in the extruder and the die and the die swell. The measured pressure profile was higher than the predicted pressure profile in the screw channel but lower in the die. No values were compared for the solid conveying section and even in the initial part of the melting zone. The temperature in the die showed a discrepancy of 1 to 5 °C between the measured

and predicted values but the variations in temperature where the solid bed broke off was not commented upon. The die swell values agreed well. It seemed that the simplifying assumptions for modelling purpose did not make a difference in terms of accuracy at the die exit but questions about their validity and accuracy can be raised in the up channel sections of the extruder. Also, the way the different zones were specified and connected were not specified.

Zavadsky and Karmis [63] developed a more detailed model which incorporated fewer simplifying assumptions. They included a delay zone between the solid conveying zone and melting zone. The flow of solid in the solid conveying zone was non-isothermal and the pressure distribution non-isotropic but the flow in the hopper was isothermal. They also obtained friction as a function of temperature. They incorporated the Tadmor model [51] in the melting zone assuming the flow in the film to be that of a power law fluid and they assumed a linear temperature profile in the melt film. Again, in the melt conveying zone a power law model was assumed with provisions to update the power law exponents for temperature and shear rate variations. They assumed that the melt conveying zone started when the solid bed decreased to 10 % of its initial value. This was done to account for the broken solid bed, but the way in which it affected the results was not discussed. The foregoing additional features made their approach more comprehensive than the others [61, 62]. The program output contained additional information such as cross channel temperature and pressure profiles, average residence time, development of film thickness in the delay zone, average film thickness of the film in the melting zone and property changes along the down channel direction. The program could also have been used to predict an optimum screw design for a given output with particular melt parameters or processing conditions. When compared to the experimental values at the die exit, there was an error of 5 % in temperature and a maximum of 30 % in the pressure values. The temperature profile at the boundary of the solid conveying zone was not smooth and the authors ascribed it to the assumption of isothermal condition in the hopper but do not elaborate on the exact reason.

Vriyayuthakorn and Kassahun [64] were the first to attempt a 3-D finite element model for the plasticating extruder. Using the method of weighted residual and employing standard

Galerkin formulation techniques, the equations of mass, momentum and energy were solved. The temperature dependent thermal conductivities and specific heats were used but their actual forms were not reported. The temperature dependent specific heat capacity function was used to account for the phase change during melting. A master curve for shear rate dependent viscosity was constructed. The author made no mention of how the solid transport was modeled in either the solid conveying zone or the melting zone. They mention that difficulties arising out of constant solid bed velocity or the breaking up of the solid bed were solved. However, they do not report how these were achieved from the modeling viewpoint. Also, boundary conditions for the different zones were not specified. The temperature and pressure profile along both the down channel and the cross channel sections were better represented on a 3-D plot and were in better agreement with the experimental data. The authors claimed that the cooling experiment observations of encapsulation of solid bed or breaking up of the bed in the melting zone were predicted. The 3-D finite element approach was obviously superior in modeling extruder structural features like channel curvature and thus could improve the flexibility if used in design of the extruders.

Recently, Wagner [70] has reported simulation of soya dough containing 50 % moisture in a single screw extruder by 3-D finite element technique. The food doughs exhibit properties similar to polymers. This simulation method could be an important step towards simulating single screw extruders because it can predict the temperature and pressure profiles in the extruder without solving separate governing equations for the different phases. The author used a 3D finite element code, called FIDAP for the simulation purpose. By using Galerkin form of weighted residuals the FIDAP to transformed the model equations for the extruder, to the finite element form and then solved the resulting system of algebraic equations. The penalty formulation method was used in formulating the problem. The generation of a mesh to describe the screw geometry was discussed in detail. The description of various boundary conditions was reported. It was also reported that the viscosity of the fluid was represented by power law fluid with constant coefficients. For the temperature range of operation, the specific heat and thermal conductivity was assumed to be constant. The limitation of the au-

thor's work with respect to the inability to incorporate temperature dependent viscosity was discussed. The energy equation could not be fitted into the model and thus was a potential source of error. She also reported the problems owing to dicretization of the domain especially in the curved sections of the extruder. The agreement between the results of the numerical simulation and the experimental values of the pressure was not good. Although the trends were similar, the experimental values did not match the predictions from the simulation but the agreement on the velocity profile was better.

There have been attempts to model the different zones in the extruder (61-64,70). Most of these have been confined to 2-D modeling though a few (64,70) 3-D modeling attempts have also been reported. The governing equations in the melt conveying zone have been well developed and standard solutions are given in the literature [49,77]. The solutions for the governing equations in the solids conveying zone have been somewhat difficult because of the absence of determination of proper friction coefficients [49,54,55] at the different surfaces in the extruder channel. The accuracy of the solution of the governing equations in both of these regions are subjected to obtaining correct property values. On the other hand, the melting zone owing to its complex two phase nature has been the most difficult to model. The melting mechanisms vary with polymers. The variations have been attempted to be incorporated into the original simple melting model in refs. [56] and [78]. These variations have been in terms of changing solid bed velocities, temperature dependent power law fluid, different forms of mass and energy balances in the solid, melt and interphase region etc. There has been no single model that can account for melting of all the polymers. Although a particular model may have helped to predict better for one polymer, it has failed to predict the melting for other polymers. No specific governing equations take into account the gradual fusion, instead of a sharp melting point, as is the case with PVC. All the models have been developed for polymers which have sharp melting points.

2.6 CONCLUSIONS OF THE LITERATURE REVIEW AND THE PROPOSED RESEARCH

The published work in the literature on PVC morphology and rheology and the processing of PVC in single screw extruders have been reviewed. It was observed that the rheological behavior of PVC is governed by the fusion characteristics of the particulate structure that exists in the melt state [13-15,25-29,34,40-43]. These structures persist at high temperatures and retain their crystallinity at processing temperatures that will be encountered in the extruder in this research. Owing to the remnant crystallinity, the PVC melts fail to attain zero shear viscosity even at temperatures until 190 or 200 °C and instead display yield stress behavior at low shear rates.

Plasticizers have been shown to affect the rheological properties like viscosities [8,30,31,36] but the mechanism by which this influence is exerted is not clearly understood. The effect of plasticizers on fusion of the melt flow units or the primary particles has not been investigated. Answers to how they affect the primary particle fusion or the exact manner in which they change the microdomain distribution have not been satisfactorily reported. Also the effect of plasticizers on the change in flow mechanism from the particulate to the melt or fused state needs to be investigated in detail.

The rheological properties of both rigid and plasticized PVC were also affected by the previous shear and thermal history of the material arising out of differences in the degree of fusion [11,36]. This fact introduces difficulty in using viscosity shear rate data from other investigations for samples whose preparation histories are unknown or have not been reported in detail. However, a systematic study of the relative influence of the three plasticizers, used in this research, on the viscosity shear rate data has not been reported. A comprehensive set of viscosity shear rate data for plasticized PVC at temperatures encountered in the extruder is thus absent. Data for temperatures below 170 °C are rarely reported. The viscosity

data have to be obtained over the temperature and shear rate of interest for differently plasticized PVC samples and then fitted to the viscosity empiricisms to be used in the numerical simulation. The yielding behavior of plasticized PVC at low temperatures and shear rates needs to be determined because fluid models incorporating yield stress will be used to model solids flow in the extruder.

Thermal properties and friction coefficients are important factors that are required for numerical predictions of the behaviors of polymers in extruders. The specific heats and thermal diffusivities for PVC plasticized with the three different plasticizers of interest have not been reported. Both the specific heat and the thermal diffusivity data need to be generated as a function of temperature and plasticizer type. The effect of plasticizers on friction coefficients has not been reported. But the effects of temperature, molecular weight and glass transition temperature on the the friction coefficients in rigid PVC have been reported [80,93,94]. The effect of surface roughness, sliding velocity and normal force have also been studied but conclusions regarding their effect are varied. New friction coefficient data needs to be generated for plasticized PVC.

Different melting mechanisms in single screw extruders for PVC have been reported [49,51,52,53]. Melting mechanism where the melt accumulated at the pushing flight has been reported for both rigid and plasticized PVC [49,51]. Some studies also reported melt accumulation at the trailing edge for rigid PVC [52,53]. It was observed that plasticizers affected fusion time in standard a ASTM laboratory test [37,67]. The differences in the fusion time values was thought to cause differences in pressure development and flow rates. The exact cause of these differences could be in the way the plasticizers affected the melting mechanism in the extruder. No investigation of the plasticizer on the melting mechanism has been reported. More specifically, studies to illustrate the effect of plasticizer on the morphological progression have not been reported. The effect of different plasticizers on fusion of PVC in extruders has not been linked to changes, if any, in the melting mechanism.

All the three zones of the extruder have been modeled. The different mechanisms in the different zones have been studied and the governing equations for each zone has been de-

veloped. The equations developed for predicting the pressure and temperature rise in the solids conveying zone have been presented in references [54] and [55]. The governing equations for the melting and melt conveying zones could be obtained elsewhere [49, 51, 56, 58, 77]. All these theories have been developed for polymers with sharp melting points.

In keeping with the above models, rigid and plasticized PVC have been modeled as a polymer with sharp melting point. In reality, gradual fusion of the PVC particulate structure takes place as the polymer moves down the extruder channel and this fact has not been taken into account. Also the two different flow regimes, particulate and fused or melt-like, have not been taken into account in the models. No report on the modelling of the differences in the fusion rates because of the plasticizer type and how the plasticizers may affect the development of the melting zones have been published. In order to simulate extrusion, accurate input data on the material properties are necessary. Properties such as viscosity-shear rate data and thermal properties have been reported for rigid PVC [51]. The viscosity was obtained as a function of temperature and shear rate by a regression fit from the viscosity shear rate data obtained from capillary rheometer at different temperatures. Since specific heat and thermal conductivity were observed to change slightly with temperature and even less with pressure, they were treated as constants. Different values for the thermal properties were used for solids and melts [51]. It is obvious that these property values from the rigid PVC formulation cannot be used for the plasticized samples in this study. In reference [61] plasticized PVC extrusion was modeled and the temperature and pressure profiles were predicted but no properties were reported and no mention was made of the plasticizer type or level.

One of the objectives of this research is to simulate the extrusion process of plasticized PVC using finite element method and to see whether any observed differences in the extrusion behavior owing to the plasticizer type can be predicted. Numerical simulation of PVC extrusion which considers the effects of plasticizer type and content has not been performed. The effect of plasticizers on the melting mechanism of PVC and on the lengths of different zone boundaries in the extruder is yet to be studied. A finite element code, FIDAP, will be used for simulation in this research. The simulation efforts will focus on predicting the pressures,

temperature, flow rates, etc in the melting and the melt conveying zone and also on numerical predictions in the solids conveying zone. The equations developed in [54] and [55] can be used for the solids conveying zone. PVC displays yield stress behavior at lower temperatures and this fact will be used to model the solids conveying zone as a fluid with yield stress by using the finite element code. Both solids and fluids with yield stresses display plug velocity profiles. At low temperatures, fluid models incorporating yield stresses probably depict the fluid behavior more correctly than a power law type model and low temperature fluid behavior is assumed to approximate solids behavior. The last two above-mentioned facts are the reason for attempting to model solids conveying as a fluid with yield stress. The equations and the boundary conditions for the melt conveying zones could be used for both the melting and the melt conveying zones with different viscosity empiricisms for the different phases. Although it is well established that shear flow conditions exist in the extruder and the finite element code (Fidap) can only handle Generalized Newtonian Fluids constitutive equation, the exact form of the shear rate dependent viscosity for each zone will be determined after a detailed examination of the viscosity - shear rate relations at different temperatures. Also the transition temperatures for different flow mechanisms need to be considered and the viscosity empiricisms changed accordingly.

From the conclusions inferred from the literature review and the discussion in this section, the following objectives are proposed for this study :

1)Investigate the effect of plasticizer type on the extrusion behavior of polyvinyl chloride in a single screw extruder. It would be of interest to observe if the plasticizer type introduces any differences in the extrusion behavior with regards to the pressure profiles, flow rates, power requirements, temperatures, etc. or whether it affects the melting mechanism in the extruder. The three plasticizers of interest are :a)DIDP (Di-isodecyl pthalate), b)DHP (dihexyl pthalate) and c)DOP (2-ethyl hexyl pthalate).

2)Determine whether physical properties such as viscosity, yield stress, density, thermal diffusivity, specific heat, friction coefficients, etc. reflect the effect of the plasticizer type. Also how fusion affects viscosity, density and flow mechanism of plasticized PVC will be investigated.

3)Use the finite element code, FIDAP, to simulate the extrusion behavior of plasticized PVC in a single screw extruder. The simulation will be performed in 2-D and if possible in 3-D. The numerical simulation will specifically attempt to predict the differences with respect to pressure development, flow rates, temperatures, etc. in the extruder arising out of the differences in the plasticizer type. Also the solids conveying will be modelled as a fluid with a yield stress. The simulation results will be compared to the experimental values.

In the next two chapters the methodology and the techniques which will be involved in carrying out the objectives of our research will be described.

3.0 EXPERIMENTAL APPARATUS AND PROCEDURE

Towards the end of the last chapter, the objectives of this research were presented. In this chapter the experimental methods used to attain part of these objectives will be outlined. These include a description of the materials used, the apparatus used for analysis and the specific methods used to obtain the experimental data. The results from the experiments, which are described in this chapter, together with their respective error bars (i.e. the variation about the reported mean values of the measured quantities) will be discussed in Chapter 5. The tables referred to in this chapter are placed at the end of this chapter.

3.1 MATERIALS

PVC powders of average molecular weights in the range of 155,000 were supplied by Exxon Corporation for use in this project. The plasticizers that have been used for this research are DIDP (Diisodecyl Pthalate, molecular weight 447), DHP (Dihexyl Pthalate, molecular

weight 334), and DOP (2 ethyl hexyl Pthalate, molecular weight 391). Epoxidized Soyabean Oil (which acts as a lubricant and plasticizer), Mark 7101 (a liquid stabilizer) and stearic acid (a lubricant) are the other ingredients of the PVC mix. For every 100 grams of PVC, 5 grams of ESO, 2 grams of Mark 7101, 0.25 grams of stearic acid and 40 grams of either of the three plasticizers have been used. Two different preparation methods, viz. dry blending and pelletizing of PVC mixes, have been used for preparing the starting materials for the experiments. The pelletized samples were received directly from Exxon. Dry blending was performed in the laboratory in order to obtain a homogeneous mixture by following a procedure that was supplied by Exxon Corporation.

3.1.1 Sample preparation

A Hobart mixer with an external jacket was used to dry blend the PVC with other additives. Hot silicon oil was circulated in the jacket to heat up the PVC mix. A temperature progression was followed to slowly heat the PVC powder while the various additives were added at different temperatures.

PVC was heated and stirred in the Hobart mixer to a temperature between 50 and 60 ° C. A mixture containing a particular plasticizer, ESO and Mark 7101 was then added to the PVC powder and it was allowed to homogenize with the PVC powder for a period of 3 to 4 minutes. The combined mixture was heated to 85 ° C in 12 to 14 minutes, while being vigorously stirred. At this point stearic acid was added to the mixture. It was then heated to a temperature between 90 and 95 ° C for the next 10 minutes. The mixing was reduced to a slightly slower rate and continued for another 10 minutes while the temperature of the mixture was maintained between 100 and 105 ° C. The batch was then dropped into a cooling bath containing an ice water mixture and slowly stirred for another 10 minutes until the temperature of the batch fell below 40 ° C. It was then stored in plastic containers.

Initially, the addition of the plasticizer mix made the PVC mixture quite sticky but as the liquids were absorbed by the PVC particles, the whole mixture became free flowing. Caution was necessary when heating the mixture at temperatures between 100 and 105 ° C as overheating of the sample might lead to over drying of the PVC mix. Before starting to characterize the material properties, the level of homogeneity achieved through the dry blending process was successfully tested. A capillary rheometer was used to measure the viscosity of two different batches. Table 3.1 show the variation in viscosity between two different batches at three different shear rates at 180 and 190 ° C. The small difference in viscosity of less than 0.9 % indicates that it is possible to make homogeneous batches, with reproducible properties, by dry blending process.

The plasticized PVC pellets were extruded at approximately 180 ° C as per information available . from Exxon Corporation. In this method a homogenized mixture of PVC and the additives, at room temperature, were the starting materials. The pelletization was possibly performed using an extruder, cooling trough and a pelletizer.

3.2 *APPARATUS*

The experiments that have been conducted to achieve the research objectives fall into two categories. First, studies were conducted to observe the effect of plasticizers on the extrusion process in a single screw extruder. After this the effect of plasticizers on the material properties were studied. A brief description of each apparatus, its pertinent operating information and the range of experimental conditions are included in this section.

3.2.1 Extruder Experiments

Extrusion experiments were performed using a Killion 4335 one-inch diameter, 20:1 L/D laboratory scale single screw extruder having a screw with a compression ratio of 2:1. An explanation of the operating principle of single screw extruders has been given previously in chapter 2. The extruder is equipped with three temperature controllers for the heaters on the barrel. A fourth controller is used to control the temperature of the die which is heated by three band heaters. Four pressure transducers are mounted in the barrel at distances of 9.75 inches, 12.75 inches, 15.75 inches and 18.75 inches, respectively, from the feed end. The end of the barrel can be screwed on to a flange which is connected to a cylindrical front section that leads to the die. This initial cylindrical section has a diameter of 0.75 inches but tapers to a 1/8 or 1/16 inch diameter capillary. Screw characteristics are listed in Table 3.2. The pellets or the dry blended materials, fed through the feed hopper, are melted by heat and shear and come out as melt through the die. In these experiments, the barrel temperature was progressively increased from the feed end to the die. The barrel temperature setting varied between 146 and 180 ° C and the die temperature setting was between 175 and 185 ° C. The smaller diameter die required higher temperature to keep the pressures, generated in the extruder, within the safe operating ranges of the pressure transducers. Screw speeds ranged from 15 to 45 rpm. Higher screw speeds could not be achieved as it would have lead to pressure build-ups beyond the permissible ranges of the pressure transducers.

For the extruder runs, certain parameters that characterized the extruder performance were observed and recorded. For a particular screw speed, the pressures were monitored for steady state operations by observing the strip chart recorders attached to the pressure gauges. Pressures, amperages and flow rates were recorded after a steady state was reached. The pressure readings fluctuated between a minimum and a maximum depending on whether the center of the channel or the screw flight was sweeping below the transducer. The average pressure reading has been reported in the results section in Chapter 5.

In the second section of the extruder studies 'cooling experiments' were conducted to study the effect of plasticizers on the melting mechanism and fusion of PVC in the extruder [48,49]. In these experiments, after the extruder has reached a steady state during a run, it was stopped and cooled. A device which is referred to as a screw puller was fabricated. This enabled the pulling of the screw from the barrel with material on it. A yellow colored die was added to the polymer feed to distinguish between the solid and the melted or the fused polymer. The material was recovered in the form of a coil which started forming in the solids conveying zone, especially for the powdered samples. Unlike the powdered samples, the pellets formed no coils for part of the solids conveying zone. Only the material near the melting zone, in front of the leading flight, started to form a continuous coil. The helical polymer ribbon was sectioned and two sets of experiments were performed. In the first case the formation and the development of the melt zone was studied. In the second case thee effect of plasticizer on the the progression of fusion in the extruder was investigated by scanning electron microscopy.

Another type of extruder experiment was performed to generate data to test the solids conveying model. The barrel temperature was maintained constant from the feed end to the discharge end. The values of the barrel temperatures were between 90 and 135 °C and were thus not high enough to initiate fusion of the PVC in the extruder. Instead of a die, only a flange was attached to the end of the extruder. As no melting or fusion of PVC mixes take place, these experiments are termed as "dry extruder run".

3.2.2 Scanning Electron Microscopy (SEM)

SEM studies were done on a Jeol JSM 35 C machine with an accelerating voltage of 15 KV. The materials from the 'cooling experiments' were sectioned and then fractured after cooling them in liquid Nitrogen. The fractured samples were mounted on aluminum stubs,

sputtered with gold and examined under the SEM at a magnification of 150 to 2000. This helped in studying the progression of fusion and how it was affected by the plasticizer type.

3.2.3 Capillary Rheometry

An Instron Capillary Rheometer (ICR 3211) was used to determine the viscosities of different dry blends and pellets between temperatures of 140 and 190 ° C. The corrected wall shear rates covered were from 2 1/s to about 110 1/s which covered the range of shear rates that were encountered in the extruder. The shear rates encountered in the extruder have an upper limit of approximately 50 1/s for screw speeds up to 45 rpm.

The capillary rheometer works on the principle of forcing a quantity of fluid through a capillary of known geometry. The capillary is placed at the end of a reservoir, called the barrel, and the temperature of both the capillary and the barrel can be controlled simultaneously. After the desired operating temperature has been reached, the scale for measuring the plunger force is calibrated. The sample is then placed in the barrel and a stainless steel plunger is used to push the material through the barrel and the die. The speed of the plunger could be varied by a set of gears. The constant plunger speed and the dimensions of the capillary affect the flow rate through the capillary and the pressure on the plunger. The resistance force on the plunger is measured by a load cell which is capable of measuring forces up to 2000 kg. The diameter of the set of capillaries that have been used is 0.07 inches and the length to diameter ratios (L/D) of the capillaries were 7.82, 21.4 and 40. At each temperature and for every plunger speed, the experiments were repeated at least two to three times to ensure the repeatability of the response of the material and to estimate the error bars for the recorded data.

For a given die, the forces on the plunger at different plunger speeds were recorded at steady state conditions. The forces were obtained from the strip chart recorders used to measure the force on the plungers. The shear stress was calculated from the force on the

plungers, area of the plunger cross section and geometry of the die. The apparent shear rates (i.e. shear rate for Newtonian fluid) was calculated from the flow rate and the capillary diameter. The shear stress - apparent rate data was obtained for all the three capillaries. The correction for the entrance pressure loss was calculated using the pressure drop and apparent shear rate data from three capillaries by using the well-known Bagley plots [81]. This correction was applied to wall shear stresses. Again a correction was employed to account for the non-Newtonian behavior of the polymer sample by applying the Rabinowitsch correction factor [82] for the apparent shear rates. The viscosity was determined by the ratio of the corrected wall shear stress to the corrected wall shear rate. These calculations to obtain the viscosity - shear rate data from the plunger speed and the force on the plunger were done with the help of a software package [83].

3.2.4 Capillary Rheometer to Measure Density

Two types of compression tests were done on the dry blended and pelletized PVC samples. For the dry blended samples, a capillary (dc = 0.07 inches and L/D = 40 or 21.4) was attached to the end of the ICR. Samples were placed in the barrel and extruded at different plunger speeds varying from 0.06 to 0.3 cm/min. For each speed, material was collected for a specific amount of time and its weight was noted. From the plunger speed and the time of its travel, the volume of the extruded material was calculated. From the weight and the volume of the extruded material its density was calculated. The force on the plunger was divided by the area of the plunger to determine the pressure at which the density was calculated. This was done for temperatures of 160, 170 and 180 ° C. Thus densities were available at discrete values of pressures at four different temperatures.

For a continuous range of density values, a second type of test was done. The end of the ICR was sealed with a plug. When the tip of the plunger touched the top of the plug in the

empty barrel, the position of a marker attached to the plunger was noted. The marker was screwed on to the plunger and its position read against a ruler. A known weight of pelletized PVC sample was put in the barrel and the plunger was brought down at a speed of 0.1 cm/min or slower. At certain intervals, the plunger was stopped and the force on the plunger was maintained manually for a short period of time. The position of the marker attached to the piston was again noted and the value of the force on the plunger was recorded. From the amount of piston displacement the volume of the samples were calculated at different plunger positions and these values were used to calculate the densities. The conical shape of the end of the plunger is taken into account when calculating the volume of the material between the plunger and the plug. Corresponding to each plunger position, the forces on the plunger are divided by the barrel cross-section to obtain the pressures. The measurements were done at 150, 170 and 190 ° C. The main source of errors arose from not being able to determine the uniformity of the compacted material in the barrel. In fact at lower temperatures, the material appeared less compacted near the bottom, as fragments of individual pellets could still be identified. It was difficult to estimate the error bars between various experimental runs. Thus it seemed that the uncertainty in the compaction could be minimized by increasing the number of repeat runs for each samples. This method was unsuitable for dry blended samples as the powder would stick to the sides of the ICR barrel and thus introduce errors in calculating the amount of material that was being compressed.

3.2.5 Rotary Rheometry

Rheological properties at low shear rates and in the dynamic mode were measured using a Rheometrics Mechanical Spectrometer (RMS model 605). These data were used to comprehend the material behavior especially at low shear rates and temperatures and to calculate the yield stress of dry blended PVC samples. Experiments were conducted between

140 and 170 ° C. The shear rates for the steady shear experiments ranged from 0.01 to 0.1 1/s. Higher shear could not be achieved as the normal forces developed in the materials exceeded the safe operating ranges of the RMS. The shear rates used for the dynamic experiments ranged from 0.02 to 100 rad/s. Strain sweep experiments were run at 140, 150 and 160 ° C to determine the linear region in which the dynamic experiments were to be conducted.

The RMS is a rotary rheometer with the lower plate being flat and the top plate being either conical or flat corresponding to cone and plate or plate and plate geometry, respectively. The top plate of the rheometer is connected to a motor which can rotate the plate in either clockwise or counterclockwise direction and thus enables the study of steady shear viscosity. The motor can also oscillate the top plate to generate dynamic property data. The bottom plate is connected to a normal force and torque transducers. The sample was placed in the gap between the cone and plate or between the two parallel plates. With a sample in the gap, the rotation caused a torque and normal force to be transmitted through the fluid to the bottom plate. These signals were detected by transducers at the bottom plate and were sent to the microprocessor after analog to digital conversion of the signals. These raw data together with the plate dimensions and the gap width were processed to obtain values of viscosity, normal force, etc. in the steady shear mode. In the dynamic tests the outputs were storage modulus G′, loss modulus G″ and complex viscosity η^*.

The plate and the cone were 2.5 cm. in diameter. The gap setting for the parallel plates were between 0.8 to 1.0 mm and was 0.05 mm for the cone and plate. As mentioned earlier, measurements were done at temperatures between 140 and 170 ° C. At lower temperatures the PVC samples do not undergo much fusion and have a tendency to slip [14,29] and special procedures were followed to overcome the slippage. After the scale to measure the gap was calibrated at one particular temperature, the samples were put in between the plates and heated slowly till 190 ° C. At about 180 ° C, nitrogen supply was turned on to provide an inert atmosphere. The gap spacing was slowly diminished and it resulted in the material exerting some normal force on the plates. At temperatures lower than 180 ° C, the normal forces relaxed slowly but some residual normal forces were still recorded on the indicator. At 190 °

C the excess materials were scraped off from between the plates and the gap was still further reduced to its final value. The final values depended on whether parallel plates or cone and plate was being used. The temperature was raised to 210 ° C to let the normal stresses relax completely. The plates and the samples were then slowly cooled to the final test temperature. As the cooling progressed, the material possibly contracted and pulled the plates inwards to a register a negative normal stress usually below 170 ° C. This negative normal stress increased in magnitude as the temperature was progressively lowered. Although initially some steady shear experiments were done, because of the problem of high normal stress, even at lower shear rates, experiments were performed in the dynamic mode. Parallel plate attachment in the RMS was used for all the dynamic experiments.

3.2.6 Differential Scanning Calorimetry

The Perkin Elmer DSC4 was used to study the thermal transitions and the specific heats of the PVC samples. The operating principle of the DSC is based on the fact that when a material undergoes a change of state it liberates or absorbs heat and that this change of state can be initiated by the application of the heat itself. A programmed linear rise in temperature is brought about in the sample and in an inert reference material. Any thermally induced changes occurring in the samples are then recorded as a differential heat flow. These are normally displayed as peaks on the DSC scan. By using special software it is possible to calculate the enthalpy changes associated with the process as well as other thermal properties like specific heat as a function of temperature. A DSC scan was generated to examine the thermal transitions of the pellets and the dry blended PVC between 70 and 220 ° C at a heating rate of 20 ° C per minute. This trace and a baseline trace (inert reference) between 70 and 220 ° C were used as an input to a software package to calculate specific heat as a function of temperature. Initially the same procedure was used to determine the specific heat of a standard sapphire sample. The specific heat of the sapphire sample was then compared

to the previously determined specific heat value. For any particular baseline the relative differences between the experimental and the standard specific heat enabled the calculation of correction factors at each temperature. The specific heat values of the PVC samples using the same baseline were then corrected using the correction factor associated with that particular baseline. The correction factors ranged from 3 to 5 %.

3.2.7 Thermal Diffusivity Measurement

An apparatus using the principle of Laser Flash technique was used to measure the thermal diffusivity of the PVC samples. It is shown schematically in Fig. 3.1. More detailed description of the apparatus is found elsewhere [96].

Samples of dry blended PVC were compression molded (at about 125 - 130 ° C) into thin discs measuring about 2 mm in thickness. From these discs, specimens were cut to fit a graphite sample holder. Each sample was coated with graphite powder and the sample together with the holder were placed in the oven in an inert nitrogen atmosphere. A laser flash was directed on to the sample via a gold surface mirror and through a fused silica window to the top of the oven. The transient temperature at the lower face of the specimen, induced by the laser pulse at the top surface, was monitored by a remote optical sensor. The response from the optical detector was recorded and stored in an oscilloscope. From the temperature response, T 1/2, which is the time for the lower surface to reach its maximum temperature was noted for each laser flash. From this value and from the thickness of the sample, a value was calculated for the thermal diffusivity. Corrections were applied for heat loss by convection from the sample disc at temperatures higher than room temperature. The measurements were done at 4 or 5 temperatures between 70 and 170 ° C. At every temperature for every sample the T 1/2 values were measured for three runs and an average value was used for the calculation of thermal diffusivity. Below 100 ° C, the signal to noise ratio of the laser sensors was

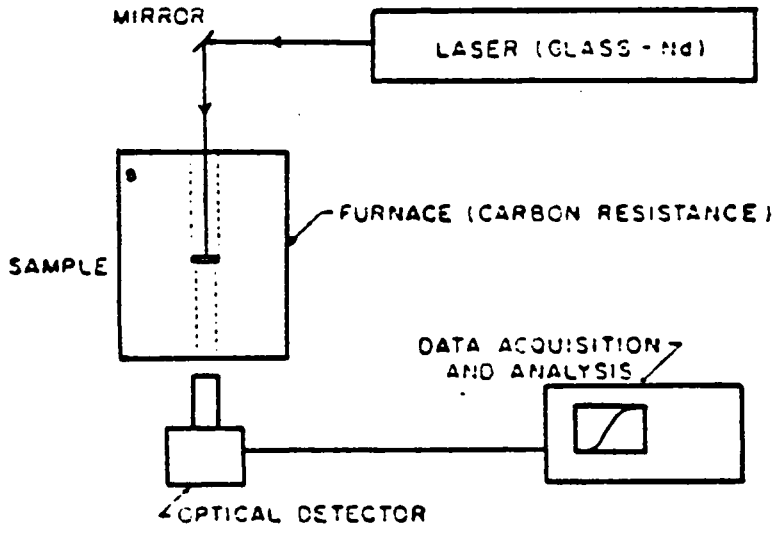

— Principal components of laser-flash diffusivity apparatus used in this study.

Figure 3. 1. Schematic of Laser Flash Diffusivity Apparatus

too large and interfered with the data acquisition. Above 170 ° C, the laser passed through the PVC samples almost instantaneously thus precluding any meaningful measurement of response time for T 1/2.

3.2.8 Measurement of Friction Coefficients

The friction coefficients were measured using a pin-on-disk apparatus which is described in detail elsewhere [93]. In essence, the experiment consists of measuring the tangential force on a cylindrical pin-shaped polymeric material when the latter is held against a rotating disk. The pin is pressurized by compressed nitrogen and by controlling the pressure of the nitrogen it is possible to vary the normal load on the pin. The whole apparatus is shielded to prevent heat loss and the temperature within the shielded cavity can be regulated by a temperature controller that is connected to the electrical heaters. The PVC samples were extruded from the ICR at 140 ° C using a 1/8 inch diameter capillary. Small pieces of these extrudates are held in a sample holder that screwed on to the end of the cylinder which is pressurized by nitrogen. Once the nitrogen pressure has been set, the tangential force is calibrated by applying weights on the sample holder in the tangential direction. For a more detailed description refer to [93]. The nitrogen pressure was set between 3.5 to 3.9 psi gauge which corresponded to a maximum normal force of approximately 6 Newtons. The disk was rotated at a speed of 36 rpm, the pin was placed 1.3 cm from the center of the rotating disk. The speed of the disk and the pin to center of the disk simulate the condition in the solids conveying zone at a screw speed of 35 rpm. The average surface roughness of the disk was 0.22 μm. First the disk was allowed to rotate freely and then the sample was lowered on to the disk. The relative motion between the stationary sample and the rotating disk exerted a tangential force on the sample. This tangential force was read off a strip chart recorder. The ratio of the tangential to the normal force gives us the friction coefficient. Friction coefficients were measured between 20 ° C to 135 ° C and at each temperature, the calibration was done

for the tangential force. Beyond 125 ° C the material was so soft that it some times broke from the sample holder under the abrasive action of the rotating disk. The experiments had to be performed several times as the scatter in the data between the repeat runs was large. A detailed discussion of the errors associated with the experiments, and how the experimental values of the friction coefficients relate to the actual values of the friction coefficients existing in the extruder will be presented in section 5.1.4.

Table 3. 1. Viscosity Comparison of Two Separately Prepared Dry Blended Sample

Material : DIDP dry blend

	Viscosity (Pa.S)			
	180°C		190 °C	
$\dot{\gamma}$ (1/s)	B1	B2	B1	B2
5	4820	4810	2072	2089
10	3175	3160	1573	1561
30	1630	1644	1015	1006

B1 and B2 are the two batches

Table 3. 2. Specifications of the single screw extruder

Barrel inside diameter = 2.54 cm
Screw L/D = 20:1
Screw Lead = 2.54 cm
Flight Width = 0.4 cm
Screw Channel Depth : feed end = 0.4572 cm
discharge end =0.2286 cm
Non-tapered feed end - 1 screw turn
Tapered section - 18 screw turns
Non-tapered discharge end - 1 screw turn
Helix angle at the Barrel = 17.65 °

4.0 FINITE ELEMENT FORMULATION

4.1 INTRODUCTION

The finite element method (FEM) is a computational technique used for obtaining approximate discrete solutions to continuous boundary value problems by reducing the latter to a set of algebraic equations. The method begins with discretizing the domain into geometrically simple subdomains called elements which are connected at the nodes. The FEM uses a piecewise application of the variational method and casts the given equation in the variational form [84]. In the process, a weak formulation of the differential equation is obtained which recasts the differential equation to an equivalent integral form by trading the differentiation between a test function and a dependable variable. In addition, the variational formulation also facilitates the classification of the boundary conditions into natural and essential boundary conditions.

To determine an approximate solution using the variational method, different methods like Ritz, Galerkin, etc. have been suggested [84]. All of these methods seek an approximate solution of the field variables in the form of linear combinations of suitable approximating polynomials or interpolating functions. The parameters or the coefficients in the linear com-

binations are determined such that the approximate solution satisfies the weak form. This necessitates rewriting of the main equation (now in variational form) for each element using the interpolating functions. At this point, all the elements are assembled according to the principles of continuity of the field variables at the nodes. After imposing proper boundary conditions, the system of equations is solved for the nodal values of the primary variables. A continuous global solution at any location in the problem domain is obtained by using the approximate polynomials.

As a computational technique, FEM has some distinct advantages. It allows easy handling of complex geometries and imposition of a variety of boundary conditions. The method is flexible enough to allow successively higher degrees of polynomials for approximation purposes without reformulation of the entire problem. It is more efficient than the finite difference method for handling problems with very large degrees of freedom. The FIDAP code incorporating all these features employs the FEM technique for solutions of isothermal/nonisothermal viscous incompressible flows [85,86].

The FIDAP is a general purpose computer program that uses the FEM to simulate many classes of incompressible flows. Presently, it can handle only Generalized Newtonian Fluid (to be henceforth to referred to as GNF) constitutive equation with proper boundary conditions and isothermal or temperature dependent physical properties. It uses the Galerkin method of weighted residuals to obtain approximate solutions for both isothermal and non-isothermal incompressible viscous fluid flow problems. For the complete list of FIDAP's capabilities and options, the reader is referred to [85]. The complexities of the problem that can be handled by FIDAP are governed by and limited to the storage capabilities and the computation time for executing the code.

In the Galerkin method of weighted residuals, substitution of an approximate polynomial for the dependent variable, when the latter is acted upon by a differential operator, results in a residual or an error in the solutions of the equation. In the weighted residual method the parameters, or the coefficients of the approximate functions, are determined by setting the integral of a weighted residual to zero. An examination of the weighted residual method shows

it to be a weighted integral form of the weak formulation obtained from variational methods [84]. It can be mathematically stated that the Galerkin form of weighted residual seeks to reduce the errors to zero by making the residual orthogonal to the interpolating function.

This chapter deals with the theory and the methods used for modelling the flow of plasticized PVC in rectangular extruder channels using the FIDAP code. The simulation problem of this study falls under the purview of three-dimensional nonisothermal steady-state problems. First, the governing equation for the continuous problem will be presented. This will be followed by discretization of the continuous problem, evaluation of various coefficient matrices and formulation of the resultant algebraic system. Discretization of the domain, imposition of boundary conditions and entering of the material property data will be discussed. Finally, the solution strategies of the algebraic system will be addressed.

4.2 FORMULATION OF THE CONTINUOUS PROBLEM

The equations that are to be solved for the flow of a fluid through an extruder channel are arrived at by applications of certain physical principles. These are conservation of mass, linear momentum and energy. With particular reference to the simulation problem dealt with in this work, certain simplifying assumptions have been taken into consideration. These are as follows :

(i) The problem is a steady state one.

(ii) Density variations are negligible. In other words, an incompressible fluid is being considered.

(iii) The enthalpy is a function of temperature only.

(iv) The fluid motion is laminar and of low enough Reynolds number such that the inertial terms are negligible compare to the viscous terms.

Also, the momentum equations are expressed in terms of divergence of the stress tensor. This representation has an advantage when Galerkin FEM is applied to the equations in a continuous problem. The incorporation of the divergence of the stress tensor in the momentum equation results in natural boundary conditions that can be interpreted physically as the components of stress acting on a fluid along its boundary. The boundary terms are almost identical to the stress-divergent form when the Galerkin FEM is applied to the Navier-Stokes equation, but the latter have no corresponding direct physical interpretation. With the above simplifications, the equations presented next are expressed in Cartesian tensor notations with summation of repeated indices implied. The three equations of change that describe the non-isothermal fluid flow problem are equations of conservation of mass, conservation of linear momentum and the energy equation.

The equation of conservation of mass is :

$$U_{i,i} = 0. \qquad (4.1)$$

where U_i is the velocity component in the x_i direction, $U_{i,i}$ means $\sum \frac{\partial v_i}{\partial x_i}$ (i.e. differentiation with respect to 'j' or 'i' is referred by (,j) or (,i), respectively.

The equation of conservation of linear momentum is :

$$\rho U_j U_{i,j} = -\sigma_{ij,j} \qquad (4.2)$$

where ρ is the density, $\sigma_{ij,j}$ is the total stress tensor.

For a fluid the stress tensor can be expressed as follows :

$$\sigma_{ij} = -P\delta_{ij} + \tau_{ij} \qquad (4.3)$$

where δ_{ij} is the Kronecker delta and τ_{ij} is the extra stress.

If ε_{ij} is the strain rate tensor of the rate of deformation tensor and is given by $0.5(U_{i,j} + U_{j,i})$, then the GNF constitutive equation determines the nature of the relation between τ_{ij} and ε_{ij} through the viscosity empiricism η

The energy equation is:

$$\rho C_p U_j T_{,j} = (kT_{,j})_{,j} + \eta\Phi \qquad (4.3)$$

where T is the temperature, C_p , is the specific heat, k is the thermal conductivity, $\eta\ \Phi$ is the viscous dissipation term and $\phi = 2\varepsilon_{ij}\varepsilon_{ij}$

The boundary conditions necessary to define the kinematics of the problem are specified by a combination of velocities, tractions, temperatures and heat fluxes. The differential equations are subjected to the boundary conditions

$$u_i = U_i(s)$$

$$t_i = t_i(s) \qquad (4.5)$$

$$T = T(s)$$

$$q = (kT_{,j})n_j(s) = q_c$$

Here t_i is the boundary traction component, q is the total heat flux, q_c is the convective heat flux and s is the boundary parameter - implying that the quantities are evaluated along the boundary contour for which n_j is the outward unit normal.

The equations (4.1 to 4.4) together with the boundary conditions (4.5) define the complete fluid flow problem and form a complete set necessary for determination of velocity, pressure and temperature fields in the fluid.

FIDAP can compute solutions to different kinds of flow fields depending on the options specified by the user. In isothermal flows, there are no temperature dependent properties and the energy equation is discarded. In weakly-coupled flows, the momentum equation is first solved independently for velocity and pressure fields. With a known velocity field the energy

equation is then solved directly for the temperature distribution. The properties are updated depending on the new temperature profile and the procedure is repeated until the preset tolerances are reached. Isothermal and weakly-coupled flows are the classes of problems that have been dealt with in this study. The third type or the strongly-coupled flows are for conditions that incorporate full set of equations includes simultaneous solution of all the three equations of change. It is not applicable to the present problem.

4.3 CONSTITUTIVE EQUATION

As mentioned in the previous section, in addition to the equations of change it is necessary to have a constitutive equation (an equation which expresses the relation between the stress and the rate of deformation) in order to solve for the unknown velocity and stresses. In choosing a constitutive equation, attention should to be paid to the rheological properties which can best characterize the particular flow problem that is being solved. Also caution must be exercised in selection of a constitutive equation since it is the mathematical representation of the fluid behavior. The FIDAP code can handle GNF constitutive equation in which the extra stress is a function of the rate of deformation. In FIDAP, for Newtonian fluid, the viscosity can be constant or temperature dependent. A number of non-Newtonian models, such as Bingham fluid and Power law model, are also provided. It is also possible to provide an user supplied subroutine in which an user defined viscosity empiricism link the stress and rate of deformation. For this thesis the subroutine option will be used.

Before discussing the different empiricism that may be employed for different section of the extruder, it will be helpful to review the flow conditions existing in the extruder. The choice of the viscosity function will depend on the temperatures existing in the extruder. At lower temperatures, particulate flow exists where as at higher temperature, the flow behavior is

similar to that of a melt [13-15, 25-31, 34, 36, 40-43]. As will be seen in section 5.1.2, the transition from particulate to melt flow for plasticized PVC blends takes place at 165 ° C. Both above and below 165 ° C (till 150 ° C), rigid and plasticized PVC has been modeled as a power law fluid [8, 31, 49]. In this thesis, plasticized PVC will be modeled as a temperature dependent power law fluid in which the viscosity empiricism, η, will be given by :

$$\eta = m|\dot{\gamma}|^{n-1} \qquad (4.6)$$

with both consistency term, m, and power law index, n, being Arrhenius type functions of absolute temperature. $|\dot{\gamma}|$ is the magnitude of the shear rate.

Alternatively, viscosity can be expressed in terms of shear rate and temperature in a single expression as

$$\ln\eta = f(\ln\dot{\gamma}, T) \qquad (4.7)$$

The ln(viscosity) will be a quadratic function of both ln(shear rate) and temperature. The viscosity expression still predicts shear thinning behavior. There will be two expressions for viscosity above and below 165 ° C. The detailed expressions will be presented in section 5.1.2.

PVC has also been known to display yield stress behavior at temperatures as high as 190 ° C, a phenomenon which could become quite important at temperatures of 150 or 160 ° C. Fluid models like Bingham and Herschel Bulkley can be used to predict the flow behavior at these temperatures.

The constitutive equation for Bingham fluid can be written as

$$\tau = -\left\{\eta_0 + \left[\frac{\tau_0}{|\dot{\gamma}|}\right]\right\}\dot{\gamma} \qquad \text{for } \tau \geq \tau_0 \qquad (4.8)$$

$$\dot{\gamma} = 0 \qquad \text{for } \tau < \tau_0$$

where τ is the shear stresss, τ_0 is the yield stress, η_0 is the Newtonian viscosity and $\dot{\gamma}$ is the shear rate.

The constitutive equation for Herschel Bulkley fluid can be written as

$$\tau = -\{m\,|\dot{\gamma}|^{n-1} + \left[\frac{\tau_0}{|\dot{\gamma}|}\right]\}\dot{\gamma} \qquad \text{for } \tau \geq \tau_0 \qquad (4.9)$$

$$\dot{\gamma} = 0 \qquad \text{for } \tau < \tau_0$$

where τ_0 is the yield stress and m and n are power law parameters.

If τ in equations 4.8 or 4.9 is divided by $\dot{\gamma}$, the resultant expression for viscosity is obtained. The actual viscosity expression for the Herschel Bulkley fluid that will be used is as follows :

$$\eta = -\{m\,|\dot{\gamma}|^{n-1} + \left[\frac{\tau_0}{|\dot{\gamma}|}\,[1 - \exp(-N\dot{\gamma})]\right] \qquad (4.10)$$

The actual viscosity expression for the Bingham fluid that will be used is as follows :

$$\eta = -\eta_0 + \left[\frac{\tau_0}{|\dot{\gamma}|}\,[1 - \exp(-N\dot{\gamma})]\right] \qquad (4.11)$$

It has been shown by Papanastasiou [89] that incorporation of the exponential term (1 - exp (-N | γ dot. |)) with τ_y for Bingham fluid allows the Bingham fluid to be treated as a continuum with out any break for the flow and the non - flow regimes. Equation 4.11 holds uniformly in the yielded and unyielded region. It was shown by him that above a certain value of N, "a quick stress growth can be achieved at relatively very low strain which is consistent with the behavior of the material in its practically unyielded state." The reason why the temperature dependent power law expression is preferred over the expression incorporating yield stresses in the melt zones will be discussed in section 5.1.3. Briefly, the importance of the

yield stress effect diminishes with increase in temperature and the power law model adequately describes the fluid behavior at temperatures existing in the melt zones.

Also, the isothermal solids conveying will be modeled as fluid having yield stress and using the viscosity emiericism in eqns. 4.10 or 4.11. Here again it will be seen in section 5.1.3 that Herschel Bulkley model will be used. It is assumed that fluids at low temperatures can approximate solids behavior. The expression developed in refs. [53] and [54] assumed that the solids moved as a plug in the solids conveying zone. Similar profiles are obtained for fluids with yield stresses when they flow through rectangular channels or circular pipes. There is is a core region where the plug flow occurs and where the stresses are less than yield stress. The similarity in shape of the velocity profiles between the solids and the fluids with yield stress and that fluids with yield stress interpret the fluid behavior more correctly for PVC at low temperatures are the rationales behind attempting to model solids conveying as fluids with yield stress using the Fidap code.

4.4 MESH GENERATION

In the finite element method, the problem domain is divided into a number of geometrically simple elements. Their number, type, size and shape and density have to be given consideration during the discretizing process. The domain has to be discretized to be as close to the exact geometry as possible with the admissible types of elements. Another important factor needs to be considered while discretizing the domain. This is to have finer meshes where the gradients of the spatial variable are steep. In general a refined mesh is necessary where there is a large change in geometry, material properties, boundary conditions or solutions of the spatial variables. The discretizing errors may be reduced by increasing the number of elements. The increase in the number of elements improves the accuracy of the solution but at the expense of additional computational costs. Also, the sol-

utions are not affected by the mesh refinement beyond a certain degree. Fidap allows mesh refinement in which all the previous nodes are incorporated in the finer mesh but retains the same order of the approximation for the solution is retained.

It has been stated previously that when high gradients of the field variable exist, it is advisable to use a finer mesh where as a coarse mesh suffices in areas of lower gradients. While refining the meshes, one also needs to be careful regarding the aspect ratios of the elements. If the fluid behavior is highly non-Newtonian (i.e. the fluid is characterized by low power law index, 'n' and high 'm'), the aspect ratios of the elements have to be lower than fluids whose behavior is more close to Newtonian. If aspect ratios are too large the stiffness matrices (associated with the algebraic system of equations for each element) is ill-conditioned and it may be difficult to invert them.

The FIDAP's mesh generating program, FIMESH, was used for 2-D and 3-D discretization of the single screw extruder. Elements are usually categorized in the FIMESH program by combination of velocity-pressure approximation used for the element. The temperature is approximated by the same basis function as the velocity. Four node quadrilaterals and eight node bricks are the elements used in 2-D and 3-D cases, respectively. For four node quadrilaterals, the velocity components and the temperatures are approximated using bilinear interpolation functions. For eight node brick they are approximated by trilinear interpolation functions. For both of these elements, the pressure discretization is done by a piecewise constant discontinuous pressure approximation. The geometrical coordinates of the problem domain, the element type and the input boundary conditions are used to generate the input file for the FIDAP code. The details of the mesh generation procedure can be found in the FIDAP manuals [85].

4.5 PENALTY FUNCTION APPROXIMATION

Often the finite element method is not applied directly to the system of equations presented above. By using the penalty function method, the continuity equation is treated as a constraint and the continuity requirement is weakened and replaced by

$$U_{i,i} = -\varepsilon P \qquad (4.12)$$

where ε is the penalty parameter and typically is in the order of 10^{-10} to 10^{-12} for the problem in this research work. The penalty finite element model allows the computation of velocities at each element of the finite element mesh. Since the pressure is absent in the model, it should be computed by some alternate means and is recovered in the post-processing step from the velocity field by use of the expression $P = \frac{1}{\varepsilon} U_{i,i}$.

The penalty method offers a significant advantage over other formulations because by penalizing or decreasing one degree of freedom at each node, it reduces the number of unknowns that have to be solved. In problems involving large numbers of nodes, such as a 3-D or large 2-D problems, the reduction of the matrix size leads to a reduction in the computer storage capabilities and computation time. The penalty method will be used solving the simulation problem described in the research objectives. The magnitude of the viscosity determines the value of the penalty parameter [84]. If ε is too large, then the constraint is not satisfied. On the other hand if it is too small, the computer-round off errors can lead to trivial solutions. In the current study, there is a large variation in viscosity with temperature but a penalty parameter value of 10^{-12} was found good for the whole range.

Earlier a description of the fluid flow problem that is being studied has been presented as a continuous formulation. The discretization of the continuous problem will be presented next and will be followed by the finite element formulation of the discretized system.

4.6 DISCRETIZATION OF THE CONTINUOUS PROBLEM

The finite element method is a piecewise application of the variational method that leads to a set of algebraic equations with finite degrees of freedom. The degrees of freedom depend on the mesh size and the number of field variables. Initially the method focuses on one element. The discrete representation of the entire region is obtained through an assemblage of elements such that the inter-element continuity of velocity and temperature is maintained.

The finite element method begins with discretization of the continuous domain into elements which have simple geometries. The elements are fixed in space and within each element the dependent variables are approximated by interpolating functions. These functions are used to interpolate the dependent variables according to the number of nodes in the element. An individual element is isolated and the temperature, velocity and pressure fields are approximated by

$$\begin{aligned} U_i(x) &= \phi^T U_i \\ p(x) &= \psi^T P \\ T(x) &= \theta^T T \end{aligned} \qquad (4.13)$$

where U_i, P and T are column vectors of elemental nodal point unknowns and ϕ, ψ and θ are column vectors of the interpolating functions. The same interpolating functions (also called basis functions) are applicable for velocity and temperature, which is an unnecessary but cost-effective restriction. The pressure interpolating function can be of lower order than either the velocity or temperature interpolating functions, but as stated earlier it will be penalized.

The substitution of the approximations into the field equations and the boundary conditions yield the following set of equations :

$$\begin{aligned} f_1(\phi, \psi, \theta, U_i, P, T) &= R_1 \quad \text{Momentum} \\ f_2(\phi, U_i) &= R_2 \quad \text{Incompressibility} \\ f_3(\phi, \theta, U_{i,i}) &= R_3 \quad \text{Energy} \end{aligned} \qquad (4.14)$$

where R_1, R_2 and R_3 are the residual errors resulting from the approximation of equation 4.1 to 4.5.

As stated previously, the Galerkin form of weighted residuals seek to reduce these errors to zero by making the residuals orthogonal to the interpolation function for each element.

Applying the Galerkin procedure to equations 4.14 and use of approximations in equation 4.13lead to the following equation :

$$[\int_v \psi \frac{\partial \phi^T}{\partial x_i} \, dv \,] \, U_i = 0 \; [- \varepsilon (\int_v \psi \psi^T \, dv \,) \; P] \qquad (4.15)$$

$$\int_v (\rho \phi U_j \frac{\partial \phi^T}{\partial x_j} \, dv \,) \, U_i + [\int_v \frac{\partial \phi}{\partial x_i} \psi^T \, dv \,] P + [\int_v \eta \frac{\partial \phi}{\partial x_j} \frac{\partial \phi^T}{\partial x_j} \, dv \,] \, U_i + [\int_v \eta \frac{\partial \phi}{\partial x_j} \frac{\partial \phi}{\partial x_i} \, dv \,] \, U_j$$
$$= \int_s t_i \phi \, ds. \qquad (4.16)$$

$$[\int \rho C_p \phi U_j \frac{d\theta^T}{dx_j} \, dv \,] T + [\int_v k \frac{d\theta}{dx_j} \frac{d\theta^T}{dx_j} \, dv \,] \, T = - \int_s qc \, \theta \, ds + \int_v \eta \, \Phi \, \theta \, dv. \qquad (4.17)$$

In deriving the above equations, the Green-Gauss theorem has been used to reduce the second order diffusion terms in the momentum and energy equation to the first order terms plus a surface integral. The appearance of the surface integrals containing the applied surface stresses (traction) and heat fluxes correspond to the natural boundary conditions for the problem. Also the inertial terms in the momentum equations have been considered as a weakly- coupled non-isothermal flow in Fidap can not exclude the inertial terms in the momentum equation without excluding them or the convective terms in the energy equations. The exclusion of the latter will introduce errors in an non-isothermal flow problem. Anyway, the contribution from the inertial terms will be negligible compared to the viscous terms because of the low Reynolds number in these problems.

Combining the momentum-energy equation into a single matrix equation produces a system of the form:

$$
\begin{bmatrix}
2K_{11} + K_{22} + K_{33} & K_{12} & K_{13} & 0 & -C_1 \\
K_{21} & K_{11} + 2K_{22} + K_{33} & K_{23} & 0 & -C_2 \\
K_{31} & K_{32} & K_{11} + K_{22} + 2K_{33} & 0 & -C_3 \\
0 & 0 & 0 & L_{11} + L_{22} + L_{33} & 0 \\
-C_1^T & -C_2^T & -C_3^T & 0 & 0
\end{bmatrix}
\begin{bmatrix} U_1 \\ U_2 \\ U_3 \\ T \\ P \end{bmatrix}
+
\begin{bmatrix}
\sum A_i(U_i) & 0 & 0 & 0 & 0 \\
0 & \sum A_i(U_i) & 0 & 0 & 0 \\
0 & 0 & \sum A_i(U_i) & 0 & 0 \\
0 & 0 & 0 & \sum D_i(U_i) & 0 \\
0 & 0 & 0 & 0 & 0
\end{bmatrix}
\begin{bmatrix} U_1 \\ U_2 \\ U_3 \\ T \\ P \end{bmatrix}
= \begin{bmatrix} F_1 \\ F_2 \\ F_3 \\ G \\ 0 \end{bmatrix} \qquad (4.18)
$$

where

$$K_{ij} = \int_v \eta \frac{\partial \phi}{\partial x_j} \frac{\partial \phi^T}{\partial x_i} \, dv$$

$$C_i = \int_v \frac{\partial \phi}{\partial x_i} \psi^T \, dv$$

$$L_{ij} = \int_v k \frac{\partial \theta}{\partial x_i} \frac{\partial \theta}{\partial x_j} \, dv$$

$$A_i(U_j) = \int_v \rho \phi U_j \frac{\partial \phi^T}{\partial x_i} \, dv$$

$$D_i(U_j) = \int_v \rho C_p \theta U_j \frac{\partial \phi^T}{\partial x_i} \, dv$$

$$F_i = \int_s t_i \phi \, ds$$

$$G = -\int_s q_c \theta \, ds + \int_v \eta \Phi \theta \, dv$$

When a penalty formulation is used the row and column corresponding to the variable P are deleted and the term $\frac{1}{\varepsilon} CM_p^{-1}C^T U$ is added to the left-hand side of the equation where $C = (C_1, C_2, C_3)^T$ and $M_p = \int_v \psi\psi^T dv$.

Writing $U = (U_1, U_2, U_3)^T$, $L = L_{11} + L_{22} + L_{33}$, equation 4.10 can be reduced to the form:

$$\begin{bmatrix} A+K+\frac{1}{\varepsilon} CM_p^{-1}C^T & 0 \\ 0 & D+L \end{bmatrix} \begin{bmatrix} U \\ T \end{bmatrix} = \begin{bmatrix} F \\ G \end{bmatrix} \quad (4.19)$$

In the above matrix form, A and D represent the convection of momentum and energy, respectively. K and L represent the diffusion of momentum and energy respectively. F and G are the forcing functions for the system in terms of traction, heat flux and viscous dissipation.

As mentioned previously, the above derivation has focused on a single element. These element equations for the entire domain are assembled and superimposed in such a way that the continuity of velocity and temperature is preserved at all the nodes. The continuity is enforced through approximate summation of equations for nodes common to adjacent elements. This assembly procedure results in a system of matrix equations of the form

$$[K]\, U = F. \quad (4.20)$$

where [K] is the global stiffness matrix, U is the unknown global vector of the dependent variables at the nodes and F is the global vector composed of external forces and and boundary conditions.

4.7 EVALUATION OF THE MATRIX COEFFICIENTS

In the last section various element matrices have been defined. They are integrals of the various interpolation functions and their derivatives. The evaluation of these integrals is carried out by the use of a numerical quadrature procedure after reducing the matrix equations in terms of the natural coordinates of the elements.

Although the FIDAP program allows a few alternatives to the user, the Gauss quadrature method is generally used. In general the fourth order integral is used for evaluation of the diffusion terms in the stiffness matrix when dealing with non-Newtonian fluids. Again for the evaluation of the inertial term, the integration order can be 3 or 4 depending on the type of element being considered.

For evaluation of the penalty term, the reduced integration method is adapted as the use of full Gauss quadrature leads to over-constraining the system. Generally, the reduced integration uses a one point Gauss quadrature for multilinear elements. These include the 4 node quadrilaterals or the 8 node bricks that have been used in the present simulation problem. It leads to piecewise constant pressure for multilinear elements.

4.8 BOUNDARY CONDITIONS

In this section the various boundary conditions that have been imposed will be discussed. The specified velocities and temperatures constitute the essential boundary conditions. The number of specified primary variables at the nodes result in a decrease in the number of degrees of freedom. In the present problem no slip boundary conditions are imposed, i.e. all velocities are constrained to be zero at the screw walls and fluid in contact with

the barrel will have the barrel velocities. The heated barrel temperature is specified as temperature boundary condition of the fluid in contact with the barrel.

Two types of surface forces or fluxes are possible in the current simulation problem. They are applied heat flux and applied traction forces or stresses. The applied stress boundary condition is of the form

$$F_i = \int_s \phi t_i ds = \int_s \phi \sigma_{ij} n_j ds \qquad (4.21)$$

By expressing the surface of the element parametrically, the boundary conditions can be expressed in an integral form similar to the coefficient matrices. These are then evaluated by numerical integration methods. The process is detailed in the FIDAP manual [85]. It ought to be remembered that the applied stress boundary conditions are in terms of the total traction vector. The total traction vector is dotted with the unit normal to the boundary to obtain the normal stress on the boundaries. The normal stress usually have contributions from both the pressure and the viscous terms and reflect their net effect. In absence of normal stresses due to the viscous forces in the constitutive equation, the normal component of the total traction vector essentially represents the isotropic pressure term. In the present problem the extruder flow is modeled by the superimposition of a drag and a positive pressure-driven flow in the extruder conduit. The pressures at both end of the mesh are specified as the net stress at the two ends.

Since viscous dissipation is not going to be considered, the heat flux is of the form

$$G = \int_s \theta q_c ds \, . \qquad (4.22)$$

A computation procedure similar to the stress boundary condition is also carried out in this case. The screw is solid and can not dissipate any heat flux for all practical purposes except where it connects to the motor. This fact is specified in the heat flux boundary condition as zero heat flux at the walls and at the root of the screw.

4.9 SOLUTION PROCEDURE

The solution of the assembled discrete matrix equation **[K(U)] U = F** is the most time-consuming stage of the analysis. Here K is the global stiffness matrix, U is the unknown global vector composed of the dependent variables and F is the global vector composed of external forces and boundary conditions. Owing to the amount of time involved in this process, the selection of a particular solution strategy is important. This is especially true in 3-D cases for highly nonlinear problems or problems with coupled physical phenomena. Thus for a set of nonlinear equations, certain facts such as the solution algorithm, convergence rate and efficiency, radius of convergence, etc. are key issues. The degree of nonlinearity of the equation dictates the use of the type of iterative procedure that will be employed.

The fixed point methods and the Newton type methods are the two categories of solution strategies. Successive substitution (SS), which belongs to the first category, has a large radius of convergence but its rate of convergence is slow. Newton-Ralphson (NR) and Quasi-Newton (QN) methods belong to the second category in which a Jacobian of the stiffness matrix has to be evaluated. In the NR method, the convergence is quadratic and thus faster if only the initial solution vector is within the radius of convergence. Unfortunately, the radius of convergence can be small and the LU decomposition of the stiffness matrix and the Jacobian evaluation at each step make the Newton-Ralphson method as time consuming as the successive substitution method. In the Quasi-Newton method, the faster convergence rate of the NR method is still obtained. However the LU decomposition and the updating of the Jacobian matrix is performed in a simpler manner at each iteration step rather than recomputing the Jacobian every time. Here the Jacobian is updated by a first order approximation of the previous Jacobian matrix.

Keeping the above facts in mind, the following iteration strategy has been employed. An initial solution associated with the linearized Stokes solution is first obtained. Then about 5 to 10 iterations are performed using the S.S. method to bring down the relative error below

0.01 and this usually brings the radius of convergence within the radius of the Newton methods. Finally the Q.N. method is used for successive iterations until the final tolerance is achieved. For 2-D problems as the solution times are relatively small compared to 3-D problems, S.S. was used to solve all the way till the final tolerance limit. The time involved in updating the input file for new tolerance limit, change the solution procedure and resubmitting the revised input files for the 2-D cases did not justify the amount of time saved by changing the solution procedure.

5.0 RESULTS AND DISCUSSIONS

In this chapter the results of the effect of plasticizers on the extrusion of PVC will be presented. The chapter will be divided into three main sections. The first two will cover the experimental aspects of the study and the last will cover the numerical results. The purpose of the experimental sections will be to satisfy the first two objectives of the research proposal. In section 5.1 the effects of plasticizers on physical properties that are important to the extrusion process will be discussed. Having gained the knowledge of the physical properties, the effects of the plasticizers on the extrusion process will be presented in section 5.2. The findings of section 5.2 will be correlated with those from the first section. Also the efforts will be directed at understanding the mechanisms of the extrusion of plasticized PVC. Numerical results will be presented in the last section of the chapter. The tables referred to in this chapter are placed at the end of this chapter.

5.1 EFFECTS OF PLASTICIZERS ON PHYSICAL PROPERTIES

Before the effects of plasticizers on the extrusion process are presented, the effects of plasticizers on physical properties that are known to govern the extrusion characteristics like pressure development, flow rates, temperature profile, etc. will be discussed. Some of these physical properties have been incorporated as input variables in the existing numerical models and will also form the input variables for the proposed models. These properties can be classified as rheological, thermal and frictional properties. Frictional properties are not required for the proposed solids conveying model but will be used to test the proposed models to the existing ones. The proposed solids conveying model entails determination of the yield stress and results of such tests will also be included in this section. In the following text, the DIDP, DHP and DOP plasticized dry blends will be referred to as DIDP dry blend, DHP dry blend and DOP dry blend, respectively. Similarly, the three plasticized PVC pellets will be referred to as DIDP pellets, DHP pellets and DOP pellets in the rest of this thesis.

5.1.1 Viscosity Measurements

The viscosity shear rate data for the three dry blended PVC mixes between 150 and 190 ° C are shown in Figures 5.1 to 5.5 and with detailed values in Tables 5.1 to 5.3. The viscosity-shear rate data for the pelletized samples for the same temperature range are shown in Figures 5.6 to 5.10 and with detailed values Tables 5.4 to 5.6. In Figures 5.1 to 5.10, it was not possible to represent the error bars as they are of the same size as the symbols representing each data point. The spread of the data about the reported mean is 3 to 5 %. To ensure an easy comparison between viscosities of different mixes, Tables 5.9 and 5.10 have

been constructed. Here for a range of temperature and shear rates, the viscosities of DHP and DOP plasticized PVC dry blends and pellets have been expressed as the ratio of the DIDP plasticized PVC dry blend and DIDP plasticized PVC pellet viscosity, respectively. The shear rates have been chosen so that they cover the entire range of shear rates that were encountered in the extruder for screw speeds between 15 and 45 rpm. The viscosities used in preparing Tables 5.9 and 5.10 were calculated using the power law parameters from Tables 5.7 and 5.8. These power law parameters, between 150 and 190 ° C, were obtained by fitting power law models to the viscosity shear rate data for each dry blended and pelletized PVC samples in tables 5.1 to 5.6. Statistical regression methods were used to calculate the power law parameters.

A comparative study of the effects of the plasticizers on the viscosities of the dry blends reveal certain trends. It is obvious from Figures 5.1 to 5.5 that for the dry blends, the DIDP mixes exhibit the highest viscosity followed by DOP and DHP mixes, respectively. When compared to a 2 to 3 % spread in the data at higher temperatures and 3 to 5 % spread at lower temperatures, the difference in viscosity between DIDP and DHP dry blends appear to be significant at all temperatures between 160 and 190 ° C. This can be observed from the viscosity ratios between DIDP and DHP dry blend as seen from Table 5.9. The differences in viscosities are higher for lower shear rates, and these differences diminish as the shear rates are increased. For 150 ° C and above a shear rate of 20 1/s, the differences in viscosity between DIDP and DHP dry blends drop sharply. Although it is larger than the deviation in the data, a difference in viscosity of 6 to 7 % may not be construed as significant because of the uncertainty in the nature of the flow at these low temperatures, The uncertainty in the nature of the flow arises owing to the behavior of the plasticized PVC at low temperatures such as 150 ° C. The flow of plasticized PVC at these low temperatures take place more by slippage at the wall than by molecular deformation [13,14,28] and it might not be proper to characterize the flow by viscosity-shear rate data which do not take into account the effect of the slippage at the walls. A look at the power law parameters in Table 5.7 also demonstrates the highly non-Newtonian behavior of the PVC mixes at 150 and 160 ° C. As expected as the temperature

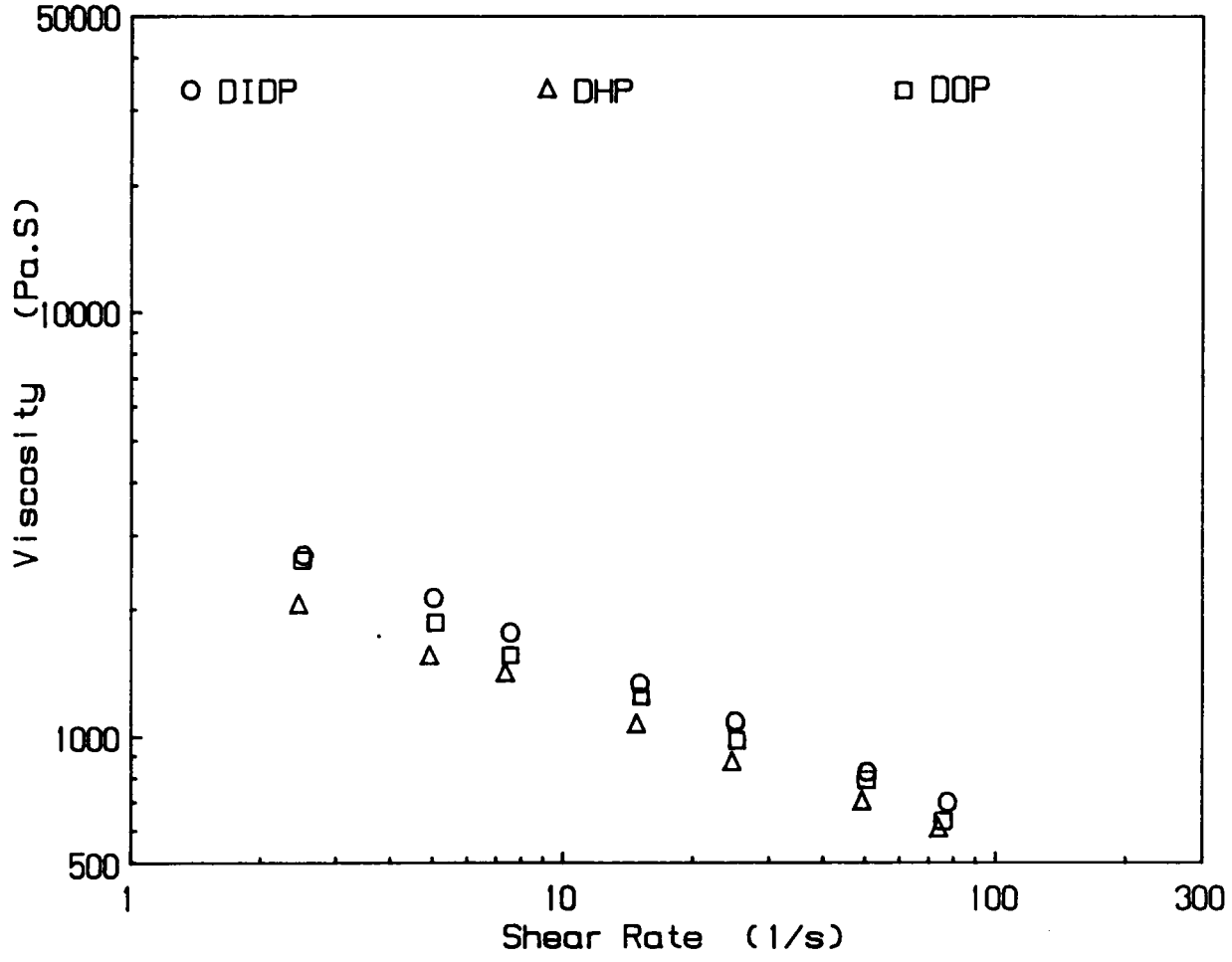

Figure 5. 1. Viscosity Shear Rate Data for PVC dry blends at 190 ° C

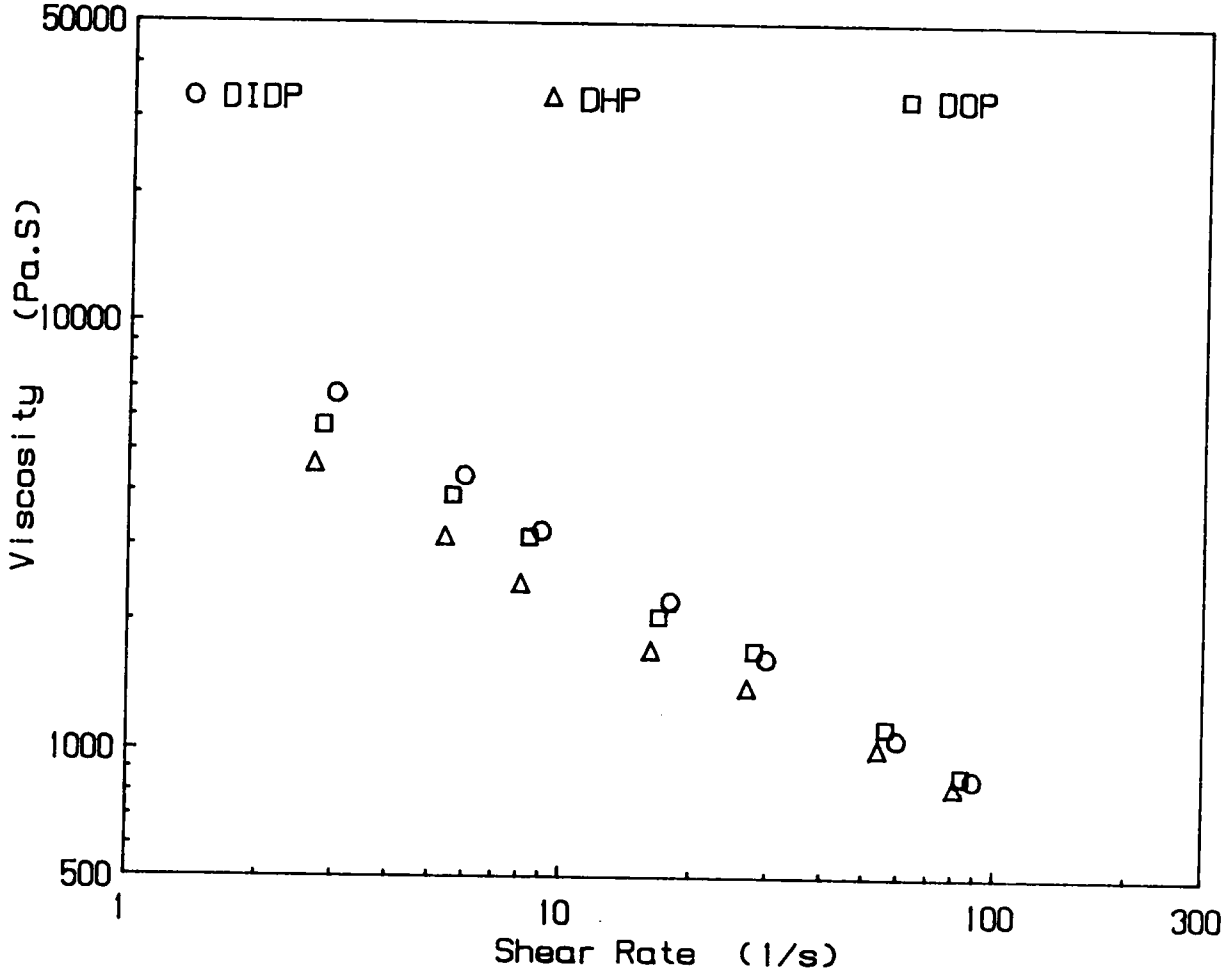

Figure 5. 2. Viscosity Shear Rate Data for PVC dry blends at 180 ° C

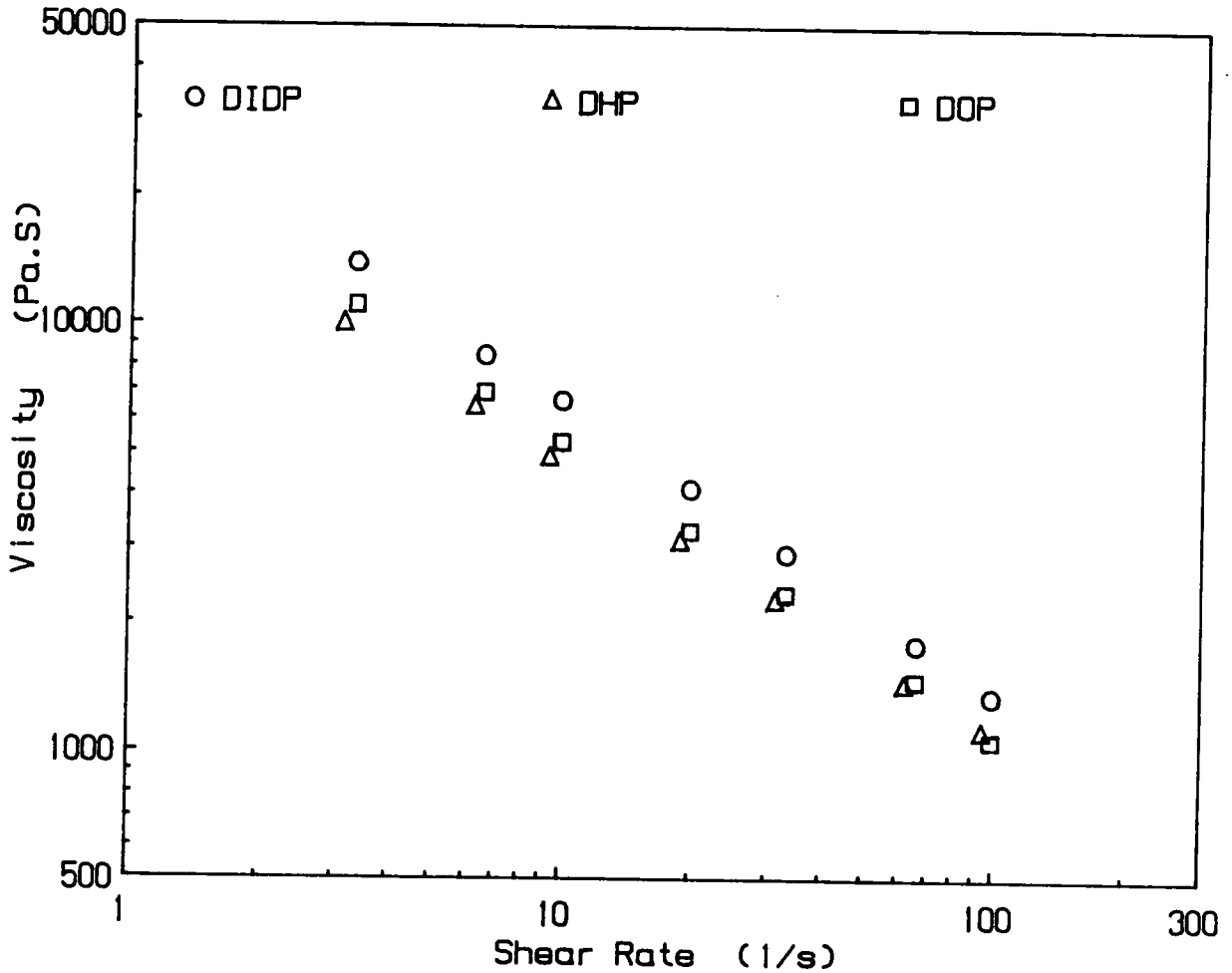

Figure 5. 3. Viscosity Shear Rate Data for PVC dry blends at 170 • C

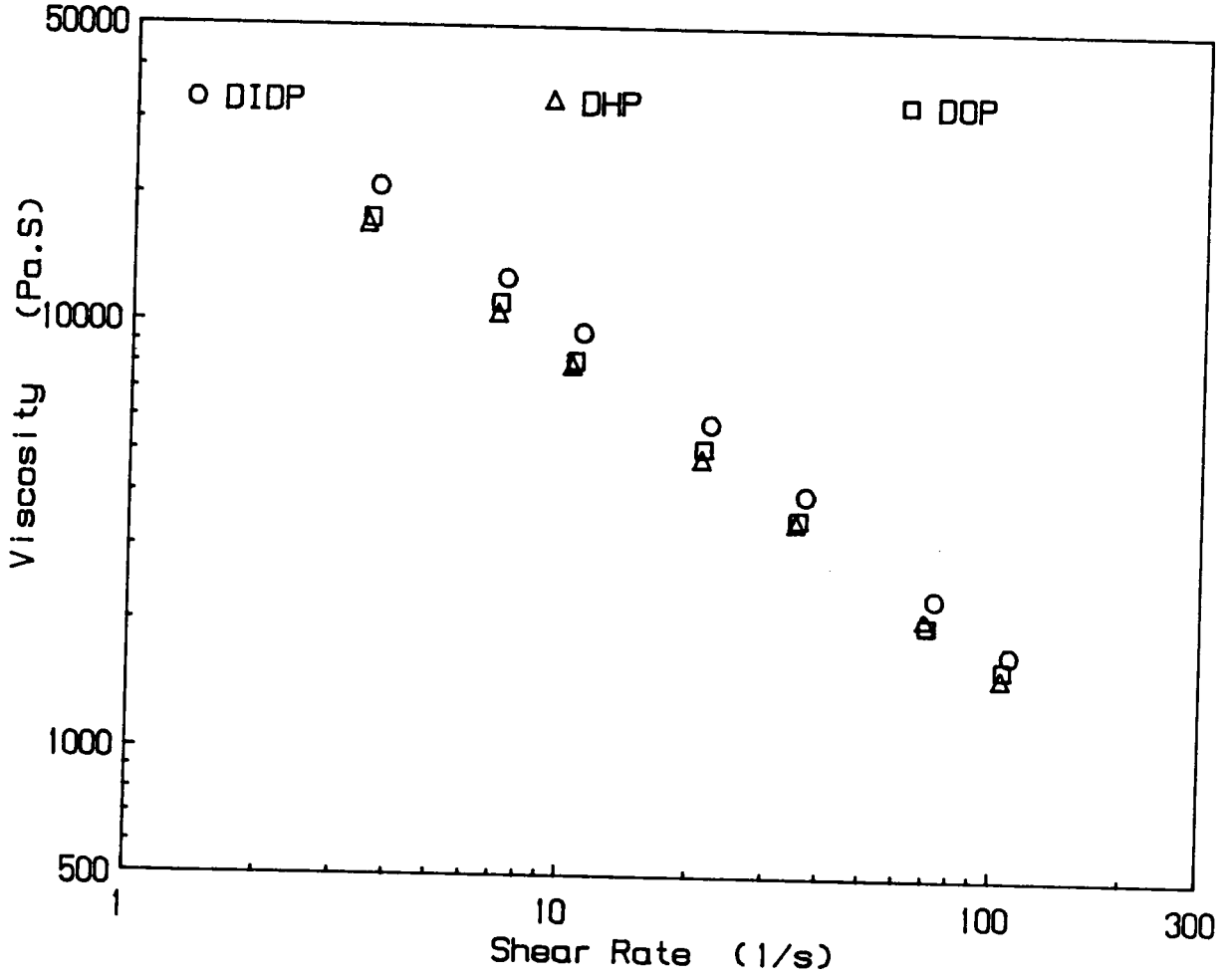

Figure 5. 4. Viscosity Shear Rate Data for PVC dry blends at 160 ° C

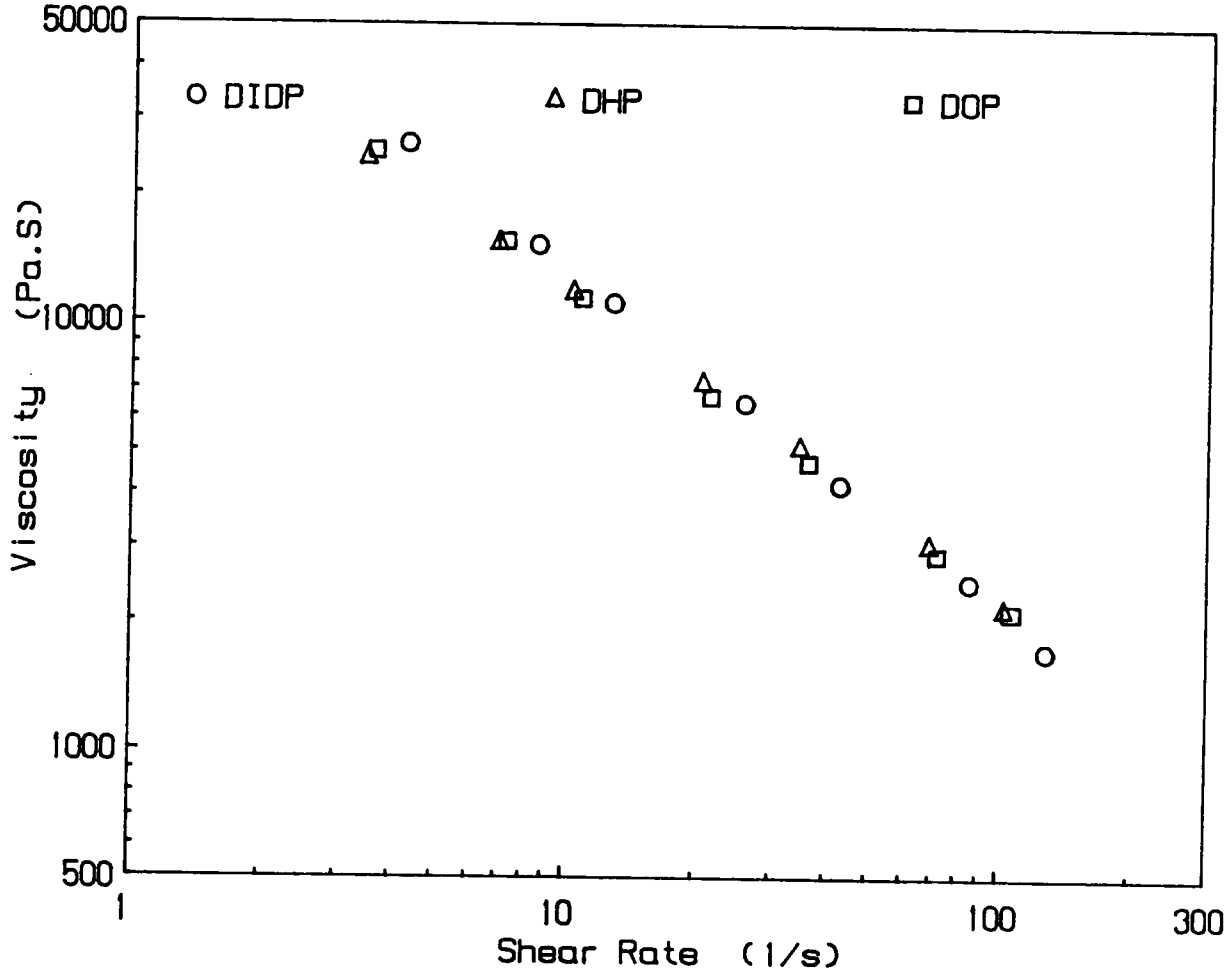

Figure 5. 5. Viscosity Shear Rate Data for PVC dry blends at 150 ° C

decreases, the power law index, n, decreases and the consistency term, m, increases. The effect of temperature on power law parameters follow the same trend for all the three blends. In general plasticizers tend to reduce the viscosity of PVC, but between 160 and 190 ° C for the same plasticizer loading, the viscosity of DHP plasticized dry blend is substantially lower than that of the DIDP plasticized dry blend.

A comparison between the DIDP and DOP dry blend viscosities indicates a trend similar to that between the DIDP and the DHP dry blends, but the difference in viscosity is less distinctive as seen in Table 5.9. At 180 and 190 ° C, the differences in viscosities between the DIDP and the DOP dry blends are not as large as was the case for the DIDP and the DHP dry blends. But considering the high degree of repeatability of experimental measurements and lower deviation about the reported mean at high temperature, the DIDP dry blend still seems to exhibit a higher viscosity. The differences in viscosities of DIDP and DOP dry blends at 170 and 160 ° C are more pronounced than at the higher temperatures but the data at 150 ° C precluded any definite conclusions.

The general direction or the trend of the viscosity shear rate data for the pellets are very similar to those of the dry blends. Here also, the DIDP pellets show substantially higher viscosities than the DHP pellets between 160 and 190 ° C. The differences diminish with increase in shear rates. Additionally at 150 ° C, the differences appear to be significant at lower shear rates but are indistinguishable at higher shear rates as observed from Table 5.10 and Figures 5.6 to 5.9. Also from Table 5.10, it is observed that the differences in viscosity between the DIDP and DOP plasticized pellets are not as large as the differences in viscosity between DIDP and DHP pellets. The viscosity differences between DIDP and DOP pellets at 190 ° C are marginally above the deviation in the data. Unlike the dry blends, the viscosity differences between the DIDP and the DOP pellets are more substantial at 180 ° C as well as 170 and 160 ° C. At 150 ° C, the difference in viscosities between the DIDP and the DOP pellets are not at all significant especially considering the nature of the flow at that low temperature. The presence of surface irregularities of the pellet extrudates and the difficulty in obtaining consistent data in the capillary rheometer at 150 ° C indicated a flow phenomenon possibly dominated

by slippage at the capillary wall. The severity of the problem was far greater for the pellets than for the dry blends. A definite correlation between the viscosities or the viscosity ratios of the dry blends and pellets could not be established. The pellet viscosities are slightly higher than the dry blend viscosities. Although in general the viscosity ratios appear to be slightly larger for the pellets than for the dry blends, there are some exceptions to this trend that can be identified by examining tables 5.9 and 5.10.

Before drawing any further conclusions on the effect of plasticizers on the viscosity data, it is necessary to focus on the compaction studies of plasticized PVC and then interpret the viscosity and compaction data together.

5.1.2 Compaction

It has been repeatedly emphasized in the literature that compaction and fusion play a dominant role in the melt flow of PVC [21,22,65,66]. The studies of the effect of plasticizer on the fusion of PVC have been attempted through observations of the melting mechanism in section 5.2.2. In this section, the effect of plasticizers on compaction has been reported by observing their effect on density measurements. Also, these tests were used to provide support for the dual-valued activation energy of PVC melt flow that has been detected so often in the past [25 - 28]. In chapter 3, two different methods for density measurements have been outlined in detail for dry blends and pellets. In the first method, densities were obtained at discrete values of pressure at three different temperatures. A second type of test was done in which the densities were measured for continuous changes in the pressure. Both methods have been discussed in section 3.2.3. The results from both the continuous and discrete types of tests were compared for all the three plasticized PVC pellets. It was observed that the density values from both sets of experiments overlap each other in the pressure ranges above 4825 KPa (or 700 psi). This suggests that at least for the higher pressures, the density values from any one of the types of tests could be used in numerical calculations.

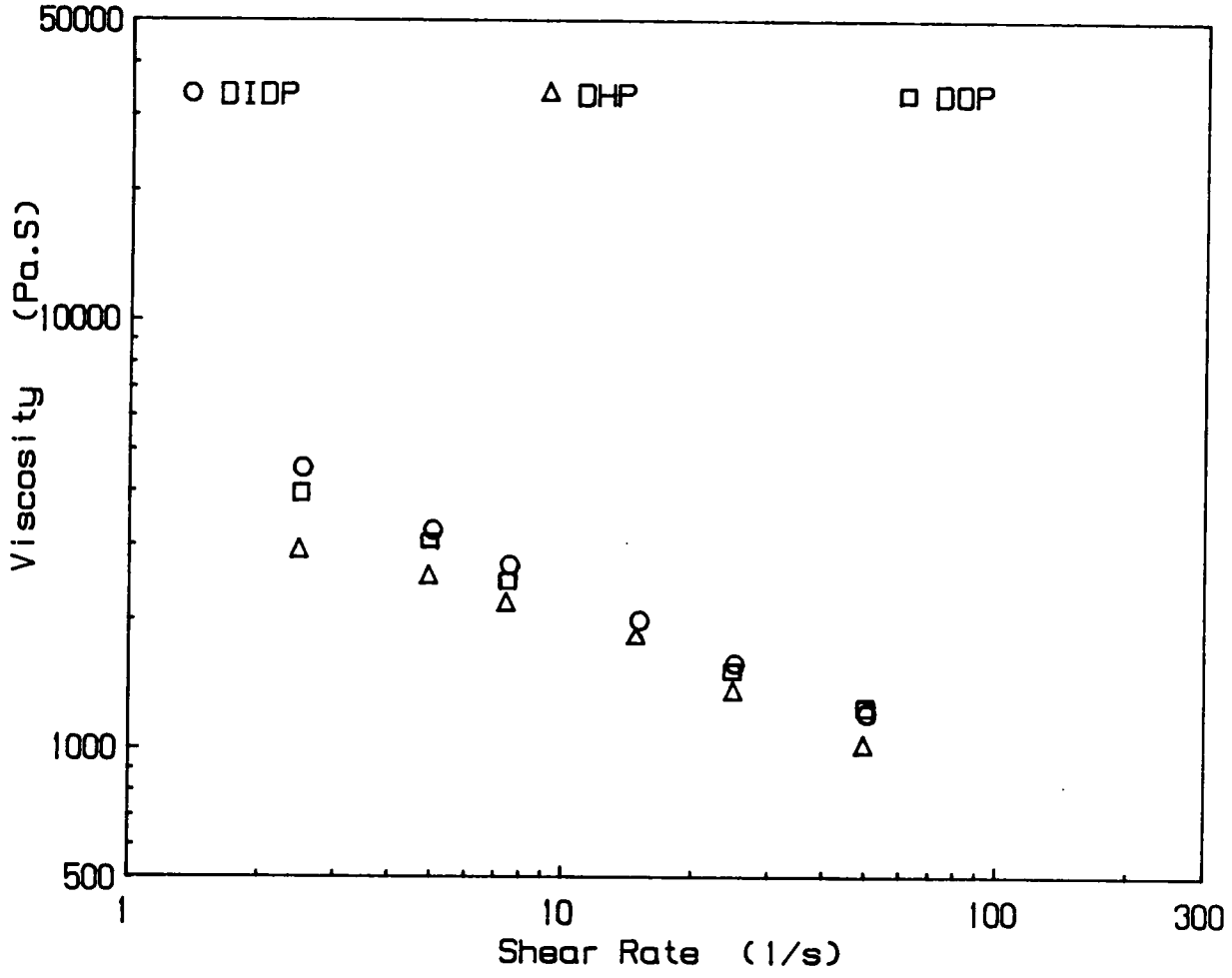

Figure 5. 6. Viscosity Shear Rate Data for PVC Pellets at 190 • C

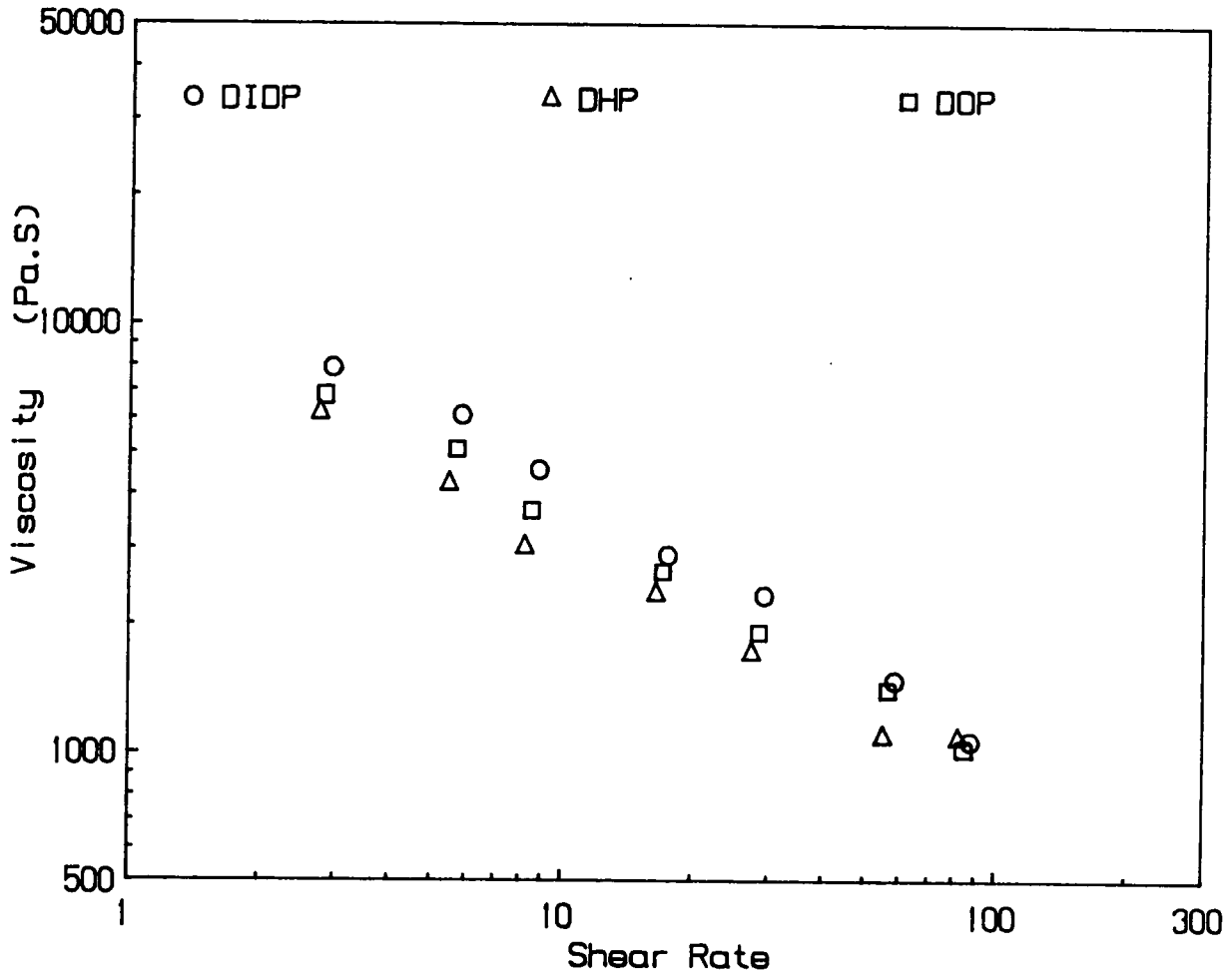

Figure 5. 7. Viscosity Shear Rate Data for PVC Pellets at 180 ° C

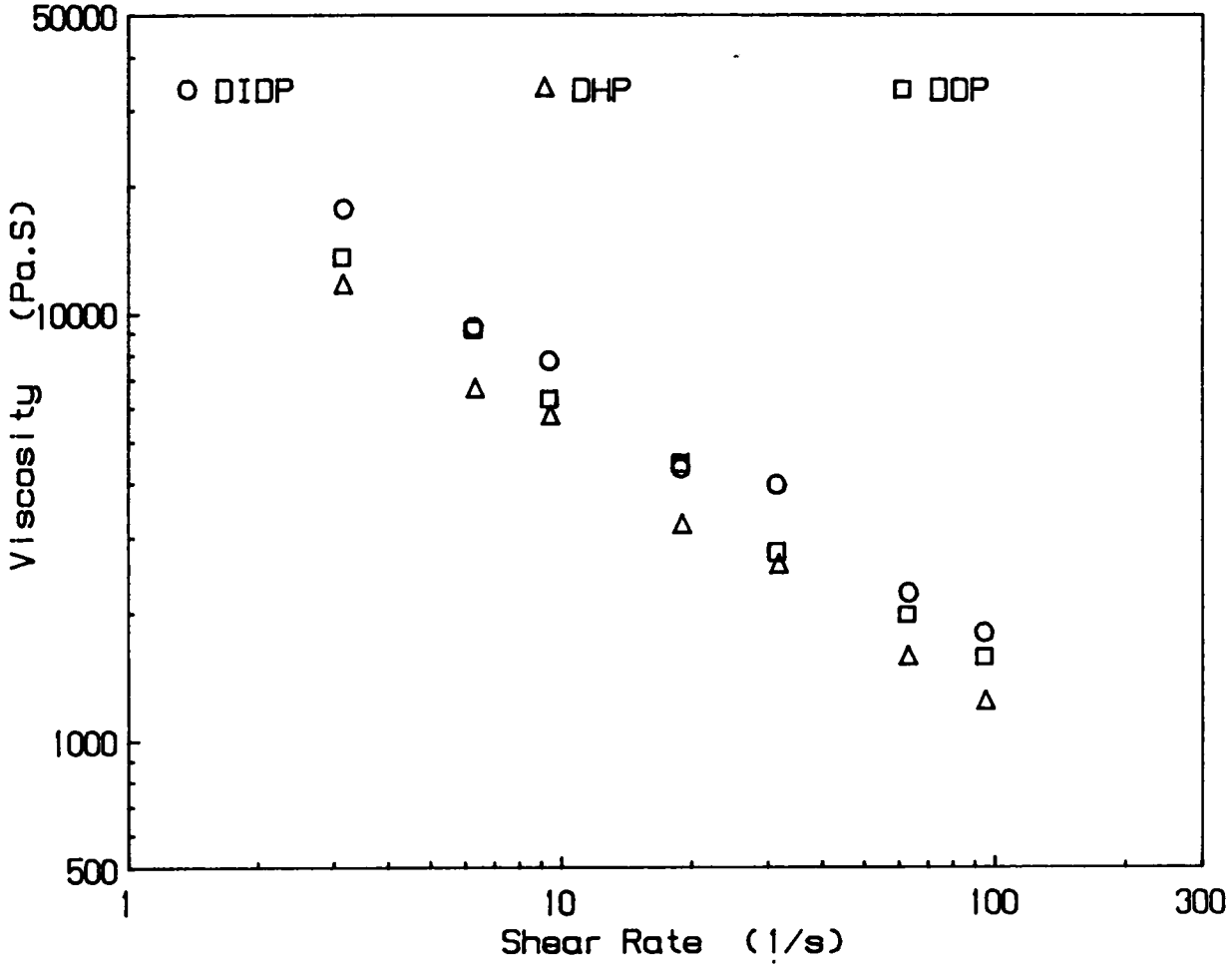

Figure 5. 8. Viscosity Shear Rate Data for PVC Pellets at 170 ° C

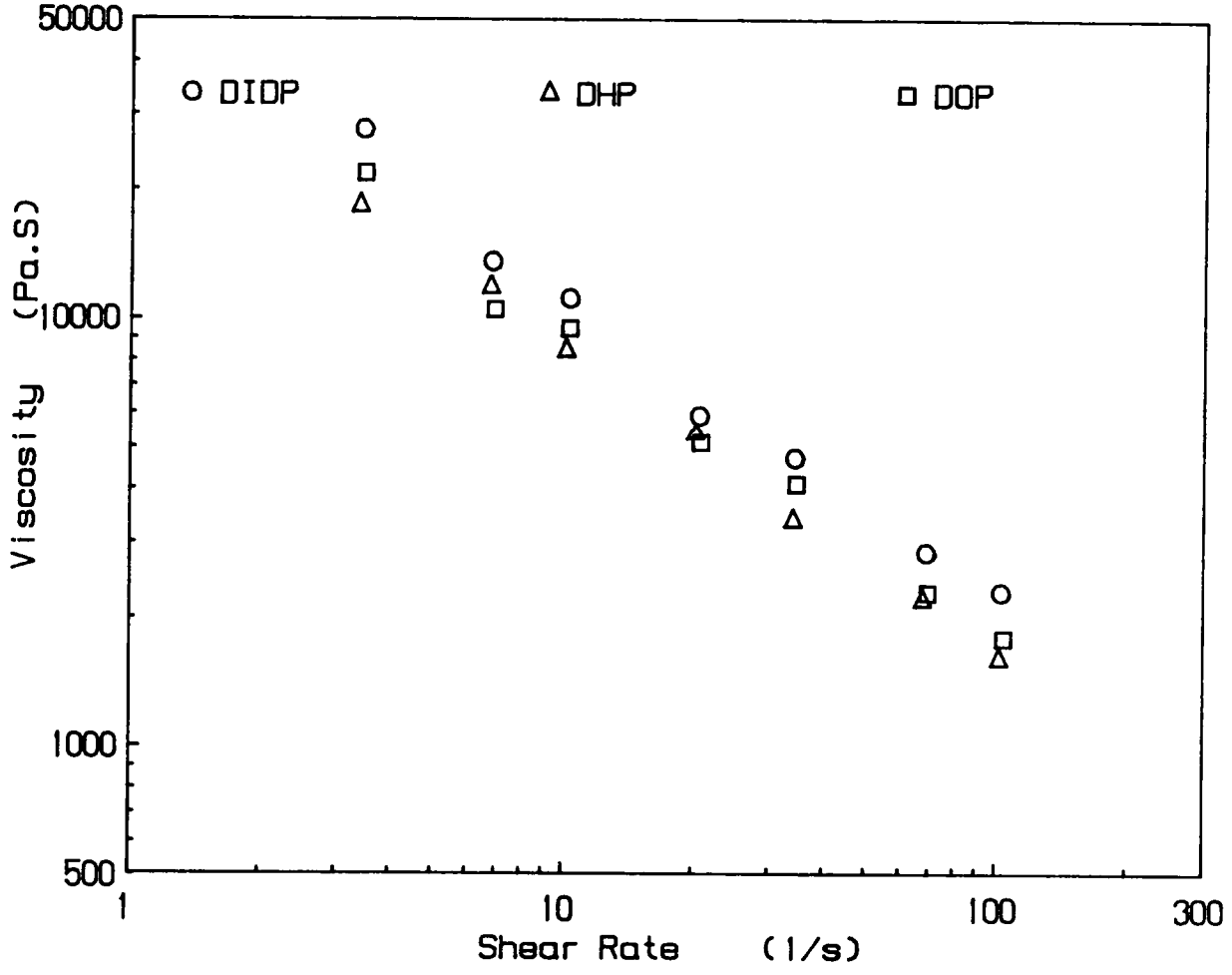

Figure 5. 9. Viscosity Shear Rate Data for PVC Pellets at 160 ° C

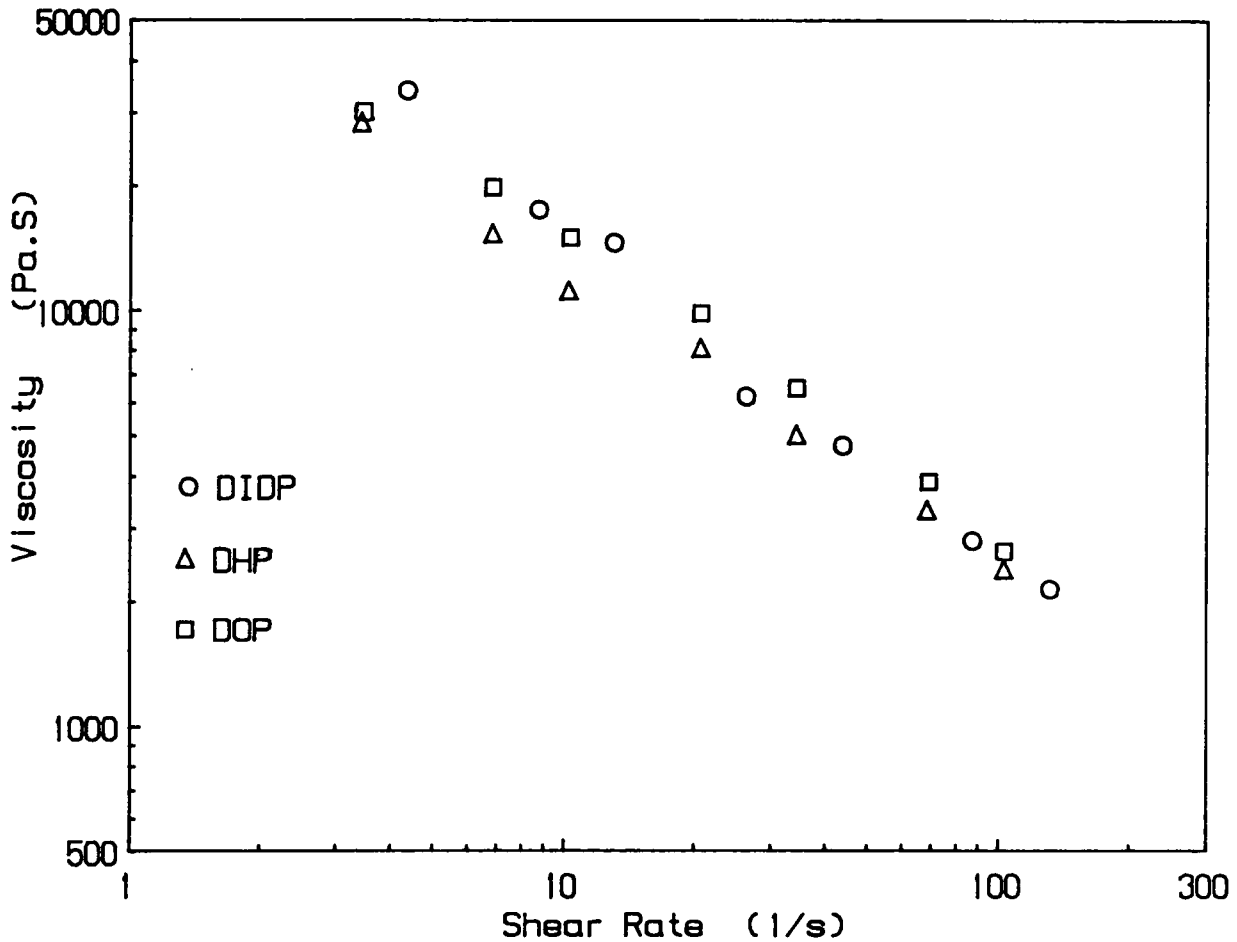

Figure 5. 10. Viscosity Shear Rate Data for PVC Pellets at 150 ° C

The density variations of PVC pellets with pressure at three different temperatures are presented in Figures 5.11, 5.12, and 5.13. For 150 and 170 ° C, the density increases with increase in pressure until about 500 to 600 psi (3450 to 4150 KPa). Beyond 600 psi (4150 KPa), the densities tend to become constant. This is expected because of the incompressible nature of the PVC melts at these temperatures. The higher density is attained through higher fusion between the PVC particles under high pressure or temperature. In the extruder runs, the maximum pressures encountered were in the range of 3300 psi (22750 KPa). Within this range, the plasticizers have no effect on density measurements. At 190 ° C, the initial growth in density with pressure is not observed, possibly because of faster fusion at higher temperature but here also the densities tend towards a constant value. No plasticizer effect on pellet density was discernible at 190 ° C. An important source of error lay in not being able to determine the uniformity of the compacted material in the barrel. At lower temperatures, the pellets appeared less compacted at the bottom than at the top. This nonuniform compaction was reduced by compressing only a small amount of material for each test and by increasing the number of repeat runs or experiments for each sample. This also aided in eliminating, the large variation in the data.

In contrast to the continuous tests, the densities of the dry blends were determined by the second method in which the densities were calculated at discrete pressure values. The results of the compaction test for the dry blended samples are presented in Figures 5.14 to 5.16. For a particular plunger speed, the variation in the values of the plunger force (and thus the pressure) was approximately below 4% and the variation in density was below 3%. It has been mentioned earlier that the plasticizer type did not affect the density of the pellets. The same conclusion was also true for the dry blends. Instead of constructing plots similar to Figures 5.11 to 5.13, which corroborated the conclusion that the plasticizer type did not affect the dry blend density, the densities of DIDP dry blends were plotted against pressures at three different temperatures of 160, 170 and 180 ° C in Fig. 5.14. Figures 5.15 and 5.16 were similarly constructed for DOP and DHP dry blends, respectively. From these figures it is observed that the densities are not affected by temperature changes beyond 160 ° C In other words above

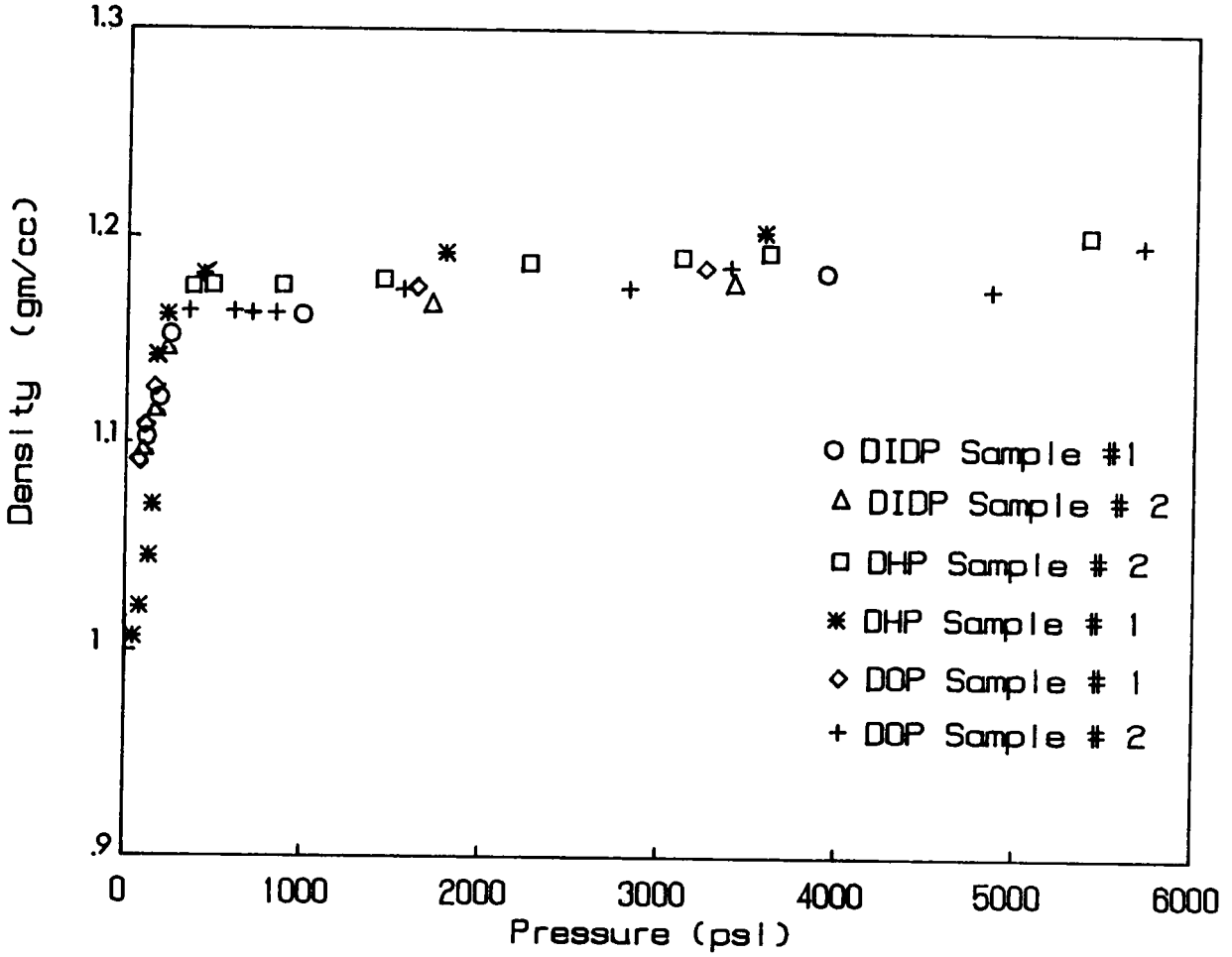

Figure 5. 11. Density of Plasticized PVC Pellets at 150 ° C

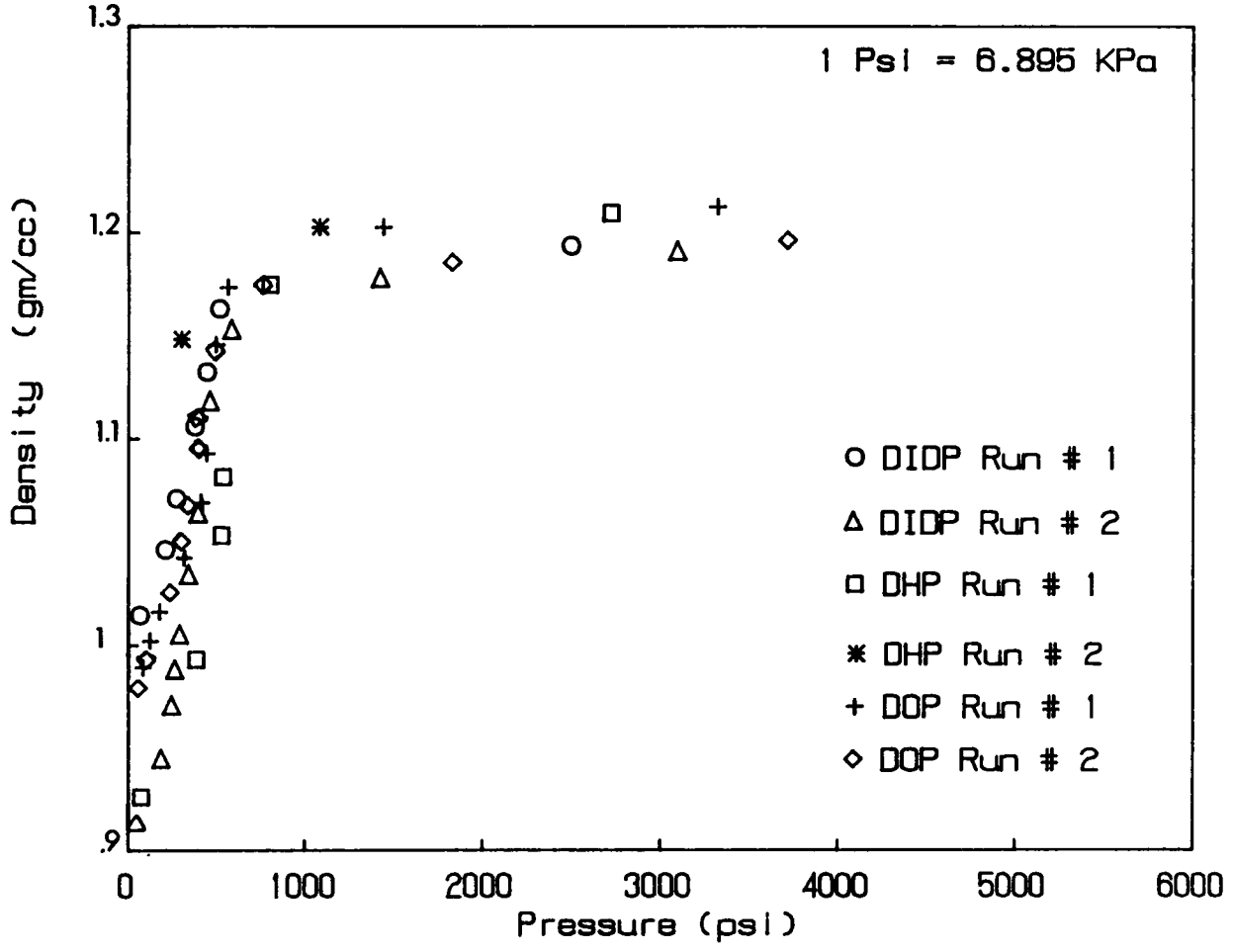

Figure 5. 12. Density of Plasticized PVC Pellets at 170 ° C

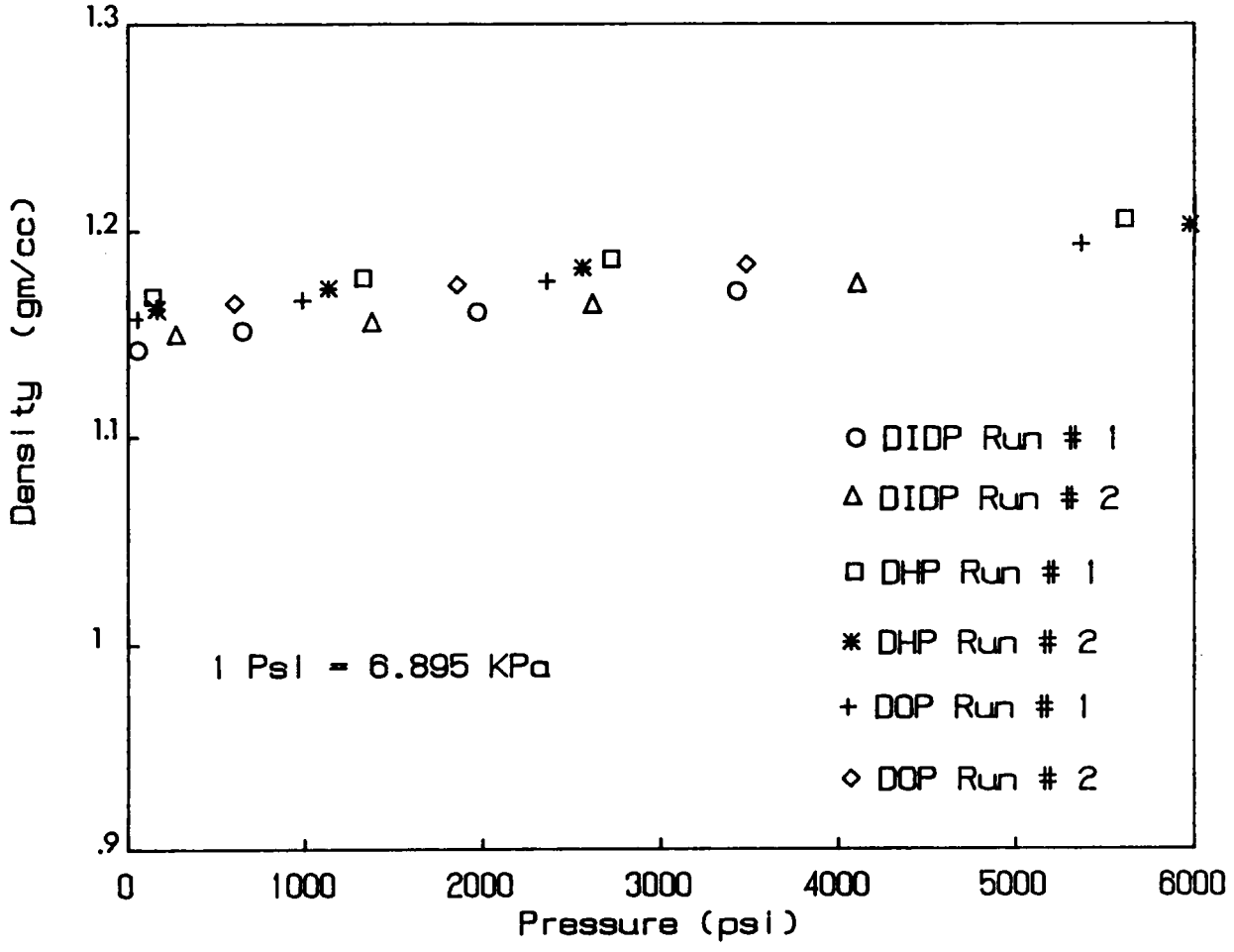

Figure 5. 13. Density of Plasticized PVC Pellets at 190 ° C

160 ° C and in the pressure ranges in Figures 5.14 to 5.16, the dry blended samples are fused and compacted to their final density and become incompressible in nature.

An interesting observation was made during the dry blend compaction test. It was seen that the dry blend extrudates from the ICR at 170 ° C and above had a clear or transparent appearance. Recalling the basic definition of fusion as a clearing of the PVC melt owing to the interdiffusion and penetration of the amorphous chains in the primary particles, the clear extruded above 170 ° C possibly signified a high degree of fusion and was indicative of a more pure melt state. In contrast, at 160 ° C and below, the extrudates had a translucent appearance. The transition in the melt flow behavior of PVC in which it loses its particulate identity and forms a more cohesive fused state has given rise to dual-valued activation energy for the flow [24-28]. For rigid PVC the critical crossover temperature is between 180 and 190 ° C. If the transparent extrudates are associated with the fused state and the translucent ones with the particulate behavior of flow, the Arrhenius' plots of plasticized should indeed show two activation energy levels. In other words if plasticized PVC dry blends had two flow mechanisms, one above and one below a critical temperature, then there would be a break in the Arrhenius' plot at the critical temperature.

Accordingly, Arrhenius' plots were constructed for DIDP and DHP dry blends and can be seen in Figures 5.17 and 5.18. Three shear rates were chosen for each material, and they covered the range of shear rates experienced in the extruder. The abscissa represents the inverse of temperature in ° K. For each shear rate the first three points (corresponding to 190, 180 and 170 ° C) lie in the highly fused or melt region while the last two points (corresponding to 160 and 150 ° C) lie in the particulate flow region. The change in the slope of the Arrhenius plots or the critical transition temperature for both the dry blends is seen to occur at about 165 ° and does not appear to be greatly affected by the shear rates that are experienced in the extruder. The mechanism of flow for plasticized PVC at the critical temperature changes from a particulate flow to a more melt-like behavior at 165 ° C. Thus the plasticizers are able to reduce the transition temperature from particulate to melt flow by 20 ° C from that of rigid PVC. It may be recalled that at processing temperatures up to 185 ° C used for this research, the

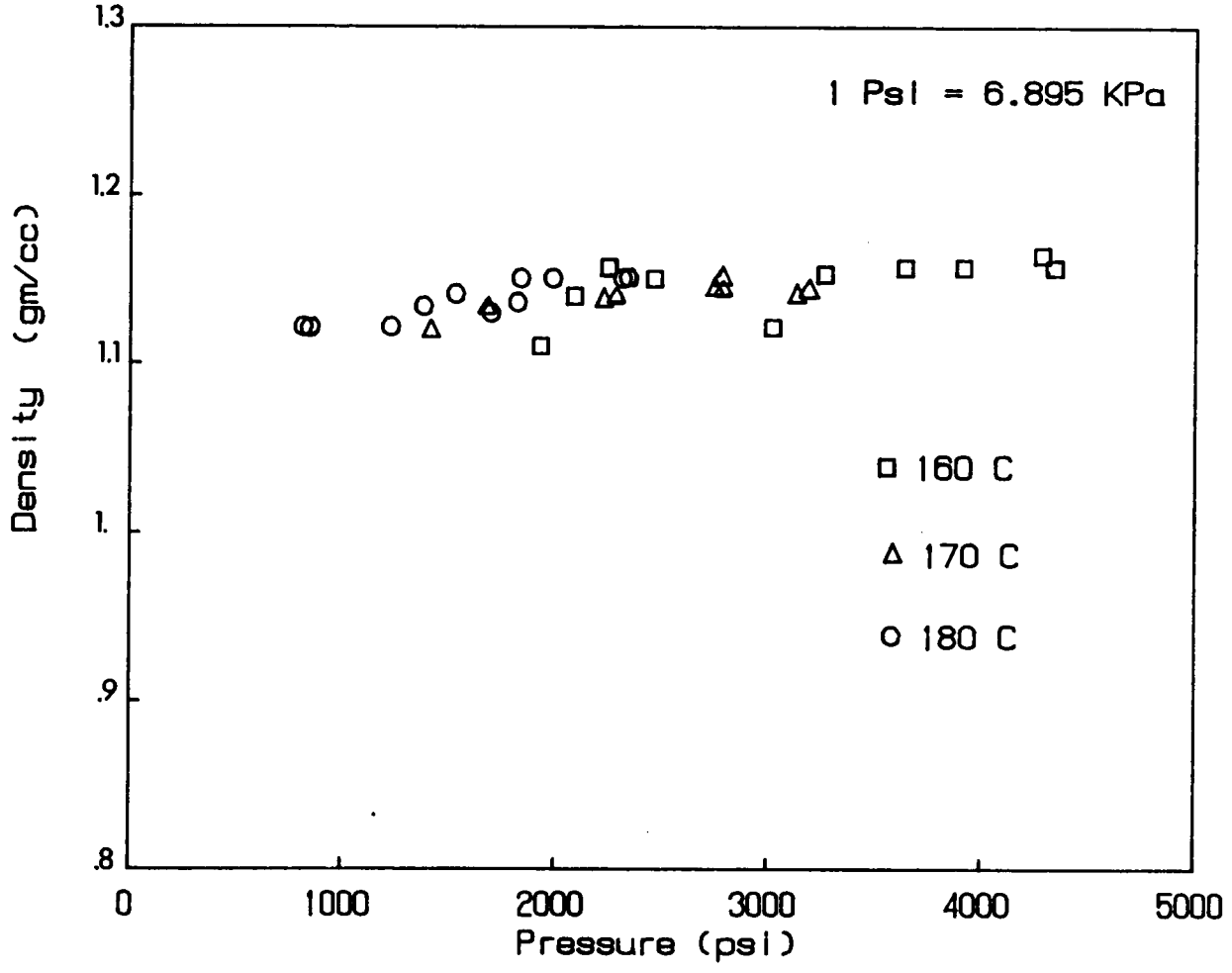

Figure 5. 14. Density of DIDP Plasticized PVC Dry Blends at different temperatures.

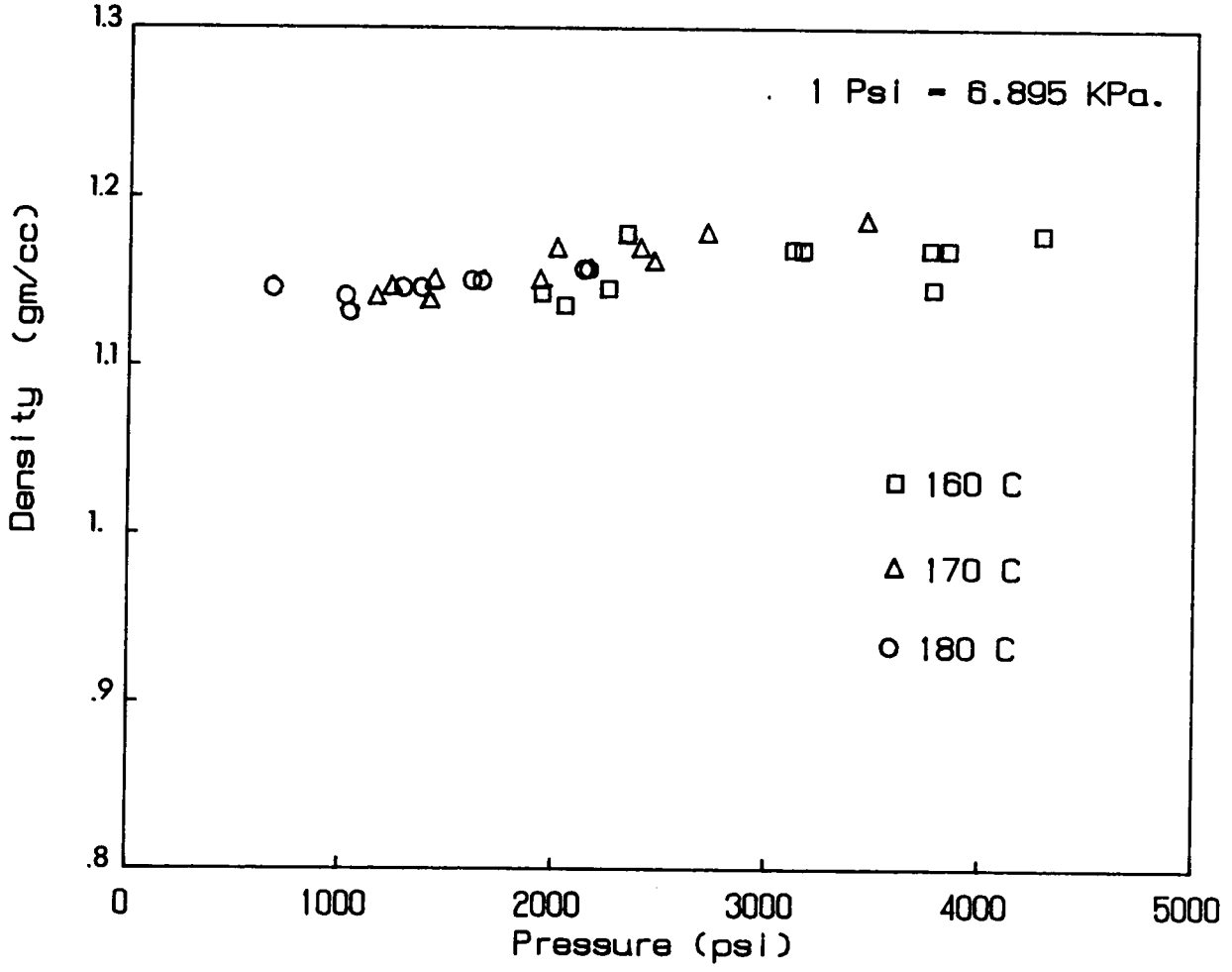

Figure 5. 15. Density of DHP Plasticized PVC Dry Blends at different temperatures.

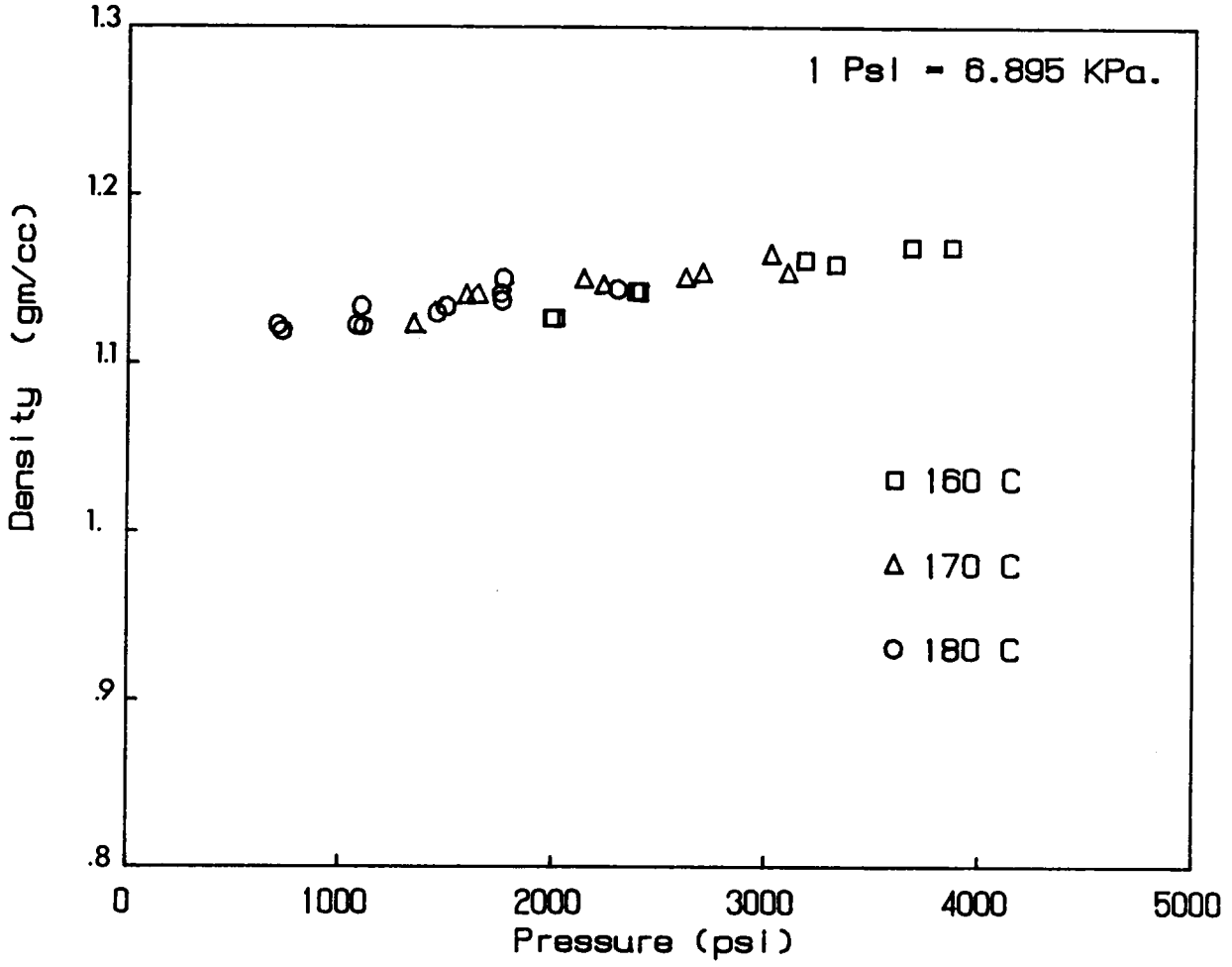

Figure 5. 16. Density of DOP Plasticized PVC Dry Blends at different temperatures.

PVC crystallites in the microdomains are very much present [73] for rigid PVC and possibly also for plasticized PVC. Although the fused state exhibits a melt flow behavior, one should not loose sight of the fact that a breakdown of the crystalline microdomain structures has not taken place; and that above the critical temperature, the fusion has proceeded far enough for the PVC mixes to behave as a homogeneous melt. In some of the scanning electron microscope pictures to be presented in section 5.2.2 , there is evidence that these crystalline microdomains are present even when the melt has turned clear at temperatures in excess of 175 or 180 ° C.

The density measurements were not affected by the plasticizer type. But during the density measurement tests, observations were made that provided insights into the flow mechanism of plasticized PVC. The dual-valued activation energy flow curves exist for both plasticized PVC as they did for rigid PVC. In the former case the critical temperature is decreased by approximately 20 ° C from the latter for a 40% plasticizer loading.

The experimental data at temperatures between 150 and 190 ° C have been fitted to power law models as shown in Tables 5.7 and 5.8. For the numerical work, it is desired to express viscosity as a function of both temperature and shear rates. These viscosity expressions will enable the continuous calculation of viscosities at any shear rate and at any intermediate temperatures other than the discrete experimental ones. Two types of regression analysis were performed with the viscosity - shear rate data at different temperatures. In the first case, the log (viscosity) was expressed as a second order function of log (shear rate) and temperature. In the second case, a power law expression was fitted to the data in which both the inertial term, m, and the power law index, n, were expressed as Arrhenius type function of the absolute temperature. SAS regression procedures [91] and IMSL subroutine DBCLSF (which is based on a modified Levenberg-Marquardt algorithm) [92] were applied to obtain the first and second types of expressions, respectively. As the flow energetics changed at 165 ° C, two sets of expressions - one above and one below 165 ° C - were computed. These expressions are presented in Table 5.11. Both the expressions fitted the experimental data quite well. The lowest experimental shear rates were approximately 2

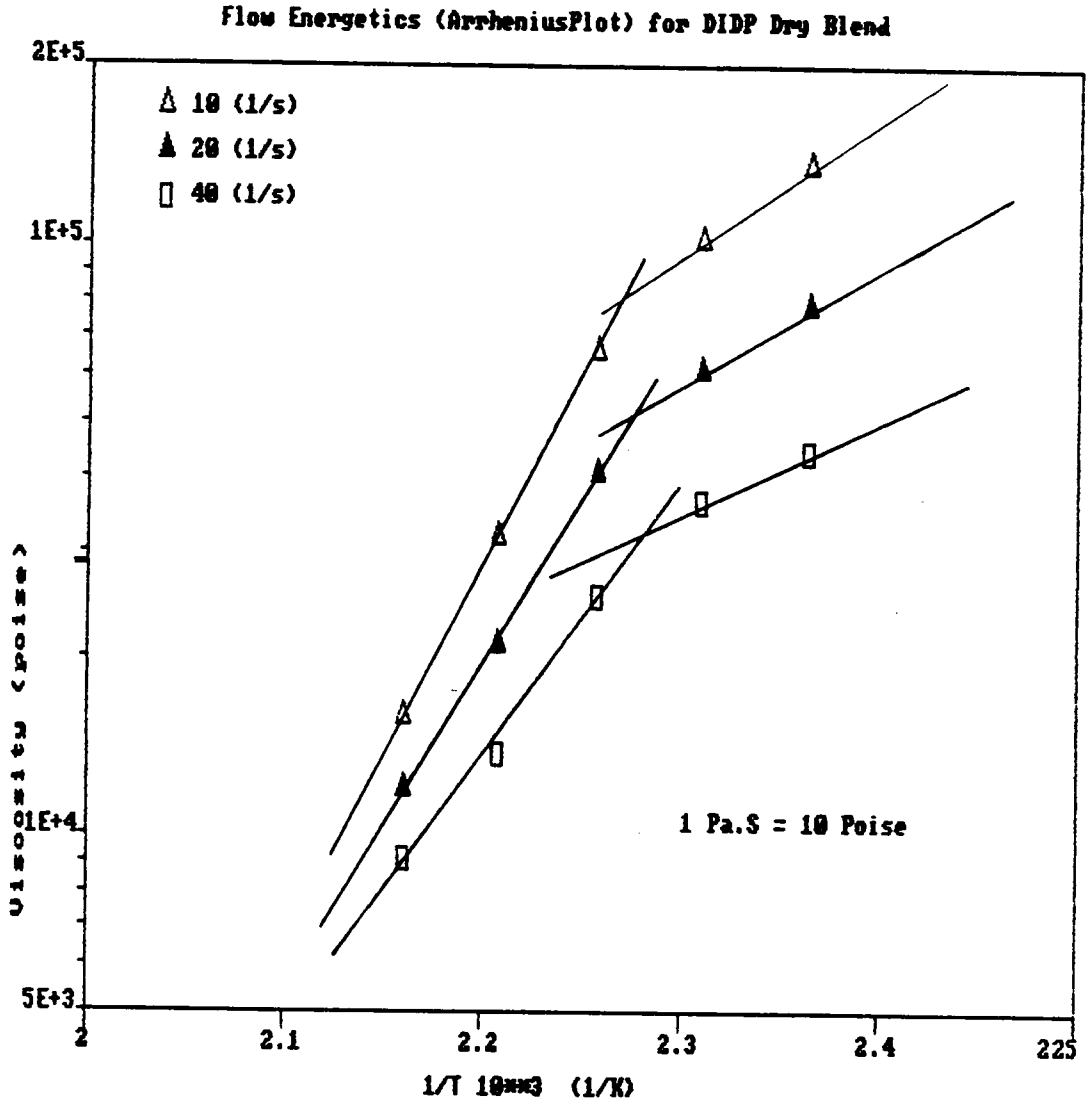

Figure 5. 17. Flow Energetics (Arrhenius Plots) for DIDP Dry Blend

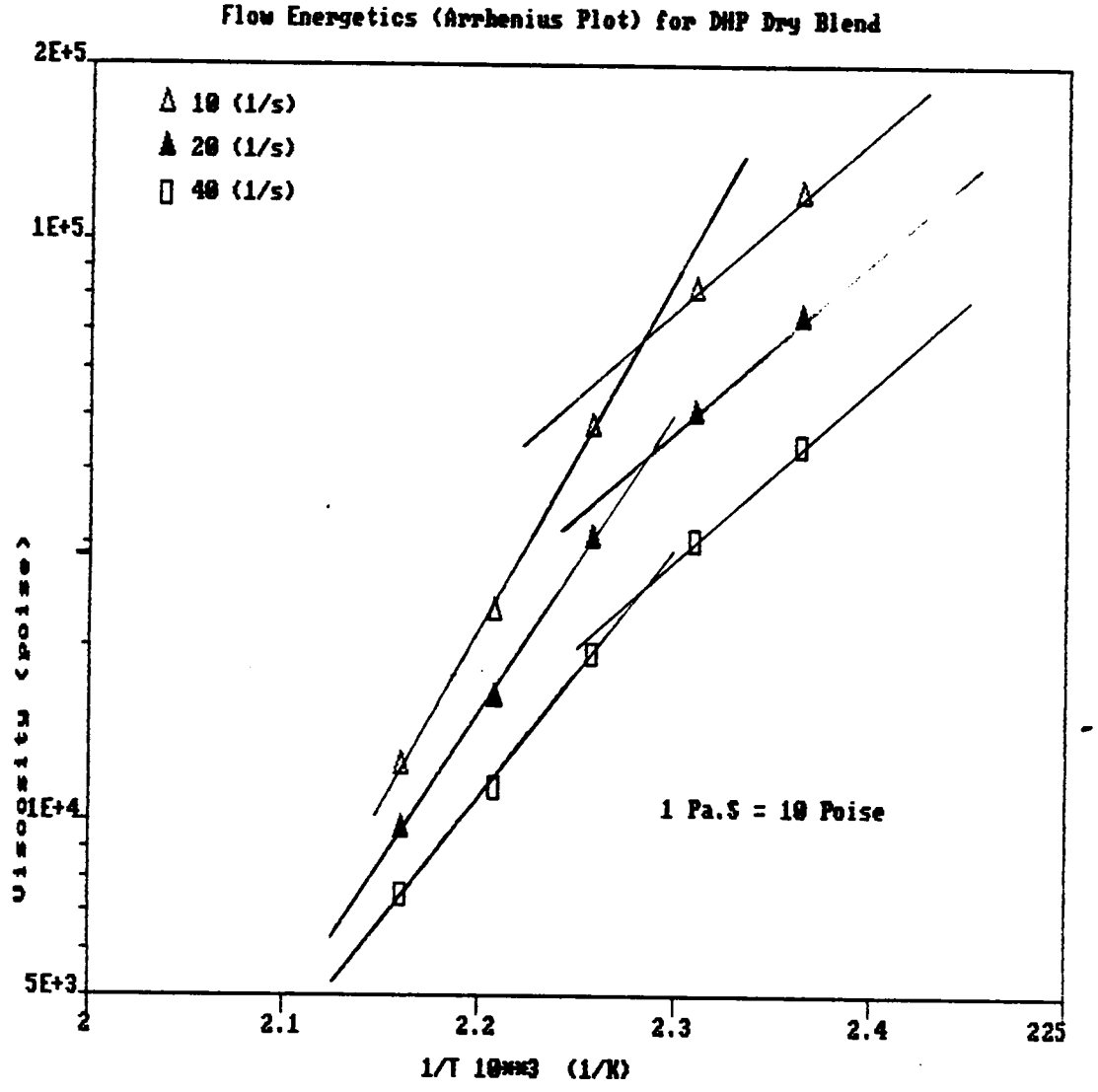

Figure 5. 18. Flow Energetics (Arrhenius Plots) for DHP Dry Blend

1/s. Both type of regression expressions predicted viscosities that matched well with viscosities that were extrapolated using power law parameters, from (Table 5.7), for shear rates between 2.0 and 0.1 1/s. Below a shear rate of 0.1 1/s, the quadratic regression expression varied considerably from the predictions made by the power law and the second regression expression. In section 5.3 which deals with numerical results, the reasons for choosing one regression expression for viscosity over the other for the numerical simulation purposes will be discussed. As a check, viscosities calculated using these regression expressions were used to calculate the ratios of viscosities between DIDP and DHP dry blend. These ratios matched the ratios of the viscosities obtained from power law parameters in Table 5.9 fairly closely.

Recasting the expression for viscosity, as a function of shear rate and temperature, was not done for the pellets and the DOP dry blends as the numerical work will only be done with DIDP and DHP dry blends. Arrhenius' plots were not constructed for the viscosity data of the plasticized PVC pellets. There was no clearing of the pellets at 170 ° C and above and thus there was no visible proof or demonstration of any change in the nature of flow from particulate to a more fused state. It was therefore deemed unnecessary to present Arrhenius' plots as there was no physical phenomenon to compare them with.

In sections 5.1.1 and 5.1.2 the effect of plasticizers on the viscosity shear rate data and compaction have been presented. The plasticizer type gives rise to significant differences in viscosity between DIDP and DHP dry blends and pellets especially above 160 °C. The differences between DIDP and DOP plasticized mixes are usually smaller and sometimes are negligible at high shear rates. The compaction tests were not influenced by the choice of plasticizers but the compaction studies provide insight into the dual nature of the PVC flow. It is observed that the plasticizers decrease the transition temperature at which the flow mechanism of PVC changes from particulate to fused or melt-like by about 20 ° C from that of rigid PVC. It is in the fused or the melt-like state, where the greater interdiffusion between the PVC particles take place, that the plasticizer effect on viscosity is more prominent.

5.1.3 Yield Stress Measurements

PVC has been said to display yield stresses even at temperatures above 190 ° C [88]. This is not unnatural considering the presence of crystallites in the microdomains at the processing temperatures up to 190 ° C or even up to 200 ° C [73]. While the values of the yield stress might be small at higher temperatures, where fusion has progressed to a high degree, they could possibly influence the flow behavior at low temperatures. The proposed solids conveying model in this thesis treats the solid as a fluid with a yield stress, and this necessitates the determination of yield stresses. Materials with yield stress deform and start to flow when subjected to external stresses higher than the yield stress. The fluids which display Newtonian behavior after they start to deform and flow are called Bingham fluids, while for Herschel Bulkley fluids, the fluids behave like a power law fluid once the total external stress exceeds the yield stress. In the rest of this chapter the Bingham fluid and Herschel Bulkley fluid models will be referred to as BF and HB fluids, respectively. As the numerical simulation work will be done only for DIDP and DHP plasticized dry blends, yield stresses will be determined only for these two dry blends.

Usually two methods are commonly cited in the literature for measurement of yield stress. A graph of log (shear stress) versus log (shear rate), obtained by means of cone and plate attachment in the RMS, shows a linear portion which is parallel to the shear rate axis and this may be extrapolated to give a yield stress [86]. This same result could be achieved by plotting viscosity vs shear stress. The shear stress where the viscosity starts to rise asymptotically is assigned the yield stress value. In the second method, the $(\text{shear stress})^{1/2}$ is plotted against $(\text{shear rate})^{1/2}$ or $(\text{modified shear rate})^{1/2}$ and the intercept with the ordinate is the measure of the yield stress [87]. The second method has been mainly used for polymer solutions. In the second method, the shear rate is modified by the viscosity ratios of the disperse and continuous phases. The $(\text{modified shear stress})^{1/2}$ - $(\text{shear rate})^{1/2}$ has also been used for rigid PVC [88] but in chapter 2 the method has been questioned for the way the

modified shear stress was measured. So for the present study the first method of yield stress determination will be followed. This requires obtaining the steady shear or the dynamic data using the RMS.

Dynamic measurements in the RMS were used to determine the yield stresses, and the reason why they were preferred over steady shear experiments will now be discussed. Initially, the steady shear experiments were carried out with the parallel plate device attachment in the RMS at 150, 160 and 170 ° C. A special technique, as discussed in Chapter 3, was employed to put the sample between the plates, set the gap width and relax the normal stresses in order to measure in the steady shear mode. But as the temperature was lowered below 170 ° C to 160 ° C, residual stresses built up in the samples. The increase in the magnitude of the normal stresses with the increase in shear rates prevented any data being recorded beyond a shear rate of 0.05 1/s as it overloaded the load cells of the RMS. These experiments were difficult to perform and only two or three data points were obtained between shear rates of 0.01 and 0.05 1/s at 150 ° C. At times experiments had to be aborted owing to build up of large normal stresses even at low shear rates. Lower shear rates were tried but the response time was too long. Also it was not possible to to obtain any data at 140 ° C. To overcome the obstacle of large normal stress with the steady shear experiments, it was decided to try using the RMS in the dynamic mode and use the dynamic data to determine the yield stress. Earlier it was indicated that a plot of shear stress vs shear rate or a plot of viscosity vs shear stress can be used to determine the yield stress for a material. In absence of steady shear data, the dynamic data had to be used for this purpose and the complex viscosity, η^*, was plotted against the storage modulus, G′. It might have been more accurate to plot η^* against G* which is equal to $\sqrt{G'^2 + G''^2}$, where G″ is the loss modulus. But considering the fact that at low frequencies, the G′ values are larger than the G″ values by almost an order of magnitude, it will not have caused much difference in the ultimate value of the yield stress.

The dynamic mode experiments have to be conducted at optimum strain values. The strains should be in the range where the viscoelastic response of the material is linear but is in the measuring range of the transducers attached to the bottom plate of the RMS. For ma-

terials with yield stress, the shear stress - shear rate curve shows a linear region parallel to shear rate axis. This linear region which indicates yielding behavior often occurs at shear rates lower than 0.1 1/s. Thus it is the dynamic mode behavior of the material at angular frequencies lower than 0.1 rad/s that might be indicative of the yield phenomena. So At 140, 150 and 160 ° C, strain sweeps were run with the DIDP dry blend at angular frequencies of 0.03 and 0.05 rad/sec. in order to determine the strain at which the dynamic experiments were to be performed. The RMS was run with the parallel plate device attachment The results of the strain sweeps are presented in Figures 5.19 through 5. 21. The torques experienced by the lower plate were as low as 4 gm - cm and as high as 300 gm - cm for the three strain sweep experiments. Usually torque values over 2 gm - cm are large enough to have reliable measurements from the RMS in the dynamic mode. The DIDP samples demonstrated a linear behavior for both the storage modulus, G' and loss modulus, G" until a strain rate of 11 %. A strain rate of 6%, which lies in the middle of the linear region, was chosen for all subsequent dynamic mode experiments.

Although dynamic mode experiments will be used for determining the yield behavior of the plasticized PVC samples, it will be interesting to observe the comparisons between the steady shear and dynamic experiments and also what experimental errors are possible for the latter cases. The problem of finding the optimum strain value for linear response has already been presented. The other most obvious question that can be raised is whether no-slip boundary conditions existed at the plates at the lower temperatures. The fact that a large negative normal force pulled the plates inwards in absence of a shearing (or oscillatory) motion suggests that there was no slippage between the material and the plates. Towards the end of this section the results of the steady shear experiments will be presented and they will be compared to the results of the dynamic experiments which will be discussed next.

The dynamic tests on DIDP dry blends were carried out between 130 and 170 ° C at intervals of 10 ° C and results are presented in Figures 5.22 to 5.26 and Tables 5.12 to 5.15. The dynamic response is measured for varying angular frequency, ω. In the rest of this chapter ω will be referred to as frequency instead of angular frequency. The variation about the mean

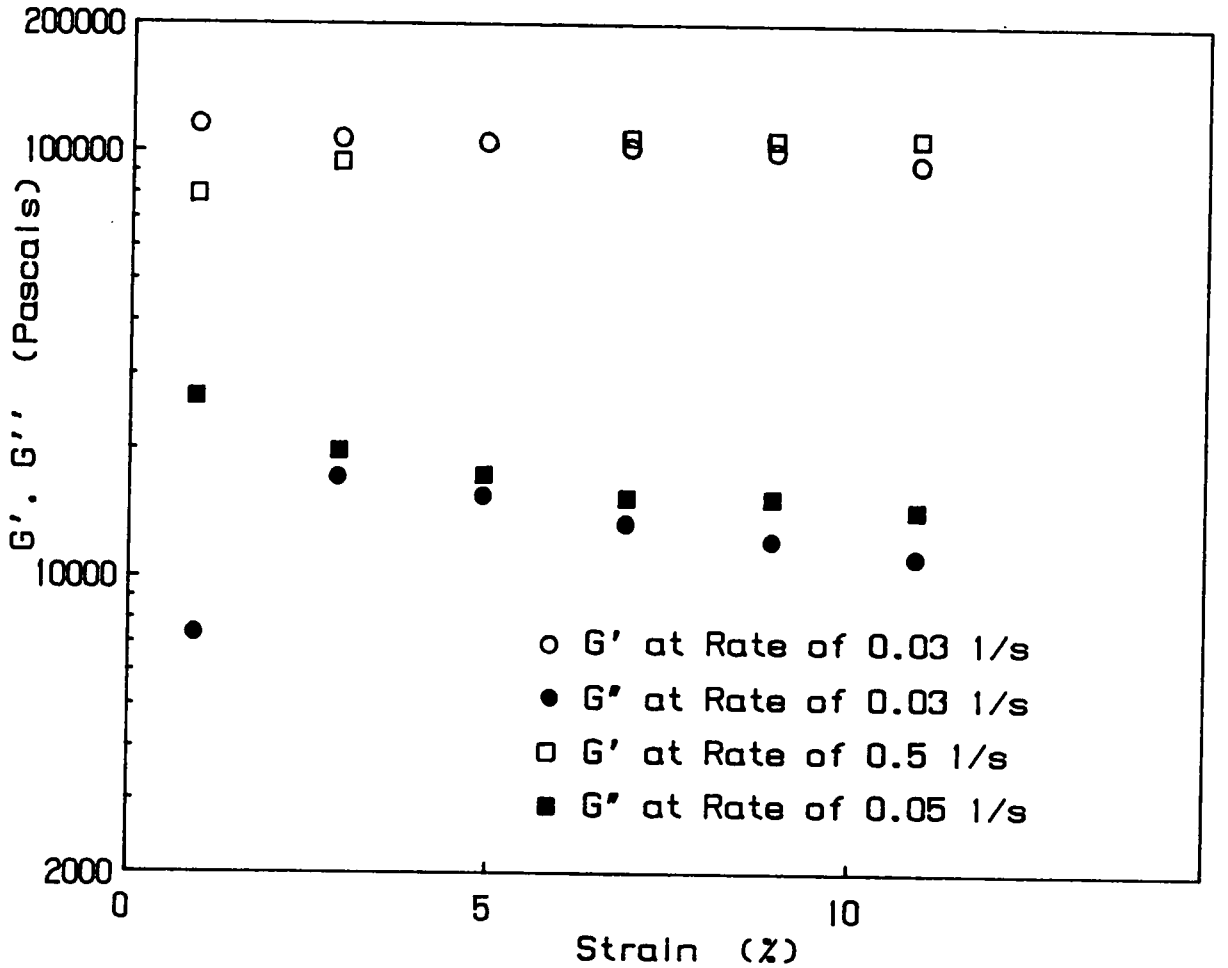

Figure 5. 19. Strain Sweep Experiment of DIDP Dry Blends at 140 C: Rate refers to angular frequency

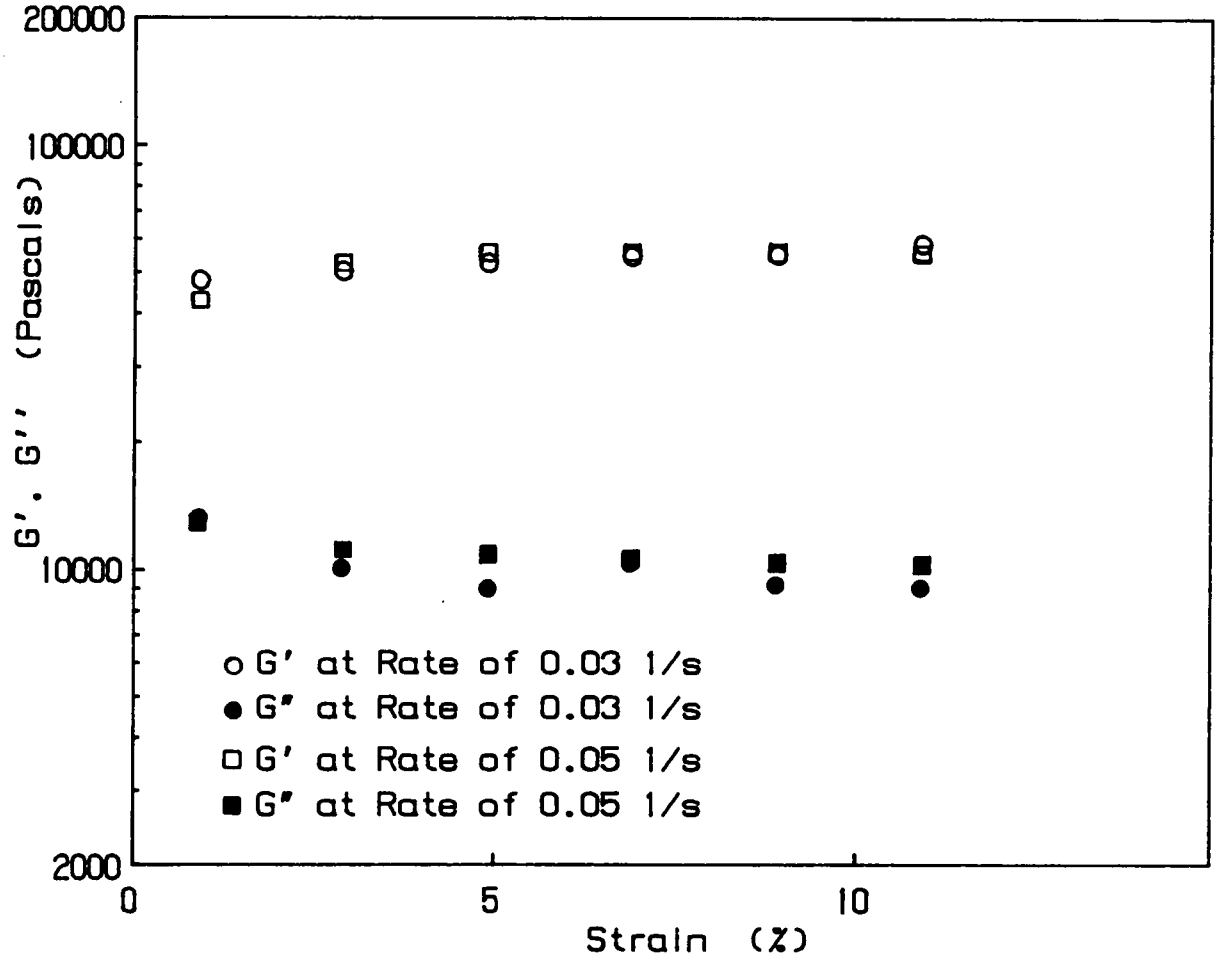

Figure 5. 20. Strain Sweep Experiment of DIDP Dry Blends at 150 C: Rate refers to angular frequency

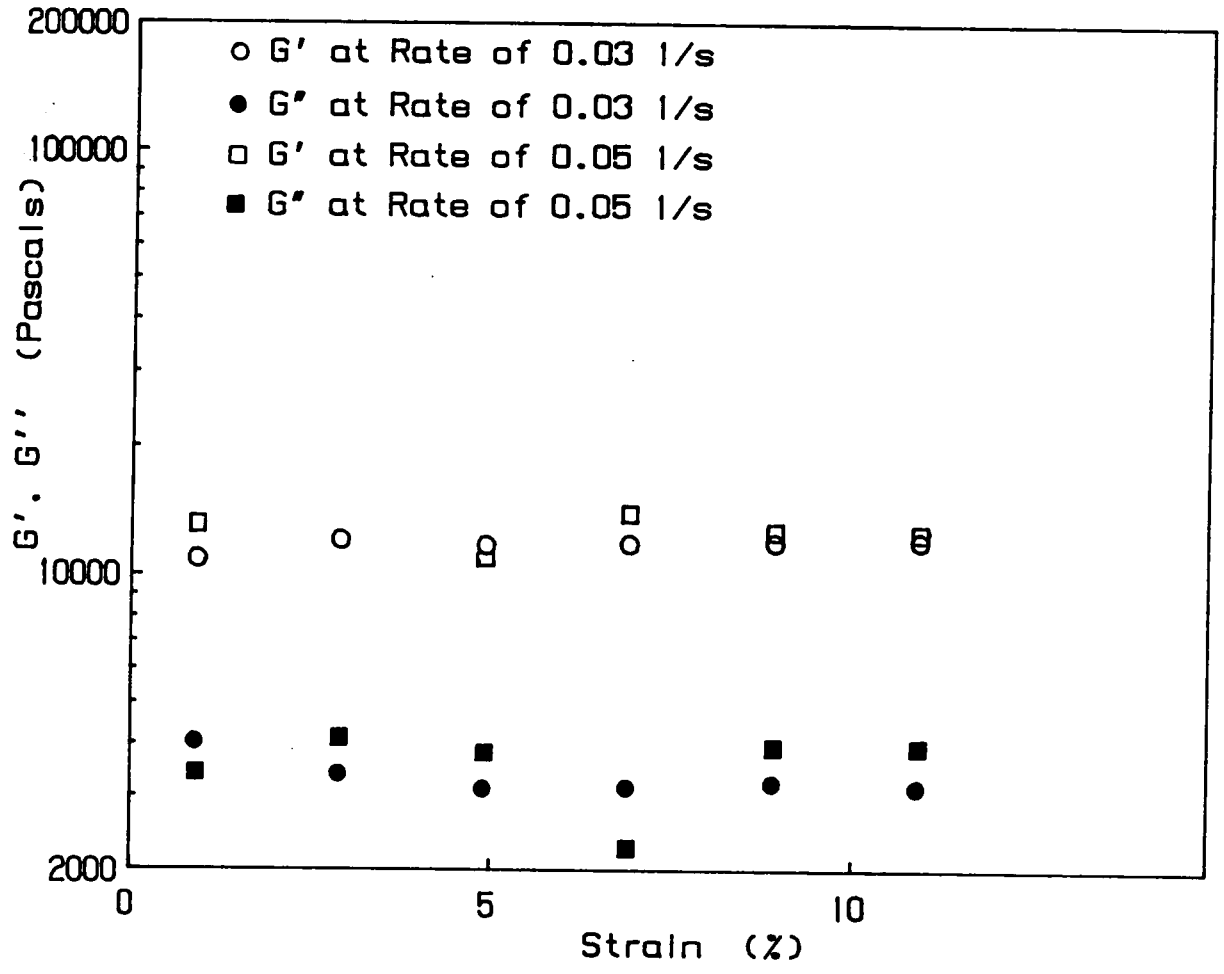

Figure 5. 21. Strain Sweep Experiment of DIDP Dry Blends at 160 C: Rate refers to angular frequency

of the reported data is less than 4 % and the error bars are the size of the symbols representing these data points. At 170 and 160 ° C as seen in Figures 5.25 and 5.26, respectively, G′ and G″ rise monotonically with frequency for almost the entire frequency range as expected for polymer melts. However at frequencies lower than 0.03 or 0.04 rad/sec. and at 160 ° C, there is a tendency, albeit not very apparent, that the moduli values are leveling off with frequency. For a solid, the elastic properties of the material are not a function of frequency [90]. For this reason the leveling off of the G′ can indicate a behavior similar to solids. It has been shown that if a material displays yield stress behavior, its shear stress - shear rate curve (or the storage modulus - frequency curve) levels off below a critical shear rate (or frequency) [86,87] and in this region the material behaves like a solid. At frequencies or shear rates higher than the critical value, the stresses are higher than the yield stress and the material deforms and flows like a fluid. At 160 °C, the DIDP dry blend seems to be possibly displaying yield stresses below 0.03 or 0.04 rad./sec. (Fig. 5.25). From Fig. 5.24 it is observed that at 150 ° C the levelling off of the moduli values of the DIDP dry blend occurs at about the same frequency as 160 ° C. At 130 and 140 ° C and at much higher frequencies the moduli values tend to become parallel to the frequency axis (Figures 5.22 and 5.23). At lower temperatures, the levelling off of the moduli values takes place at higher frequencies and the presence of the yield stress in the material is possibly more unambiguous.

The dynamic tests were repeated for DHP dry blends between 130 and 170 ° C and the results are presented in Figures 5.22 and 5.27 to 5.30. They are also tabulated in Tables 5.16 to 5.19. An examination of the DHP dry blend dynamic data provides similar trends as with the DIDP dry blend. The yield stress phenomenon is conspicuously noticeable at 130 and 140 ° C and even at frequencies above 0.1 rad/sec, while at 150 ° C it appears to be present at lower frequencies. At 160 ° C, it is difficult to determine whether the DHP dry blend is displaying a yield stress in the measured frequency range. But on the whole at 160 and 170 ° C the moduli values rise monotonically with frequencies; i.e. the material is displaying more melt like behavior.

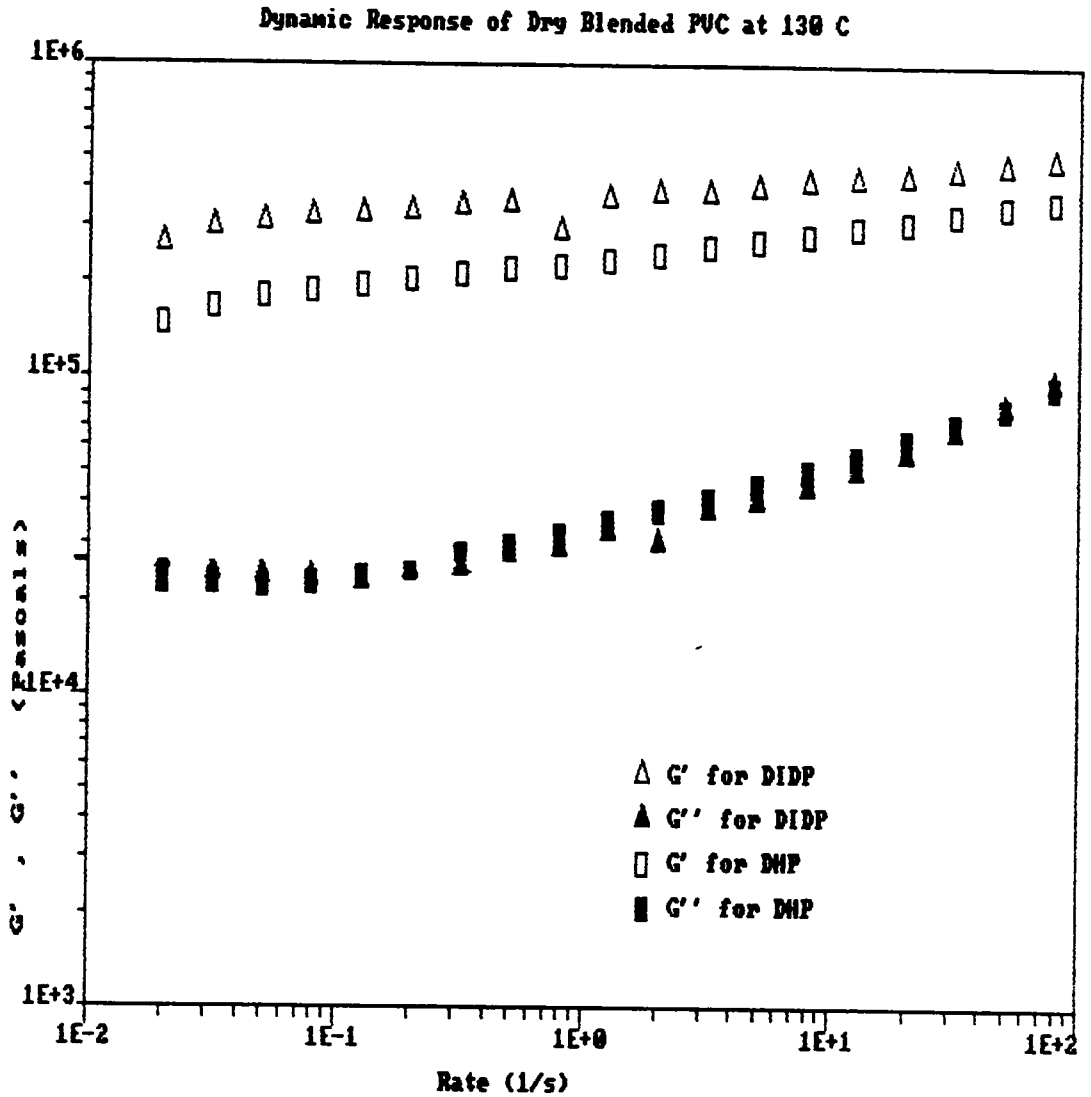

Figure 5. 22. Dynamic Response of PVC Dry Blends at 130 C: Rate refers to angular frequency

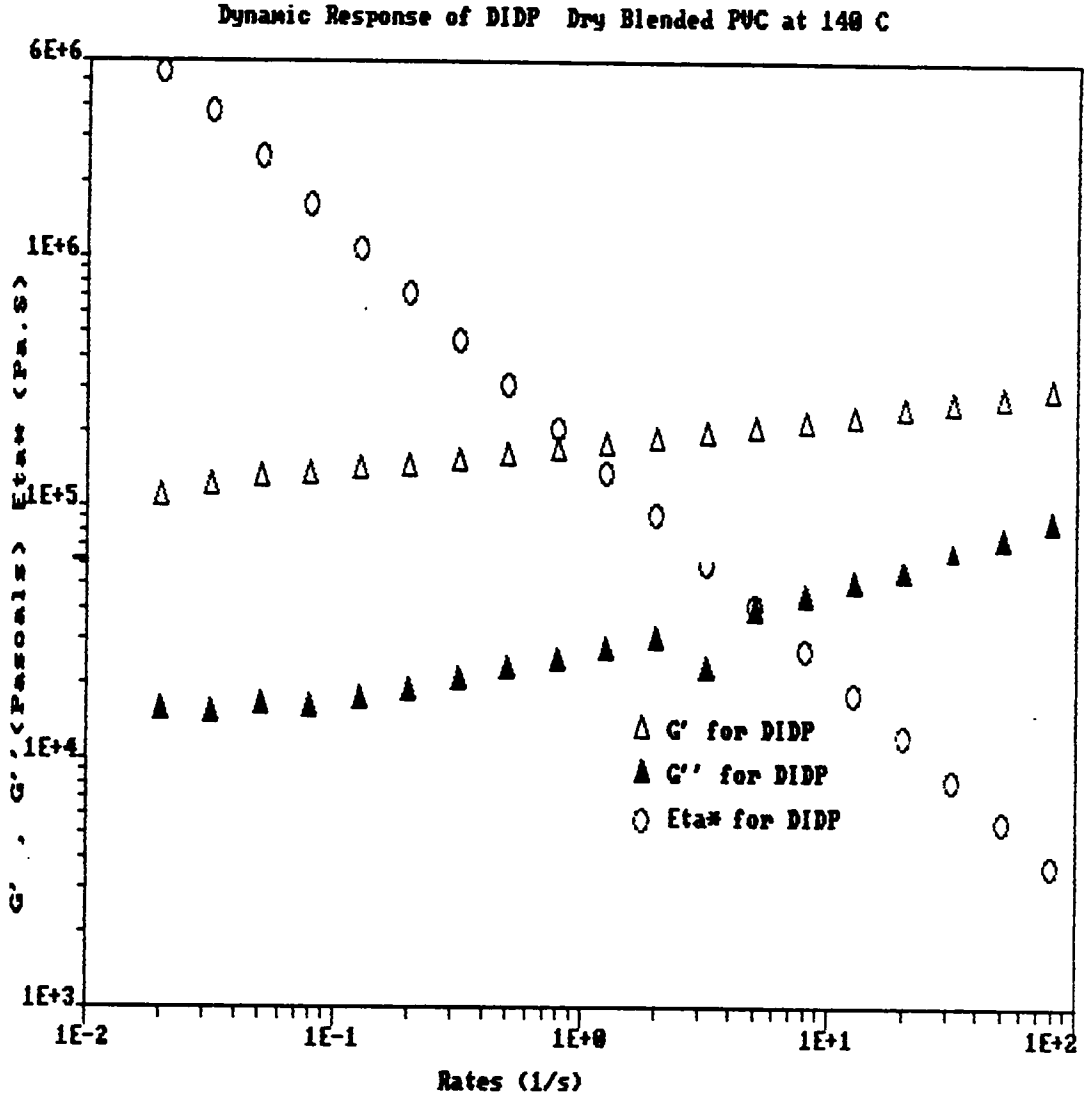

Figure 5. 23. Dynamic Response of DIDP Dry Blends at 140 C: Rate refers to angular frequency

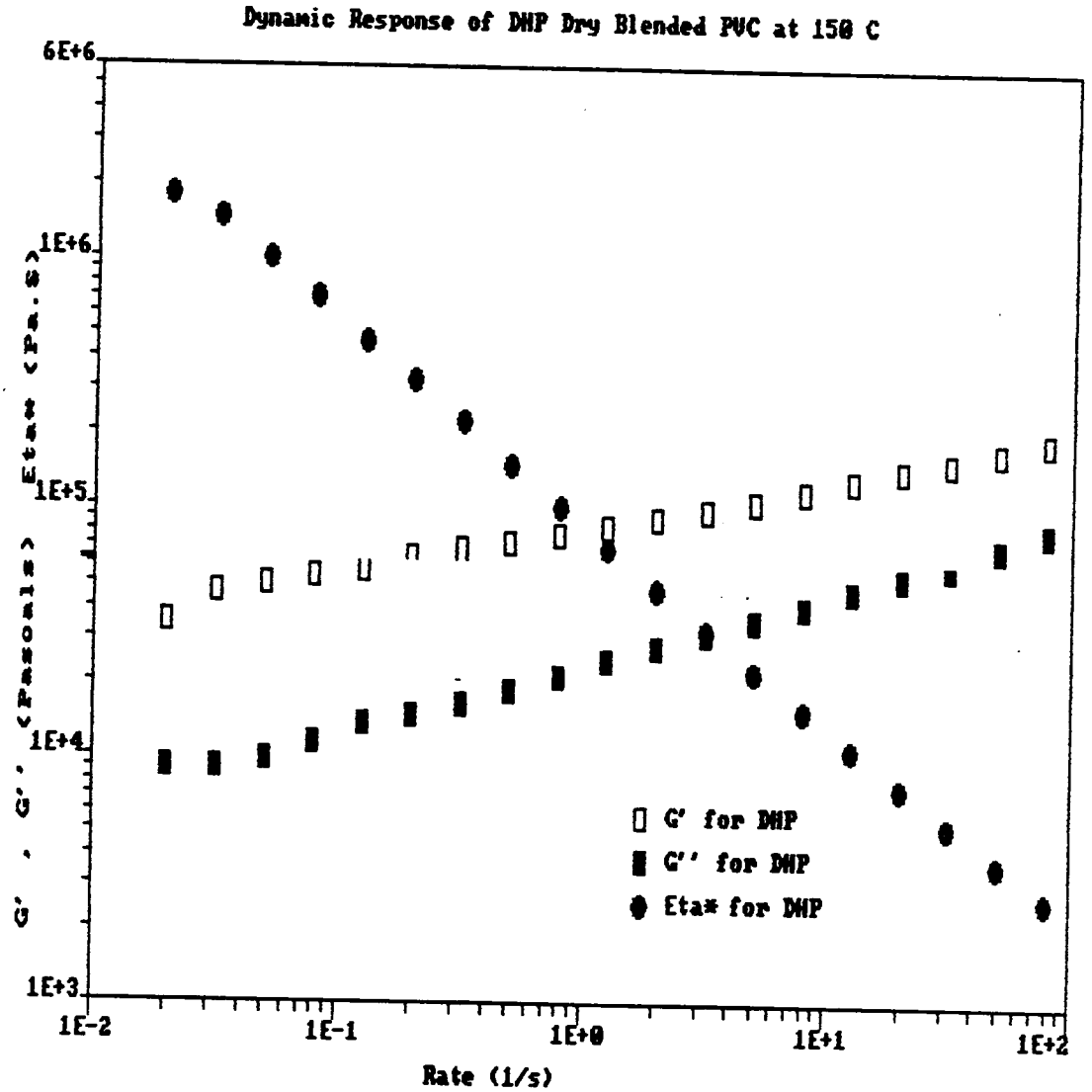

Figure 5. 24. Dynamic Response of DIDP Dry Blends at 150 C: Rate refers to angular frequency

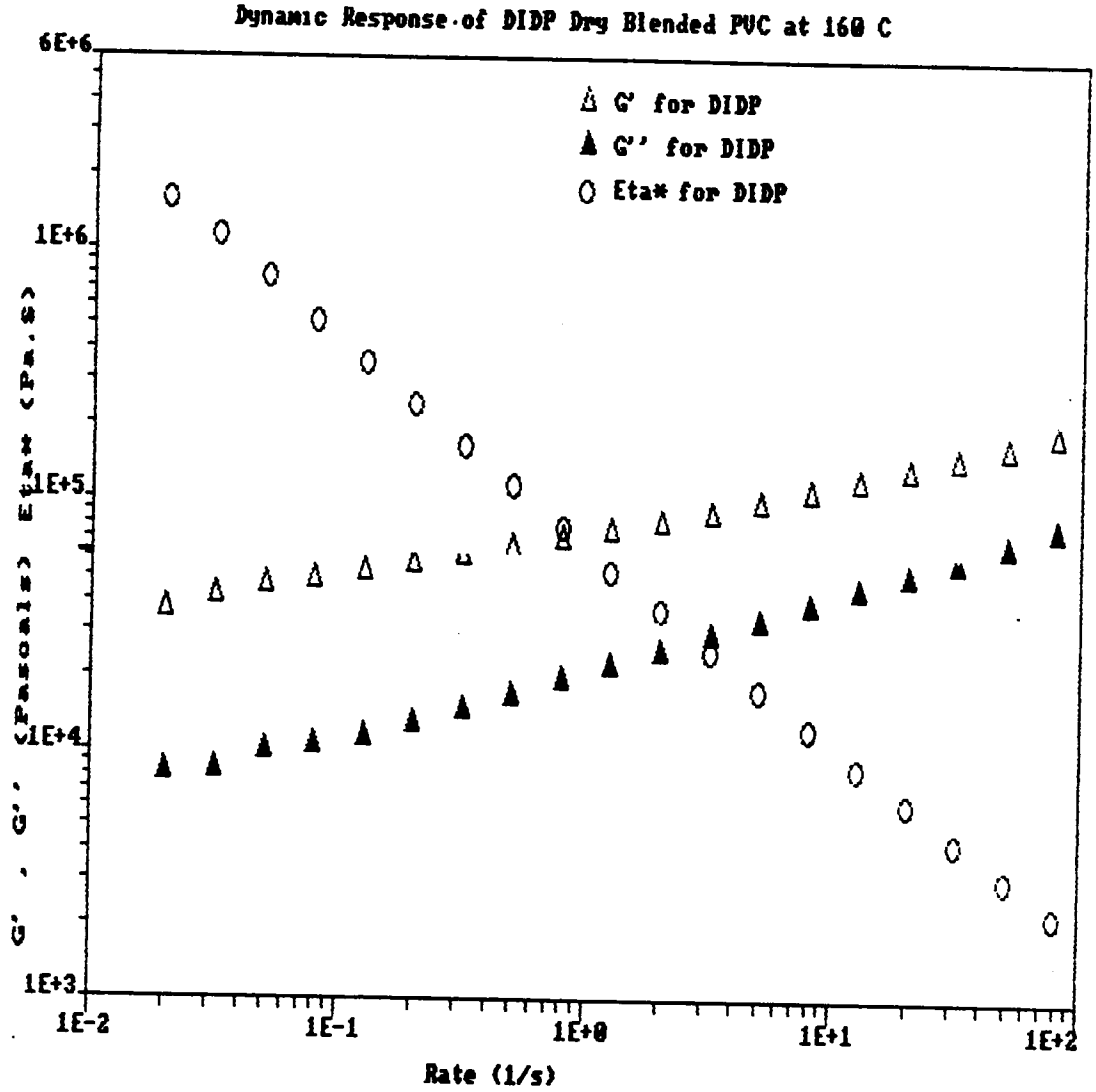

Figure 5. 25. Dynamic Response of DIDP Dry Blends at 160 C: Rate refers to angular frequency

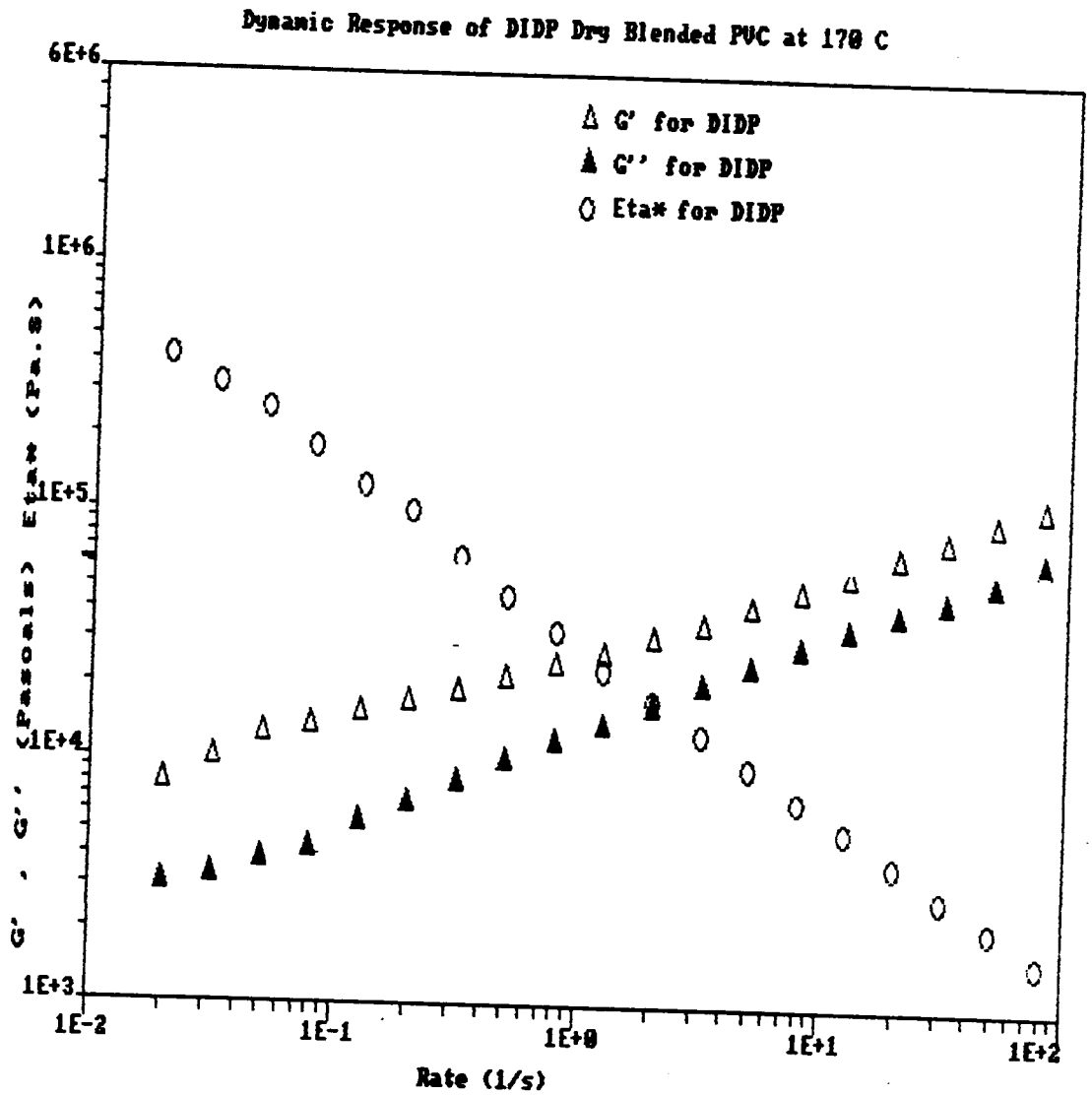

Figure 5. 26. Dynamic Response of DIDP Dry Blends at 170 C: Rate refers to angular frequency

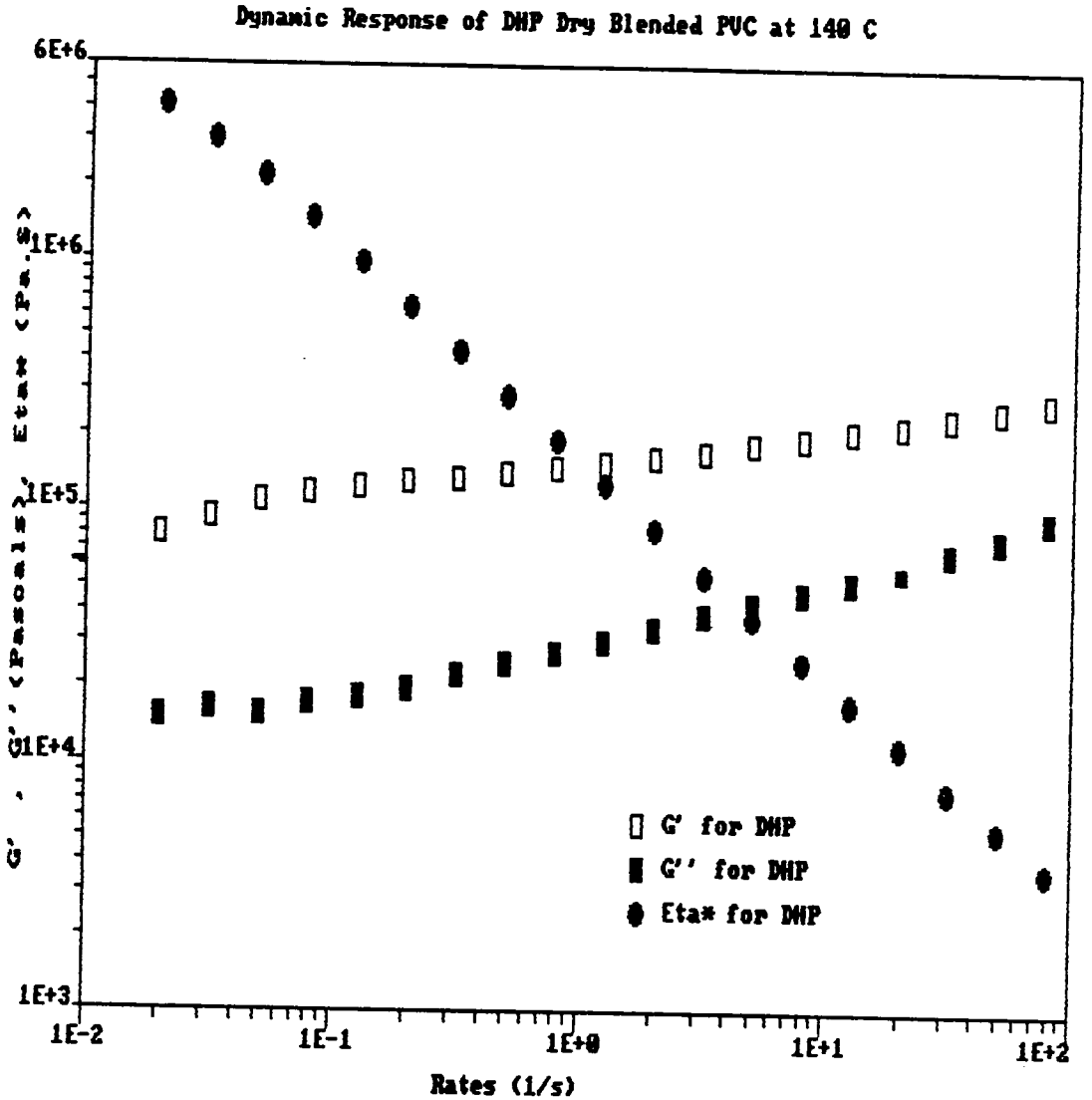

Figure 5. 27. Dynamic Response of DHP Dry Blends at 140 C: Rate refers to angular frequency

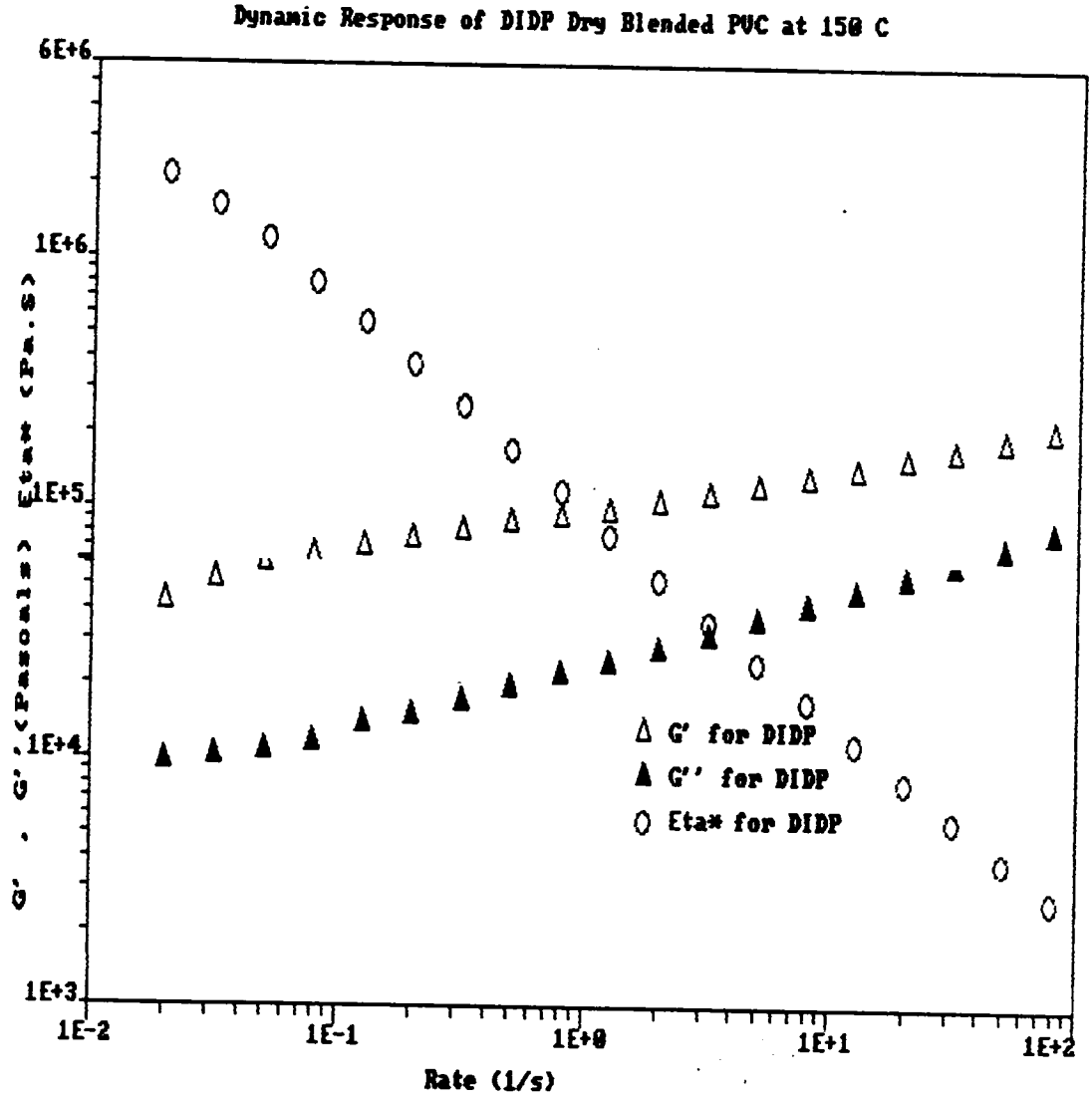

Figure 5. 28. Dynamic Response of DHP Dry Blends at 150 C: Rate refers to angular frequency

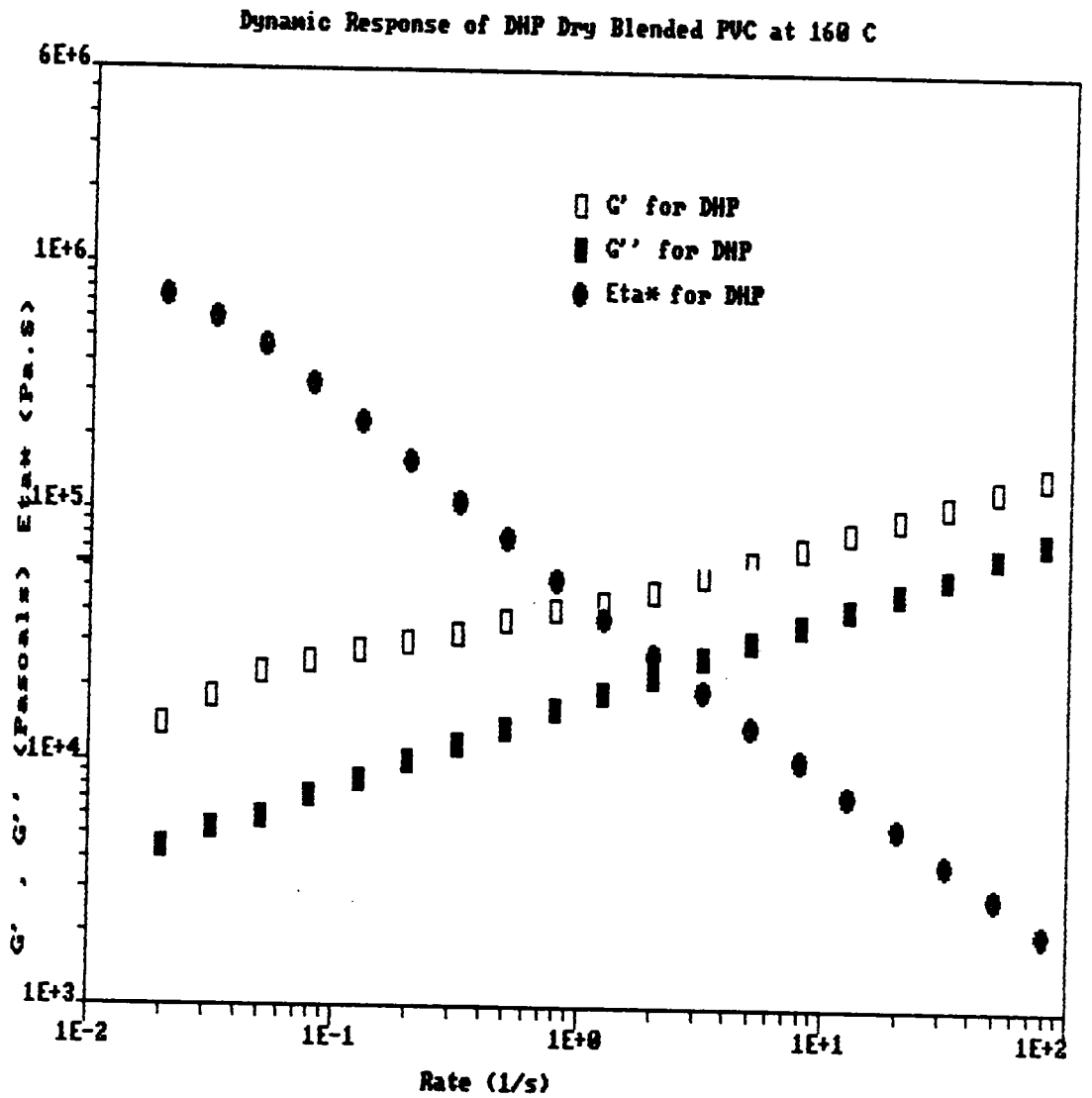

Figure 5. 29. Dynamic Response of DIDP Dry Blends at 160 C: Rate refers to angular frequency

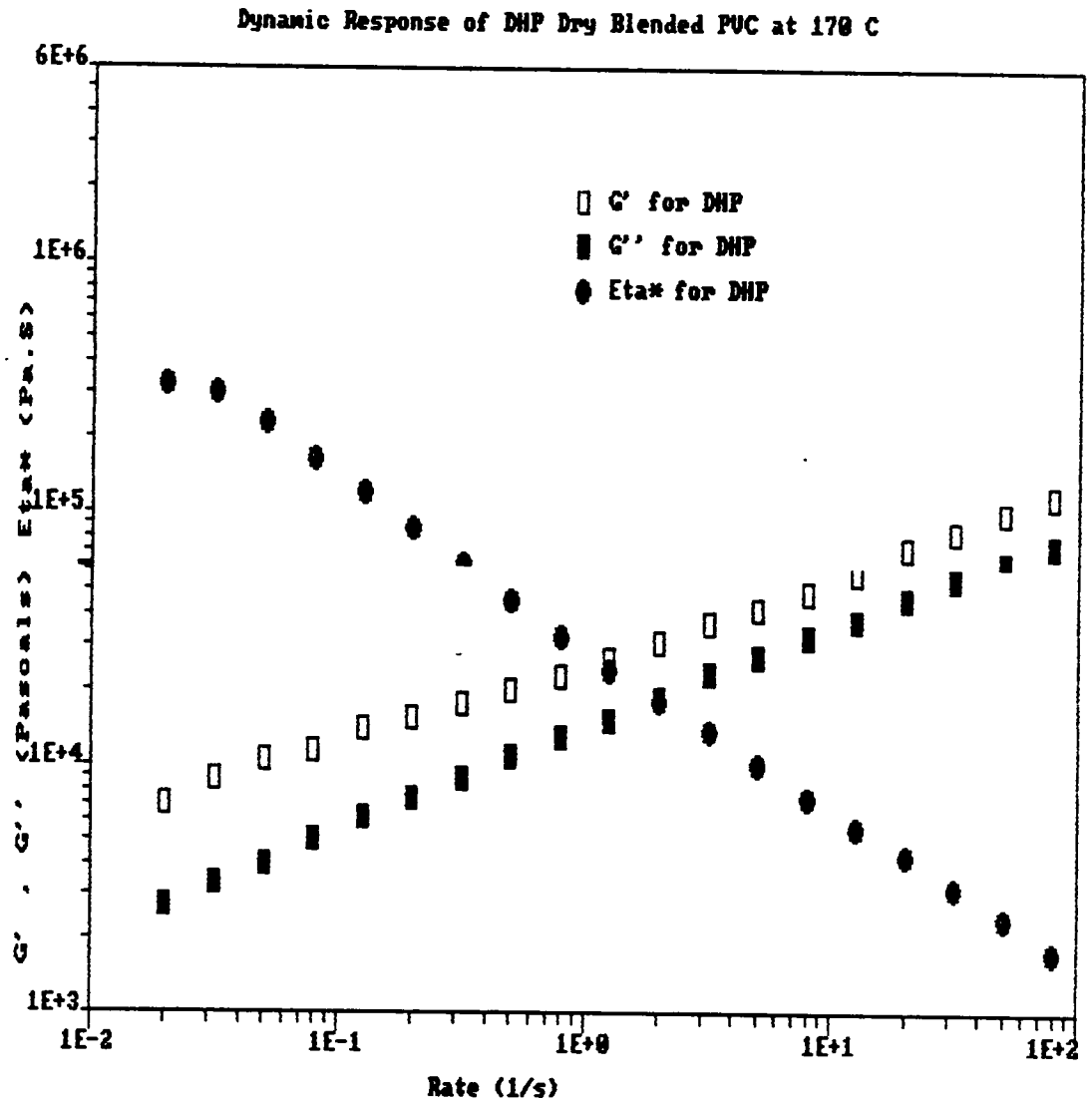

Figure 5. 30. Dynamic Response of DHP Dry Blends at 170 C: Rate refers to angular frequency

Having established the phenomenon of yield stresses quite conclusively between 130 and 150 ° C, the next logical step is to determine their magnitudes. The yield stresses are determined from the the η^* Vs G′ plots of the DIDP and DHP dry blends which are presented in Figures 5.31 and 5.32. The G′ values where the η^* Vs G′ curves start to go up asymptotically are the yield stresses at those temperatures. From Figure 5.31, it can be observed that definite yield stresses can be obtained for the DIDP dry blend at 130 and 140 ° C. At 150 and 160 ° C, the exact values of G′, where the curves start to rise asymptotically, are not quite distinct. The location of the yield stresses from the η^* Vs G′ plot are not clearly obvious and thus needs to be estimated. It can be recalled that in Figures 5.22 to 5.25, the levelling off of G′ with frequency at 160 ° C was not as distinct as it was at 130 or 140 ° C. This fact could indicate that the yield behavior might not be as dominant a feature at 160 ° C as it is for the lower temperatures and thus makes the determination of the yield stress from the η^* Vs G′ plots somewhat ambiguous at 160 ° C or higher. The weak presence of the yield behavior for the DHP dry blend, especially at 160 °C, is also supported by the η^* Vs G′ plots for the DHP dry blend in Figure 5.32. Here also the yield stresses were much easily determined at 130 and 140 ° C than at 150 and 160 ° C. At 160 ° C, the G′ value where the η^* Vs G′ curve starts to go up asymptotically is not very distinct and the yield stress had to be estimated. The yield stresses at various temperatures are tabulated in Table 5.20. The DIDP dry blend exhibited higher yield stresses than the DHP dry blends. As expected, the yield stresses decreased with increase in temperature. They decreased by almost one order of magnitude as the temperature was increased from 130 to 160 ° C.

The next task is to fit the viscosity shear rate data at the lower temperatures to a fluid model that incorporates the yield stress. It might be emphasized here that the viscosity shear rate data between 150 and 190 ° C have already been fitted to i) power law models at discrete temperatures and ii) to two continuous temperature-dependent power law models covering two separate temperature ranges above and below 165 ° C. Because of the weak presence of the yield stress and the ambiguous nature of determining the yield stresses at higher temperatures, it was decided not to fit the data at 160 and 170 ° C by a Bingham or Herschel

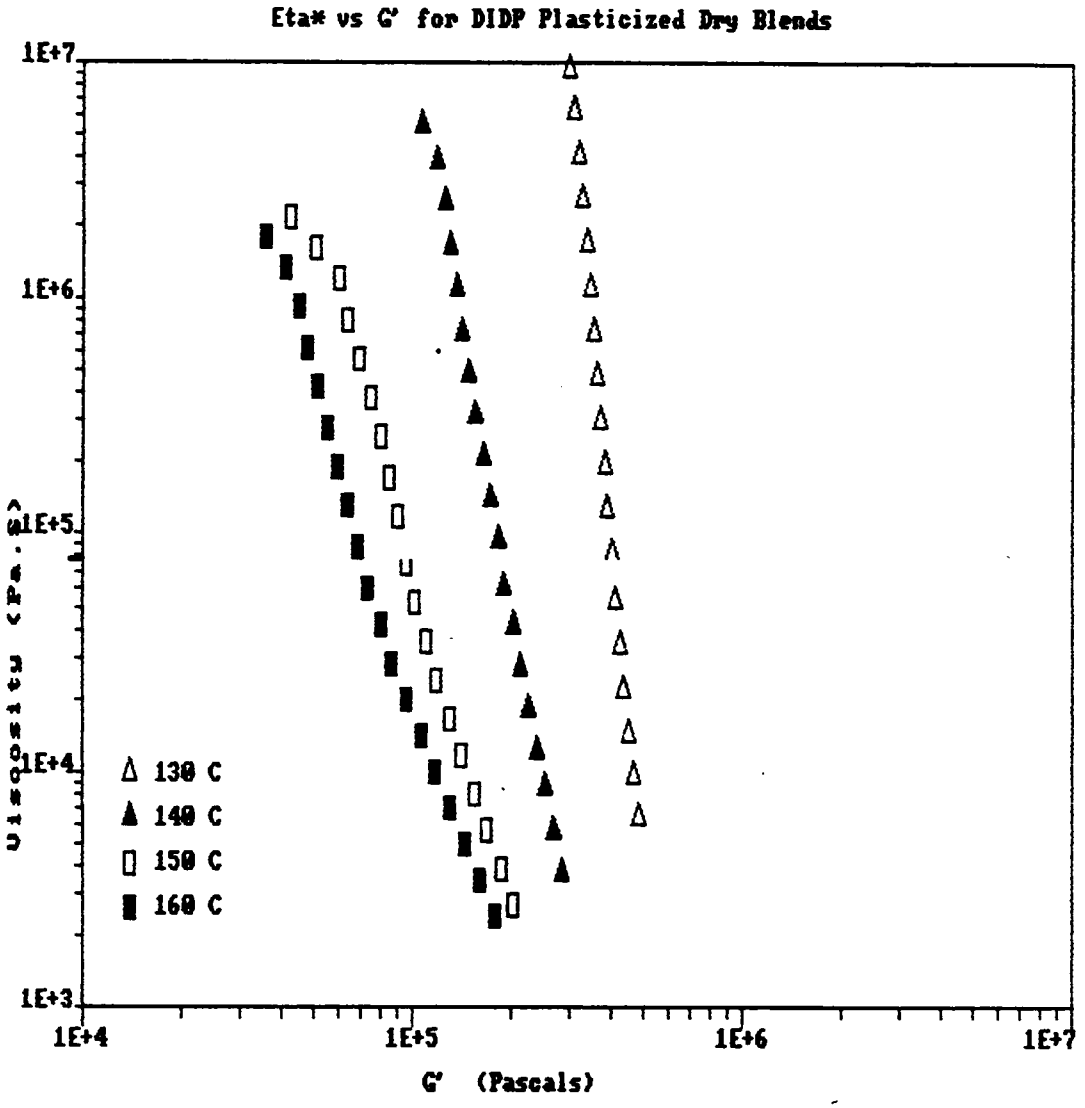

Figure 5. 31. Complex Viscosity vs Storage Modulus Plots for DIDP Dry Blends.

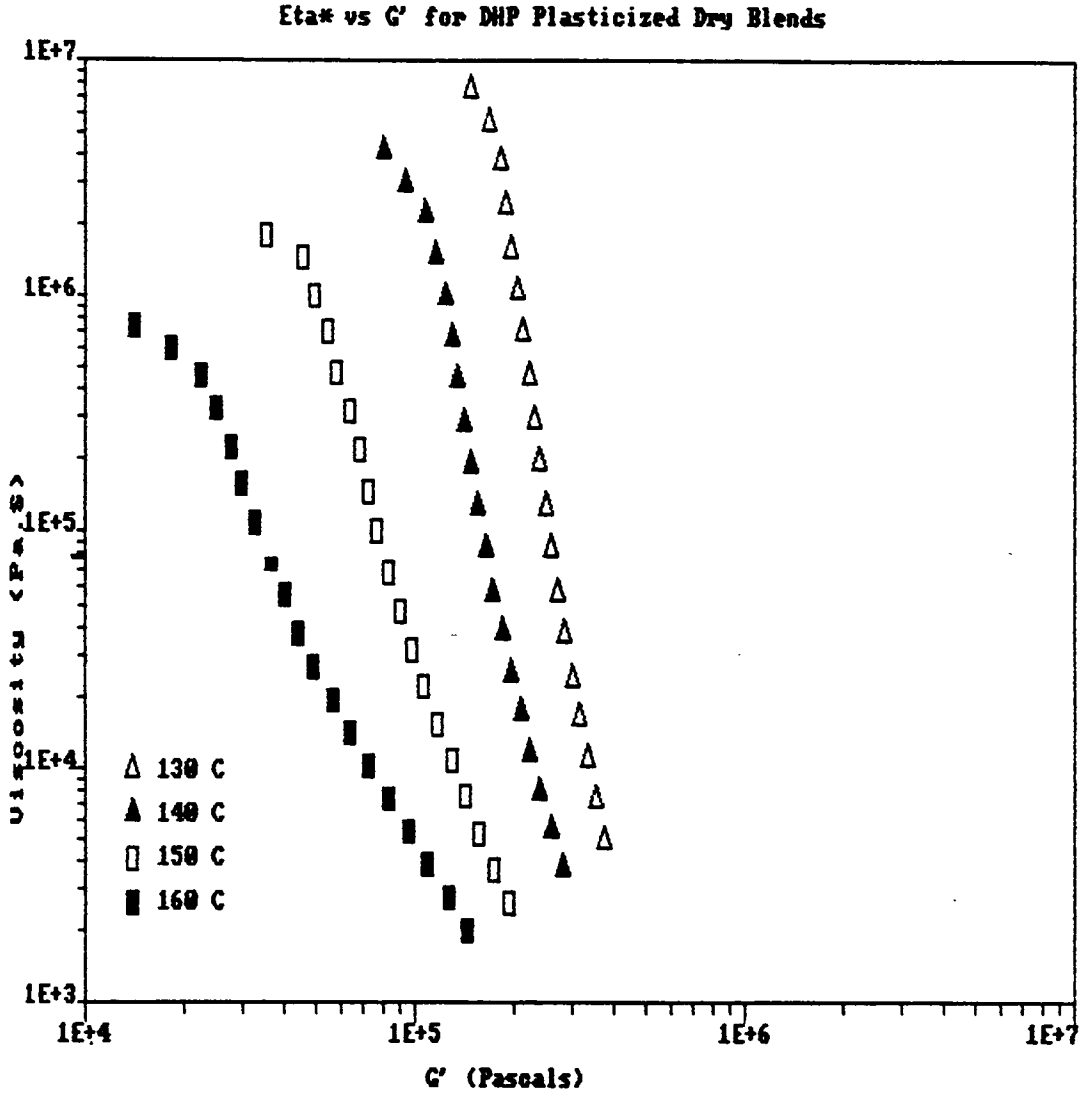

Figure 5. 32. Complex Viscosity vs Storage Modulus Plots for DHP Dry Blends.

Bulkley model. No flow curve were obtained at 130 ° C owing to the difficulty in measuring the viscosity at that temperature with the ICR. In Table 5.21 the BF and the HB parameters for DIDP and DHP dry blends at 140 and 150 ° C are presented. Figures 5.33 and 5.34 show a comparison of the HB and BF models fits to the shear stress - shear rate data of the DIDP and DHP dry blends at 140 ° C. At 140 ° C, it was observed that the HB model provided a superior fit for the shear stress-shear rate data for the DIDP and the DHP dry blends than the BF model. The same was true at 150 °C for both the dry blends. The power law parameters associated with the HB fluid are very different when the HB model is fitted to a set of data at 140 ° C than when a simple power law model is fitted to the same data set. The incorporation of the yield stress in the HB fluid makes the viscosity of the power law fluid much smaller than the viscosity of the power law fluid without any yield stress when both are are fitted to the same data. This is evident from the eqn. 5.1 as shear stress is decreased by the value of the yield stress before determining the power law parameters:

$$\tau = \tau_y + m\,|\dot{\gamma}|^n \qquad (5.1)$$

where τ is the shear stress, τ_y is the yield stress, $|\dot{\gamma}|$ is the magnitude of the shear rate and 'm' and ' 'n' are the power law parameters .

Also, the data at 150 ° C have been fitted to both power law and HB model. Both models seem to fit the data well and the results do not conclusively show that one model is better than the other. As was the case at 140 ° C, the power law fluid portion of the HB fluid is less viscous than just the power law fluid without yield stress, when both models were fitted to the same data. The difference in viscosities or the power law parameters between the power law fluid of the HB model and that of a pure power law fluid at 150 ° C is smaller, than at 140 ° C. This is because the lower yield stress values at 150 ° C have a lesser influence on determination of the viscosity parameters as seen from eqn. 5.1. This fact reinforces the earlier statements that the yield stress might not be a dominant factor affecting the flow rates at higher temper-

atures. However, from the modeling viewpoint in section 5.3, it will be seen that at 150 ° C the viscosity of the PVC dry blended mixes will be modeled as a power law fluid rather than as a HB fluid. Although both models can fit the viscosity data at 150 °C quite well, modeling of the HB fluid will involve one extra parameter and was thus avoided.

The reason for which dynamic experiments were preferred over steady shear experiments for determining yield stresses was mentioned in the beginning of this section. For this research, G′ values were used to determine the yield stresses. Utracki and co-workers [88] had used G″ measurements for calculation of yield stresses to fit the modified Caisson plots but they had not satisfactorily explained the rationale for doing so. Figures 5.35-5.37 contain a comparison of the steady shear and the dynamic data at 150, 160 and 170 ° C for lower shear rates and frequencies. It was not possible to run steady shear experiments at 140 ° C because the normal stresses were too high. A large number of runs had to be performed at 150 ° C to obtain data points from steady shear experiments as high normal stresses interfered with the data collection. This fact perhaps may invalidate the shear stress values from the steady shear experiments. From Figures 5.35 and 5.36 it appears that at 150 and 160 ° C, G″ values follow the shear stress (or τ) more closely than G′. At 170 ° C, the G′ and τ values match better (Fig. 5.37). The validity of interpreting a fluid property like the loss modulus, G″, at low temperatures, when the material is behaving more like a solid, may be questioned. So the overlapping of the loss modulus or G″ (from dynamic experiments) at low frequencies with the shear stress (from steady shear experiments) at low shear rates may not be a sound basis upon which conclusions can be drawn. Even if G″ was selected as a basis of yield stress measurements, it would have resulted in much lower values for the yield stress than the results reported here. If this yield stress together with the viscosity shear rate data were fitted to a HB model, the effect of incorporating the yield stress on viscosity would have been negligible as seen from examining eqn. 5.1. In such circumstances, it is obviously advisable to use the power law model because the HB model introduces one more variable without really affecting the material parameters.

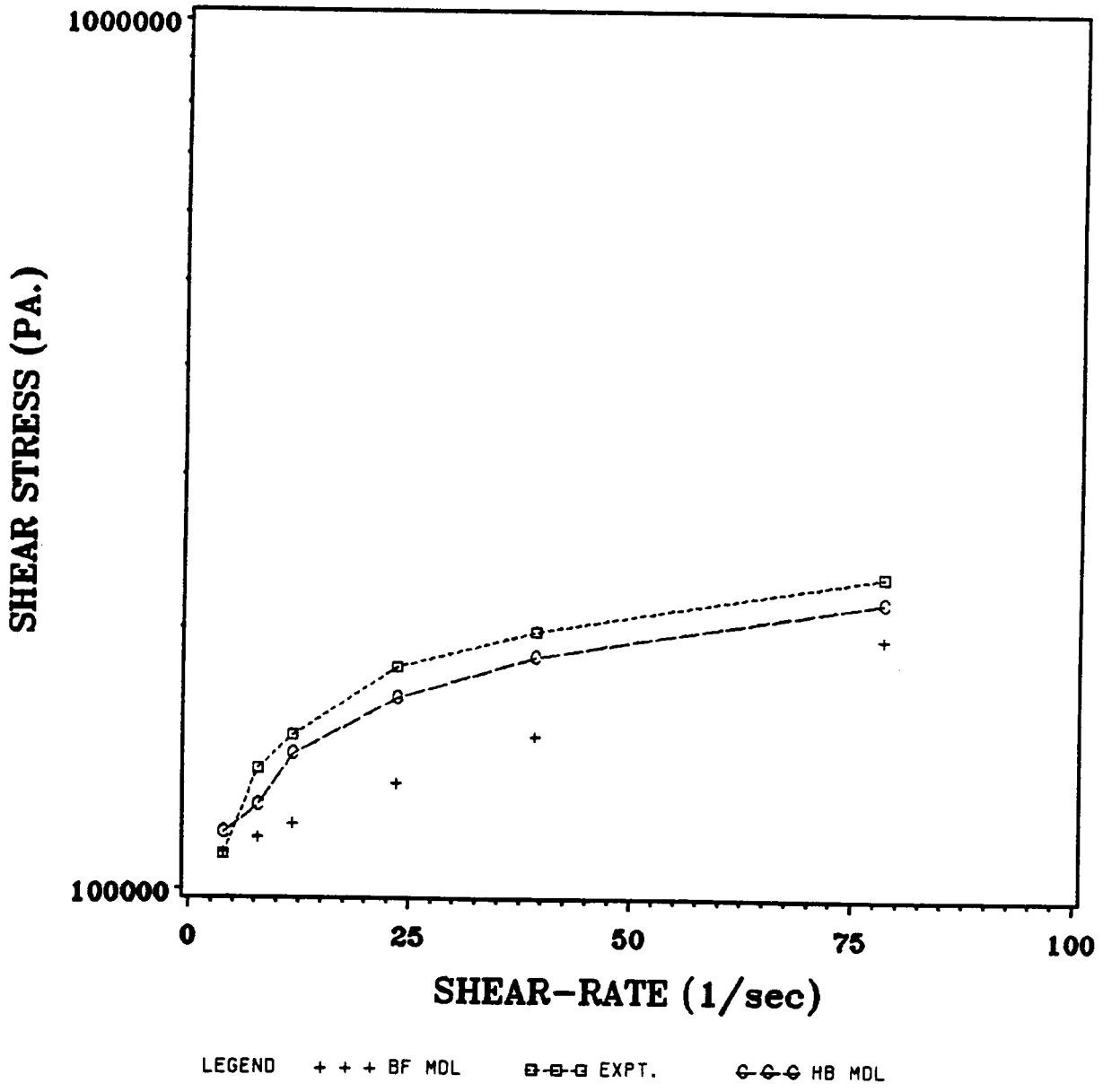

Figure 5. 33. Fitting various models to the DIDP dry blend shear stress-shear rate data at 140 ° C

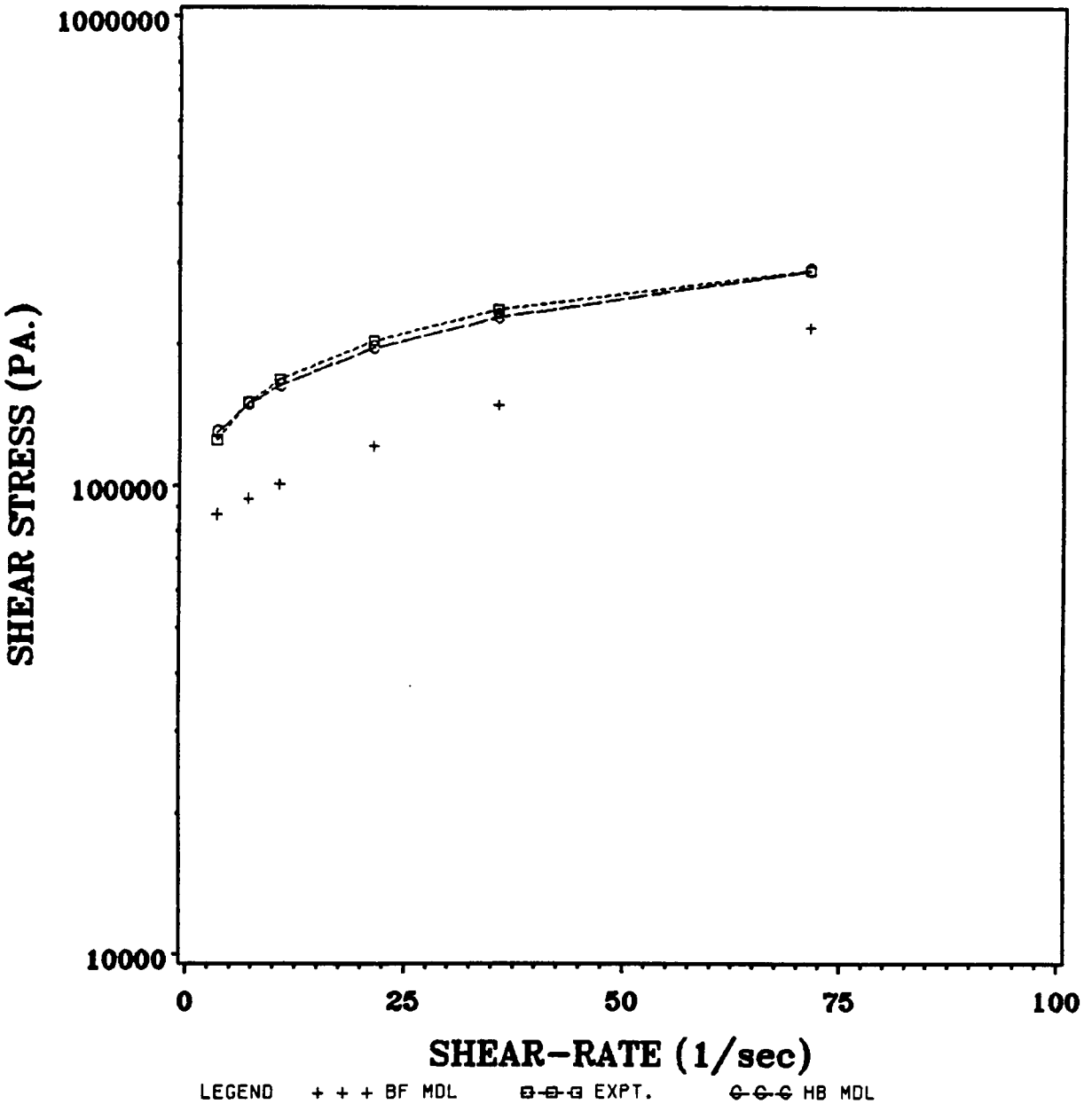

Figure 5. 34. Fitting various models to the DHP dry blend shear stress-shear rate data at 140 ° C

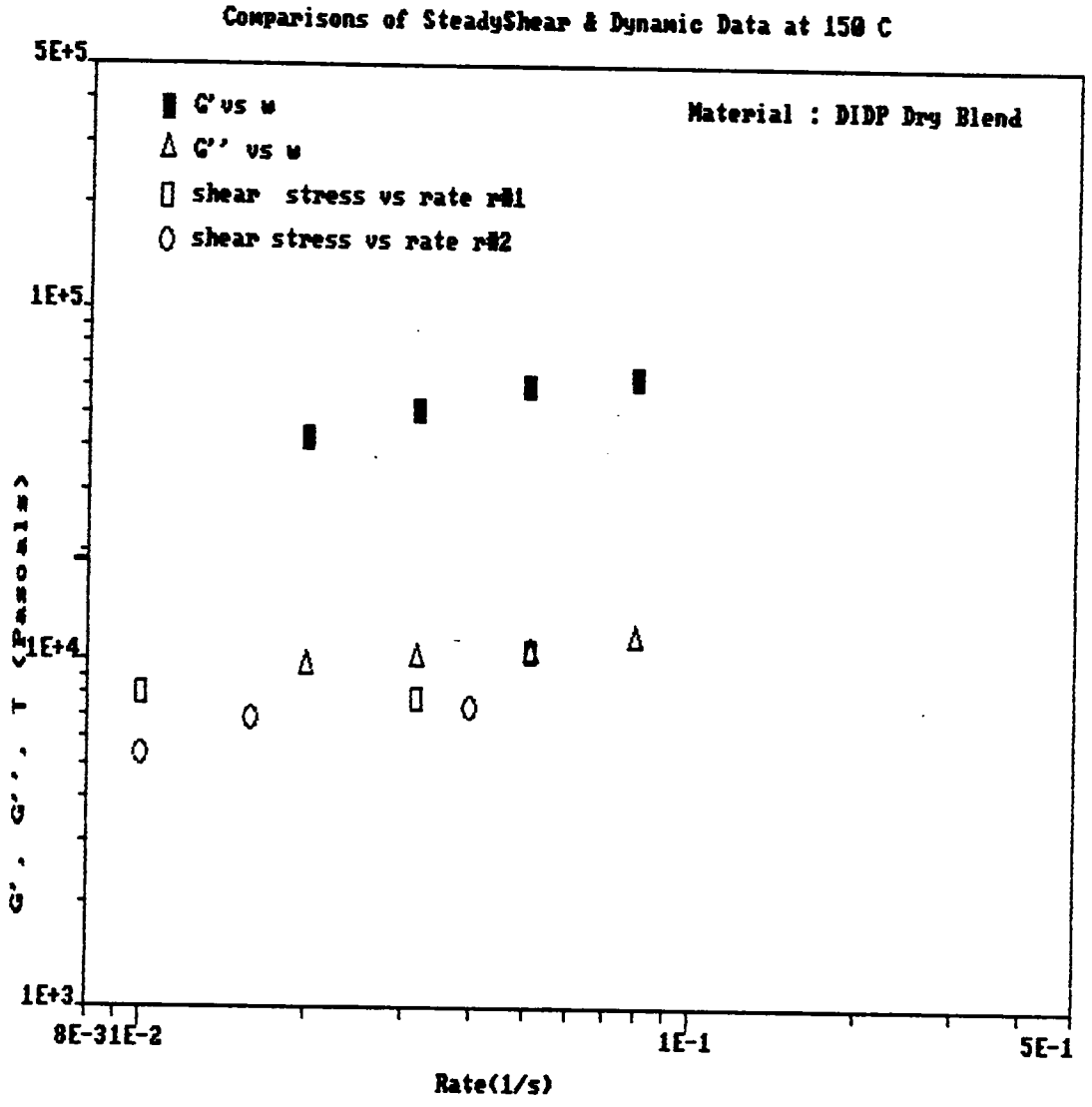

Figure 5. 35. Comparisons of Steady Shear & Dynamic data for DIDP dry blend at 150 ° C

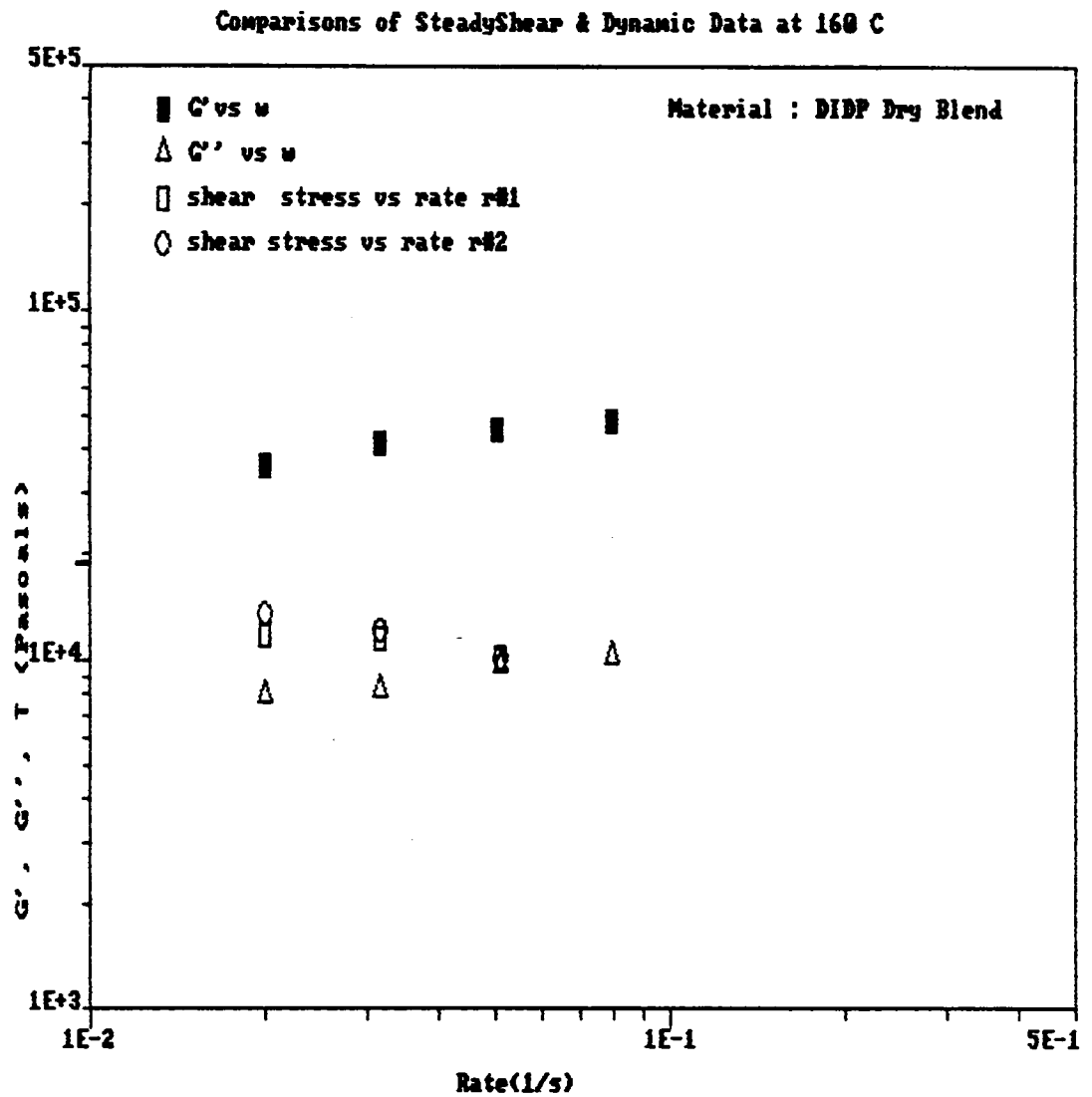

Figure 5. 36. Comparisons of Steady Shear & Dynamic data for DIDP dry blend at 160 ° C

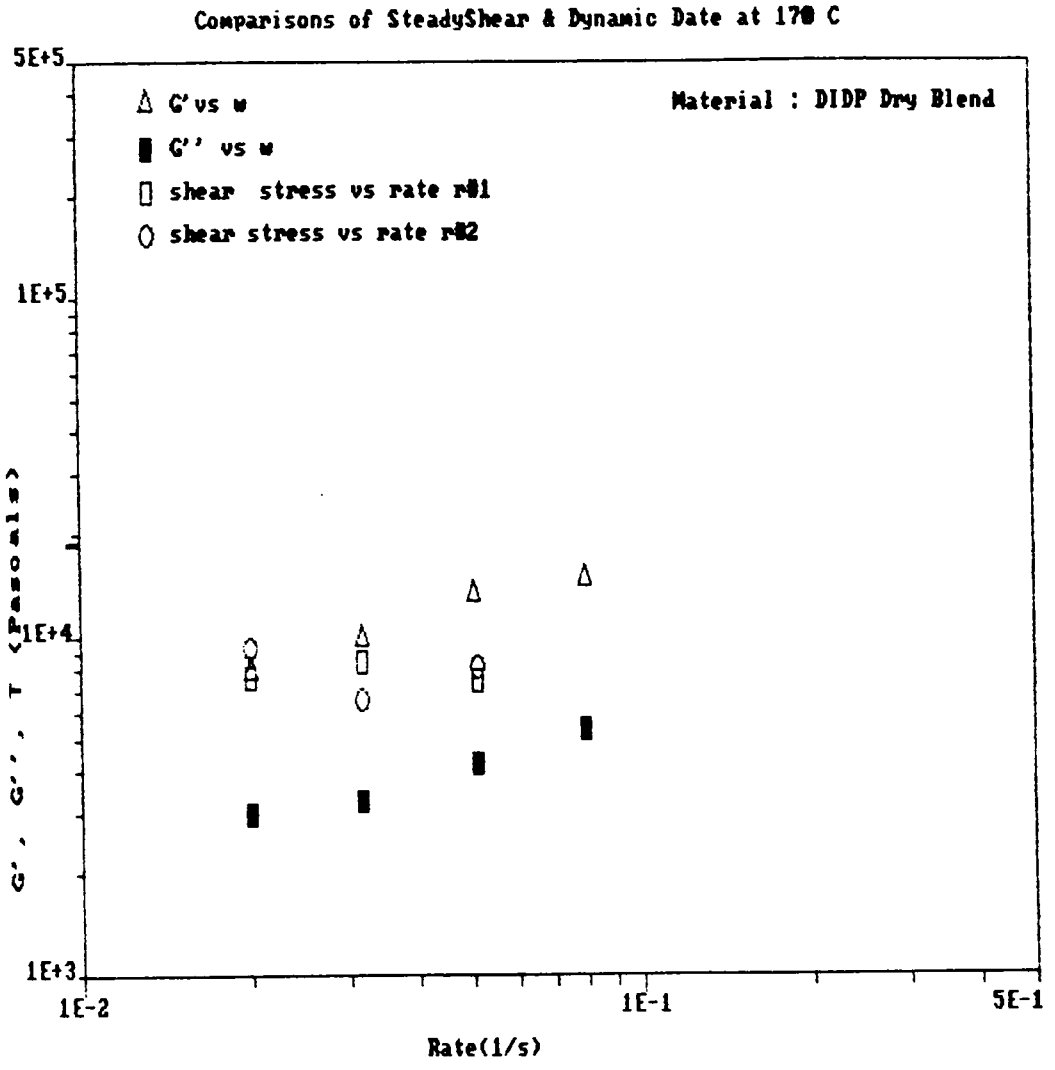

Figure 5. 37. Comparisons of Steady Shear & Dynamic data for DIDP dry blend at 170 ° C

In this section the results of the dynamic mode experiments performed on the RMS to determine the yield stresses and the evaluation of constants for fluid models that incorporate yield stresses have been presented. Both the DIDP and the DHP plasticized dry blends showed definite yield stress behavior especially below 150 ° C and the behavior became more prominent at lower temperatures. The DIDP dry blend showed higher yield stress values than the DHP dry blend. At 140 ° C the HB fluid model fitted the capillary rheometer data for both dry blends better than the BF model. With this, the rheological measurements for fulfilling the research objectives have been completed. In the next two sections, the measurement of thermal properties and friction coefficients will be discussed.

5.1.4 Determination of Thermal Properties

Extrusion is affected by thermal properties like specific heat and thermal diffusivity and conductivity. In this section the measurement of the thermal properties will be reported together with the investigation of whether the plasticizer type has any effect on the thermal properties for both the pellets and the dry blended PVC. Also, it is important to examine what kinds of thermal transitions the plasticized PVC undergoes when it is processed from room temperature to about 190 ° C in the extruder. First the thermal transitions and the calculations of specific heat will be discussed. This will be followed by the thermal diffusivity results.

The experimental procedures used to obtain thermal scans by means of the Differential Scanning Calorimeter have been presented in chapter 3. Briefly, a scanning rate of 20 ° C/min was chosen and the thermal transitions were observed between 40 to 210 ° C. The DSC scans presented in this chapter are representations of repetitive experimental runs. In general, three runs were performed under identical conditions to establish the repeatability of the results. Small variations were observed but these are expected probably because of minor variations in the homogeneity of the sample and in the sampling procedure. When quantitative evalu-

ations of the DSC scans were made for specific heat measurements, the small variations in the scans were possibly reflected in the small variation in the specific heat values.

In Fig. 5.38, the DSC scan of rigid PVC, i.e. without any additives, is shown. It shows a glass transition or TG at about 85 ° C and no sharp endothermic transitions are observed until 200 ° C. In Figures 5.39 and 5.40, the DSC scans of dry blended DIDP and DHP mixes are displayed. The TGs seem to be depressed depressed from 85 or 90 ° C to approximately 65 to 70 ° C but as the scans start 25 ° C earlier at 40 ° C, the actual TG determination could be wrong and the TG possibly depressed further. The plasticizer type does not seem to influence by how much the TG of the PVC mix is depressed. Here also, until 190 ° C, no endothermic peaks are observed. There are small exothermic peaks seen in the DIDP dry blend scan at about 170 ° C and in the DHP dry blend scan at about 165 ° C. No plausible reasons could be attributed for these exothermic peaks. The endothermic peaks between 205 and 210 ° C for the DHP dry blend coincide with the reported crystallite melting point of approximately 210 ° C that has been reported previously for rigid PVC [1]. The absence of sharp peaks between 70 and 200 ° C and the gradual change in slope of the DSC scans for both of the dry blends possibly signify the gradual transition from the solid to the melt state. In other words there is no complete breakdown of the loose semi-crystalline structure of PVC during the processing. This seems to mirror the gradual fusion process of PVC and is consistent with the work of previous researchers [13-15,21,22, 65,66,73].

The results of the DSC scans for the PVC pellets plasticized with DIDP and DHP are similar to those of the dry blends as seen in Figures 5.41 and 5.42. The TGs are located at about 70 to 75 ° C and no endothermic transitions, associated with melting of crystallites, were observed. The small exothermic peaks appear in both the scans at about 160 ° C. It appears less sharp for the DIDP pellets than for the DHP pellets. Also, a small endothermic peak is observed for the DHP pellets around 205 ° C which can be linked to the melting of the crystallites. However, the 10 or 15 % crystallite content was not expected to show a large melting peak in the case of either the pellets or the dry blends.

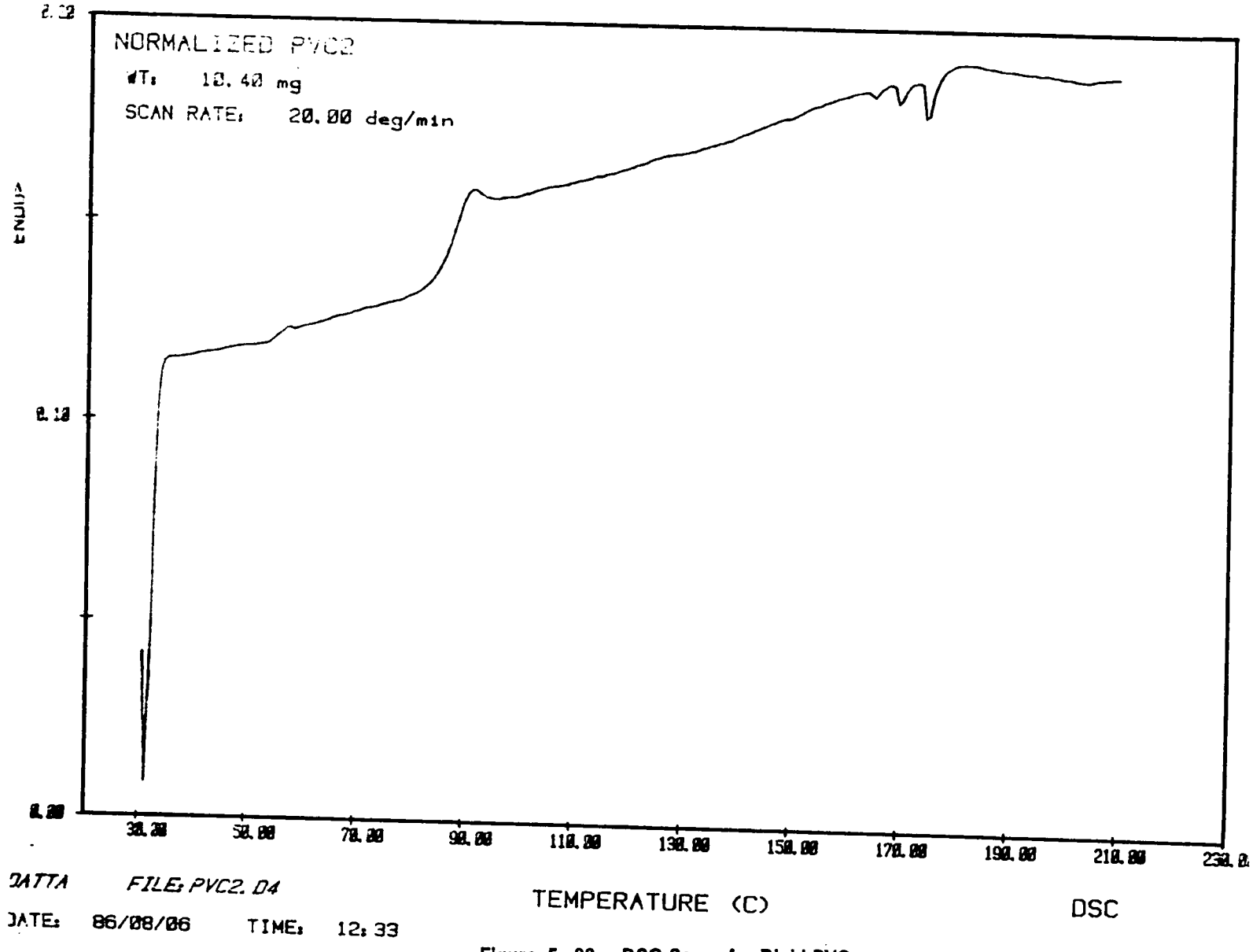

Figure 5. 38. DSC Scans for Rigid PVC

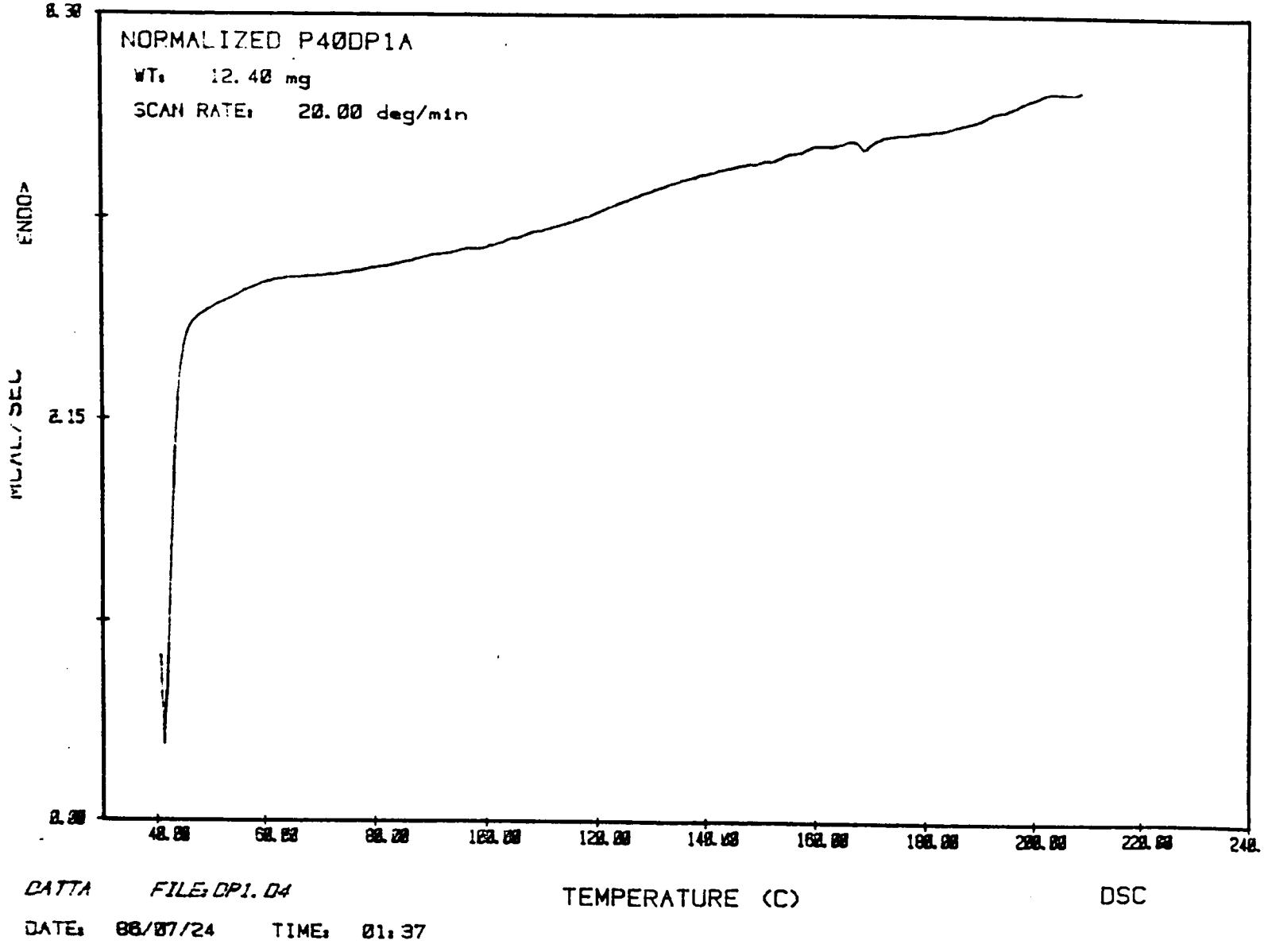

Figure 5. 39. DSC Scans for DIDP plasticized Dry Blended PVC

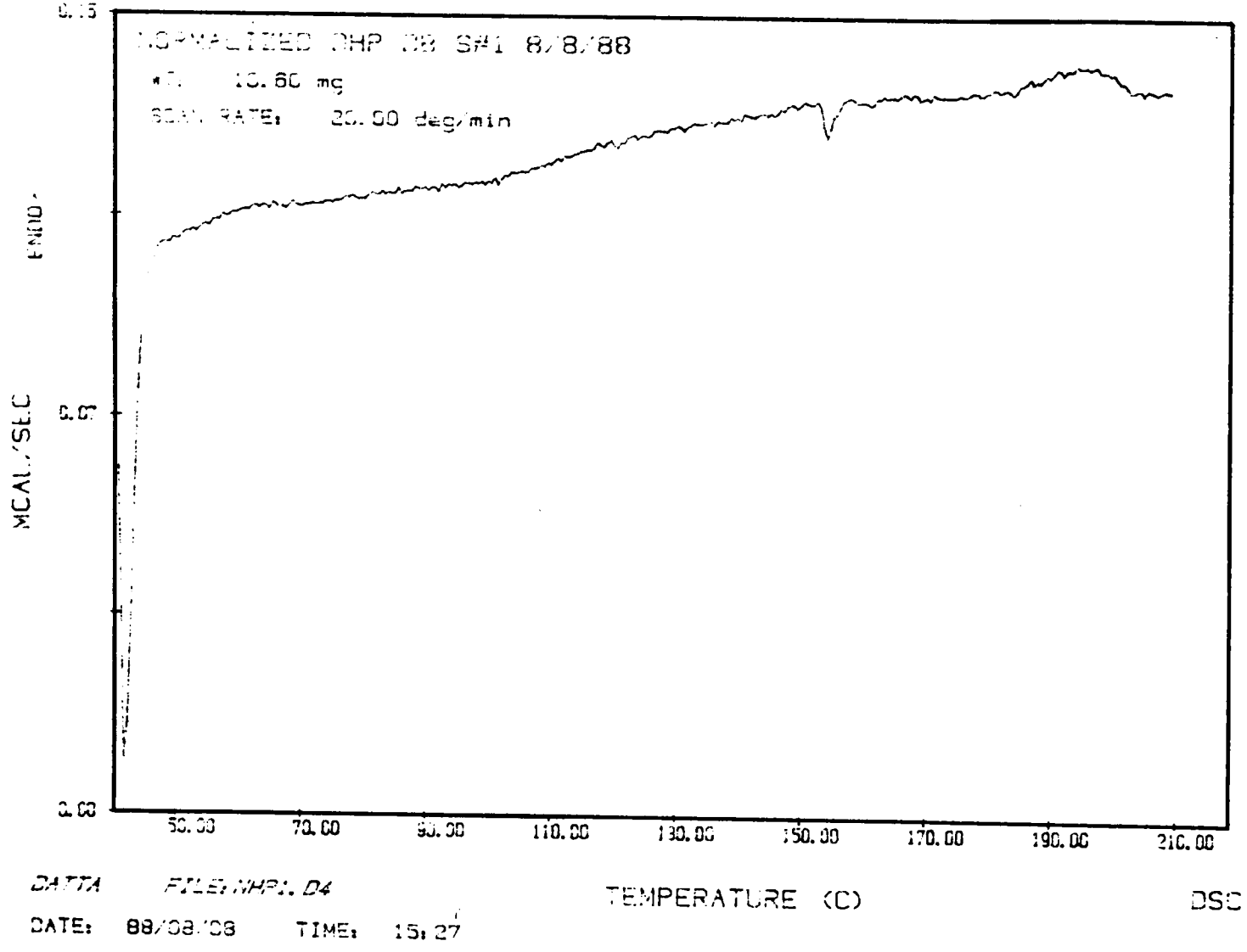

Figure 5. 40. DSC Scans for DHP plasticized Dry Blended PVC

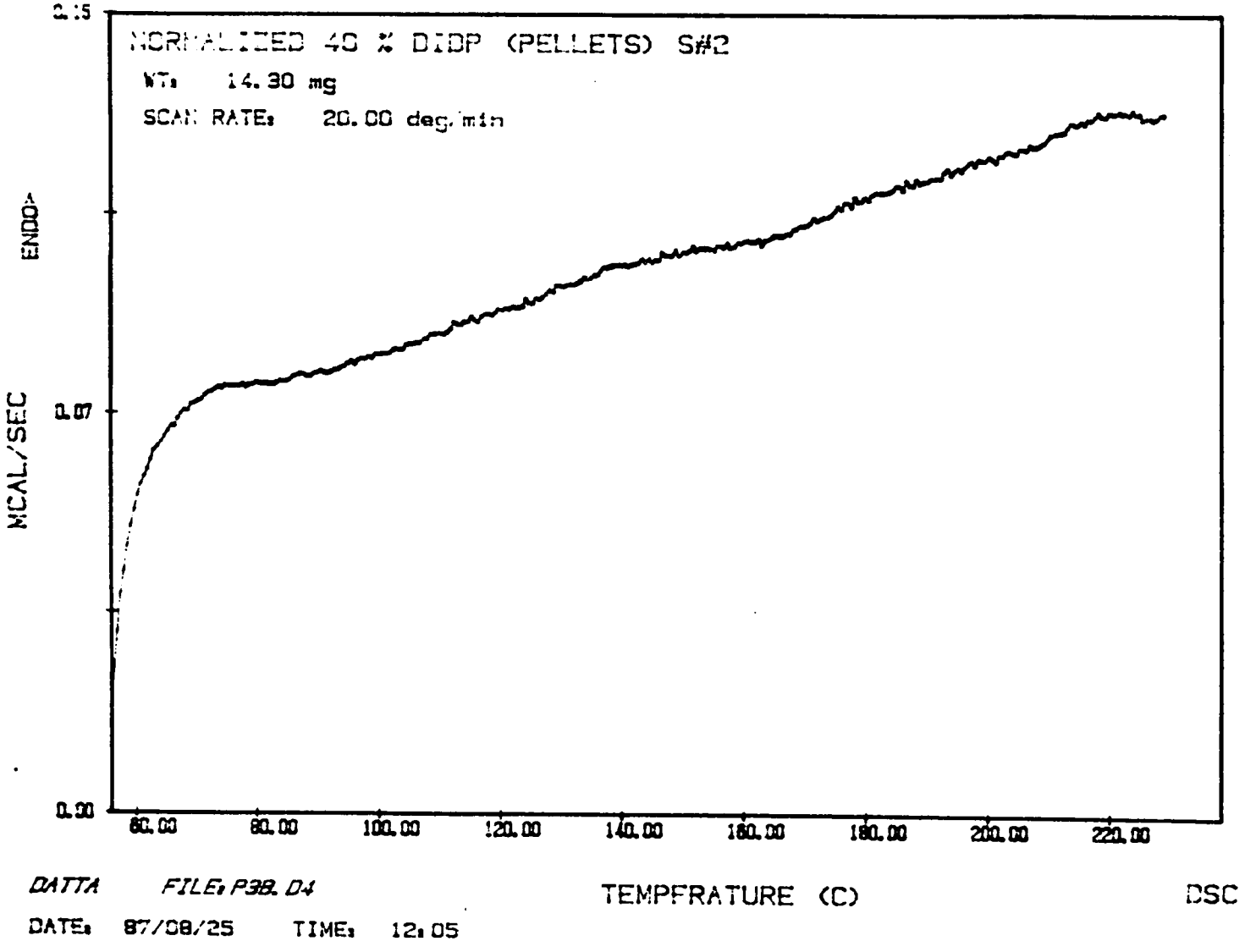

Figure 5. 41. DSC Scans for DIDP plasticized PVC Pellets

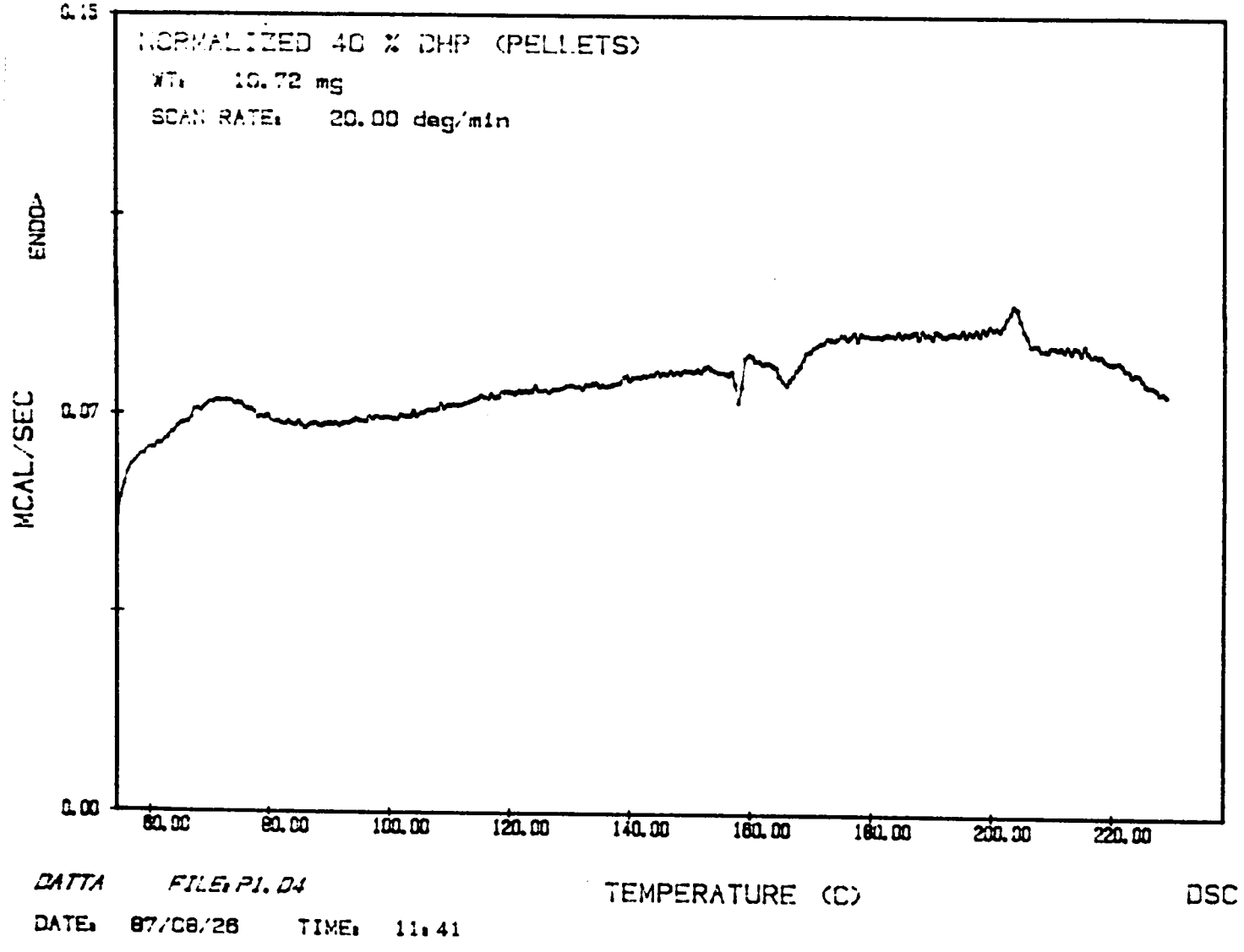

Figure 5. 42. DSC Scans for DHP plasticized PVC Pellets

The DSC scans provide insights into the nature of the changes that take place in the PVC mixes with the rise in temperature. A more quantitative method that reflects these changes is desirable for application in numerical work. When any polymeric material is heated from room temperature to its final processing temperature in the melt state, the added thermal energy raises its temperature from the initial temperature to the melting point, brings about a change of state from solid to melt and raises the temperature from the melting point to the final processing temperature. A thermal property like specific heat, which can be associated to quantify the entire heating up process, will be composed of two parts. One part will reflect the sensible heat capacity or the part linked to the temperature rise per unit mass. The other part will represent the apparent specific heat associated with the change of state per unit mass; i.e. the latent heat term is absorbed in the specific heat capacity and the problem is formulated as though there was no phase change. The total heat capacity should represent the combined effect of both and might vary with temperature. When it is heated from the initial room temperature to the final processing temperature, the specific heat capacity of plasticized PVC will account for the rise in temperature and will also incorporate the gradual change of state or fusion that takes place in PVC.

As indicated in chapter 3 with the DSC system, the specific heat of any sample as a function of temperature can be determined. This is accomplished with the aid of a special software package. To calculate the specific heat values, the software requires a DSC scan and a baseline scan between the same temperature ranges and obtained at the same heating rate. The heat capacity can be obtained in either graphical or tabulated form. But usually errors result because of problems in calibration of the system. To overcome any inherent system error, the same procedure was initially employed to determine the specific heat of a standard sapphire sample. The specific heat values of the sapphire were then compared to the already determined and tabulated specific heat values of this standard sapphire sample. For any particular baseline, the relative difference between the experimental and standard specific heats of the sapphire sample enabled the calculation of correction factors at temperatures at intervals of 5 ° C. The values of the specific heats of the plasticized PVC samples

using the same baseline were then updated using the correction factors associated with the baseline. The correction factors were approximately in the range of 3 to 5 %.

The specific heat values of the dry blends are presented in Table 5.22 and displayed in Fig. 5.43. Each dry blend was run at least three times and the values in the tables are the mean readings of these tests. The spread of the data is approximately 3% about the mean and is indicated by error bars in Fig. 5.43. Inspection of the data shows some variation in the specific heats of the three plasticized PVC dry blends. In general, the DIDP dry blend exhibits higher specific heat than the DOP dry blend, which in turn shows higher specific heat than the DHP dry blend. Although the difference is mostly larger than the error bars, especially between DIDP and DHP, it is not known whether this difference can possibly cause significant difference in the processing of PVC in the extruder.

An examination of Fig. 5.43 reveals a definite pattern in which the data points seem to lie along two lines with different slopes. The change in the slopes of this specific heat-temperature curves occur approximately between 160 and 165 ° C. The transition temperature almost coincides with the temperature change associated with activation energy changes when the flow mechanism changed from particulate to fused or melt like state. It is well documented that at TG, there is an abrupt change in the specific heat [10]. Although there are not enough data points below 75 ° C, there appears to be a leveling off of the data or changes in the specific heat below 75 ° C which at first was associated with the TG of the plasticized materials. As mentioned previously, because the DSC scans for specific heat measurements start at 70 ° C the scans can not be used to determine TGs close to 70 ° C. It might thus be inferred here that a change in the slope of the specific heat-temperature curve for the dry blends at their TG is not identifiable as was expected but the change in slope definitely occurs when the flow mechanism of PVC changes.

Table 5.23 and Fig. 5.44 display the specific heats of the pelletized PVC samples. The spread in the data was again less than 3%. The DOP exhibited slightly higher specific heat than the DHP pellet but the DIDP pellets exhibited significantly higher specific heat than the other two pellets. The difference in specific heat between DIDP plasticized pellets and the

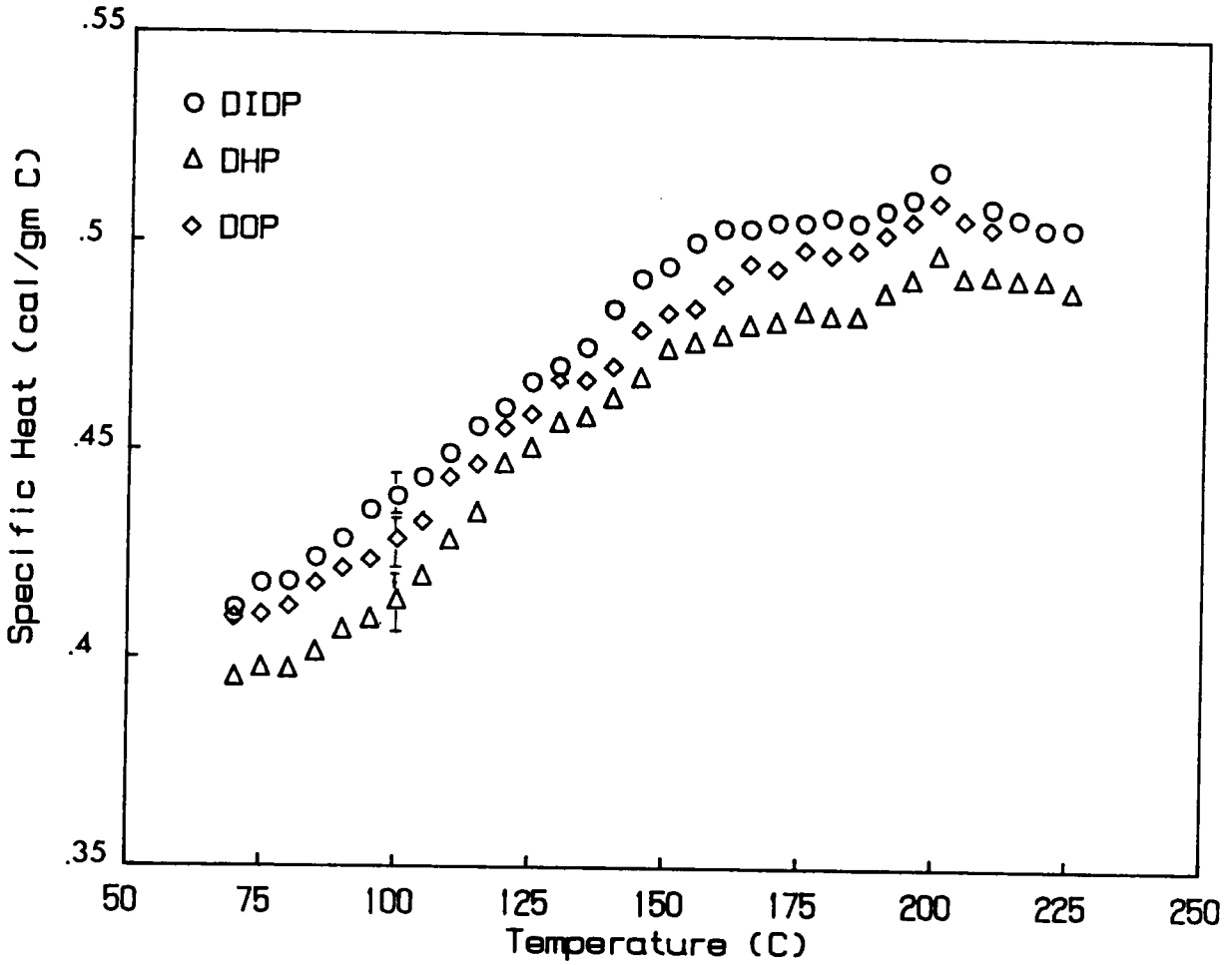

Figure 5. 43. Specific Heats of plasticized PVC Dry Blends

other two plasticized pellets is large. Since the precise preparation history of the pelletized materials is not known, it is difficult to speculate whether the shear or the thermal history during the pelletizing process were different enough to have affected the specific heat values. The change in the slope, associated with change in flow mechanism, at about 165 ° C is also present for the pellets. The change in slope is more prominent for the DIDP plasticized pellets than it is for the DHP or the DOP plasticized pellets. There is also the change in slope of the pellet specific heat vs temperature curve at 70 or 75 ° C, which may not be the TG of the materials as the change in slope occurs at temperatures close to where the DSC scans were started.

To observe whether the shear and thermal history did affect the specific heat of the plasticized dry blends, specific heats of the extrudates formed from the dry blended samples were measured. The samples were obtained from extrusion experiments performed with the 1/16 inch diameter die. The results are presented in Table 5.24 and Fig. 5.45. Comparisons of Table 5.22 and 5.24 clearly indicate that the dry blend extrudates have lower specific heat values than powdered mixes. Unlike the pellets and the dry blends, the DHP dry blend extrudates have a higher specific heat value than the DIDP or the DOP dry blend extrudates, but the difference may not be statistically significant. Again, the slope of the extrudate specific heat - temperature curves change slope at around temperatures where the flow mechanism changes.

An examination of the specific heats in Tables 5.22, 5.23 and 5.24 indicates that in general the pellets and the dry blend extrudates have lower specific heats as compared to the dry blends. As the composition of the dry blends dry blend extrudates and the pellets are the same, a difference in thermal and shear history seemed to induce a change in the specific heat. The DIDP dry blend has higher specific heat than the other two dry blends but for the dry blend extrudates, the specific heat of the DHP samples are slightly higher. It is difficult to say whether these differences are significant enough to cause differences in the extrusion process. The shear and thermal history change associated with the pelletizing procedure was not as pronounced for the DIDP pellet as was for the DHP and the DOP pellets i.e. the former

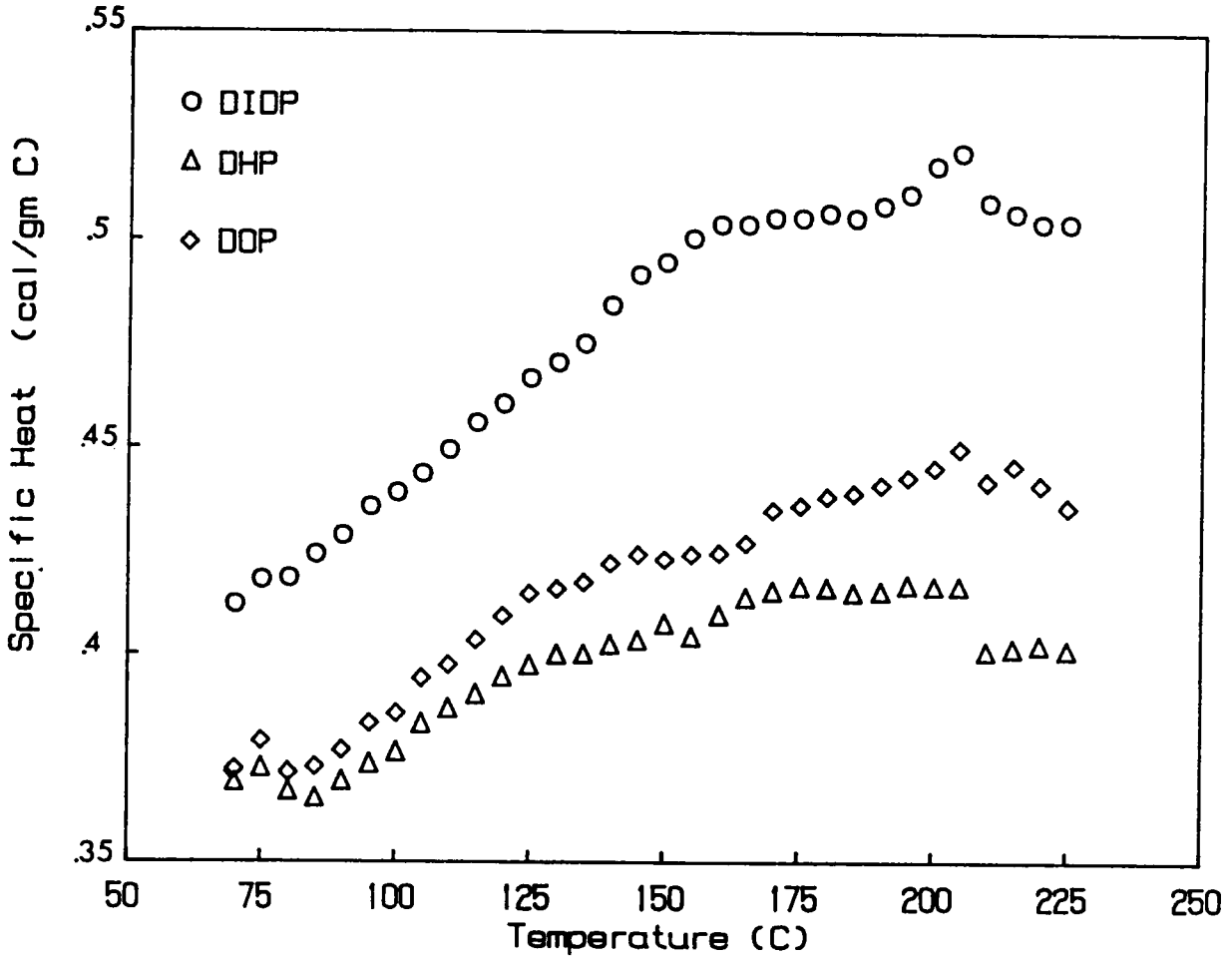

Figure 5. 44. Specific Heats of plasticized PVC Pellets

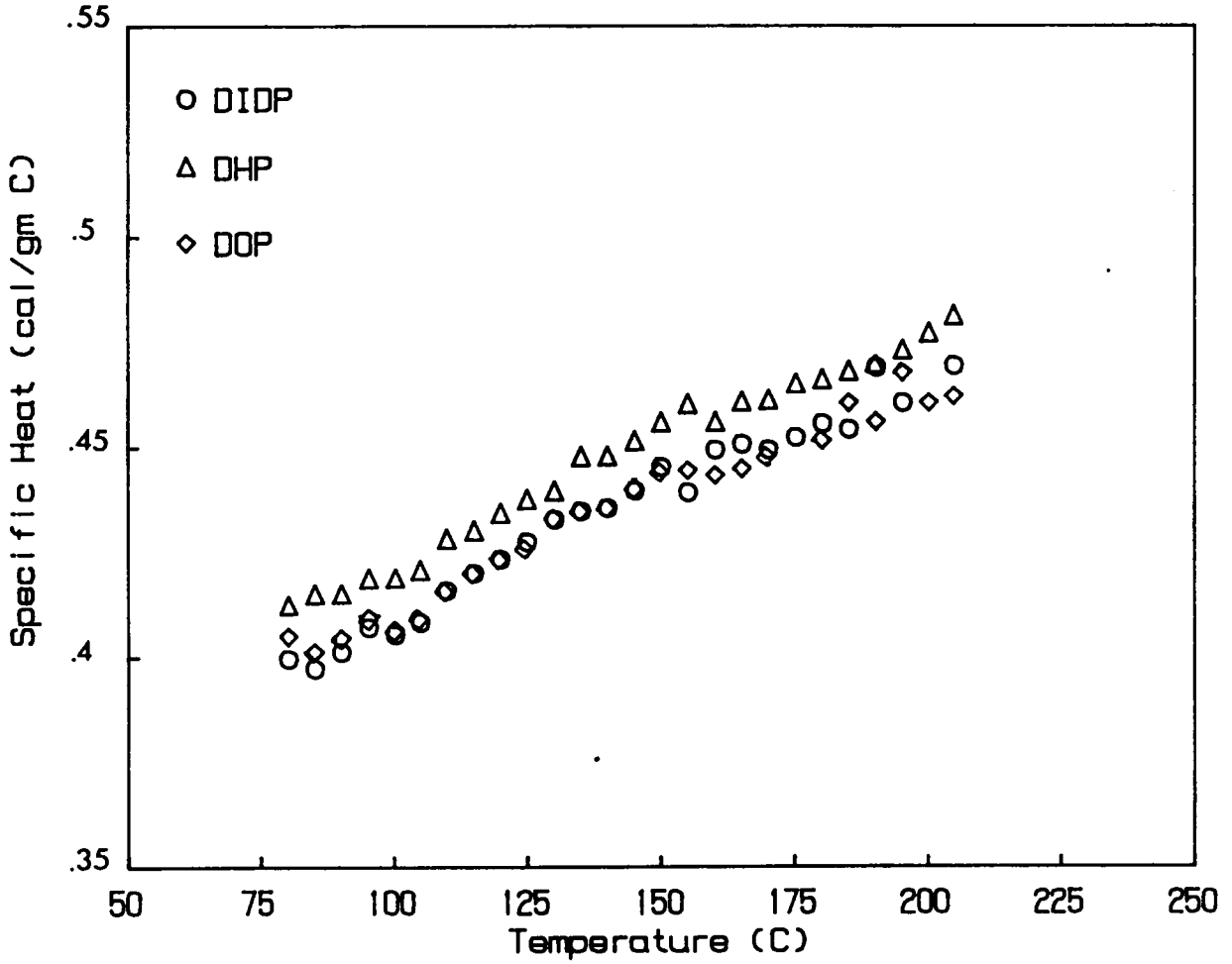

Figure 5. 45. Specific Heats of Extrudates of Dry Blended PVC samples.

have higher specific heat values than the latter samples. As the materials were processed only once through the extruder, it was deemed unnecessary to conduct a through investigation of how shear and thermal histories affected the specific heats of PVC samples. Also, for numerical purposes only a distribution of specific heat as a function of temperature is required and the data in Tables 5.22 and 5.24 supply this information.

The second thermal property that has been investigated is thermal diffusivity. The numerical methods require the evaluation of thermal conductivity rather than thermal diffusivity. No instrument to measure the thermal conductivity was available. Thus thermal diffusivity was measured and the thermal conductivity was determined from the following expression :

$$k = \alpha \times \rho \times C_p \qquad (5.2)$$

where k is the thermal conductivity, α is the thermal diffusivity, ρ is the density and C_p is the specific heat.

The experimental procedure and the theory behind the laser flash apparatus used to measure thermal diffusivity has been explained in chapter 3. In each experiment, a laser beam was directed on one face of the sample and the temperature on the other face, which increased with time, was monitored. The samples were cut from films which were formed by pressing the dry blended powder or the pellets in a hot mold. From the sample thickness and the time needed for the back surface to reach half of its final temperature value, thermal diffusivities were calculated. Corrections were applied for heat loss by convection from the samples at temperatures above the ambient.

The results of the thermal diffusivity experiments can be seen in Figures 46-48 for the dry blended samples. The experimental data are also given in Table 25. Each data point represents an average of three experimental runs. The thermal diffusivities initially decreased with temperature and then seemed to level out. But for the DHP and the DOP dry blends, it was not possible to record any data below 100 ° C. The noise to signal ratio of the amplified signals, coming from the monitored back surface of the sample, was high at low temperatures,

and this interfered with the data collection. At temperatures above 160 ° C, the laser flash passed through the sample almost instantaneously and precluded any meaningful measurement of the thermal diffusivity. There does not seem to be a significant effect of the plasticizer type on the thermal diffusivity. The laser flash technique was unsuccessful for measuring the thermal diffusivity of the pellets as the laser beam penetrated and heated up the back surface of the sample very fast. In other words the laser passed through the pelletized samples almost instantaneously. The thickness of the pressed pelletized films were changed but still no data could be obtained. The fact that the pellets and dry blends above 160 ° C allowed almost instantaneous passage of the laser beam might reflect on the state of fusion attained at higher temperatures. The pellets were fused during the preparation and therefore may have transmitted the laser beam in a manner similar to their passage through the fused dry blends at 160 ° C.

The thermal properties are not as sensitive to the plasticizer type as some of the rheological properties. The plasticizers seemingly depressed the TG of PVC by 15 to 20 ° C but it could have been still lower. The level of plasticizer loading rather than the plasticizer type determined by how much the TG was depressed. There are no sharp endothermic transitions in the DSC scans for the PVC dry blends and the pellets in the temperature range in which they are processed. The plasticized PVC samples gradually fuse from the solid to the melt state. The specific heats increase with increase in temperature and the DIDP samples register a slightly higher specific heat than the other two plasticized mixes in both the pelletized and the dry blended states. For the dry blended extrudates, the DHP samples had slightly higher specific heat values but the difference may not be significant as may have been in the case of the pellets and dry blends. Also the change in PVC from a particulate to a fused state seemed to be accompanied by a change in the slope of the specific heat-temperature curve. There was no significant difference in the measured values of the thermal diffusivities of the three dry blends between 100 to 160 ° C.

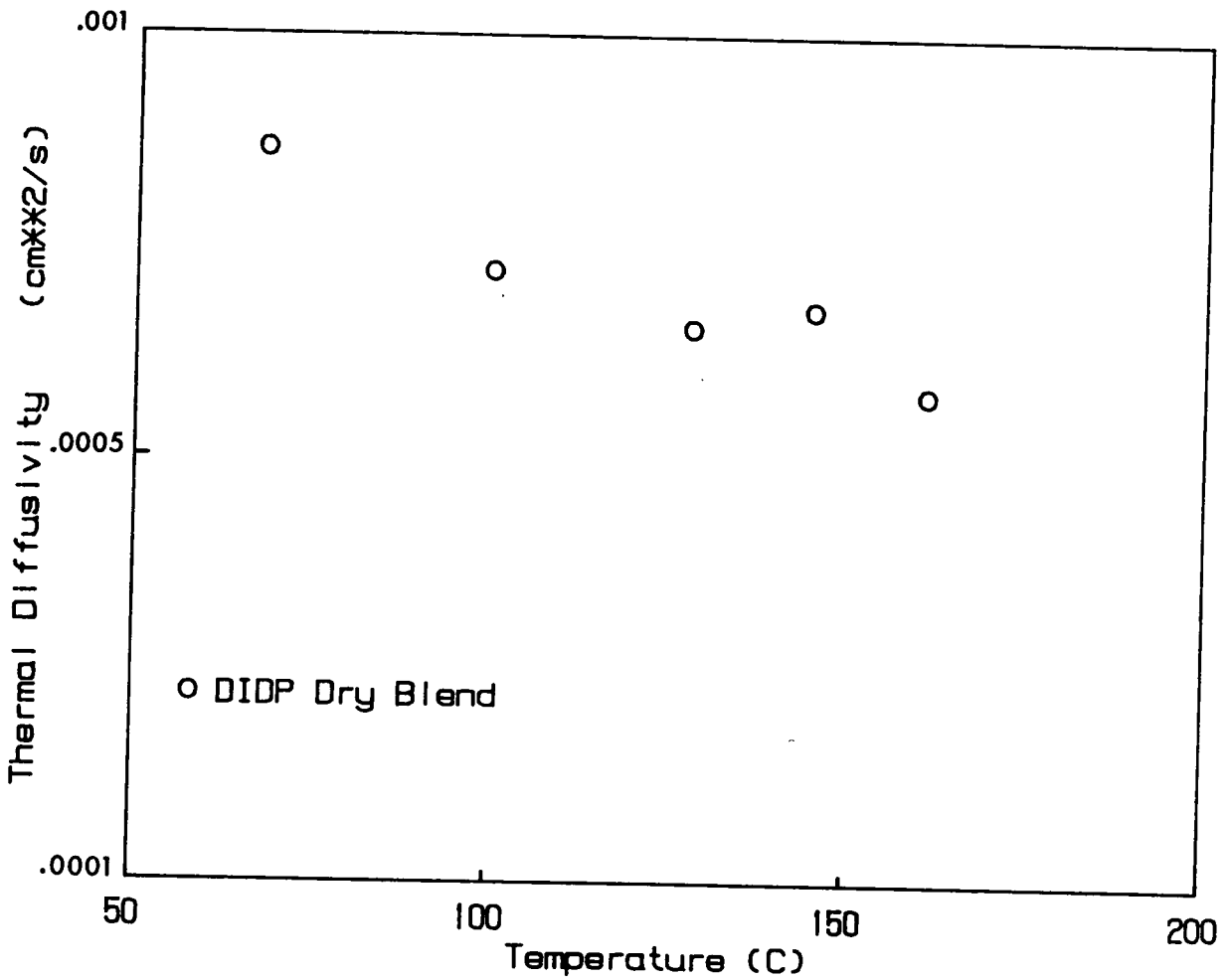

Figure 5. 46. Thermal Diffusivities of DIDP Plasticized PVC Dry Blend.

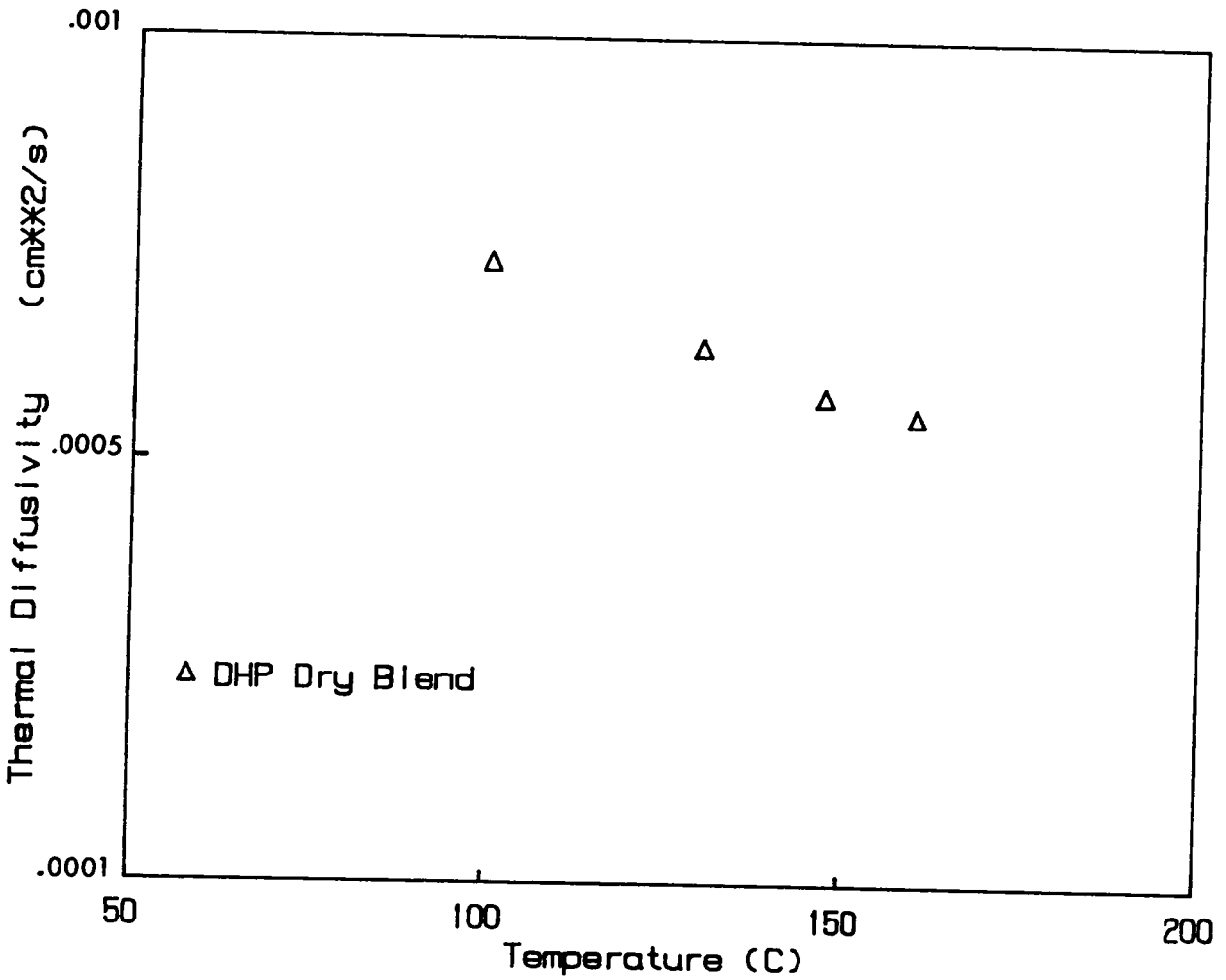

Figure 5. 47. Thermal Diffusivities of DHP Plasticized PVC Dry Blend.

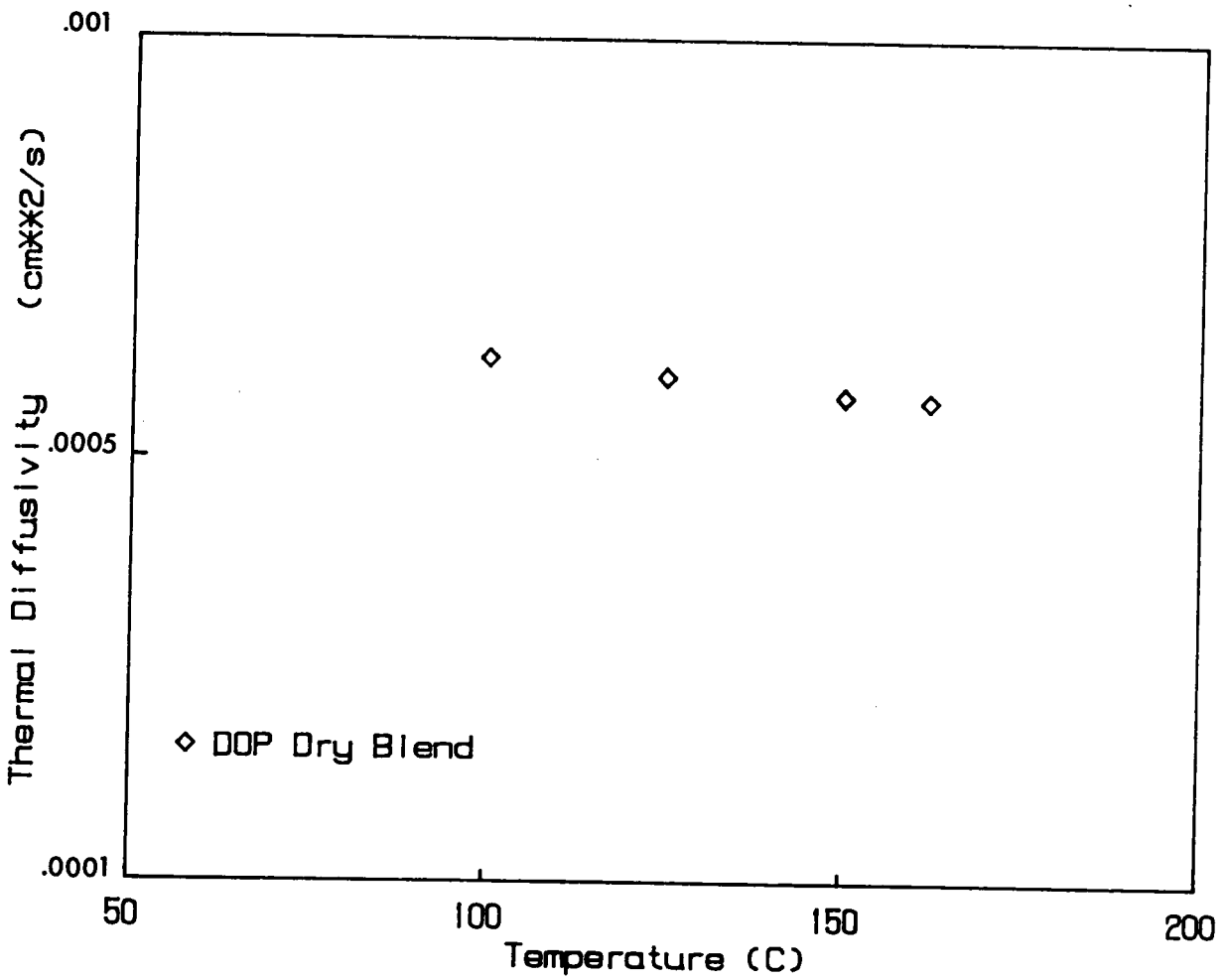

Figure 5. 48. Thermal Diffusivities of DOP Plasticized PVC Dry Blend.

5.1.5 Friction measurements

One of the objectives of this research is to model the solids conveying as a fluid having a yield stress. The results of the proposed solids conveying have to be compared with the existing solids conveying model to test the validity of the new model. The existing model requires the determination of friction coefficients between the polymer and the material of the barrel and screw. The measurement of the friction coefficient of the dry blended DIDP and DHP samples was performed against a finely machined steel surface because these materials show the most obvious differences in the extrusion performance. The key to the difference in the extrusion performance could possibly lie in their respective behaviors in the solids conveying zone which in turn is governed by their friction characteristics. The friction factors of these two materials are obtained using a pin-on-disk apparatus [93]. The sample preparation, a brief description of the apparatus and the experimental procedure have been outlined in chapter 3. The speed of the rotating disk was set to simulate the conditions in the solids conveying zone for a screw speed of 35 rpm. The equipment had to be calibrated for the tangential force. For a nitrogen pressure of 3.5 to 3.9 psi on the pin, the normal force was calculated. The tangential force was measured when the sample was lowered on the rotating disk. The ratio of the tangential to the normal force was the friction coefficient. First the friction coefficient was measured at room temperature and then at temperatures at intervals of approximately 10 ° C until the sample was so soft that it broke off from the holder above 130 ° C.

The results of the friction measurements are presented in Figures 5.49 and 5.50 and reproduced in detail in Tables 5.26 and 5.27. The average surface roughness of the disk against which the friction coefficients were measured was 0.22 μm. Ideally whatever the surface roughness value might be (within a certain tolerable variation), the final friction coefficients between the polymer and the rubbing surface reach an equilibrium or steady state value [93,94]. This is particularly true for surface roughness of the disk used in the experiments in

this thesis and also for smoother surfaces. It has been demonstrated in the past that that for surface roughness of the same order of magnitude as used here, the equilibrium or steady state friction coefficients for rigid PVC were nearly independent of the sliding speeds and surface roughness [93]. Although no formal measurements were made of the barrel and screw surface, a visual observation of these surfaces indicated that these were smoother than the disk used in the experiment. So the measured friction coefficients are probably close to the actual friction coefficient values existing in the extruder between the PVC dry blends and the barrel and the screw. There are other factors that can cause differences between the actual and the measured values of the friction coefficients and they will be discussed later. The magnitude of the measured friction coefficients fall within the same range as previously published data and the initial trend of rise in friction coefficients with temperature has also been observed [80,93]. Owing to the large scatter in the data, a comparative analysis of the data from the figure might not be a worthwhile exercise. There are certain general trends which are common in both plots. The friction coefficients rise until a temperature of 60 or 70 ° C is reached, remain somewhat constant until 115 or 120 ° C, and then start to fall. The fall in the friction coefficients at higher temperatures is expected since the material softens as it approaches temperatures, for which particulate flow can occur.

Certain legitimate concerns can be raised about facts that could have interfered with these experiments and in using the frictional coefficient data from these experiments in the numerical work. The state of compaction of the sample might not be the same as the state existing in the extruder. The normal forces that exist in the extruder are far higher than normal force of 5 or 6 Newtons that are exerted by the polymer pin on the rotating disk. Although the theory behind the measurements of friction coefficients assumed that when the normal force increased, the tangential force increased in the same proportion so that their ratio, which is the friction coefficient, remained constant. This fact has not proved to be universally true and certain variations of the friction coefficients with normal force has been observed [80]. The difference in surface roughness may not contribute to a major difference in friction coefficients as discussed previously. The disk and the extruder barrel or the screw

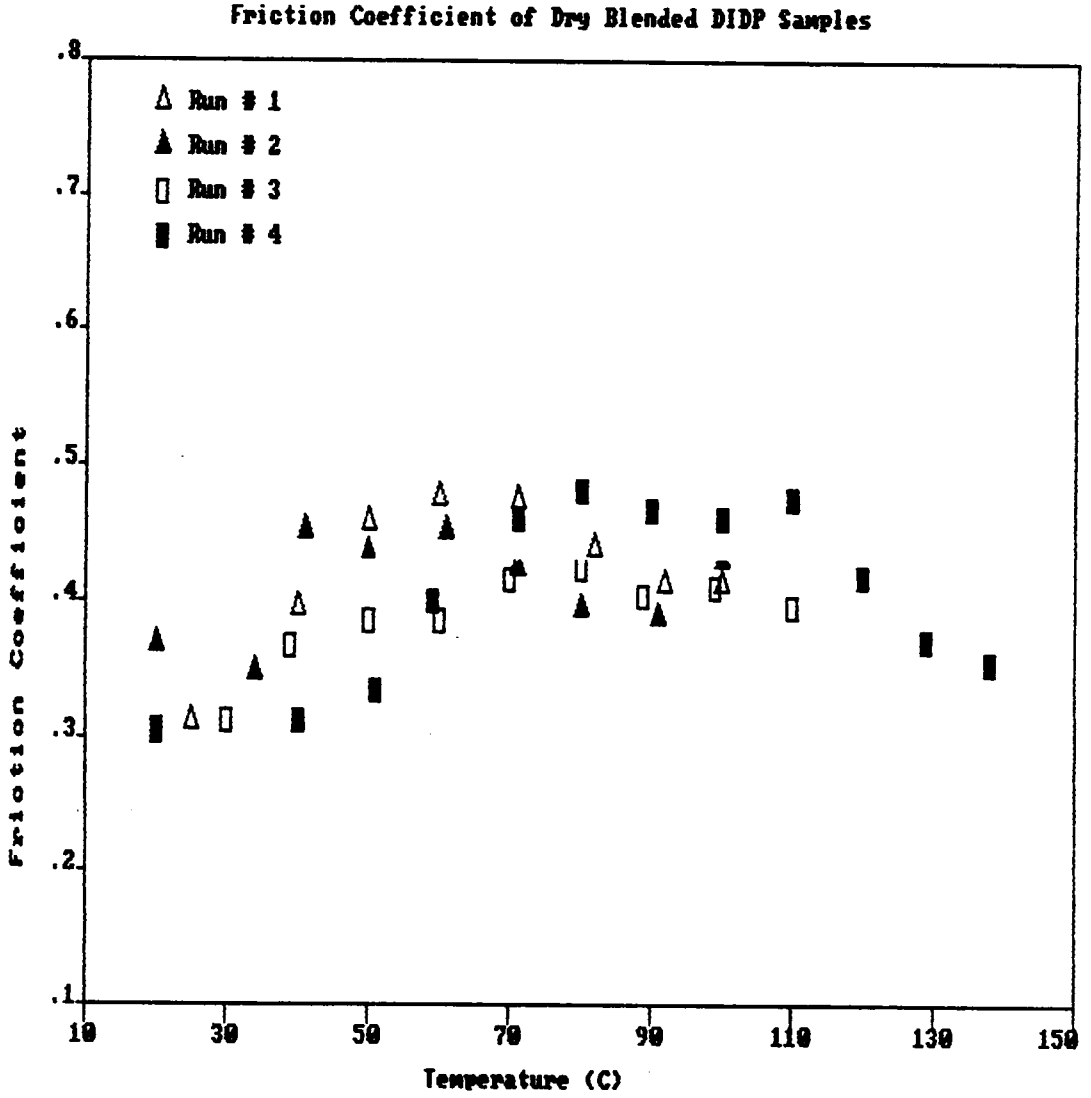

Figure 5. 49. Friction Coefficients vs Temperature of Dry Blended DIDP Samples

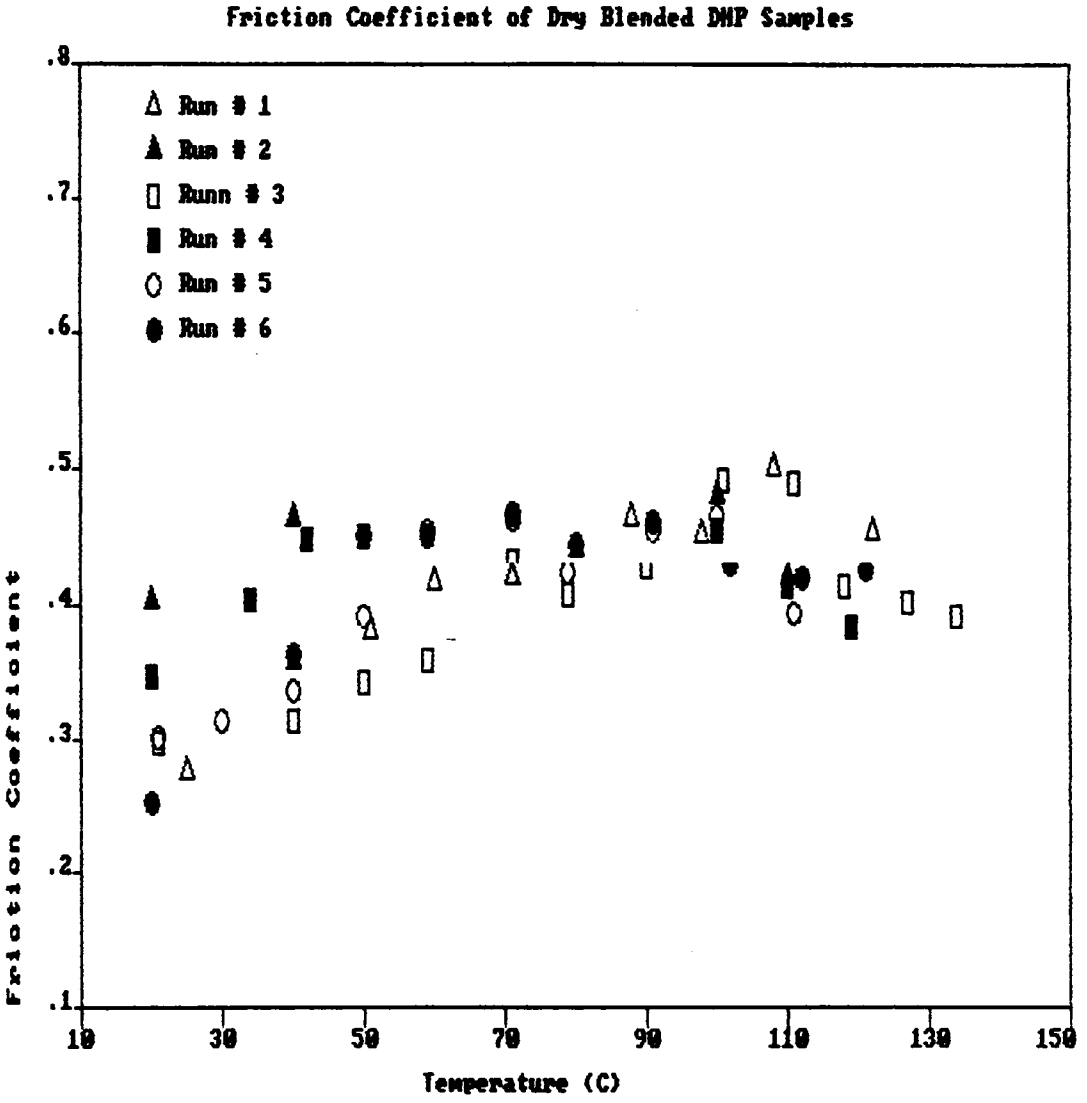

Figure 5. 50. Friction Coefficients vs Temperature of Dry Blended DHP Samples

were not made of the same material. Adhesion between sliding surfaces does influence tangential frictional forces between them but after repeated rubbing of the polymer, the friction coefficients are not much influenced by the material of the rubbed surface [80]. The pin was allowed to slide on the disk on the same track so that a polymer deposit formed on it. But no controlled experiments were performed to observe how a large number of repeated contacts between the polymer pin and the disk affected the friction coefficients. The measured friction coefficients are to be used in the existing solids conveying model which also incorporates terms like non-isotropic pressure distribution factor, ratio of friction coefficients between the screw and the barrel, etc. By manipulating these factors, other than friction coefficients, the existing models can be made to match numerical results to the experimental results. So it is seen that absolute values of friction coefficients may not be the only factor that can influence the solids conveying models.

The scatter in the friction coefficient data does not permit any definite conclusions regarding the effect of the plasticizer type. The trends and the magnitude of the friction coefficient match some of the previously published data. Still, the measurements of friction coefficients (and the solids conveying model in which they are used) are difficult to analyze as compaction, local temperature and pressure changes and solid-solid interface interactions complicate the situation.

5.2 EXTRUSION STUDIES

One of the three main objectives of this research is to investigate the effect of plasticizers on the extrusion process in a single screw extruder. At the beginning of this chapter, rheological properties that might influence the extrusion process have been observed to reflect the effect of the plasticizer type. The sensitivity of these physical properties to the

plasticizer type indicate a possibility that some differences in extrusion characteristics, such as pressure buildup, temperature profile, flow rate, etc. might be observed for different PVC mixes owing to difference in the plasticizer type. The extrusion work can be divided into two sections. In the first section the effect of plasticizers on pressure development, flow rate and amperage were recorded. This was done for both cases with the 1/8 and the 1/16 inch dies attached to the extruder and with both pelletized and dry blended samples. In the second section, 'cooling experiments' were conducted to study the melting mechanism of the plasticized PVC and to find out the effect of the plasticizers on the melting mechanism of PVC in a single screw extruder. The differences in physical properties and differences in the melting mechanism have been correlated to observed differences in the extrusion characteristics.

5.2.1 Studies on the Effect of Plasticizers on Extrusion Characteristics

To help in analyzing the results of the extruder runs, certain conditions under which the experimental variables were recorded will be addressed or re-emphasized. The pressure transducers on the extruder were positioned at turns 10, 13, 16 and 19, respectively. The pressures from each of the four transducers were recorded on strip chart recorders. As the screw flight swept past the transducer, depending on whether the edge of the flight or the center of the channel came directly under the transducer, the transducers were subjected to a maximum or a minimum pressure, respectively. The pressures recorded on the strip chart recorder thus alternated between a maximum and a minimum value. All pressures reported in this section are a mean of the two extreme values. For a particular speed, each extruder run was repeated two or three times to test the reproducibility of the results. For both the pellets and the dry blends and with the 1/8 inch die attached to the extruder, the pressure readings between repeat runs in the last two zones of the extruder varied by approximately 350 tO 861 KPa (50 to 125 psi), although occasionally the variations were as high as 1035 KPa

(or 150 psi). The variation in the measured pressure between repeat runs was the same for all three dry blends and the DHP pellets with the 1/16 inch diameter die attached to the extruder. But on a few occasions, for the DOP and the DIDP pellets the corresponding difference in pressures between the repeat runs were as high as 1725 KPa (i.e. 250 psi) in the last two zones of the extruder Later it will be observed that even these large variations do not affect the conclusions drawn from the results presented in this section. The pressure fluctuations between the repeat runs for the first transducer located at turn 10 sometimes varied by a considerable amount. This turn is normally situated in the solids conveying zone or the melting zone. The transducers might not accurately indicate the pressure readings in the solids conveying zone as they are probably not designed to respond to pressures in the solids conveying zone. The transducers, when positioned in the melting zone, probably responded to variations in pressures between the melt pool and the compacted solids and thus might be subjected to a large fluctuation in pressure. Initially some of the extruder tests pressures were recorded only from the last two pressure transducers while the first two pressure wells in the extruder were plugged off. But later they were recorded from all the four pressure transducers. Still at times, no appreciable pressures could be recorded from the first two transducers probably because the intensity of the signals were below the measurable ranges of these transducers.

The error bars or the variations between repeat runs of other measured parameters for the extruder runs are as follows. The different temperature settings for the extruder will also be discussed. The variations in the flow rates between repeat runs were between 1 to 2 gm/min at 15 to 35 rpm and up to 3 gm/min at 45 rpm. The amperage meter of the extruder can be read with an accuracy of 0.1 ampere and the variations between the repeat runs were of the same order of magnitude. The extruder is heated by three sets of band heaters that are positioned along the extruder. There were additional heaters for the dies as has been mentioned in chapter 3. Temperature settings for the heaters will be indicated for each extruder run in the tables that display the results. The heater and die temperature settings were higher for the 1/16 inch die than for the 1/8 inch die by 6 ° C for each zone. This was done

to accommodate the higher pressures that resulted with the 1/16 inch die and prevented the pressures from exceeding the safe operating ranges of the transducers. In fact even with the use of the 1/8 inch die some readings were taken with the higher barrel temperatures for screw speeds of 35 and 45 rpm.

The results of the extruder runs will be presented by two sets of data; i.e. results of two repeat runs will be provided under identical operating conditions. Conclusions will be drawn based on both sets of data. Although pressures are reported in KPa units, their equivalent values in psi will also be included in the discussion. This has been done for the convenience of the reader and also to correlate with the experimental setup in which pressures were recorded by gauges in psi units.

The extrusion characteristics with the 1/8 inch die are presented in Tables 5.28-5,31 for the dry blends and in Tables 5.32-5.33 for the pellets. From Tables 5.28-5.31, it is observed that at all four screw speeds the DIDP dry blend registered pressures of 2250 to 4140 KPa (325 to 600 psi) higher than those for the DHP dry blend in the last two zones of the extruder. However for the same zones at 15 and 25 rpms, the differences in pressures between the DIDP and the DOP dry blends are within or slightly higher than the error bars of 350 to 1035 KPa. Hence, it can not be concluded that there is a discernible plasticizer effect at lower screw speeds. However at 35 and 45 rpms, the DIDP dry blend exhibits pressures of 2410 to 4140 KPa (350 to 600 psi) higher than those of the DOP dry blends in the last two zones of the extruder. It has been reported that the DIDP dry blend viscosities were considerably larger than the DHP dry blend viscosities. The difference in viscosity between DIDP and DOP dry blends was smaller especially at higher shear rates. The dry blends with higher viscosity gave rise to higher pressures in the extruder. The DIDP dry blend having the maximum viscosity and DHP dry blend with the lowest viscosity gave rise to highest and lowest pressures, respectively, in the last two zones of the extruder. The smaller difference in pressures build up between DIDP and DOP dry blends could possibly be attributed to their smaller difference in viscosities. But based only on the viscosity difference it is difficult to comment on the magnitude of these pressure differences which are smaller at lower screw speeds and larger at

higher speeds. This trend does not seem to agree well with larger viscosity differences at lower shear rates and lower differences at higher shear rates.

Trends similar to the dry blends are observed for the differently plasticized pellets when they are extruded with the 1/8 inch die as seen from Tables 5.32 and 5.33. In general, pellets possessing higher viscosities registered higher pressures in the extruder than the corresponding dry blends when the plasticizer type was the same. Here the DIDP pellets registered significantly higher pressure values than both the DHP and the DOP pellets at screw speeds of 25, 35 and 45 rpm. The differences in pressure generated by the DIDP pellets over the other two pellets in the last two zones of the extruder for these three speeds were between 1380 to 4140 KPa (200 - 600 psi). No experiments were conducted at screw speed of 15 rpm. In light of what has been said previously, the viscosity differences can probably explain the differences in the pressure buildup. The DIDP pellet with higher viscosity gave rise to higher pressures than the other two pellets with lower viscosity. In contrast to the dry blends, there are significant differences in the pressure buildups at all screw speeds between the DIDP and the DOP pellets. No significant differences in pressure buildup were observed between DIDP and DOP dry blends at screw speeds of 15 and 25 rpm. Comparisons of the viscosity ratios of the DIDP samples and the other two mixes in Tables 5.9 and 5.10 showed that the viscosity ratios were slightly higher for the pellets than for the dry blends especially at shear rates of 20 and 40 1/s. The larger difference in viscosity ratios of the pellets as compared to the dry blends can be thought of as the reason for the higher difference in pressure profile, between the DIDP and the DOP pellets, as compared to a lower difference in pressure profile, between DIDP and DOP dry blends. However, this difference in viscosity ratio is usually small and might not be significant. Also at 170 ° C, the viscosity ratios of DIDP and DOP are larger for the dry blend than for the pellets. On the other hand, the larger viscosity ratios of the pellets over the dry blends between the DIDP and the DHP plasticized mixes are not reflected in any increased pressure differences between the DIDP and the DHP pellets as compared to the DIDP and the DHP dry blends. Thus it is difficult to comment on the magnitude of the pressure difference between the pellets and the dry blends based on their viscosity difference only. In

general with the 1/8 inch die the plasticizer effect on pressure buildup is more distinguishable between the DIDP and the DHP mixes than between the DIDP and the DOP mixes and can be possibly attributed to their difference in viscosities.

The effect of plasticizers on the extrusion characteristics can also be studied by observing their effect on power, as measured by the amperages, and flow rates registered during the process. Higher amperages and flow rates were registered for the DIDP mixes as compared to the DHP or DOP mixes with the 1/8 inch diameter die attached to the extruder. This was true for both the pellets and the powders. The amperage is indicative of the extruder motor load. The difference in amperage was always larger than the deviation between the repeat runs and the accuracy with which the meter could be read. Although the flow rates for DIDP dry blends at 15 and 25 rpm were slightly higher than for the other dry blends, the differences in flow rates were within the experimental deviation between the runs. At 35 and 45 rpms, the DIDP dry blends registered flow rates slightly higher than the deviation about the reported mean. For the same screw speeds and barrel temperatures and with the 1/8 inch diameter die attached to the extruder, the flow rates and the amperage values were higher for the DIDP pellets than the other two pellets with some exception for the flow rates at 45 rpm.

The flow conditions existing in the extruder consist of a drag flow superimposed with a positive pressure gradient flow. The rotating screw provides the potential for the drag flow and also pressurizes the molten polymer. The positive pressure flow conditions can also be changed by changing the pressures at the extruder exit or at the inlet to the die which are basically the same. This can be accomplished by changing the die dimensions. The 1/8 inch die was replaced by the 1/16 inch die. The difference in the extrusion pressures with the 1/8 inch diameter die between DIDP and DHP dry blends was distinctly higher than the difference in pressure buildup between the DIDP and DOP plasticized dry blends. It was thus decided to concentrate only on DIDP and DHP dry blends to investigate the effect of plasticizer type on the extrusion process using the 1/16 inch diameter die. This eliminated the time for preparation of extra DOP plasticized PVC dry blend. However, as all the three pellets were already

available, the extrusion experiments with the 1/16 inch die were conducted using all the three varieties of plasticized pellets.

The results from the extruder experiments with the 1/16 inch diameter die attached to the extruder followed the same trends as those observed with the larger diameter die. Both the plasticized PVC dry blends and pellets with higher viscosity gave rise to higher pressures in the extruder. This can be observed from the extrusion results in Tables 5.34 and 5.35 for the plasticized PVC dry blends and in Tables 5.36 to 5.39 for the plasticized PVC pellets. In the last two zones of the extruder at 35 rpm, the DIDP dry blend exhibited 1375 to 3450 KPa (200 to 500 psi) higher pressures than both the DHP and the DOP dry blends. At 45 rpm, the DIDP dry blend registered pressures of 1375 KPa (200 psi) higher than those by the DHP dry blend. The amperage recorded for the DIDP dry blend was higher than both the other two plasticized dry blends. Although at 35 rpm the DIDP dry blend registered slightly higher flow rates than the DHP dry blend, at 45 rpm the reverse was true. But considering the error bars of approximately 3 and 2 gm/min at 45 and 35 rpm, respectively, the difference in flow rates is not significant. With regard to the pellets, the pressure buildup for the DIDP pellets was considerably larger than that for the DHP or the DOP pellets samples for all four screw speeds. This is clearly evident from Tables 5.36-5.39. The DIDP pellets registered pressures of 2750 to 6200 KPa (400 to 900 psi) higher than that for the other two pellets in the last two zones of the extruder at 15, 25 and 35 rpms. At 45 rpm, the pressure difference decreased to a value of 1375 to 2750 KPa (200 to 400 psi). With the 1/16 inch diameter the amperage, which is indicative of the total load on the motor to transport the polymer, was larger for the more viscous DIDP pellets than for the DOP or the DHP pellets. The flow rate of the DIDP pellets was slightly larger than the other two plasticized PVC pellets at 25 and 35 rpms. But at the other two screw speeds of 15 and 45 rpm, the differences were not significant when compared to the deviation in the data between repeat runs. With the 1/16 inch diameter die as was the case with the larger diameter die, the plasticized PVC mix which has the largest viscosity gave rise to the highest pressures in the extruder. This was true for both dry blends and pellets.

In general, the use of the 1/16 inch diameter die fortified the conclusions drawn from the extrusion tests done with the 1/8 inch diameter die. Considering the experimental repeatability of the results, it has been demonstrated that both the pelletized and the powdered DIDP samples exhibited higher pressures and power requirement than the other two corresponding samples. Only a comparison between DIDP and DOP dry blend at the two lower speeds did not produce a significant difference in the pressures. The effect of plasticizers on the flow rates is not very distinct but overall the DIDP plasticized mixes, with a few exceptions, registered higher flow rates. In general, the plasticizer type is reflected in the performance of PVC in the extruder. The difference in pressure buildup has been linked to the difference in their viscosities.

5.2.2 Studies of the Melting Mechanism

In the second section of the extruder studies, 'cooling experiments' were conducted to study the effects of plasticizers on the melting mechanism and fusion of PVC in the extruder. In these experiments after the extruder had reached steady state during a run, it was stopped and cooled. Then the screw, with material on it, was pulled out. At times a yellow colored die was added to the polymer feed to distinguish between the solid and the fused or the melted polymer. The material was recovered in the form of a coil beginning in the solids conveying zone for the powdered samples. A typical polymer coil for the dry blend is seen in Fig. 5.51. Unlike the powdered samples, the pellets formed no coils for most of the solids conveying zone. Only the material near the melting zone in front of the leading flight started to form a coil. The helical polymer ribbon was sectioned and two sets of experiments were done. In the first case the formation and the development of the fused or the melt zone was studied. In the second case the progression of fusion of PVC in the extruder was investigated with the help of a scanning electron microscope.

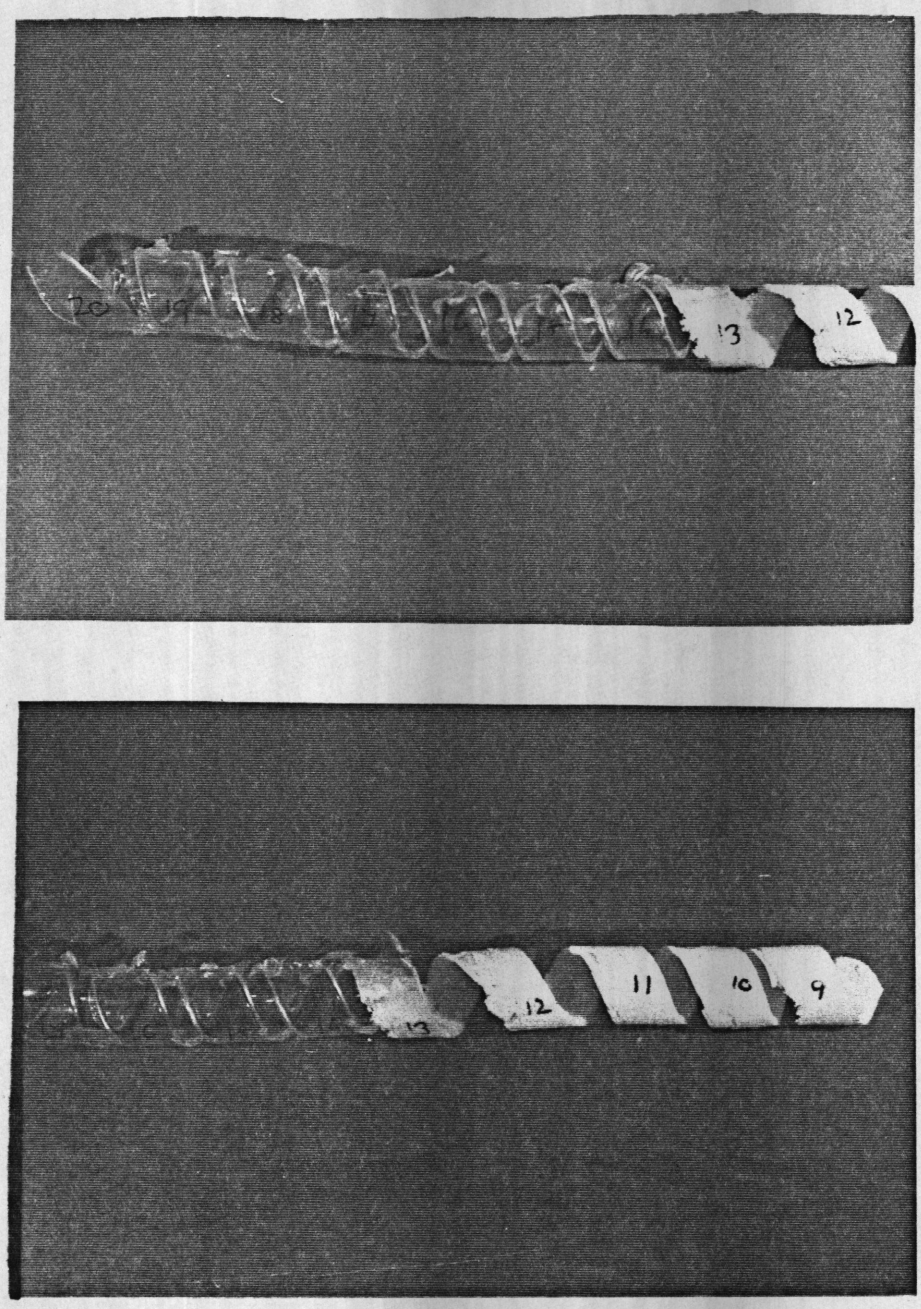

Figure 5. 51. Polymer Coils showing the change from solid to melt form occurring in the extruder.

In the first case the edges of the different sections from the polymer coils were photographed at small magnifications. In the cases where no dye was to the polymer feed, the initiation of fusion is determined from the position where dry blended PVC starts to loose its compacted solid appearance and begins to turn clear. When the yellow colored dye was used, the homogenization of the dye in the melted or fused part of the polymer coils from the 'cooling experiments' was taken to be the onset of the fusion. The difference in the coloration between the solids and the melt section of the coil helped in studying the development of fusion along the screw. The development of the fused or the melted layer was studied at 35 and 45 rpm for the dry blended PVC and at 35 rpm only for the pelletized PVC. This was accomplished for both the dies. It was clearly observed from these photographs of the edges that the fused or the melted material started to collect near the leading edge and slowly encompassed the entire channel cross-section. It has been reported for both rigid and plasticized PVC that at first a melt layer forms near the barrel surface before it starts to accumulate near the leading edge or the pushing flight [48-53]. Both the pellets and the powders showed no such melted layer near the barrel surface. In the Tadmore model [48,49] describing the melting of polymers in single screw extruders, the melt layer formed near the barrel surface is scraped by the flights and forms a melt pool near the leading edge. The last zone or the melt pool is present clearly visible in the photographs and the development of this melt zone allows one to follow the progression of the fusion along the screw.

First, the development of the fused layer along the screw will be followed for the coiled materials formed from the dry blends using the 1/8 inch diameter die at the extruder end. With the 1/8 inch die in place at 35 rpm, the DIDP dry blend started to form a melt near the leading edge (i.e. in front of the pushing flight) just in front of turn 12 and the melt pool covered the entire channel width by turn 13. The melt pool of the DHP dry blended sample started to form around turn 13 and filled the entire channel within the next two turns. For the DOP dry blended samples the melt pool started to form in front of the pushing flight at turn 13 and between turns 14 3/4 and 15 it had encompassed the whole cross-section. At 45 rpm, the melt zone formed by the DIDP dry blend covered the channel width in a span of 1/2 turn between

turns 12 1/4 and 12 3/4. The DHP dry blend, on the other hand, started to form the melt layer at turn 12 3/4 and had covered the entire channel width within one turn. The experiments conducted at screw speeds of 45 rpm were performed at slightly higher wall temperatures than the 35 rpm experiments to keep the pressures developed in the extruder within the range of the transducers. The higher wall temperatures coupled with higher screw speeds should have initiated fusion at a point earlier in the extruder (i.e. at a turn less than 12) at 45 rpm than for the 35 rpm. Apparently this did not happen. The pressure, developed in the last zone of the extruder, at a screw speed of 45 rpm and higher wall temperature was not very different from the case of a screw speed of 35 rpm and lower wall temperature. The presence of similar back pressure may have been the decisive factor as to where the site for fusion initiation was located. For higher back pressure, the initiation site is probably pushed further up the screw. This point will again be deliberated when possible explanations will be sought for the observed earlier and later clearing of the compacted solid polymer in the at the start of the melting zone owing to plasticizer type.

The objective of these studies was to see whether the plasticizer type caused the initiation of fusion and subsequent clearing of the compacted polymer in the earlier turns of the screw for one polymer and in the latter turns for a differently plasticized mix. Accordingly the fusion initiation in the earlier screw turns is called earlier fusion and fusion initiation in the later screw turns is called later fusion initiation. Thus fusion seemed to be initiated earlier for the DIDP dry blends than for the other two dry blends. Also the fusion spread across the channel faster for the DIDP dry blend. This means that the DIDP dry blend was able to encompass the entire channel cross-section within one turn from where it started to form the melt pool at 35 rpm. At 45 rpm this change occurred within 1/2 turn. For the DHP dry blend, the completion of the melt pool across the channel occurred between two turns at 35 rpm and between one turn at 45 rpm. Comparing with results of section 5.2.1, the mixes which gave rise to higher pressures fused earlier and over less distance in the extruder.

With the 1/16 inch die the melt pool formation of the dry blended samples was similar in nature to the melt pool formation with the 1/8 inch die. Here also no melt layer was observed

near the barrel surface and the melted or the fused zone encompassed the entire cross-section from the leading to the trailing edge after starting to build from the leading edge. Recalling from section 2.5, leading edge is the edge of the screw channel in front of the advancing or pushing screw flight. The rear end of the screw channel is the trailing edge. For the dry blends at 35 rpm, the melt pool formation covered the entire channel width from its initial buildup near the leading edge between turns 9 1/2 and 9 3/4 for DIDP, between turns 10 and 10 1/2 for DOP and between turns 10 1/4 and 10 3/4 for DHP dry blends. At 45 rpm,the DIDP formed a melt pool between turns 9 and 9 1/4. At the same screw speed the DHP started to form the melt pool in front of the pushing flight at turn 9 1/2. It covered the entire channel width between turns 9 3/4 and 10. Here also, the earlier fusing plasticizer mix gave rise to higher pressures. The earlier fusing mix also had higher viscosity. In the case of the 1/8 inch die, fusion was occurred sooner over a shorter distance for DIDP dry blend. In the case of the 1/16 inch die for all the three dry blends at 35 rpm and for DIDP and DHP dry blends at 45 rpm, the melt pool covered the entire channel width within 1/2 turn. Whether or not the rate of fusion was affected by the plasticizer type could not be determined.

The formation of the melt layer by fusion in the pelletized materials followed similar patterns as were observed for the dry blends both in terms of the way in which the melt zone was formed and the effect of the plasticizers on which pelletized mix fused earlier. This was true for both the dies. It has been mentioned earlier that the pellets did not form a polymer coil early in the solids conveying zone. Also, the pellets did not turn clear as the dry blends and thus fusion had to be studied by observing the homogenization of the yellow dye added to the feed. For the pelletized samples with the 1/16 inch die at 35 rpm, it was observed that the compacted solid bed encompassed the entire channel width and started to form a helical coil at turn 5 for DIDP, at turn 7 1/2 for DHP and turn 8 for the DOP pellets. For the DIDP pellets, the melt zone started to form at turn 7 and it filled up the entire channel cross-section by turn 11. For the DHP pellets, the melt pool formation appeared in front of the pushing flight at turn 7 1/2 and the melt pool buildup covered the whole channel cross-section by turn 13. Similarly for the DOP pellets, the melt pool formation took place between turns 7 3/4 and 13. The DIDP

plasticized PVC pellets which fused earlier over a shorter distance gave rise to high pressures than the other two pelletized materials. For the 1/8 inch die at 35 rpm screw speed the DIDP pellets started to compact and form a coil between turns 8 1/2 and 9 and the compacted material covered the entire channel width by turn 11 1/2. The corresponding turns where the compacted solid pellets started to accumulate and the turn where it covered the entire channel width were 11 and 15 1/2 for DHP pellets and were 13 and 16 1/2 for DOP pellets.

In general, the pellets gave rise to higher pressures than the corresponding dry blends having the same plasticizer. As mentioned earlier, it is difficult to pinpoint what caused the higher pressure profiles to be generated by the the pellets over the dry blends. The pellets fuse earlier in the screw channel and probably this leads to higher pressure development as more energy is available for pumping and pressurization of the melt. Again, it is possible that higher viscosity of the pellets gave rise to higher back pressure which in turn pushed back the zone where fusion was initiated.

It is observed that the DIDP plasticized materials have generated higher pressures in the extruder. They also compacted and formed the melt zones earlier than the other two plasticized mixes. This seems to support the hypothesis made in references [37] and [67] that the faster fusing plasticizer gave rise to higher pressures in the extruder. The early fusion and early covering of the channel width by the fused DIDP was seen for both the dry blends and the pellets. The exact locations of the zones varied by 1/4 turn for the 1/16 inch die and by 1/2 turn for the 1/8 inch die between repeat runs. But considering the fact that the experimental repeatability of the extrusion runs in section 5.2.1 was generally good, this variation in the location for the starting or completion of the melting zone is possibly an acceptable variation between repeat runs. With the 1/8 inch die, the melting zone length seemed to be affected by the plasticizer type for both 35 and 45 rpms. The difference in the melting zone lengths owing to the plasticizer type was not distinguishable for the 1/16 inch die.

From analyzing the physical properties it is difficult to find any precise reason as to why the DIDP mixes fused earlier in the channel. The thermal properties could have been responsible for earlier fusion. But the plasticizer effect did not noticeably alter the values of the

thermal properties. In fact the specific heat of the DIDP plasticized PVC mixes were slightly higher and indeed would reduce the rate of temperature buildup and delay fusion. Thermal diffusivity was difficult to measure below 100 °C and a possible difference in these values could have caused certain plasticized mixes to fuse sooner and over a shorter distance. The other property that could have affected the fusion was the friction factors and their dependence on temperature. The measurement of friction factors was not precise enough to say whether they made any difference. The compaction data also had not shown any plasticizer effect. No compaction data was obtained below 150 ° C and it is in this temperature range the possible cause for the difference may lay. Also it could have been that higher pressure buildup in the last two zones of the extruders for the DIDP plasticized mixes pushed the fusion initiation zone further up the channel. To support this it has been mentioned earlier that two screw speeds with different barrel temperatures gave rise to similar back pressure in the last zone of the extruder and in such a cases the initiation of fusion started at about the same turn in the extruder.

It may be emphasized at this point that the melt flow of PVC is governed by the fusion characteristics of PVC. Rather than a complete breakdown of the crystalline structures present in PVC, fusion causes the formation of melt zones and dominates the flow properties. The fusion arises out of an interdiffusion of the amorphous chains that link the crystallites. The study of the melting mechanism has been conducted from visual observations and low magnification photographs of the helical polymer coil from 'cooling experiments. The clearing of the PVC mixes in the ICR and the extruder and the dual value flow activation energy signify a change in the flow mechanism from particulate to a fused nature. These observations, although signifying the fused or the melt-like state, do not shed light on the changes at the microscopic levels that are referred to at the beginning of this paragraph. In the second part of the studies concerning the melting mechanism the effect of plasticizers on the progression of fusion along the screw was studied. The polymer coils were fractured under liquid Nitrogen, sputtered with gold and then examined under the SEM. The surfaces were examined at mag-

nifications of 100 to 2000. The effects of plasticizer on the progression of fusion is investigated in the following paragraphs.

Typical studies of progression of fusion will be presented in this paragraph. It may be recalled that with the 1/8 inch die at 35 rpm, the fusion started at turn 12 for DIDP and at turn 13 for DHP dry blends. The melt pool encompassed the channel width by turn 13 for the DIDP dry blend and by turn 15 for the DHP dry blend. The progression of fusion for the DIDP dry blend at 35 rpm is followed in Figures 5.52 - 5.55. At turns 9 and 10 in Fig. 5.52, the channel is composed of 100 to 150 micron PVC particles. At turn 12 1/4 in Fig. 5.53, the original 100 micron particles are still noticeable at the trailing edge. They are not as distinct near the leading edge because of the onset of fusion but the outlines of their boundaries can still be distinguished. Half a turn down the channel, at turn 12 3/4 (Fig. 5.54), the degree of fusion has progressed considerably at the leading edge, while at turn 15 (Fig. 5.55), materials from the leading and trailing edges are indistinguishable. The gradual nature of fusion is clearly demonstrated by the SEM pictures and correlate quite well with the gradual change of state that was suggested earlier by the DSC scans. The fusion to form a homogeneous mass with higher degree of interpenetration between the amorphous region of the individual particles continue long after the attainment of previously described uniform coloration or clearing of the melt across the cross section of the polymer coil. The progression of fusion for DHP dry blends at 35 rpm is followed in Figures 5.56-5.59. At turn 12 the DHP dry blends that started to fuse near the leading edge but the 100 micron particles are clearly visible along the entire cross-section. Fig. 5.56 shows the non-fused material composed of 100 μm particles at turn 9 and turn 12. At turn 13 in Fig. 5.57 fusion is seen to be initiated along the leading edge. At turn 14 in Fig. 5.58, the fusion near the leading edge has not obliterated the remnants of the 100 micron particles whose outlines are still discernible. The fusion at the trailing edge seems to start at turn 14 for the DHP dry blend. At turn 17 (Fig.5.59) all the material across the channel width appears fused. The gradual nature of the fusion is established in the case of DHP dry blends also. The study confirms that the melt formation begins at the leading edge and then spreads across the channel width towards the trailing edge. Additional comments can also be made

with regard to the plasticizer type affecting the fusion of PVC in the extruder. DIDP initiates early fusion, a fact which has been confirmed before from visual observations.

It would be interesting to investigate the effect of the plasticizer type on the degree of the fusion process taking place in the extruder. A more thorough investigation at higher magnification was thus conducted for the DIDP and the DHP dry blends at 35 rpm with the 1/16 inch die. The findings of this study will obviously attempt to support the results of the SEM pictures obtained from the 1/8 inch die. It is also expected that additional information on the effects of plasticizers on the degree of fusion might be obtained. Terminologies for different particle sizes defined in Table 1.1 will be used in the following discussion. The progression of fusion for DIDP dry blend with the 1/16 inch die is followed in Figures 5.60 to 5.65. At turn 9 1/2 in Fig. 5.60, the difference in the material between the leading and trailing edge is quite obvious. At turn 10 in Figures 5.61 and 5.62, materials from both edges appear fused but the outlines of the original particles or grains of 100 μm size are still visible. Although at higher magnification the appearance in general is structureless agglomerates, approximately 10 μm particles seem to be present. Also sub-micron particles can be identified as tiny dots and could be the microdomains. They are too omnipresent to be thought of as debris. At the leading edge at turn 12 (Fig. 5.63) the tiny submicron specks appear quite prominently among the larger 10 μm particles which seem to loose their identities. At turn 14 and 16 in Figures 5.64 and 5.65, the submicron particles seem to be homogeneously distributed in the melt in which no other larger definite particle structure can be identified.

The same basic trend could be followed for the DHP dry blends with 1/16 inch die in Figures 5.66 to 5.71. At turns 9 and 10, in Figures 5.66 and 5.67, respectively, the extent of

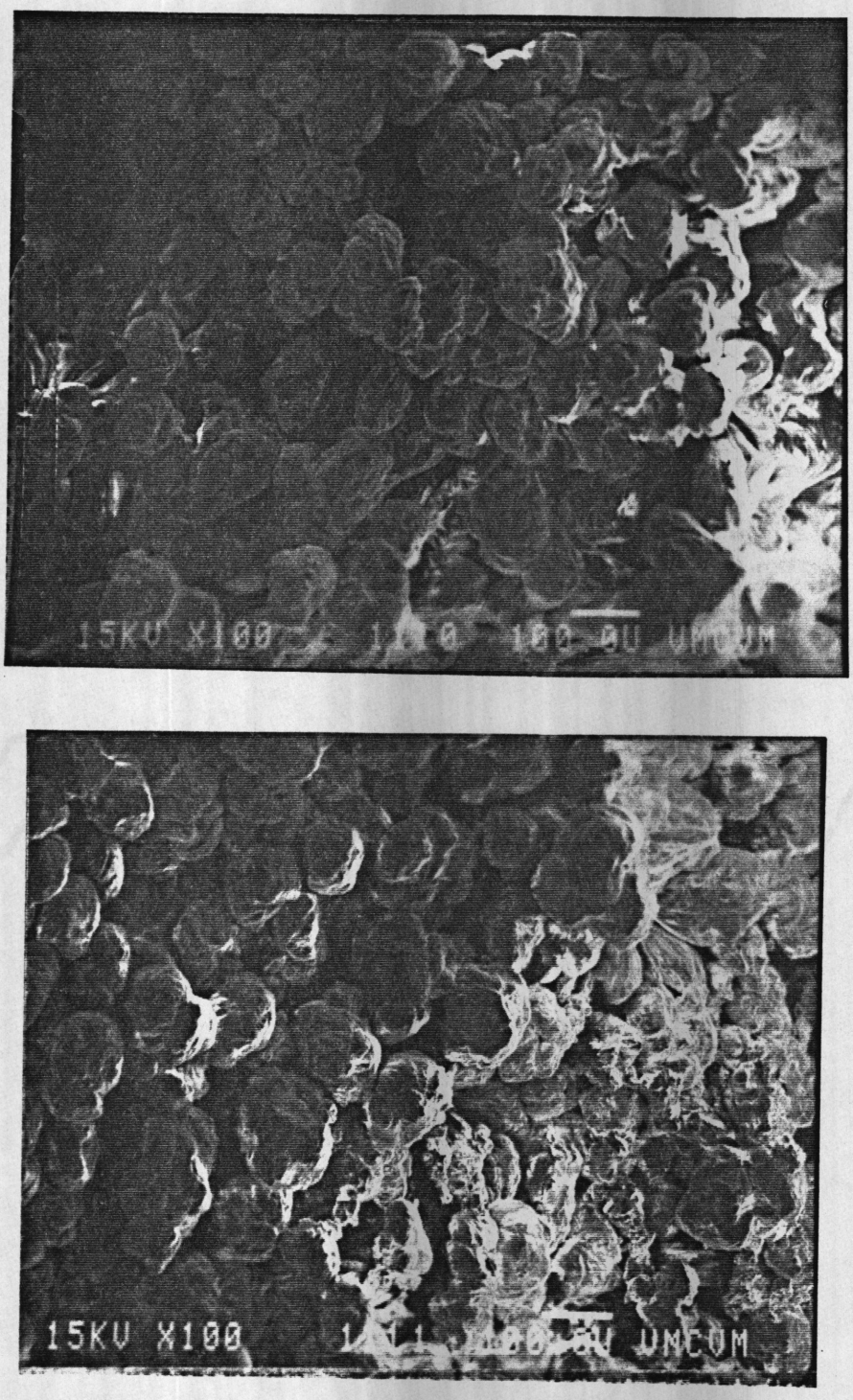

Figure 5. 52. Fusion Study of DIDP dry blend by SEM (1/8 inch dia. die) at turns 9 & 10.: Turn 9 (top), Turn 10 (bottom). Mag. 100

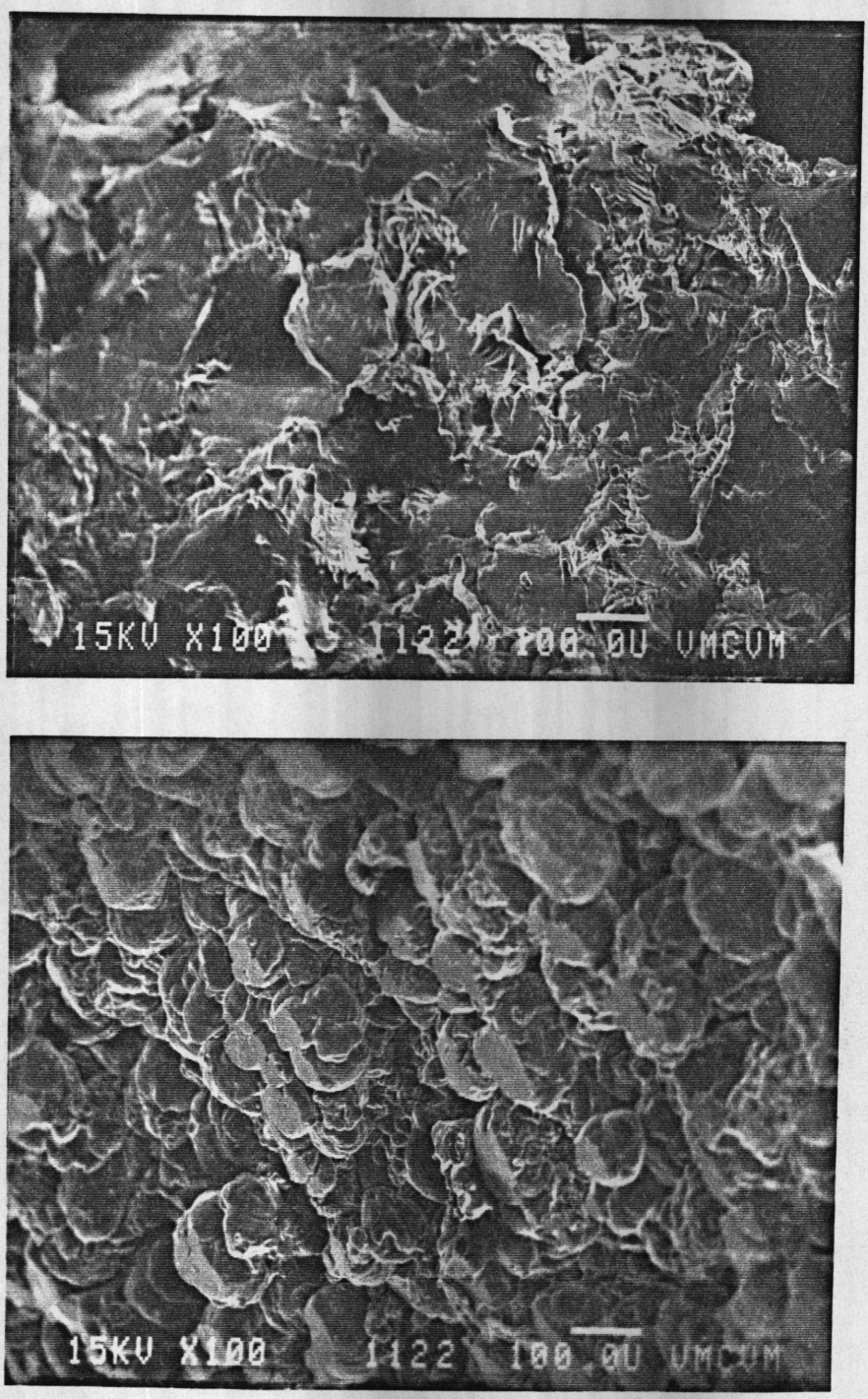

Figure 5. 53. Fusion Study of DIDP dry blend by SEM (1/8 inch dia. die) at turn 12 1/4: Leading edge (top), Trailing edge (bottom). Mag. 100

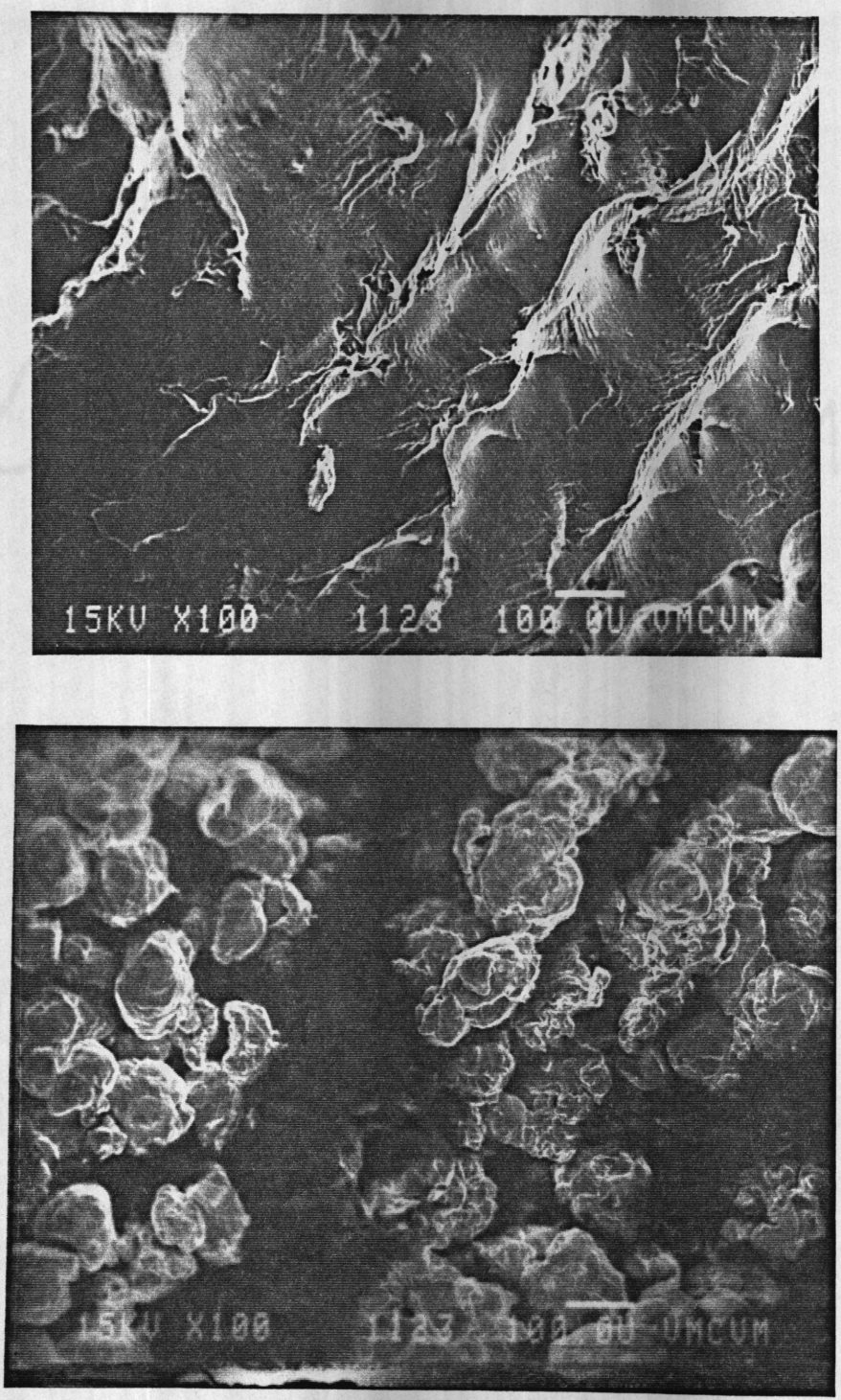

Figure 5. 54. Fusion Study of DIDP dry blend by SEM (1/8 inch dia. die) at turn 12 3/4: Leading edge (top), Trailing edge (bottom). Mag. 10 0

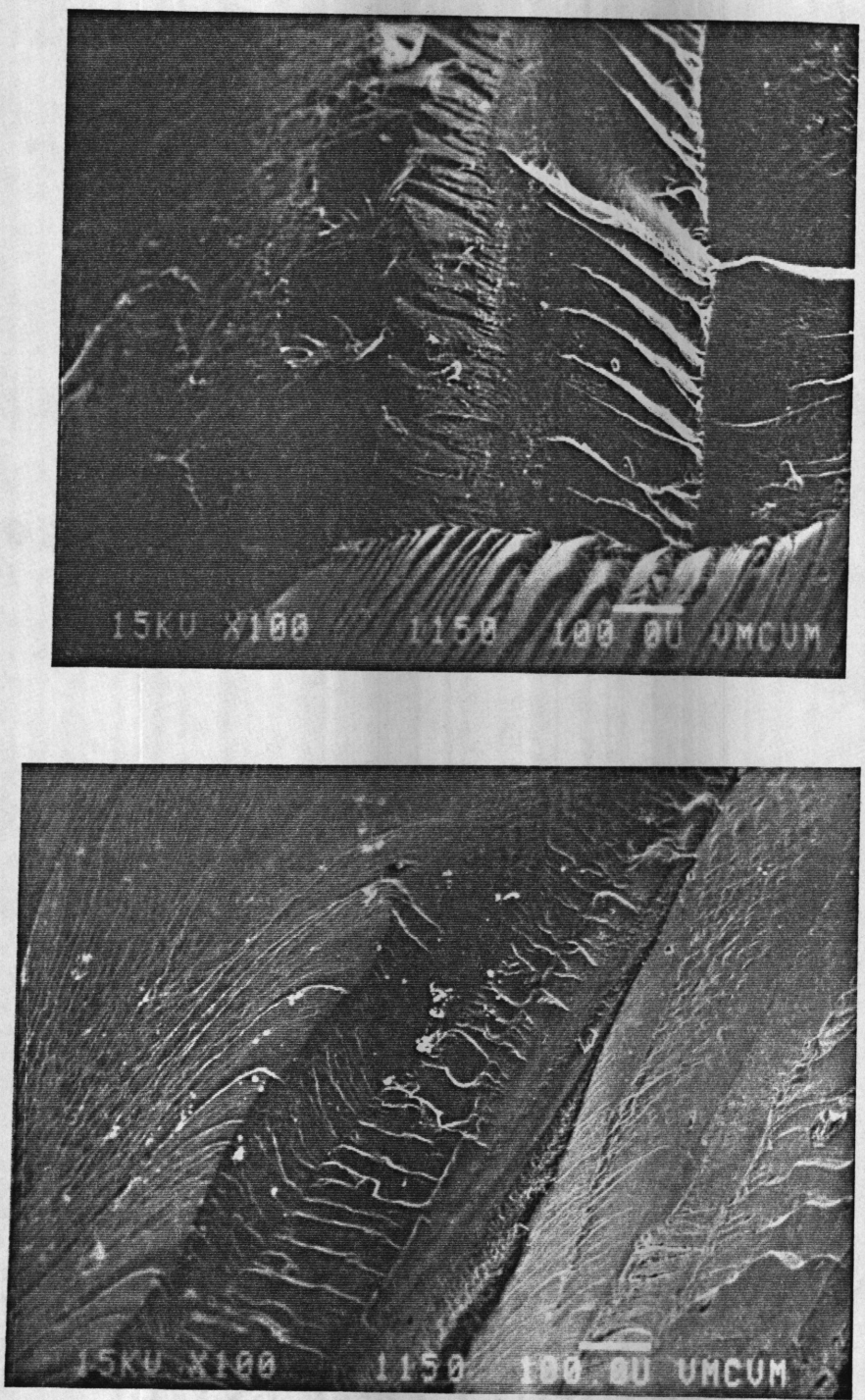

Figure 5. 55. Fusion Study of DIDP dry blend by SEM (1/8 inch dia. die) at turn 15.: Leading edge (top), Trailing edge (bottom). Mag. 100

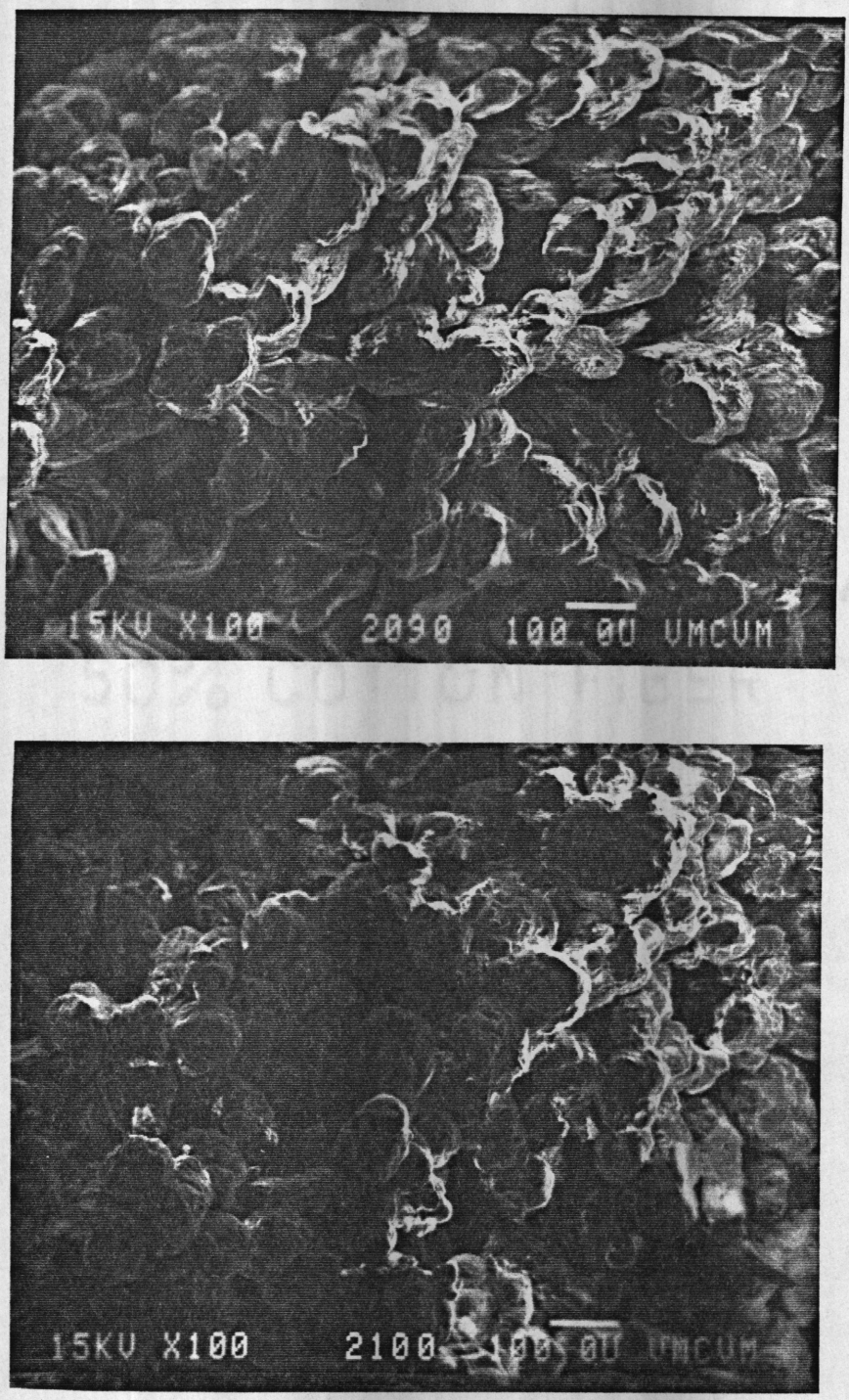

Figure 5. 56. Fusion Study of DHP dry blend by SEM (1/8 inch dia. die) at turns 9 and 12.: Turn 9 (top), Turn 12 (bottom). Mag. 100

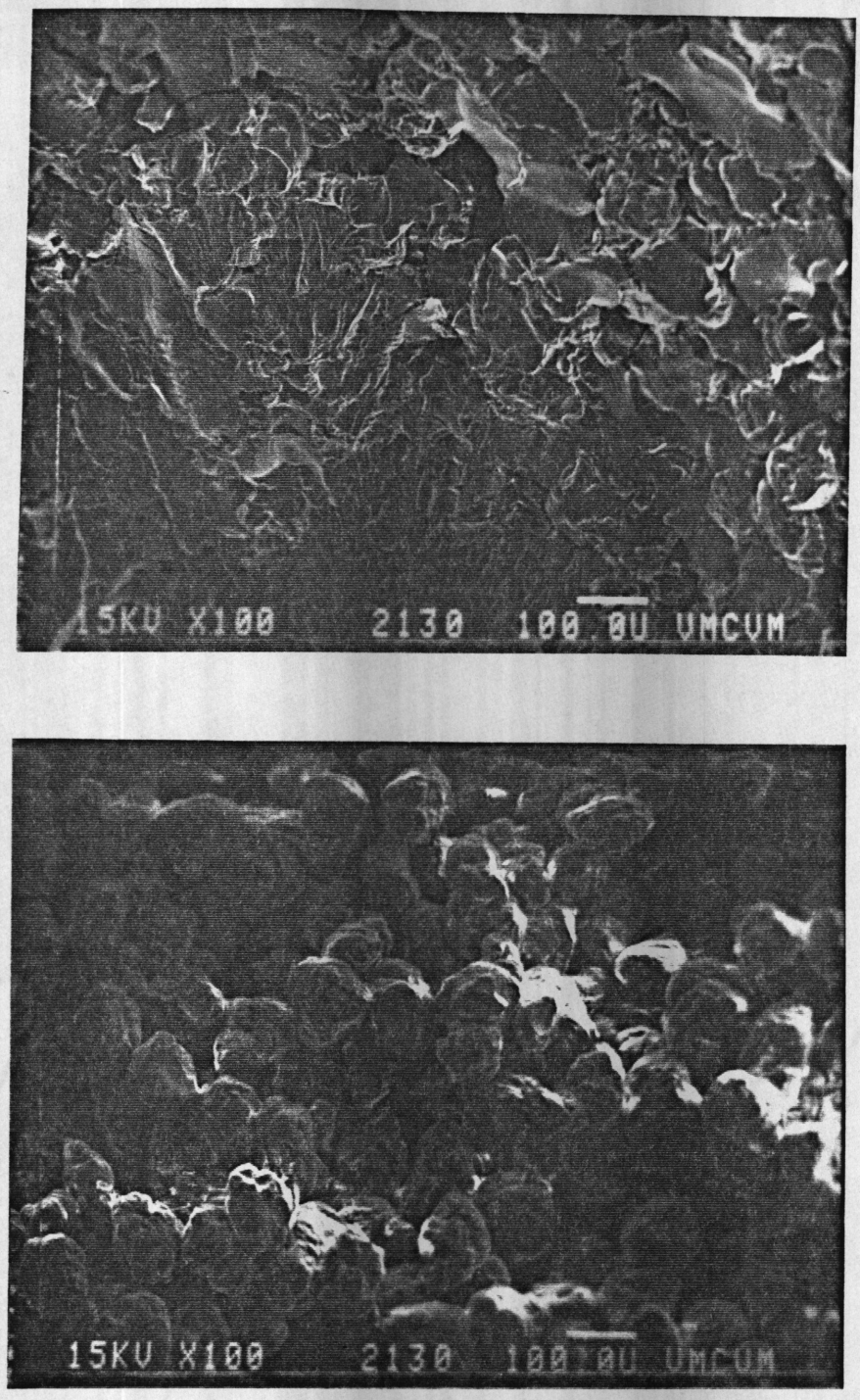

Figure 5. 57. Fusion Study of DHP dry blend by SEM (1/8 inch dia. die) at turn 13.: Leading edge (top), Trailing edge (bottom). Mag. 100

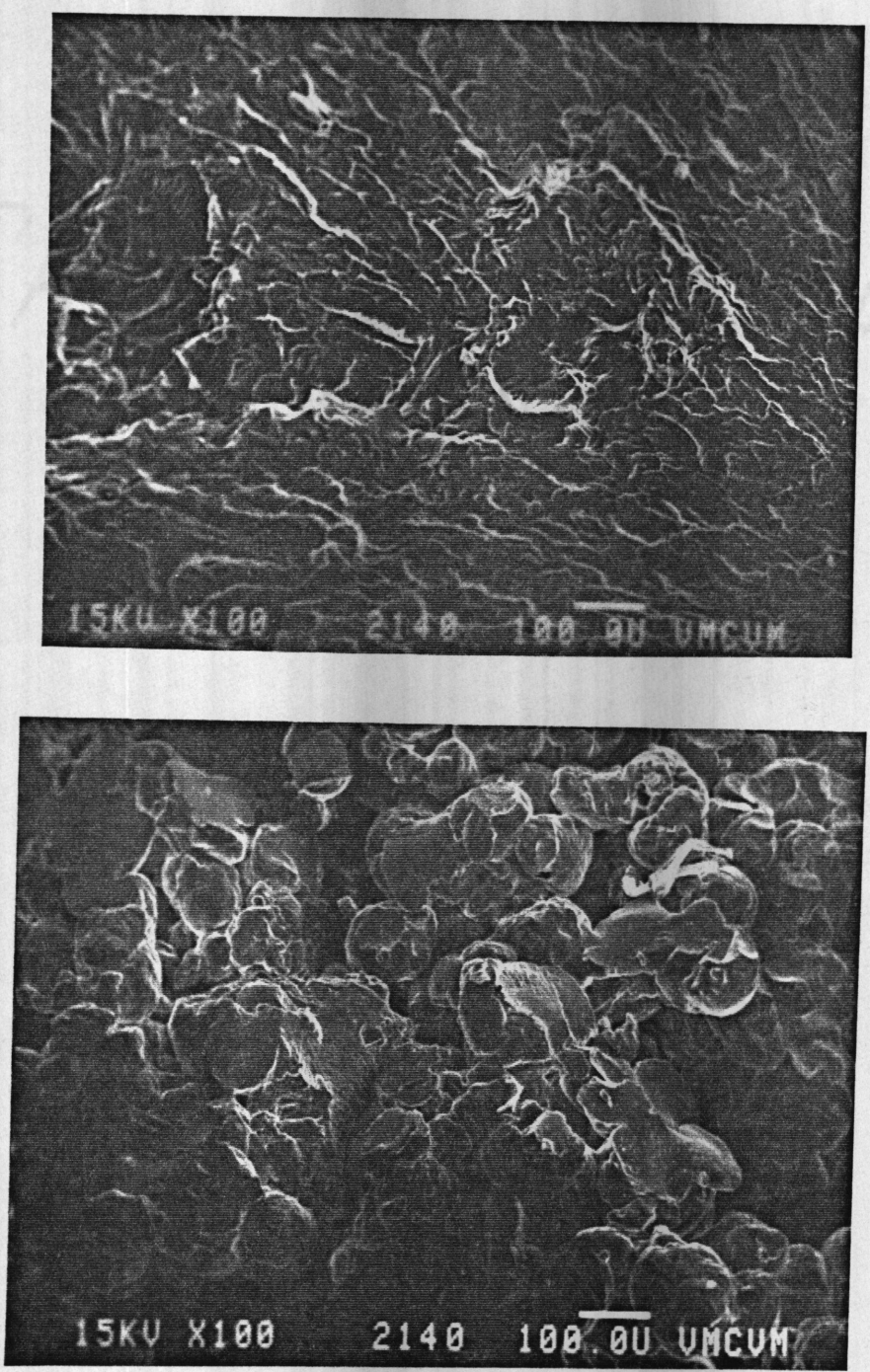

Figure 5. 58. Fusion Study of DHP dry blend by SEM (1/8 inch dia. die) at turn 14.: Leading edge (top), Trailing edge (bottom). Mag. 100

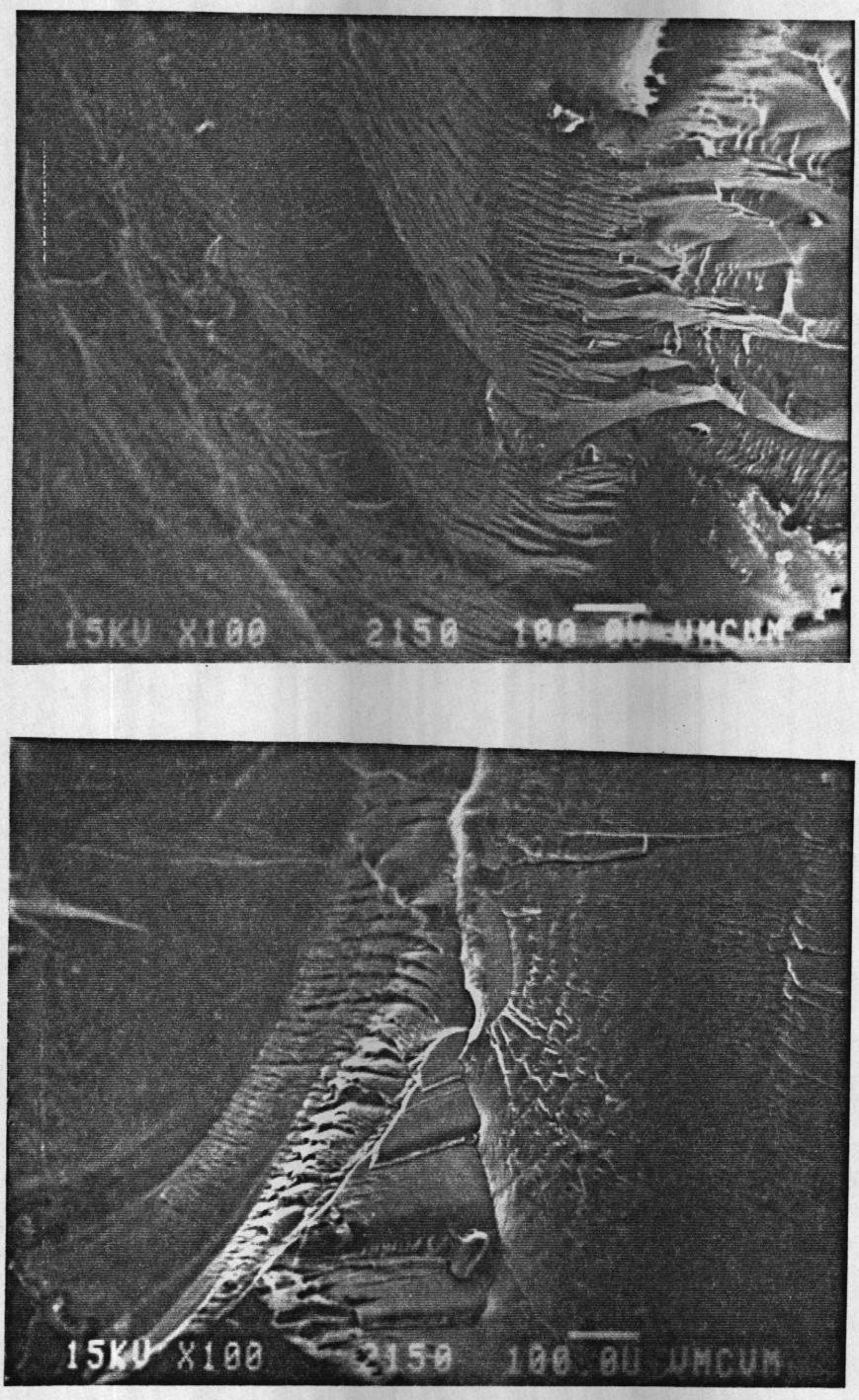

Figure 5. 59. Fusion Study of DHP dry blend by SEM (1/8 inch dia. die) at turn 17.: Leading edge (top), Trailing edge (bottom). Mag. 100

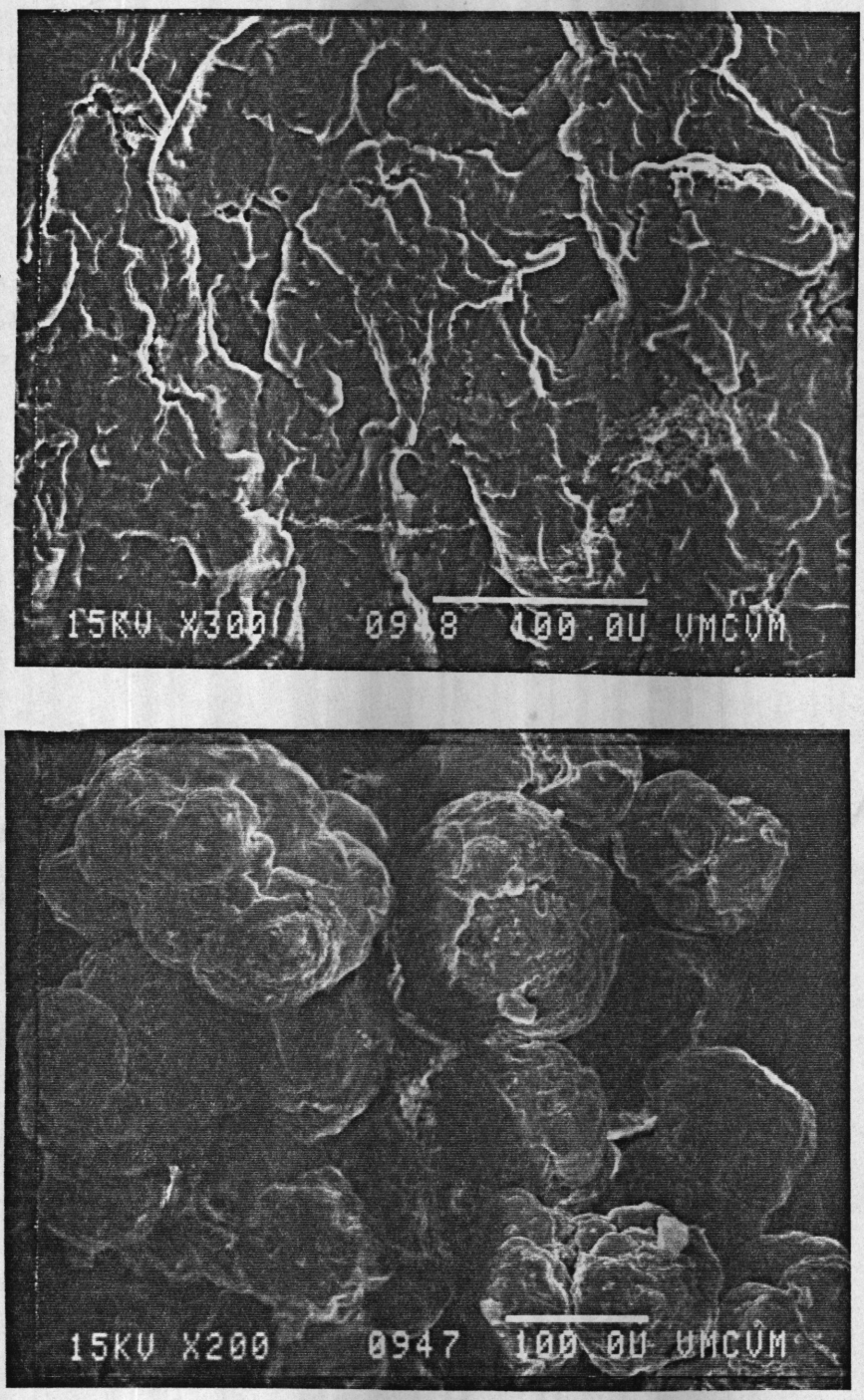

Figure 5. 60. **Fusion Study of DIDP dry blend by SEM (1/16 inch dia. die) at turn 9 1/2:** Leading edge (top), Trailing edge (bottom). Mag. 270

Figure 5. 61. Fusion Study of DIDP dry blend by SEM (1/16 inch dia. die) at turn 10.: Material from leading edge. Top mag. 200, Bottom Mag. 2000.

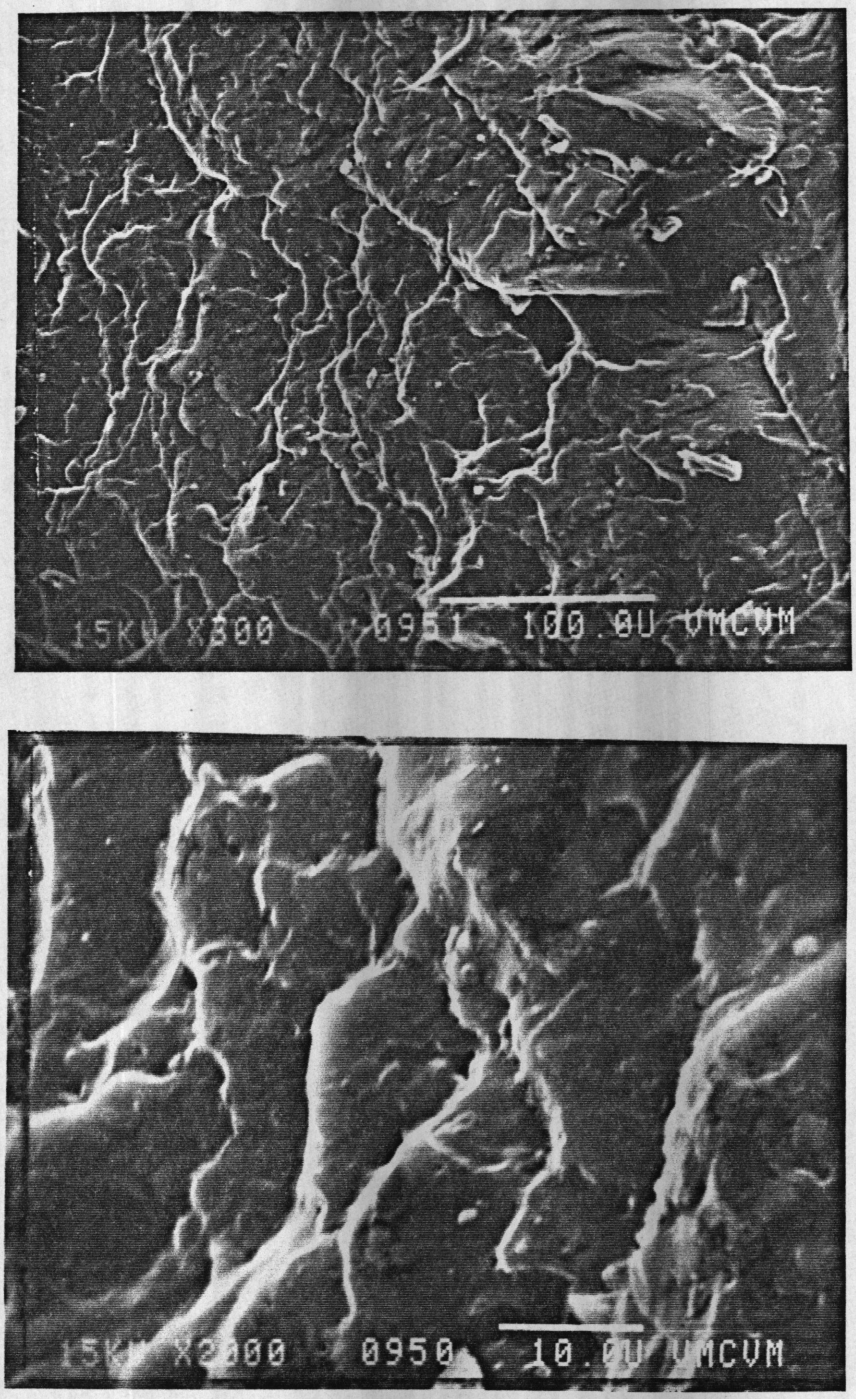

Figure 5. 62. Fusion Study of DIDP dry blend by SEM (1/16 inch dia. die) at turn 10.: Material from trailing edge. Top mag. 300, Bottom Mag. 2000.

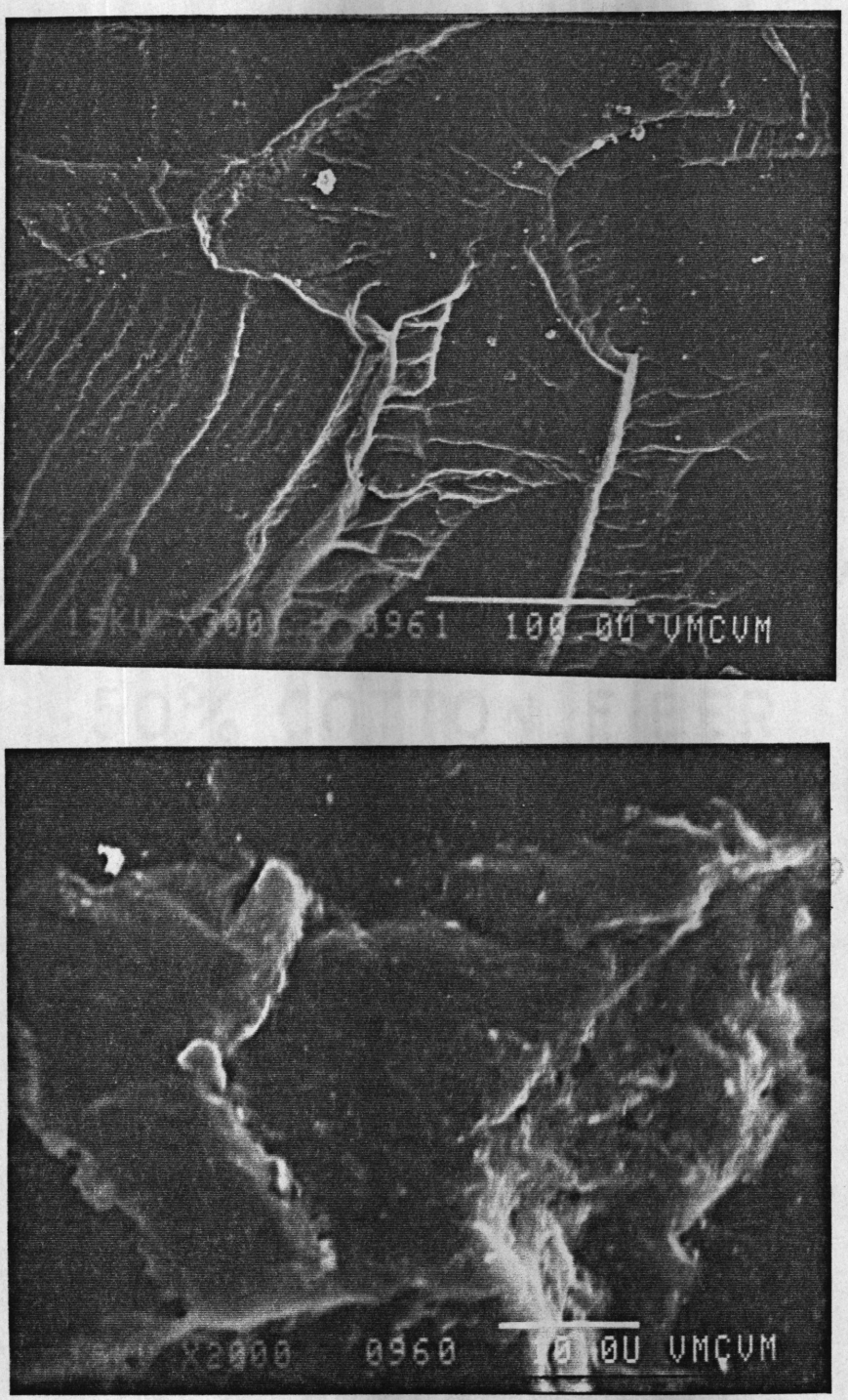

Figure 5. 63. Fusion Study of DIDP dry blend by SEM (1/16 inch dia. die) at turn 12.: Material from Leading edge. Top Mag. 300, Bottom). Mag. 2000.

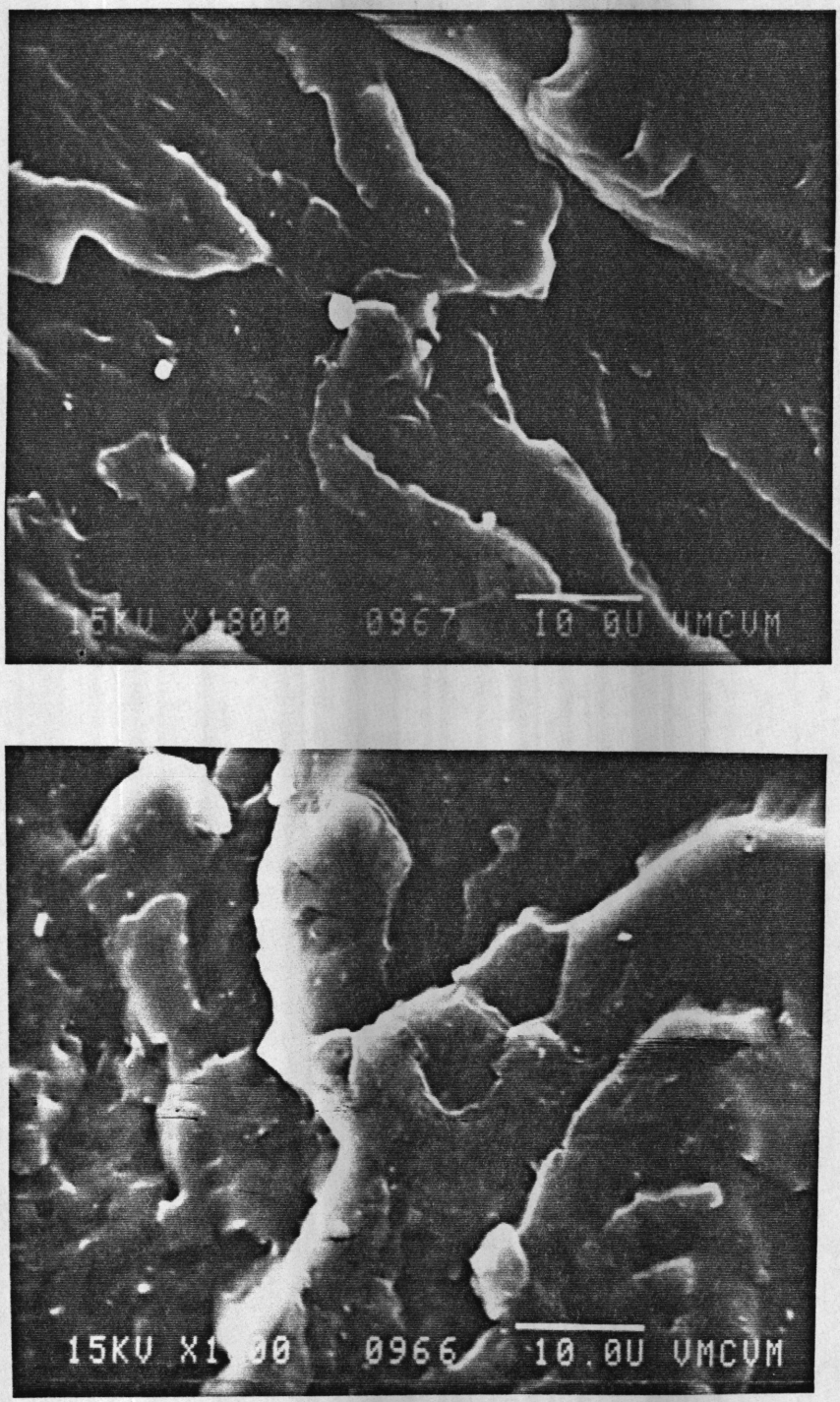

Figure 5. 64. Fusion Study of DIDP dry blend by SEM (1/16 inch dia. die) at turn 14.: Leading edge (top), Trailing edge (bottom). Mag. 1800.

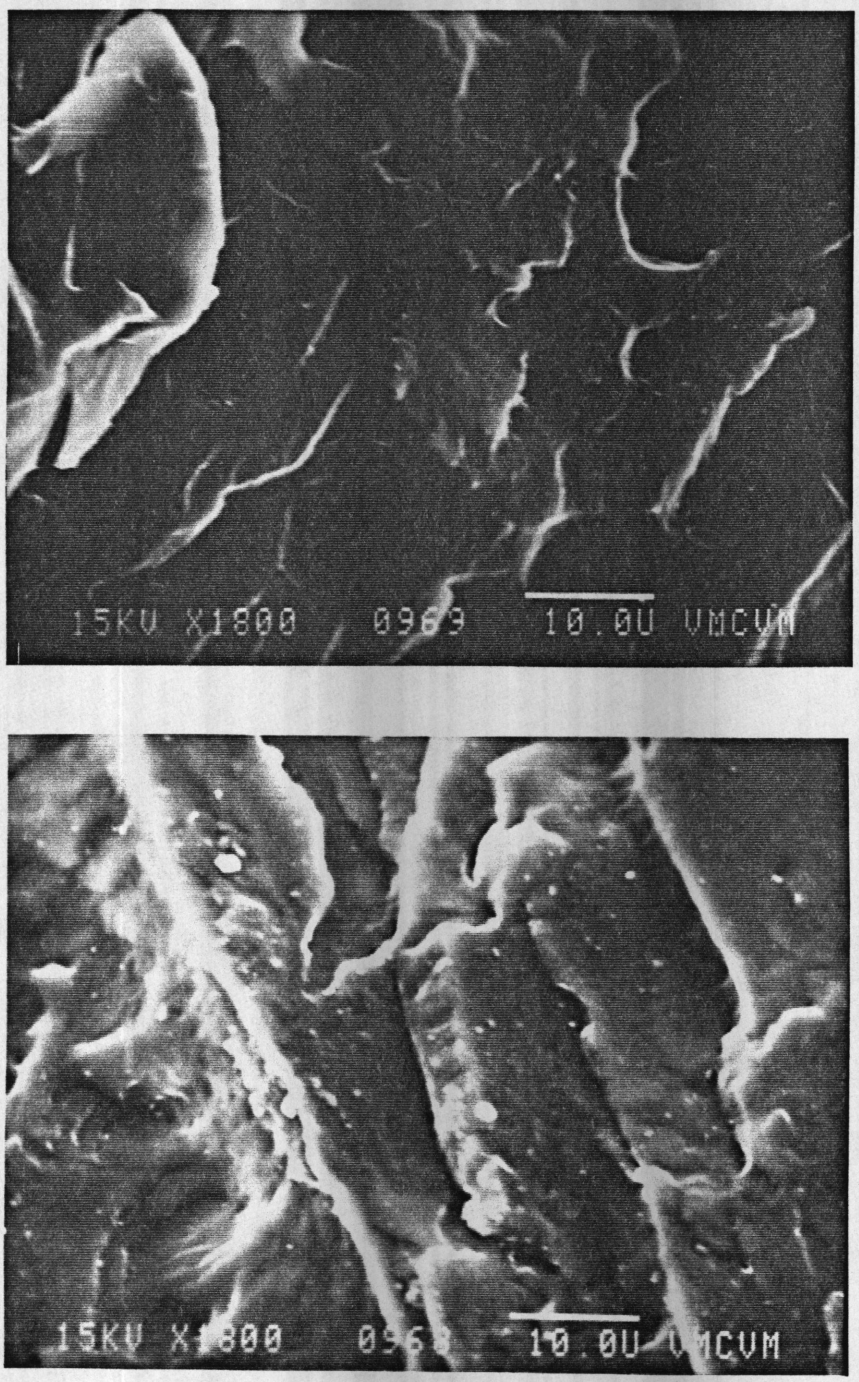

Figure 5. 65. Fusion Study of DIDP dry blend by SEM (1/16 inch dia. die) at turn 16.: Leading edge (top), Trailing edge (bottom). Mag. 1800.

fusion is much less than the DIDP dry blend at the corresponding turns. At turn 11 1/2 (Figures 5.68 and 5.69), fusion has set in at both the edges but the outlines of the original 100 μm grains are still visible. The submicron particles seem to be distributed among the larger particles or agglomerates whose dimensions are in the range of 10 μm. At turns 14 and 16 in Figures 5.70 and 5.71, the presence of larger 10 μm particles are less distinguishable. But the submicron particles, which could be the microdomains, appear less homogeneous than in the DIDP dry blend. The difference in the distribution of the submicron particles, although not very distinct, could be attributed to the plasticizer type. If submicron particles are indeed the microdomains, the plasticizer type possibly plays a role in how they are dispersed in the PVC in the extruder. The microdomains appear to be more homogeneous in the DIDP plasticized dry blend than in the DHP plasticized dry blend. The higher level of homogeneity for the DIDP dry blend could have been influenced by the higher pressures developed by the DIDP dry blend over DHP dry blend in the extruder. However too much should not be inferred from these high magnification SEM scans because the evidence is not very clear.

The SEM scans have given support to the earlier observation that plasticized mixes that give rise to higher pressures in the extruder, also fuse earlier and probably faster. The gradual nature of PVC fusion has been re-established and this is in accordance with a host of earlier experimental results. The initial 100 μm particles or grains gave way to a possible intermediate 10 μ m particles or agglomerates. Further development of fusion led to a structure less mass interspersed with submicron particles. The distribution of these submicron particles, possibly microdomains, seem to be somewhat affected by the plasticizer type but the evidence is not very conclusive.

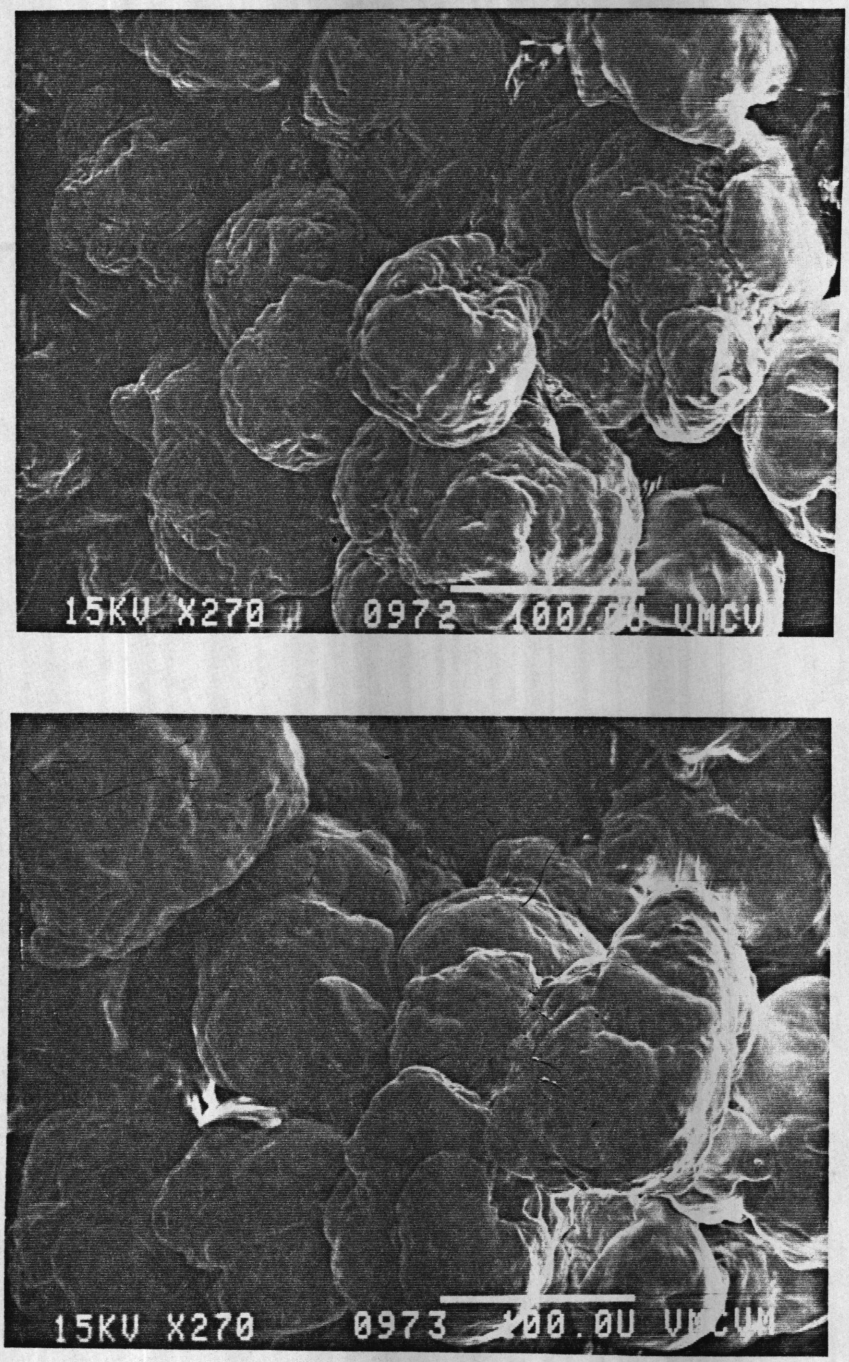

Figure 5. 66. Fusion Study of DHP dry blend by SEM (1/16 inch dia. die) at turn 9.: Leading edge (top), Trailing edge (bottom). Mag. 270.

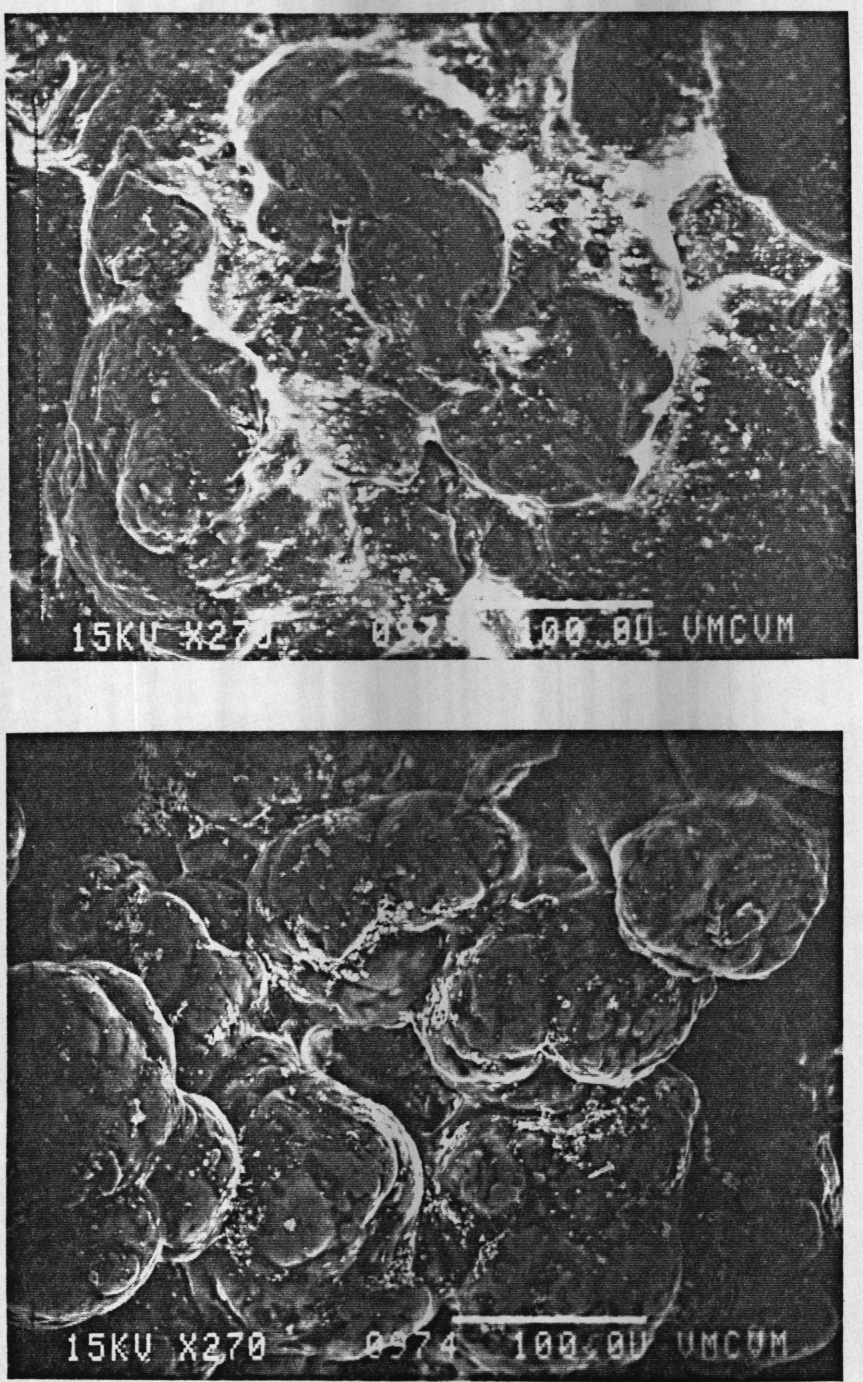

Figure 5. 67. Fusion Study of DHP dry blend by SEM (1/16 inch dia. die) at turn 10.: Leading edge (top), Trailing edge (bottom). Mag. 270.

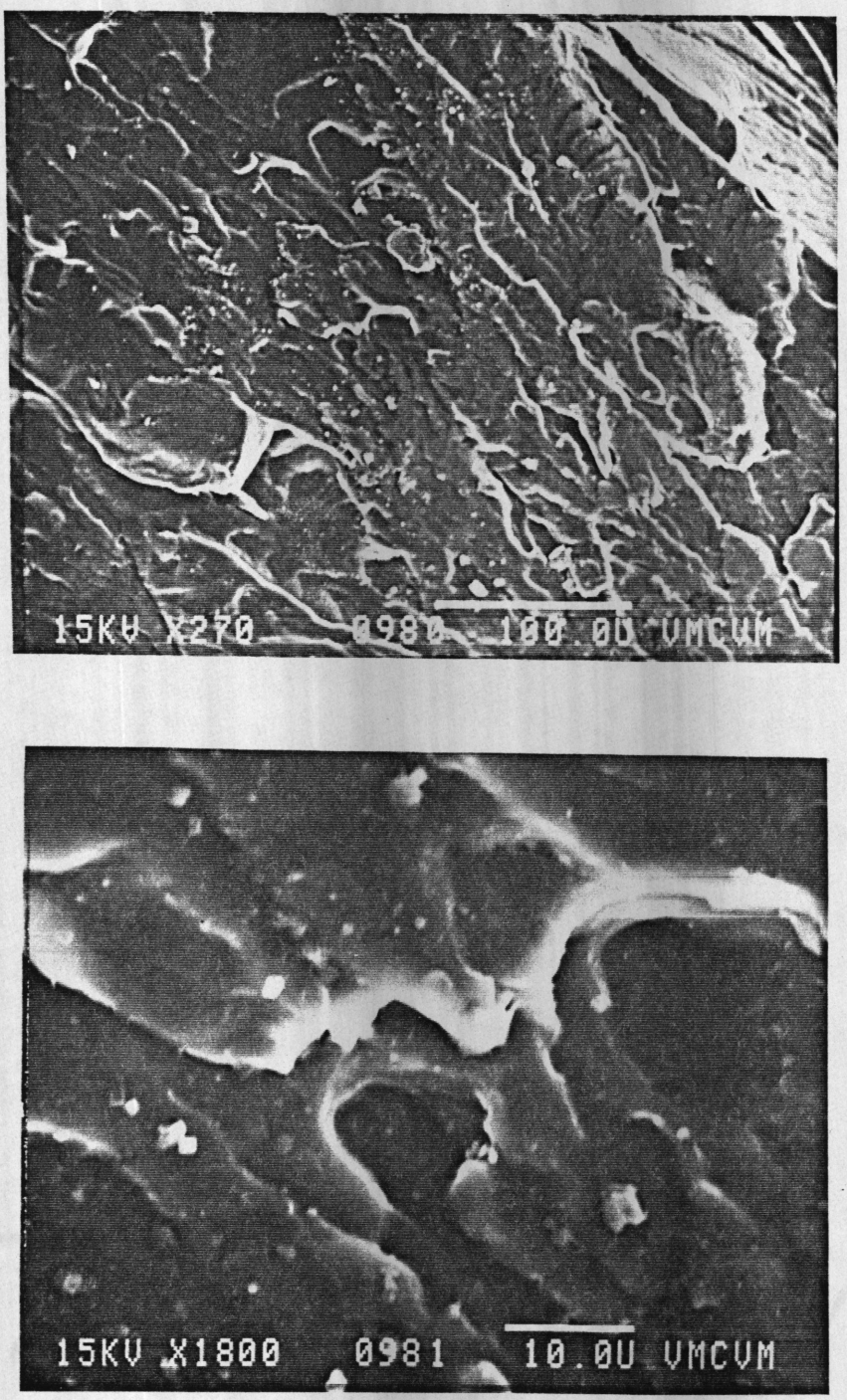

Figure 5. 68. Fusion Study of DHP dry blend by SEM (1/16 inch dia. die) at turn 11 1/2: Material from leading edge. Top Mag. 270, Bottom Mag. 1800.

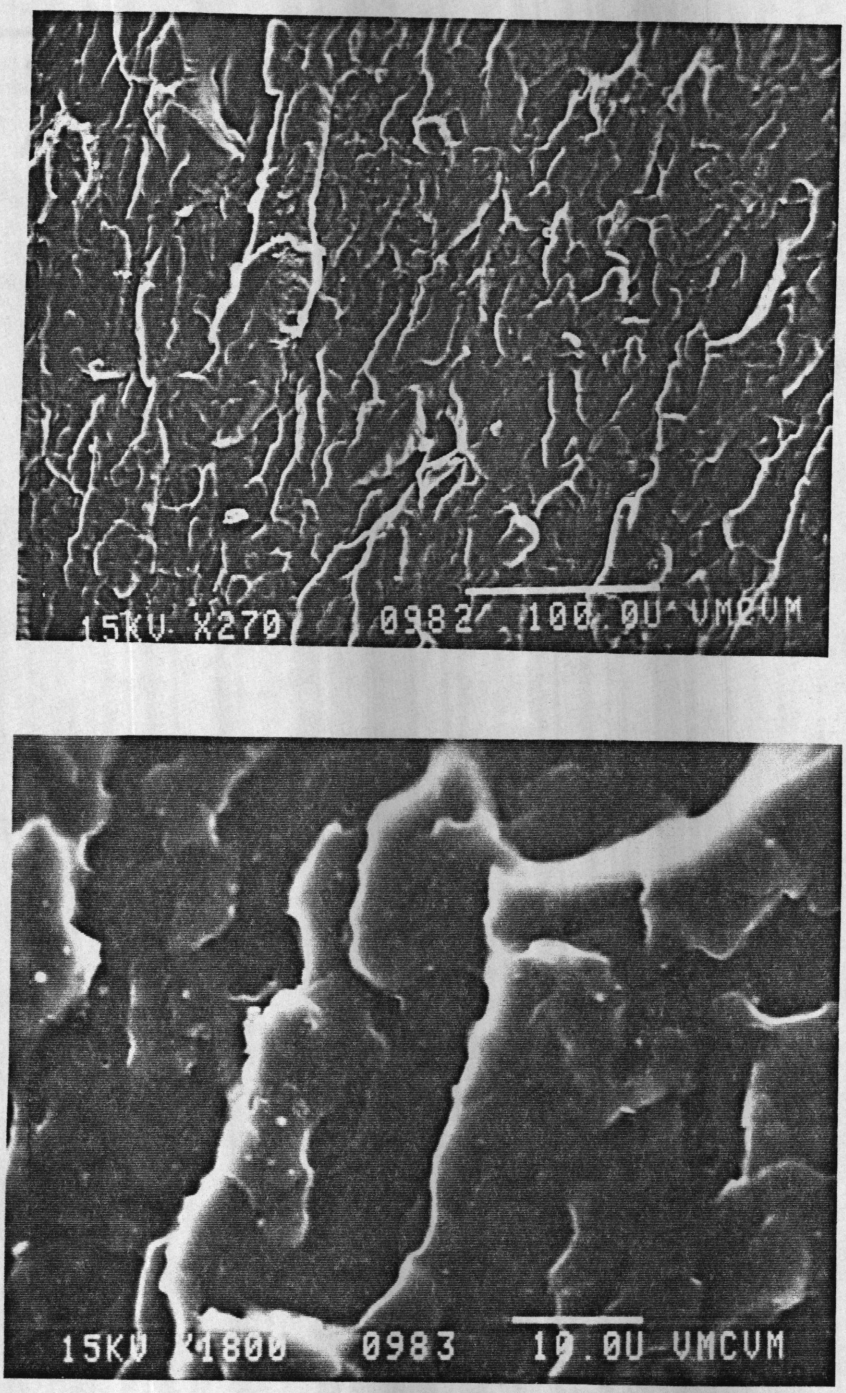

Figure 5. 69. Fusion Study of DHP dry blend by SEM (1/16 inch dia. die) at turn 11 1/2: Material from trailing edge. Top Mag. 270, Bottom Mag. 1800.

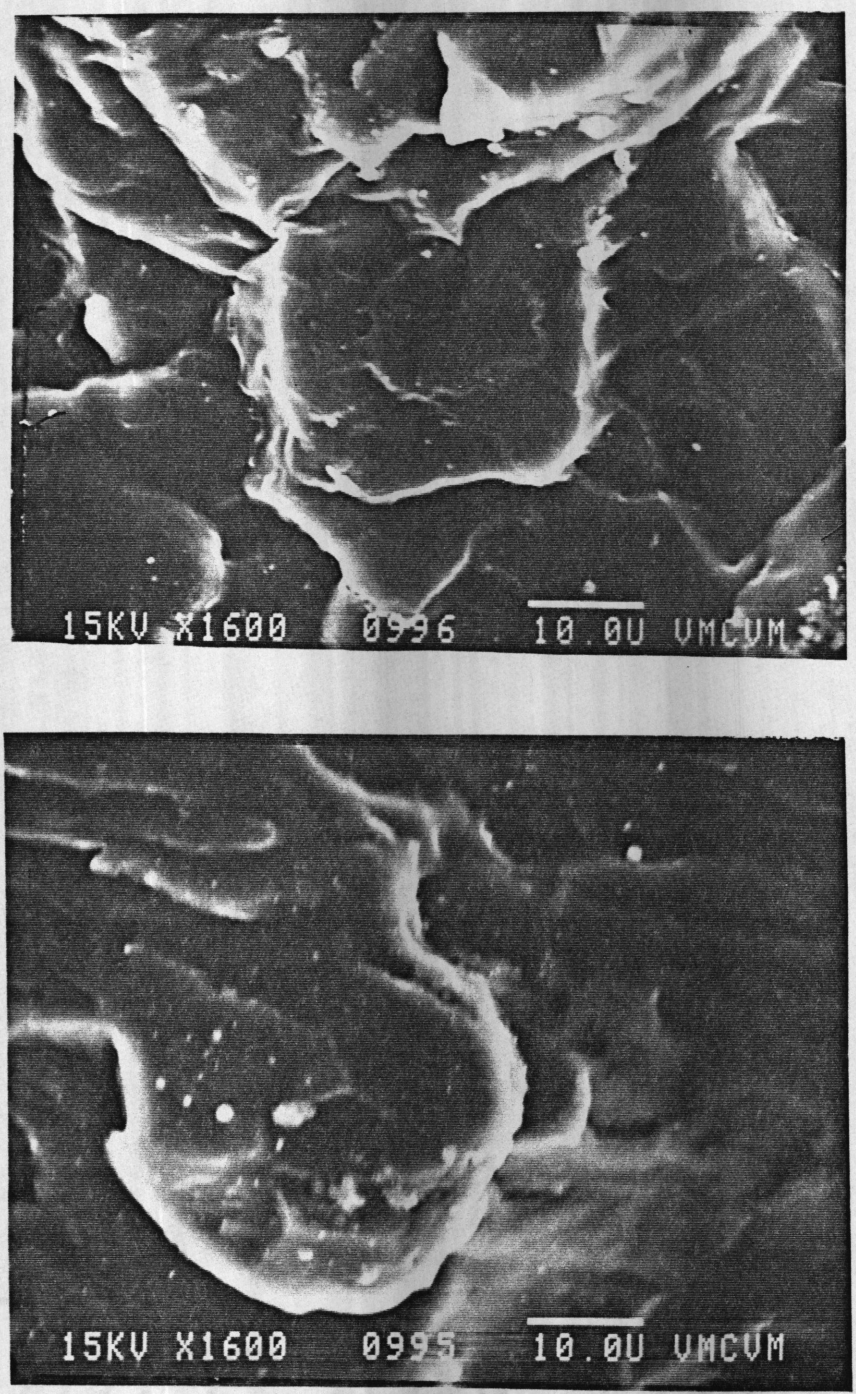

Figure 5. 70. Fusion Study of DHP dry blend by SEM (1/16 inch dia. die) at turn 14.: Leading edge (top), Trailing edge (bottom). Mag. 1600.

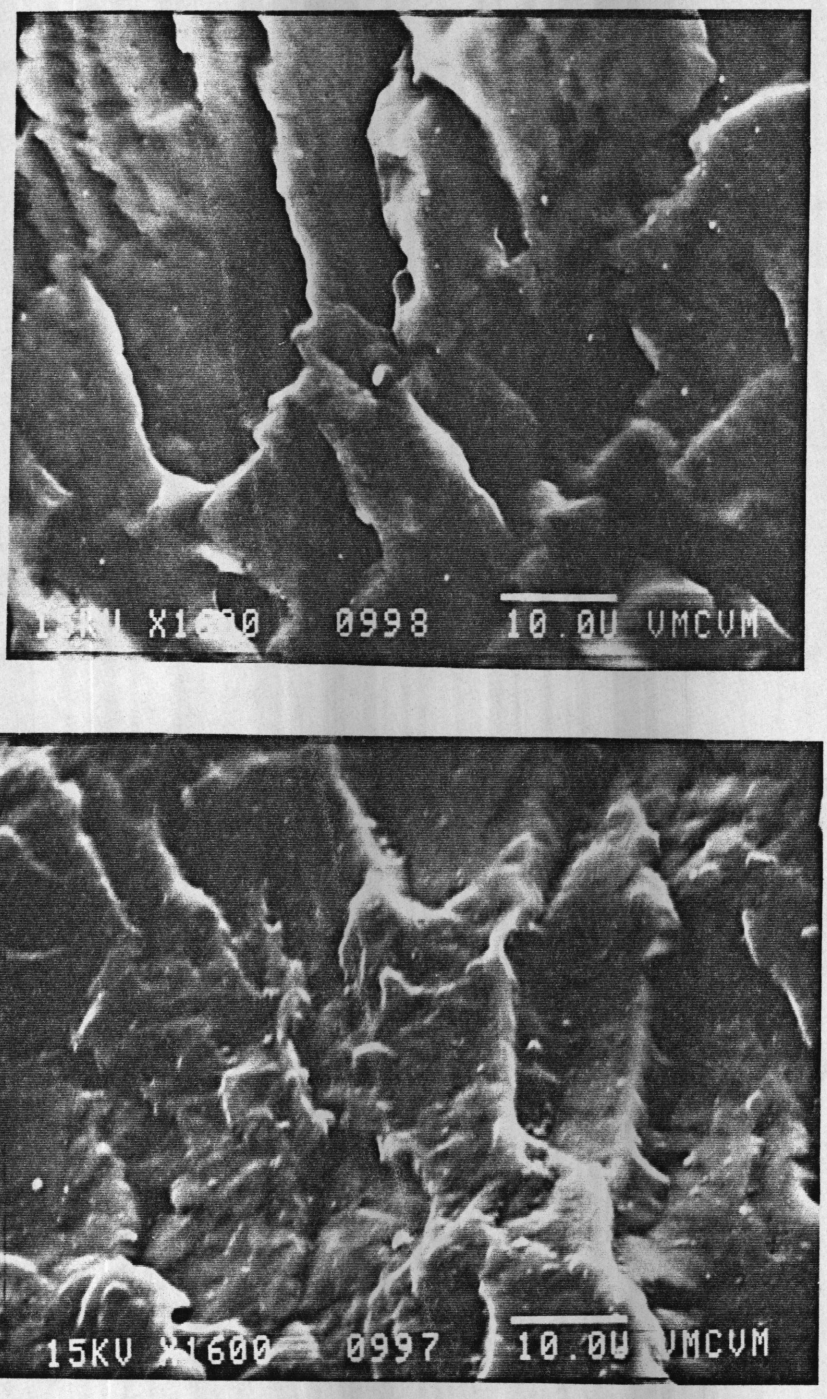

Figure 5. 71. Fusion Study of DHP dry blend by SEM (1/16 inch dia. die) at turn 16.: Leading edge (top), Trailing edge (bottom). Mag. 1600.

5.2.3 Dry Extruder Runs

Before moving on to the discussion of the numerical results, a second type of extruder run needs to be reported. In order to check the validity of the solids conveying model, experimental data had to be generated against which the models could be tested. In these experiments, barrel temperatures much below that required to initiate fusion of PVC were maintained. As no melt formation took place during these extruder runs, they are called dry extruder runs. With only the flange attached to the end of the extruder, experiments were run with dry blended DIDP at 15, 25 and 35 rpm for constant barrel temperatures settings. The maximum barrel temperature was about 135 ° C. The dry blended DIDP was preheated to maintain the isothermal characteristics of the whole experiment.

Tables 5.40 to 5.42 display the results of the dry extruder runs. From these tables it is quite apparent that beyond a certain barrel temperature, the flow rate of the solids was not affected by changes in the barrel temperature. Instead of an average value, the ranges of pressures from the transducer at turn 19 are given in the tables. There is a drop in the pressure values with an increase in the barrel temperature. The pressure varied by as much as 380 KPa (55 psi), 325 KPa (47 psi) and 560 (80 psi) for screw speeds of 15, 25 and 35 rpm, respectively, for different barrel temperatures. The friction coefficients had also not displayed a wide fluctuation with temperatures in the range of the barrel temperature settings and this could have led to solids conveying capacities not being affected. But most probably, it is the drag induced by the rotating screw that dominates the flow in the case of this dry extruder runs and the back pressure build up has very little influence on the flow rates. The results of the numerical tests, which will be discussed in the next section, indicate a dominance of the drag mechanism. The fact that the flow rates do not seem to vary with temperature might make it possible to model nonisothermal solids conveying using properties that do not depend on temperature.

Also in Table 5.43, the densities of some of the extrudates obtained from dry extruder runs at different barrel temperatures are presented. As the barrel temperatures go up, so does the extrudate density till it reaches the incompressible densities of the melted or fused PVC. The density variation with barrel temperature may be due to different degrees in fusion at different temperature. But the pressure build up in the extruder can also affect the degree of fusion. Previously, the density variation with pressure till 3450 to 4150 KPa (500 to 600 psi) was noticed in the compaction tests in section 5.1.2. This density variation will be used to explain the simulation results of the the solids conveying zone in the next section.

The dry extruder runs have provided data to check the proposed solids conveying model. For different barrel temperatures, the flow rates seemed to be governed predominantly by the screw speed and not by pressure build up in the extruder. The relative insensitivity of the flow rate to variations in barrel temperature allows the modeling of the solids conveying zone as an isothermal phenomenon.

5.3 NUMERICAL RESULTS

In the last section of this chapter, results of numerical simulations performed to fulfil the third objective of this research will be presented. All numerical simulation work (except those involving the finite difference solids conveying model) was performed using the finite element code called Fidap. Fidap can handle only GNF constitutive equation as stated earlier. Two viscosity empiricisms have been suggested in section 4.3. The solids conveying model will be modeled as a fluid with a yield stress and the viscosity empiricism will be that of a Herschel Bulkley (to be referred henceforth as HB) fluid. The melt zones will be modeled as a shear and temperature dependent power law fluid. First, it will be shown that the two main viscosity empiricisms can be used in Fidap to predict simple flows for which analytical solutions exist. This prediction of simple cases will be done for 2-D shear flows and, in some cases, for 3-D

shear flows. The viscosity models are only good for shear flows. Non-isothermal shear flow involving power law fluids will also considered. Next the results involving simulation of the solids conveying zone will be presented. It has been proposed that the solids conveying zone be modeled as a fluid with a yield stress. Fluid properties at low temperatures have to be used for solids conveying as they will possibly better represent the solids behavior than fluids at higher temperatures. The HB model fitted the capillary rheometer data better than the Bingham fluid model at 140 and 150 °C; thus the HB model will be used for simulation purposes. Both 2-D and 3-D cases for solids conveying will be considered and the numerical predictions will be tested against the experimental values. Lastly, the results of simulating the melt zones will be discussed. Only 2-D cases will be considered and the numerical and experimental results will be compared.

5.3.1 Testing of Various Empiricisms in the GNF Constitutive Models.

Although Fidap has provisions for non-Newtonian viscosity empiricisms, neither the temperature dependent power law viscosity nor the viscosity of HB fluids are included. Subroutines have to be written for these models. In fact the in-house power law model for Fidap has an error. Predictions for simple shear flows involving these two fluid models will be compared to the analytical results.

As Fidap power law model gives erroneous results, initially a subroutine for 2-D power law model was tested. Also this allows one to see how the mesh sizes have to be modified as the non-Newtonian character of the power law fluid becomes more pronounced. Drag and pressure driven flows through a rectangular slit were used as model cases, and all other numerical predictions were compare against the results obtained from these model cases. Power law parameters for the DIDP dry blend from 150 to 190 ° C, as seen in Table 5.7, were used to test the model predictions. First for a fixed pressure differential across the rectan-

gular slit, flow rates and velocities at two different locations were compared between numerical and experimental results. Initially, the power law parameters used were of DIDP dry blend at 190 ° C. The variations in both the predicted flow rates and the velocities were less than 0.3 % from the analytical results for a relative error of 0.001. With the same pressure differential, fluid properties at 180, 170, 160 and 150 °C were used to predict velocities and flow rates. The variation between numerical and analytical results increased from 0.5 % at 180 ° C to about 2 % at 150 ° C. The problems were solved by successive substitution method and the number of iterations increased from 9 at 190 °C to 35 at 150 ° C. Also the element aspect ratio had to be altered to obtain stream lines parallel to the flow direction, which is indicative of the correct solutions for drag and pressure driven flows in straight channels at low Reynolds number. The element aspect ratio to obtain parallel stream lines was above 40 for power law parameters at 190 ° C but had to be decreased to 15 for power law parameters at 150 °C. Thus for a more non-Newtonian fluid (characterized by low power law index and high consistency term), the constraint on the element aspect ratio results in increased number of elements in the mesh and the solution convergence becomes more difficult. In these cases viscosity was expressed as a function of shear rate only at discrete temperatures. But these two constraints on element aspect ratio and time of convergence will impose the same difficulty for cases when viscosity is expressed as a continuous function of temperature and shear rate like the ones presented in Table 5.11 A. Solutions of drag flows were quite accurately predicted by using Fidap.

The next logical step was to test the power law models for pressure driven flow in 3-D cases. Although not many actual simulation runs of the extruder involving power law fluid in 3-D have been performed, the test cases discussed next will be helpful in explaining the reasons why more 3-D simulation runs were not done. It is well known that the smaller the ratio of channel width to height of the channel, the greater will be the impact of the retaining wall on restricting the flow. For a large ratio of width to height of the channel, the flow problem effectively becomes a 2-D problem. For a fixed pressure drop and a width to height ratio of 2.0, the analytical and numerical flow rates for a pressure driven flow were compared for a

fluid having the DIDP dry blend power law parameters between 150 and 190 °C. The analytical results were obtained from reference [104]. The analytical solutions contains factors that had to be interpolated from logarithmic plots and these were used in calculating the flow rate values. This interpolation from logarithmic plots might introduce some errors in the analytical values. This is especially true at low width to height ratio of the channel and for low power law index. The variation between analytical and numerical results at 180 and 190 ° C was 0.4 and 2.3 %, respectively, at a relative error of 0.001. Initially successive substitution was used to bring down the radius of convergence and the error level to 0.01 and then quasi-Newton method was applied for faster convergence to achieve an error level of 0.001. The mesh had 7 nodes in the cross channel section and 19 nodes along the width. The elements were bricks with 8 nodes. Using the same mesh and flow conditions, the power law parameters at 170 ° C provided a discrepancy of 9 % between analytical and numerical results. The mesh was refined to include 12 elements along the cross channel and this brought down the discrepancy to 4 % but increased the computation time by almost 3 times. When the number of nodes were cut to 10, the deviation rose to 5.5 %. On the other hand, increasing the number of nodes from 19 to 25 in the channel depth cut the error between numerical and analytical results by 1.3 % but the solutions took 1.5 times more time. Decreasing the nodes from 19 to 15 along the channel depth increased the errors by approximately 1 %. The preceding facts establish the trade off between more precise answers using finer mesh and increase in computation time. It also shows that beyond a certain mesh refinement, the answers do not change significantly and in fact at times, too fine a mesh can be detrimental. Using 10 elements in the cross channel direction and using 14 or 16 elements along the channel height, the deviation between numerical and analytical results is about 6 % for the power law data at 160 °C. The deviation at 150 °C was considerably higher. Flow rates of drag flow in 3-D were accurately predicted using Fidap.

A major problem in using the power law model is that it predicts very high viscosity at very low shear rates and this is more marked at low temperatures where the power index is smaller. Also, low values of the power law index increase the mesh size. Usually polymers

tend to attain a Newtonian viscosity at low shear rates. No such leveling of viscosity was observed at low shear rates for plasticized PVC dry blends. When the pressure differential driving the flow is increased, the shear rates in the fluid increased and the deviations between analytical and numerical results decreased. Also when the effect of the wall is decreased by increasing the width to height ratio of the channel, the errors decreased. For higher pressure differential and wider channels it was thus possible to decrease the disparity between the numerical and analytical results to less than 2 % and less than 5 % even when using power law parameters at 160 and 150 ° C, respectively. The width to height ratio of the tapered extruder channel is approximately between 6 and 10 and the shear rates experienced in the extruder are approximately between 1 and 70 1/s. Here the conditions in the extruder are conducive to using the experimentally obtained power law parameters. Another factor that should be noted is the element aspect ratio. To attain parallel stream lines, the element aspect ratio dropped from 72 for power law parameters at 190 ° C to 26 for power law parameters at 150 ° C. These low aspect ratios at low temperatures will become a major impediment for not being able to do 3-D modeling for the melt zones.

Having established that Fidap can be used to predict flow rates and velocities in drag flows and pressure driven flows for power law fluids over a wide range of temperatures, it would be of interest to see how the viscosity expressions developed in section 5.1.2 are able to predict velocities and flow rates for similar flows. There are two types of expressions. In the first category, the viscosity is expressed as a power law model with the power law parameters being Arrhenius type functions of absolute temperatures. In the second case the the natural log of the viscosity was expressed as quadratic functions of natural log of shear rate and temperature or $\ln \eta = f(\ln \dot{\gamma}, T)$. Two sets of expression above and below 165 ° C were developed; 165 ° C is the transition temperature when the flow mechanism changes for plasticized PVC. By substituting for the temperature in these expressions, viscosities at discrete temperatures are obtained as a function of shear rates only. Predictions and comparisons between analytical and numerical cases using these expressions will be made only in 2-D as these expressions will be used solely for 2-D simulation purposes.

The results obtained from using $\ln \eta = f(\ln \dot{\gamma}, T)$ will be discussed first and then followed by discussion about the power law type models in which the power law parameters are functions of absolute temperature. Actual viscosity expressions of the form $\ln \eta = f(\ln \dot{\gamma}, T)$ above and below 165 ° C are presented in Table 5.11 A. Using the viscosity expressions for DIDP for a fixed pressure drop across a rectangular channel, the deviation between numerical and analytical results varied between 2 to 6 % for temperatures between 190 and 170 ° C. For the quadratic viscosity function at 150 and 160 °C, the deviation between the numerical and analytical results vary by as much as 10 % or higher if the pressure differentials is unchanged from the one used for cases between 170 and 190 ° C. The more viscous materials at lower temperatures flowing under the same pressure drop as at higher temperatures, give rise to lower shear rates in the material and cause large errors in flow predictions. If the pressure differential is increased at lower temperatures so that shear rates are higher, the errors can possibly be reduced. It has been mentioned in section 5.2.2 that at shear rates below 0.1 1/s, the viscosity predictions from the quadratic viscosity function and the power law models diverge. So if pressure differential is increased, the shear rates increase and the predictions from the above two models agree better. For a temperature of 160 ° C, Raising the pressure drop by 60 % increased the shear rates to above 0.1 1/s and reduced the errors in the flow rate predictions to less than 2 %. As will be seen later in section 5.3.3 the shear rates in the extruder will be approximately between 1 and 70 1/s for the cases that will be considered and no problem is envisaged in velocity or flow predictions at those shear rates. The second model in which the viscosity expression was similar in form to the power law model was tested for flow rates under pressure driven flows at 150 and 160 ° C. The constants used in this model are given in Table 5.11 B. Here the deviation in the flow rate was larger than the previous case where viscosity was expressed as a quadratic function of function of shear rate and temperature. Also it took 2 to 4 more iterations to achieve the same tolerance level irrespective of its value. No test was done for the second model above 165 ° C as the first model had proved to be adequate in the higher temperature range and proved to be better in the lower temperature range.

Non-isothermal flows will be considered for simulation purposes and the next task is to see whether Fidap can make correct predictions for non-isothermal flows involving power law fluid. There is no analytical solution of non-isothermal flow of power law fluid with varying properties. Indeed the non-isothermal flow of power law fluid with with constant properties can only be solved numerically. In reference [105] and [106] the non-isothermal pressure driven flow for a power law fluid with constant properties have been solved using finite difference techniques. The solutions were obtained using dimensionless quantities and for power law fluids of n=0.25 and n=0.5. No viscous dissipation was considered. The power law index of 0.25 and 0.50 almost covered the range of power law indices for DIDP and DHP dry blend as seen in Table 5.7. Using the power law models, discussed earlier, the predictions obtained by using Fidap for dimensionless average fluid temperature at two dimensionless distances in the flow direction were calculated. This was done for both the power law indices of 0.25 and 0.5 and the previously published data and the predictions from Fidap are shown in Table 5.44. The relative error for the Fidap calculation was 0.0001 while the relative errors or the tolerances for the finite difference cases were not reported. Also no mesh refinement was done for the Fidap calculations and the step sizes for the finite difference scheme were not reported. Considering the previous two facts, the discrepancy between the finite difference and the finite element methods is not significant. So Fidap would be able to predict temperatures in non-isothermal flows of power law fluids. This also holds good for expressions like $\ln \eta = f(\dot{\gamma}, T)$ which basically predict power law behavior.

So Fidap is seen to be capable of predicting flow rates, velocities and temperatures for isothermal and non-isothermal flows involving power fluids in 2-D and for isothermal cases in 3-D flows. Viscosity, density, specific heat and thermal conductivity are the physical properties that will be needed for simulation of the non-isothermal flows that exist in the extruder melt zones. From section 5.1, the last three properties for the dry blends are almost constant in the temperature range of 150 to 190 ° C and viscosity is the only property that is affected by temperature. It has been possible to express viscosity as a temperature dependent power

law model and the ability of the model to predict flow rates and velocity profiles from 150 to 190 ° C and for shear rates experienced in the extruder has been tested successfully.

The solids will be treated as a HB fluid and the analytical results of simple flows will be compared to the prediction from Fidap. It was shown in section 5.3 that HB fluid model fitted the capillary rheometer data better than the Bingham fluid model. The HB viscosity will be modelled as follows :

$$\eta = -\{m\,|\dot{\gamma}|^{n-1} + \left[\frac{\tau_0}{|\dot{\gamma}|}\,[1-\exp(-N\dot{\gamma})]\right] \qquad (5.3)$$

The reason for incorporating the term (1 - exp (-N $|\dot{\gamma}|$)) has been explained before and the advantages of incorporating the term in the viscosity expression in simulations of flows involving the Bingham fluid have been discussed in section 4.3. [89]. The use of equation 5.3 definitely improved upon the predictions from previous HB viscosity empiricism [98,99] that did not incorporate the term containing the exponential expression. It was observed that for pressure driven flows of HB fluid Equation 5.3 holds good both in the yielded and the unyielded regions of the flow and predicts correct velocity for the central core and the region between the core and the walls. The differences between the analytical [100] and the numerical results were smaller by using eqn. 5.3 than by using the earlier form used in reference [98] and [99]. Also the convergence was faster using the viscosity expression in eqn. 5.3 than the model used earlier.

For a pressure driven flow of a HB fluid in a straight channel, the ratio of τ_y (the yield stress) to τ_w (the wall stress) and the power law exponent, n, are the two important factors that can affect the flow rate and the velocity profile. In Table 5.45, the percentage difference between the analytical and numerical flow rates results for a pressure driven flow in a rectangular slit are presented. The numerical results are for a relative error of 0.001. For a fixed τ_y as the ratio of τ_y / τ_0 increases, the pressure differential driving the flow decreases and the deviation between numerical and analytical increases by a slight amount. Also shown in Ta-

ble 5.45 is the effect of decreasing the power law index for two different yield stress to wall stress ratios. As the power law part of the materials become more and more non-Newtonian in character, indicated by a decreasing n, the numerical results start to deviate more from the analytical results. The effect of varying the ratio of the stresses and the power law indices had similar effects on the value of the velocities. The refinement of the mesh increased the accuracy of the predictions but beyond a certain mesh refinement, the deviations between analytical and numerical results started to increase. Decreasing the relative error helped in improving the prediction but the results were not quite sensitive to lowering the relative error below 0.001.

The solids conveying will be modeled in 2-D and 3-D. The test predictions for the HB fluid were reasonably good but were done only in 2-D. To the best of the author's knowledge, there have been no published results of pressure driven flows for HB fluid in 3-D. So in the next section, the 2-D viscosity model has to be extended to 3-D. The down-channel velocity for 3-D cases will be a function of both channel depth and height. So the shear rate calculations will have to take this factor into account. If then by altering the tolerance limit and refining the mesh the solutions of the 3-D cases (under appropriate boundary conditions) do not change by any significant amount, it can reasonably be said that the 3-D model for HB fluid is working. The next section deals with the solids conveying and will apply the HB model to simulate the solids conveying as a fluid.

5.3.2 Predictions of Isothermal Solids Conveying Model

The modeling of the solids conveying zone by treating the solids as a HB fluid will be discussed in this section. The HB model discussed in sections 5.3.1 with material parameters from Table 5.21 will be used to predict results that will be compared to the experimental results from the dry extruder runs presented in section 5.2.3. The material used for solids con-

veying experiment and numerical tests is DIDP dry blend. Also the finite difference model of Tadmor et al. [54,55] for the tapered solids conveying zone will be used to predict the results of the dry extruder runs. Numerical simulation has been performed in both 2-D and 3-D.

For a large temperature range, the results of the dry extruder runs in 5.2.3 established the fact that the effect of changing the barrel temperature was not significant on flow rates as long as the barrel temperature was not high enough to initiate fusion. The barrel temperature for each run was constant along the entire barrel length. The experiments were performed for different constant barrel temperatures that varied from 90 to 130 ° C for 15 rpm and varied from 105 to 135 for 25 and 35 rpms. The barrel temperature did not affect the flow rates of the solids which seemed to be dominated by the drag induced by the rotating screw at each screw speed. The pressure at the screw exit dropped with increase in barrel temperatures. As temperature variation does not affect the solids conveying flow rate, the solids conveying is treated as an isothermal phenomenon in the temperature range used for the 'dry extruder runs'. Modeling of the solids conveying zone will thus be done only for the isothermal case.

The availability of the excellent problem solving capabilities of Fidap are made use of in order to achieve the modeling of solids conveying as a fluid. Fidap has been developed for following GNF constitutive equation and thus establishing a proper viscosity empiricism which approximates solids behavior is the first requirement for modeling purposes.

Although no experiments were performed at a barrel temperature of 140 ° C, the flow rates could not have been very different between 135 and 140 ° C especially considering the trend till 135 ° C. Fluid behavior at 130 or 140 ° C is assumed to be similar to solids behavior at 130 or 135 °C. At 140 and 150 °C, the HB fluid model fitted the capillary data quite well. It was not possible to obtain viscosity shear rate data below 140 °C. So the HB model parameters at 140 ° C can be seen as a reasonable approximation for fluid parameters at a temperature lower by 5 or 10 ° C. The dominance of drag will be reflected in the numerical experiments as was the case for the experimental observation. The assumption that the solids conveying results reported in section 5.2.3 is an isothermal phenomenon, thus a slight

deviation in physical properties should not affect the numerical prediction by a substantial amount.

Tadmor's model for tapered screw channel was used to predict the pressure rise in an extruder for a given flow rate [54,55]. The outlines of the model are given in Appendix A. In all the calculations involving Tadmor's model, the ratio of the friction coefficient at the barrel to the friction coefficient at the screw was taken to be 0.71. It is in the range of standard values for this ratio as used in references [54] and [55]. The actual ratio could have been quite different and is the first source of approximation of the existing solids conveying model. Friction coefficient is proportional to normal stress. The pressures on the barrel, flights and roots of the screw have different values but are proportional to the down channel pressure. The proportionality constant between the pressures on the different surfaces and the down-channel pressure is known as the non-isotropic pressure distribution factor (to be referred to henceforth as NIPD). It has been previously mentioned that in the existing solids conveying model, the NIPD values can be varied to match numerical predictions and experimental results and this fact is the second source of approximation for the existing model.

Although Tadmor's model is accepted, a critical analysis need to be made with regard to the factors that can influence the predictions such as NIPD and ratio of friction coefficients at the barrel and screw. This will be done following an examination of the predictions from the existing solids conveying model. For a fixed flow rate, the NIPD can be changed to vary the pressures at the extruder exit. Table 5.46 show the various NIPD values that are required to match the numerical predictions and experimental pressures from 'dry extruder runs'. For 15 rpm and a average flow rate of 18.5 gm/min, the exit pressure varied between 3000 to 6000 KPa. for different barrel temperatures. By varying the NIPD between 0.1716 to 0.1767, existing solids conveying model can predict the range of pressure from 3000 to 6000 KPa. Similarly, the variation of NIPD to match the experimental and numerical results at 25 and 35 rpms are given in Table 5.46. It can be observed that the variation in NIPD occurs within a narrow range of values at each screw speed and also among the three different screw speeds. Whether these values will be valid for another extruder with different geometry processing the same

material is difficult to predict. In fact Tadmor et al. [54,55] do not discuss the validity of the model when the extruder geometry is changed or the pressure build-up is different or the barrel temperature changes. Although the non-isothermal solids conveying has been modeled, the effect of temperature on the NIPD has not been incorporated in that model. Also in the model fitting done here, the NIPDs for all the screw surfaces and the barrel surfaces have the same value and this can surely be questioned. The ratio of the friction coefficients at the barrel and the screw is assumed to be constant. Considering the difficulty in rigorous analysis of the solids conveying zone, it can be re-emphasized that this might not be a valid assumption. Thus there are assumptions regarding both the NIPD and the friction coefficients which might not be very definite under changing processing conditions. These facts lend a certain amount of uncertainty and ambiguity to the Tadmor's model which is at present the best available tool for modeling solids conveying.

The proposed 2-D fem model of the solids conveying zone treats the solids as a HB fluid with a drag on the upper plate and an imposed positive pressure gradient in which the pressure is higher at the exit than at the entrance. For numerical purposes , the extruder is represented by 'unwinding' the screw channel and consists of a rectangular channel with the barrel being pulled at an angle to the down-channel direction as shown in Fig. 2.23. If Vb is the barrel velocity, then the down-channel component Vbz = Vb Cos (θ) and the cross-channel component Vbx = Vb Sin (θ) where θ is the helix angle and equals 17.65 ° for a square channel. In the 2-D case the upper plate moves with a velocity of Vbz and the lower plate is stationary. The geometry of the extruder channel in 2-D, subdivided into a 4 node quadrilateral, is seen in Fig. 72. The actual number of nodes is not shown here. The number of nodes the vertical direction are 17 as in section 5.3.1 it was found to be the optimum in the test cases of HB fluid in slits with comparable geometry to the extruder channel. The number of nodes in the down-channel section are 159. Initially a relative error of 0.001 was tried. When the error level was cut by 10 %, the results were affected by a very small amount. So the higher tolerance of 0.001 was maintained for all computations.

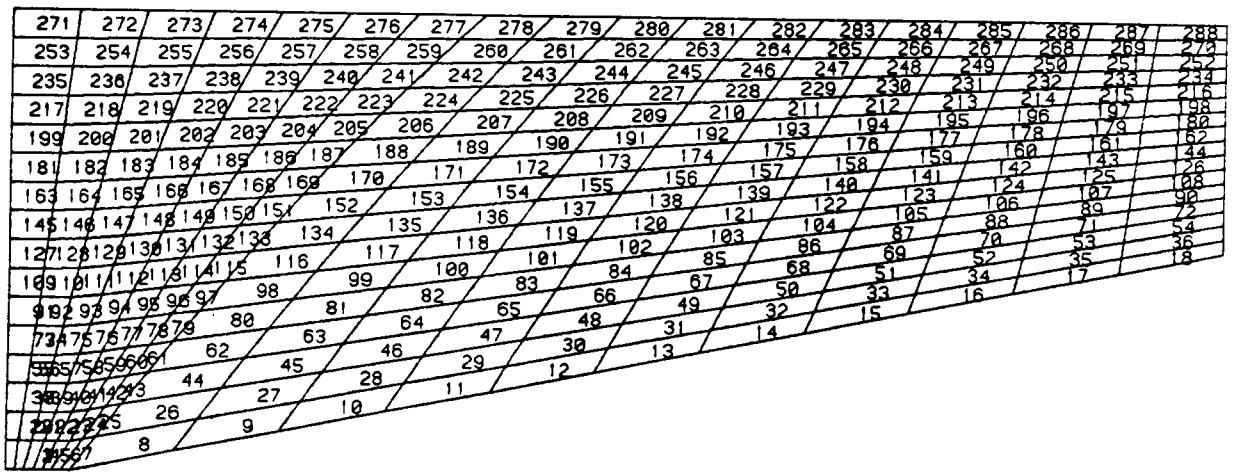

Figure 5. 72. Dimensions of Extruder Channel and Approximate Mesh for 2-D Solids Conveying Simulation.

The predictions from 2-D simulation of solids conveying is presented in Table 5.47. At each screw speed, flow rates (for a channel width of 2.54 cm) were computed by supplying the fluid properties, the velocity boundary conditions along the two edges of the channel and the pressures at two ends in the form of a traction vector. The pressure gradients are positive as they increase with distance along the channel and their values correspond to the average of the experimental range of pressures reported in Tables 5.38 to 5.40. Also reported in Table 5.47 are the flow rates of pure drag flow of HB fluid at the three speeds. It is seen from Table 5.47 that imposition of the positive pressure gradient on the pure drag flow decreases the flow rate by approximately 9 % but the large variations in the value of the positive pressure gradient have practically no effect on the flow rates. Figures 5.73 and 5.74 show the numerically predicted velocity profiles obtained at two different positions along the screw channel at 15 rpm for two different positive pressure differentials. Figures 5.75 and 5.76 show similar plots but at 35 rpm. It is clear that the positive pressure gradient and possibly the form and the magnitude of the viscosity function alters the velocity profile but no plug velocity profiles are obtained. The existing solids conveying model assumed a plug flow in the solids conveying zone [49,54,55] but the numerical predictions of the proposed model do not agree with this assumption. The drag seems to the dominant factor at all the three screw speeds and the effects of the positive pressure gradient and the fluid property seem to be comparatively small. The ranges of the pressure drop used for numerical purposes correspond to actual experimental values and within this range, the flow rates and the velocity profiles from the numerical predictions are dominated by the drag.

Before any comparisons are made between experimental and numerical results, results from 3-D numerical tests will need to be discussed. The addition of the retaining wall, 2.54 cm wide, will surely affect the velocity profile and flow rates. The velocities are constrained to be zero at the side walls. Also the top plate now has a cross-channel component, Vbx. Brick elements with 8 nodes were used for 3-D numerical work. Initially, 7 elements were placed along the width and later it was increased to 10. The change in the flow rate was 5.5 %. When the number of elements were increased from 10 to 13 elements, the flow rate pre-

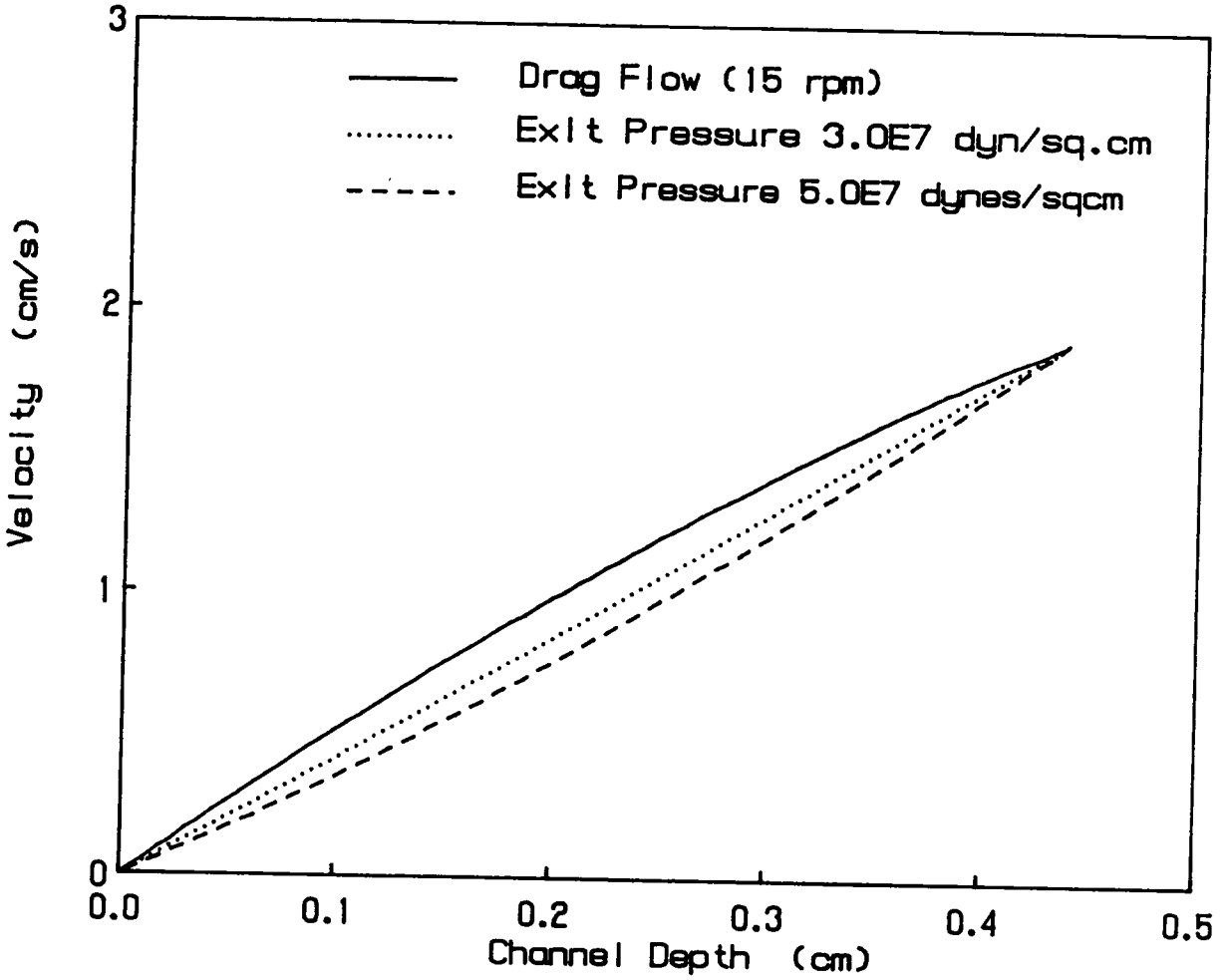

Figure 5. 73. Numerical predictions of Down Channel Velocity versus Channel Depth at different Exit Press. at 121cm (15 RPM)

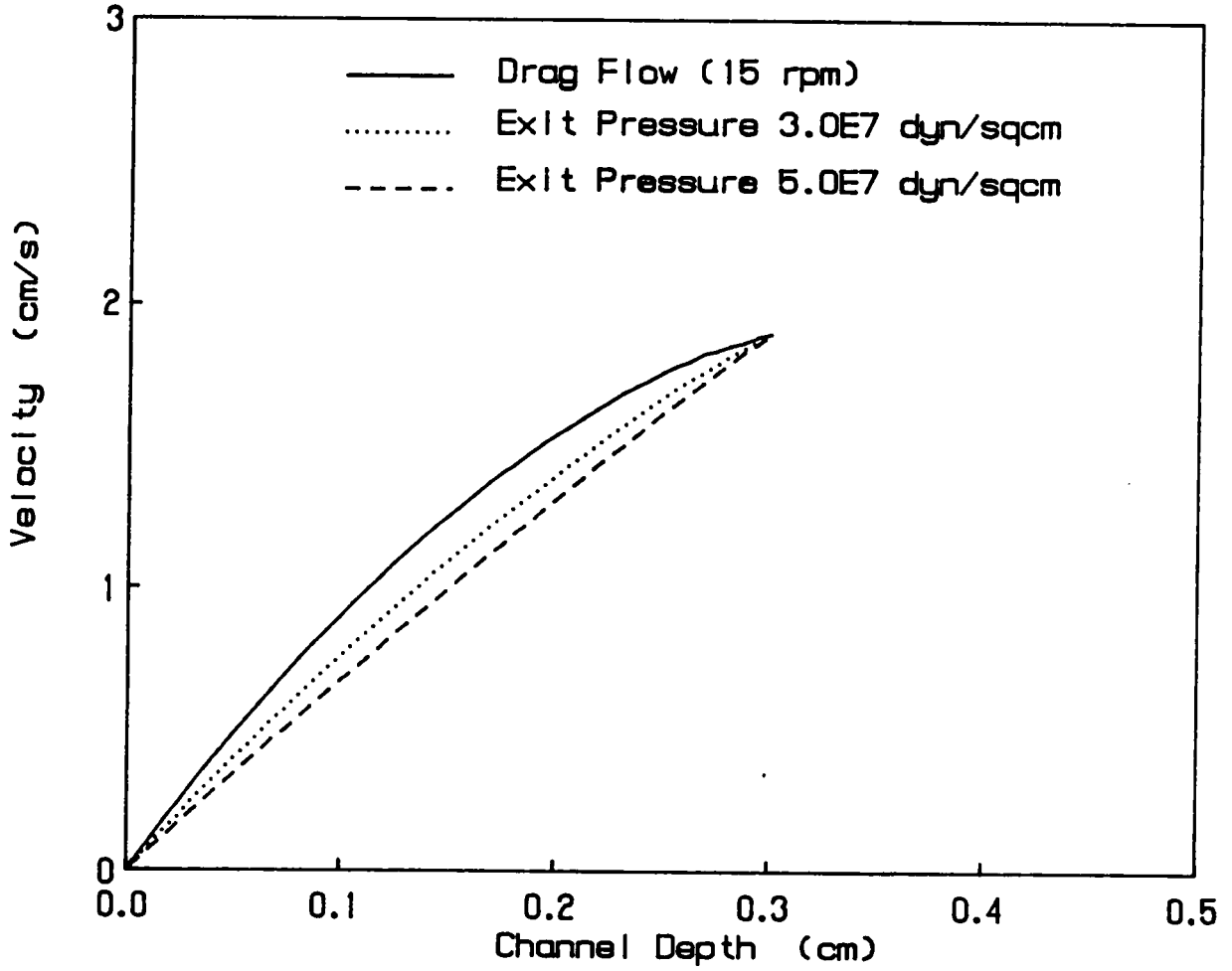

Figure 5. 74. Numerical predictions of Down Channel Velocity versus Channel Depth at different Exit Press. at 141cm (15 RPM)

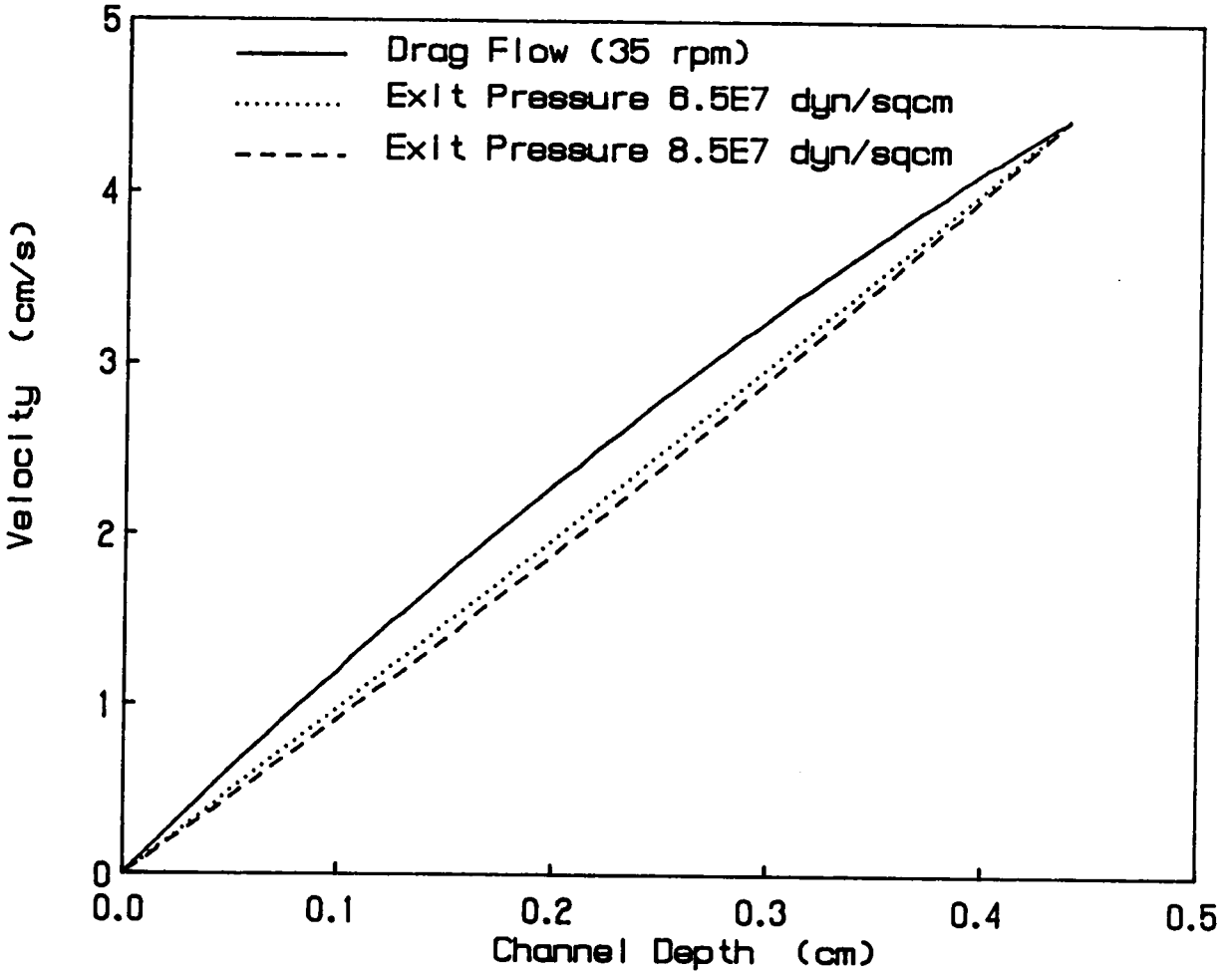

Figure 5. 75. Numerical predictions of Down Channel Velocity versus Channel Depth at different Exit Press. at 121cm (35 RPM)

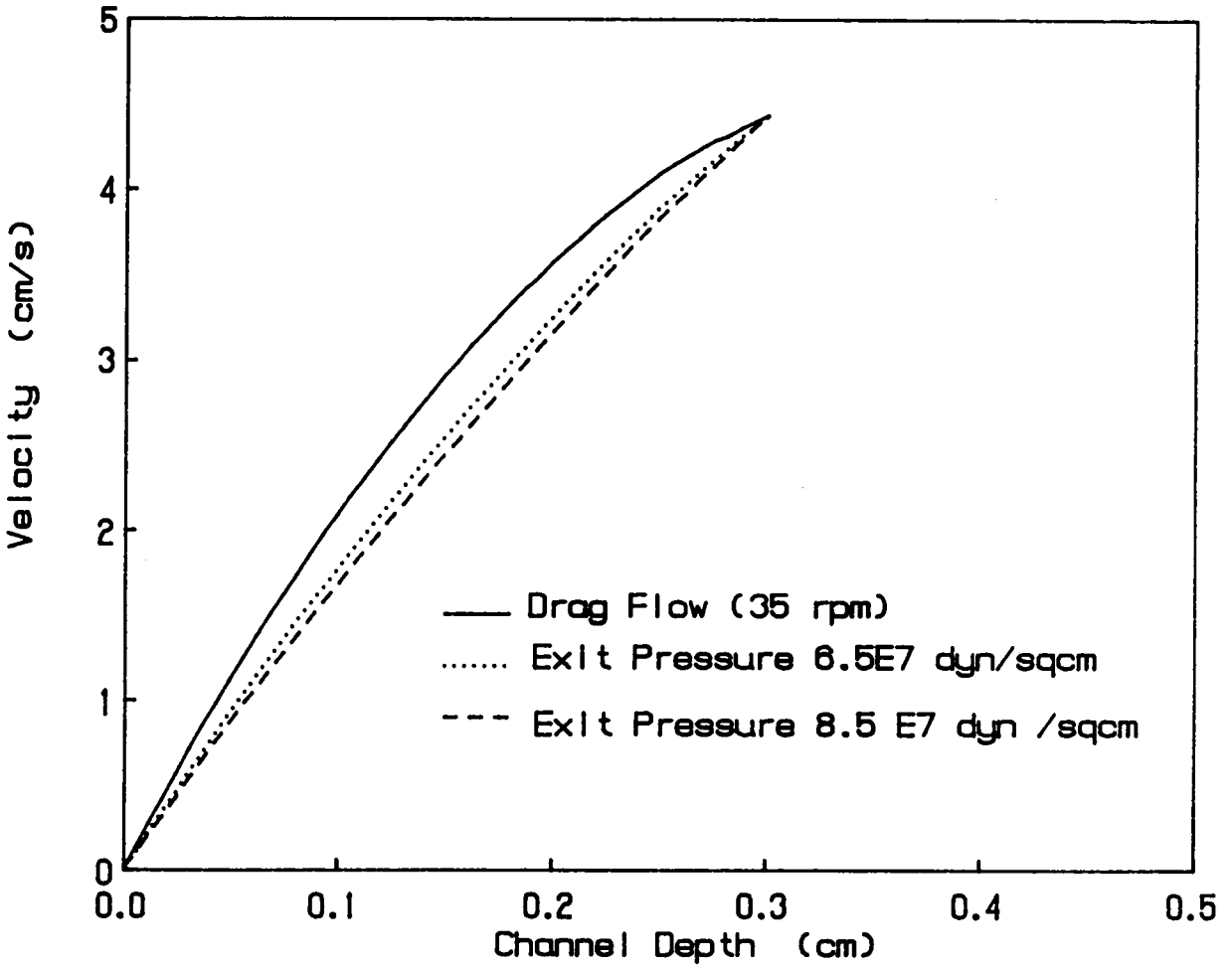

Figure 5. 76. Numerical predictions of Down Channel Velocity versus Channel Depth at different Exit Press. at 141cm (35 RPM)

diction varied by less than 2 % but the solution time increased considerably. It was decided to have 10 elements in the width direction. The number of elements along the channel height had to be reduced to accommodate the additional elements along the width. Along the height direction 10 and 14 elements were tried and as the difference was less than 2 %, it was decided to place the lower number of elements along the height. Owing to problems of large memory and computation time associated with large 3-D problems, a certain amount of accuracy probably had to be sacrificed. Even then a mesh having 4961 nodes with three velocity degrees of freedom (minus those stated in the boundary conditions) resulted from working with a coarse mesh. A relative error level of 0.001 was used for all the calculations.

The results of 3-D simulation are presented in Table 5.48 with flow rates calculated for two values of imposed positive pressure differentials (signifying two different barrel temperatures) at each of the three screw speeds. The retaining wall further reduce the flow rates from the 2-D case. The overall reduction in flow rates from the case of the pure drag flows in 2-D is 28 %, 20 % and 15 % for screw speeds of 15, 25 and 35 rpm, respectively. The effect of the cross-channel flow was negligible on the flow rates. This was found to be the case when 3-D simulation was done with or without the cross-channel velocity as a boundary condition. As was the case with the 2-D numerical tests, the drag induced by the top plate is the dominant factor and the positive pressure differentials and the fluid properties do not affect the flow rates by any significant amount. The dominance of drag was more prominent at higher speeds as evident by the lower reduction of flow rate values between 2-D drag flow and the complete 3-D model at 25 and 35 rpms. Of course mesh refinement was not done and this might have led to a small variation in the flow rate but the overall effect of the drag would still be prevalent. The extrudate density at different barrel temperatures for the dry extruder runs were presented in Table 5.43. The densities range from 0.33 to 1.16, which is the incompressible density of the melt. Table 5.49 shows the density values, at different screw speeds, which when they multiply the flow rates for 3-D cases (in Table 5.48) match the numerical and experimental flow rates. The plasticized PVC dry blend is fed as a powder to the extruder and gets compacted as it travels through the tapered screw channel. The density

of the extrudates in Table 5.43 are possibly the densities of the materials which passes through the flange attached to the extruder exit. The simulation of the solids conveying was done as a fluid which has a constant density. As the density continually varies in the extruder channel, an average density has to be assigned or ascribed to the fluid. This average density has to be somewhere in between the initial feed and the final extrudate density. The density values in Table 5.49 lie can be considered to be such average densities which allow for the solids to be modeled as a fluid. The density values in Table 5.49 lie in a narrow range and are well within the range of experimentally determined extrudate densities from dry extruder runs.

The limitations and advantages of the solids conveying model need to be investigated. The average density values in Table 5.49 are close to the final extruder densities in Table 5.43 for low barrel temperatures until 110 ° C. At higher barrel temperatures, the increase in density takes place faster but the same average density values, now intermediate between the powder and the final extrudate densities can correlate the numerical and experimental results. The different barrel temperatures did not affect the flow rates in the 'dry extruder runs' but could have affected the densities. The exact variation of density inside the extruder channel is a function of temperature, pressure and geometry of the channel and thus it is difficult to predict and determine. The average values in Table 5.49 are within the correct range of densities but whether they are realistic values or they ought to be higher and closer to the final fluid density can be debated. Also mesh refinement could alter the volumetric flow rates in 3-D simulation and this might change the required density value. A small variation in the values of NIPD factor allowed the existing solids conveying model to match the numerical and experimental pressures. Similarly, a small range in density allows correlation between numerical modeling and experimental observations for the solids conveying to be treated as a fluid with yield stress. Considering the difficulties in properly analyzing the solids conveying zone, choosing an average density (that actually exists at some point in the extruder) which aids in correlating the solids conveying to a fluid flow problem might be a rational approximation. Researchers have modeled solids as a non-Newtonian fluid [61,64] with high value of the consistency term, m, and low power law index, n. Here the solids are treated as a HB

fluid, whose yield stress phenomenon imparts it a more solid like behavior. The dynamic data of plasticized PVC have conclusively shown that at 130 and 140 °C, the material shows pronounced yield stress behavior. So treating these kind of materials as a HB fluid is more realistic than treating them as a power law fluid with high m, and low n. The power law parameters of the HB fluid are characterized by lower m and higher n than the simple power law model which does not incorporate the yield stress. The high n as explained in section 5.3.1 allows faster convergence. The high n values also leads to higher element aspect ratio which would also help in lowering the mesh size and computation time than if the solids were modeled as a power law fluid with low n. The effect of the yield stress in itself might not affect numerical results directly but its incorporation in the model gives rise to more realistic representation of the solids. Also the magnitude of the yield stress affects the power law parameters, which in turn affects the element element aspect ratio and aids in reduction of computation time. Measurements of fluid properties are relatively much easier than measurement of friction coefficients. This fact together with the availability of the Fidap code make the above-mentioned approach to model solids conveying zone as a fluids with yield stress an interesting alternative to the existing model for the zone. Additional work is needed in this area with other materials that display yield stress behavior.

5.3.3 Prediction of the Melt Zones

The melt zone simulation will cover the extruder channel from the screw turn, where fusion is initiated, until the turn 18.75, where the last pressure transducer is positioned. The 'cooling experiments' in section 5.2.2 indicate that the initiation of fusion is determined from the position where dry blended PVC starts to loose its compacted solid appearance and begins to turn clear. When the yellow colored dye was used, the homogenization of the dye in the melted or fused part of the polymer coils from the 'cooling experiments' was taken to be

the onset of the fusion. Four cases will be considered here for simulation purposes. They are DIDP and DHP dry blend with the 1/8 inch diameter die attached to the extruder at 35 rpm and the same materials with the 1/16 inch diameter die attached to the extruder at the same screw speed. In section 5.2.2 it was stated that DIDP and DHP dry blends start to fuse and turn clear at turn 12 and 13, respectively, with the 1/8 inch die. For the 1/16 inch die, the fusion initiation sites are turns 9 1/2 and 10 1/4 for DIDP and DHP dry blend, respectively. The clearing up of the material (or homogenizing of the dye) from the onset of fusion took place within 1 to 2 turns with the larger diameter die attached to the extruder and within 1/2 turn with the larger die attached to the extruder. The melting zone or the two phase zone seems to be small compared to the total number of turns in which molten polymer is found. The latter, which includes both the melting and the melt conveying zones, is defined as the melt zone in this section.

The reason why only 2-D simulation was done for the melt zone will now be discussed. The temperature in this melt zones vary approximately between 150 and 185 ° C. The element aspect ratio for 3-D flows in this temperature range had to range from 26 to 72 to obtain proper results as was seen in section 5.3.1. The lower temperatures will be present at the beginning and bottom of the melt zones because the feed materials, as explained later, are assumed to enter the simulation zone at approximately 150 °C and flow between a heated barrel and an adiabatic screw. The constraints on the element aspect ratios for a 3-D mesh of the flow domain lead to a large problem with 4 degrees of freedom (3 velocities and temperature) at each node and could not be handled by Fidap's current memory capabilities. Instead a 2-D simulation of the melt zones was performed. The cross-channel velocity component of the barrel can affect the shear rate and thus the viscosity and flow rates. The effect of the cross - channel velocity on flow rate is small for small helix angle screw. The helix angle of 17.65 ° for the screw used in this study is smaller compared to some screws in which the effect of the cross-channel velocities on the flow rates were not pronounced [101]. The cross-channel component affected the flow rates by a very small amount for the 3-D flows considered in the last section. The effect of the cross-channel on the temperature distribution could be greater

but this is again lessened by the small helix angle [102]. Also viscous dissipation is not being considered in the energy equation in this study and this fact probably reduces the effect of cross-channel velocity on the temperature distribution.

The mesh size, boundary conditions, fluid properties, tolerances, what results to be compared, etc. need to be examined before the discussion of the simulation results. A temperature of 150 ° C warranted an element aspect ratio of 15 or less in the colder parts of the extruder as discussed in section 5.3.1. Eleven and fifteen nodes were placed in the channel depth direction for simulation of the melt zones for the DIDP dry blend using the 1/8 inch die. The flow rates, velocities and the pressures (at turn 15.75) calculated for the two cases were off by 1 % and it was decided to place eleven nodes along the channel depth. A relative error of 0.001 was used for all the simulations of the melt zones as lower tolerance did not affect the numerical results. Viscosity is a function of shear rate and temperature and the model in eqn. 4.7 with parameters from Table 5.11.A were used. There were two viscosity functions for each dry blend above and below 165 ° C, which is the transition temperature from particulate to melt-like flow. The other physical properties were independent of temperature.

The various boundary conditions for the simulation purposes are as follows. No slip boundary conditions were applied with the upper plate being moved with a velocity Vbz = 4.4353 (down channel component of the barrel velocity at 35 rpm), while the lower plate was stationary. The barrel temperature was progressively raised in the experimental setup. In the simulation problems, a lower temperature was set for the first part of the mesh (corresponding to a distance of 40 cm from end of the mesh) and a higher temperature was set for the rest of the mesh. An adiabatic screw was assumed as the screw is solid with the potential of some heat loss through the end where it connects to the motor. It was stated in section 5.1.2 that clear extrudates were obtained from the capillary rheometer at temperatures above 165 ° C. The extrudates at 160, 150 and 140 were more translucent. The clearing of the dry blends from the initial compacted solid through an intermediate translucent stage in the extruder is indicative of the progression of fusion and takes place between 1 to 2 turns with the larger diameter die attached to the extruder and within 1/2 turn for the smaller diameter die attached to the

extruder. If the clearing of the dry blends is an indication of a temperature around 165 ° C, surely the temperature is lower where the fusion is initiated. From the appearance of the dry blends at the onset of fusion, an average temperature of 150 °C is assumed at the particular screw turn where fusion was initiated. It could be a little higher or lower than 150 ° C and the approximation should not introduce much error especially as the clearing of the material in the screw channel, signifying a temperature of around 165 ° C, occurs over a short distance in comparison to the total length of the melt zone. Two quantities have been compared between the experimental and numerical results to check the agreement between them. The flow rates will be calculated using a channel width of 2.54 cm and pressure at turn 15.75 will be obtained from the simulation results. These two quantities will be compared against experimental results presented in Table 5.28 for the 1/8 inch diameter die and in Table 5.34 for the 1/16 inch diameter die.

It was initially envisaged that it may be possible to model the melting zones by using different viscosity empiricisms for the solids and the melts. But the effect of the melting zone is reduced by its relative length compared to the total length of the melt zones and also continuous shear and temperature dependent viscosity functions allow for somewhat gradual change in the material characteristics as would occur in the melting zone. Again, the 2-D modeling restricts the the scope of following the melt pool formation along the channel width.

The results of 2-D simulations using the 1/8 inch diameter die are presented in Tables 5.50 and 5,51. Initially the experimental conditions were used as boundary conditions in predicting the flow rate and pressure at turn 15.75. Then the barrel temperature was varied by 2 ° C keeping the pressure differential constant. In the next case, the pressure differential was varied by varying the inlet pressure and keeping the barrel temperature constant. Considering the sensitivity of the temperature controllers and the response of the transducers in the earlier zones, the deviation between the actual recorded conditions during the experiments and the conditions used for numerical experiments in the latter cases is quite reasonable. Between successive repeat runs, the flow rate variation was 1 to 2 gm/min and the variation in pressure in the last two zones were between 350 to 860 KPa. (50 to 125 psi). With

respect to these error bars, there is excellent agreement between numerical predictions and experimental results for both flow rates and pressure at turn 15.75 for both the dry blends for experimental boundary conditions. Even when the boundary conditions are altered, within the experimental deviation range of 2 ° C for barrel temperature and 10 % variation in inlet pressure, the numerical predictions are still good. The effect of changing the barrel temperature was more noticeable than the change in inlet pressure. The numerical predictions of velocity and temperature variation along the channel depth for different screw turns are shown in Figures 5.77 and 5.78. The velocity of the DIDP dry blend was slightly higher than the DHP dry blend near the lower plate and this causes the former to have higher flow rates. The shear rates in the extruder were between 3 and 70 1/s and the temperature and shear dependent viscosity model should have no problem in predicting correct viscosities in this shear rate range. The initial difference in temperature diminishes as the materials progress along the channel. At the last turn the temperature values along the depth (not shown here) are almost the same for both the dry blends. In Fig. 5.79, the velocity streamline, pressure and temperature contours for the DIDP dry blend using the 1/8 inch diameter die are presented. These figures are not to scale and have been expanded along the width and contracted along the length. The trends of the three quantities can be observed and they seem to behave in predictable fashion. Although the inlet temperature was constrained to be 150 °C, there are some temperatures below this value and this is confined only to entry region. It has been possible to predict the differences in the extrusion characteristics of the dry blends based on their differences in physical properties by numerical simulation using finite element methods. The main difference in the physical properties is the difference in viscosity owing to the plasticizer type.

The results of the 2-D simulation using the 1/16 inch diameter die are presented in Tables 5.52 and 5.53. As with the 1/8 inch diameter die, numerical experiments were conducted with experimental conditions and with changes in barrel temperatures and inlet pressures within the experimental deviation range. For experimental conditions, the deviation between numerical and experimental flow rates was small and almost within the experimental error bars

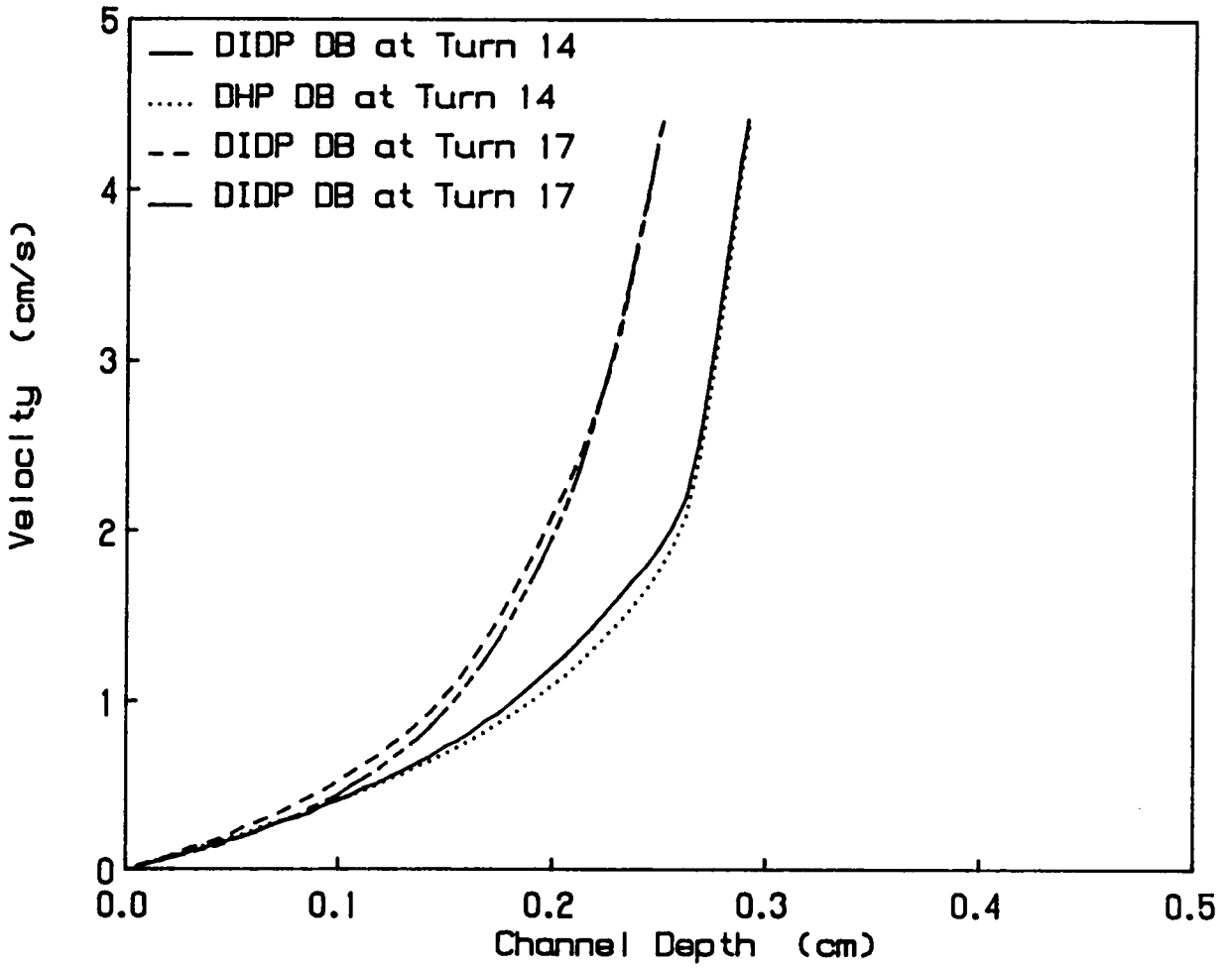

Figure 5. 77. Numerical predictions of Down Channel Velocity versus Channel Depth at different Screw Turns (1/8 inch die).

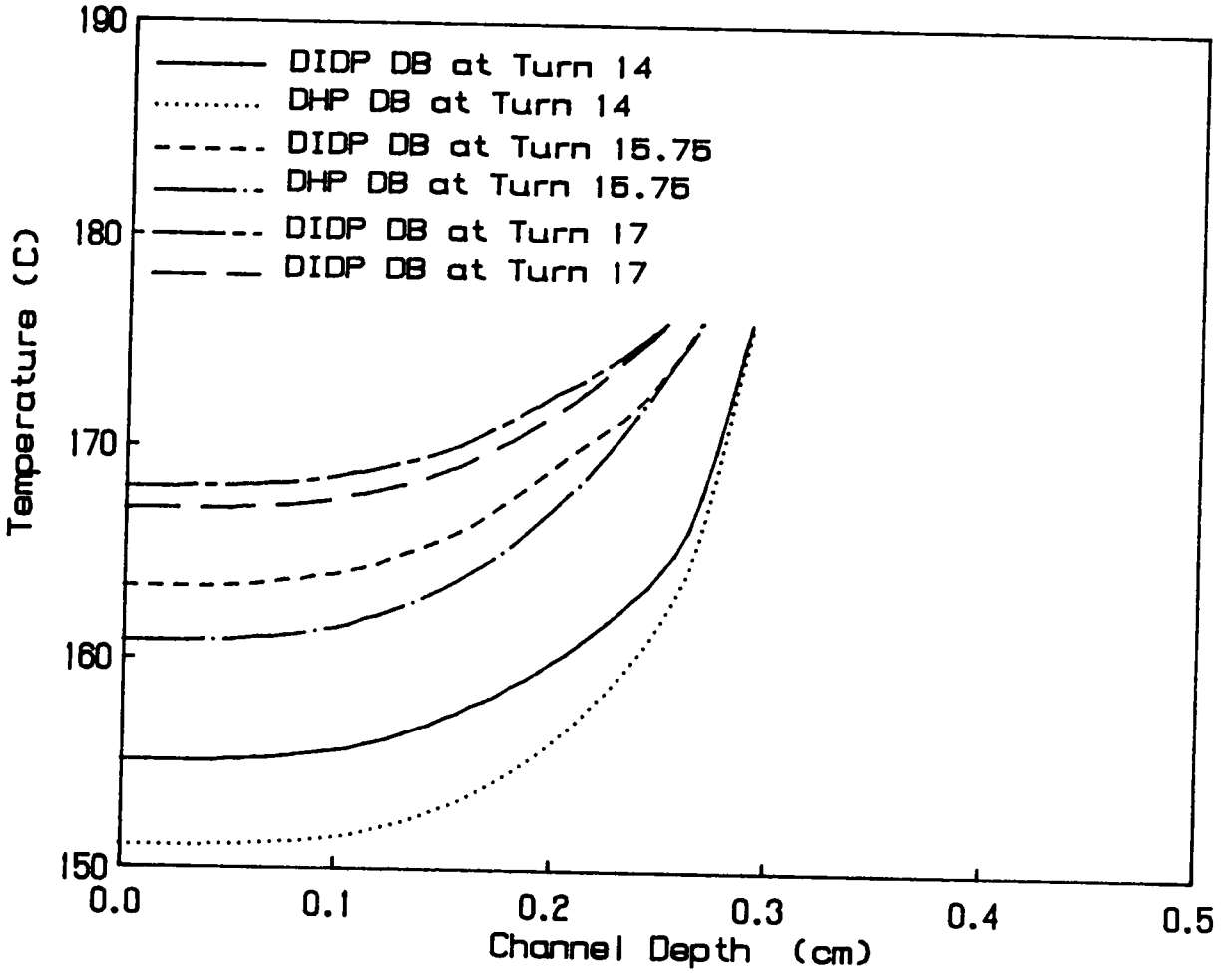

Figure 5. 78. Numerical predictions of Temperature versus Channel Depth at different Screw Turns with 1/8 inch die.

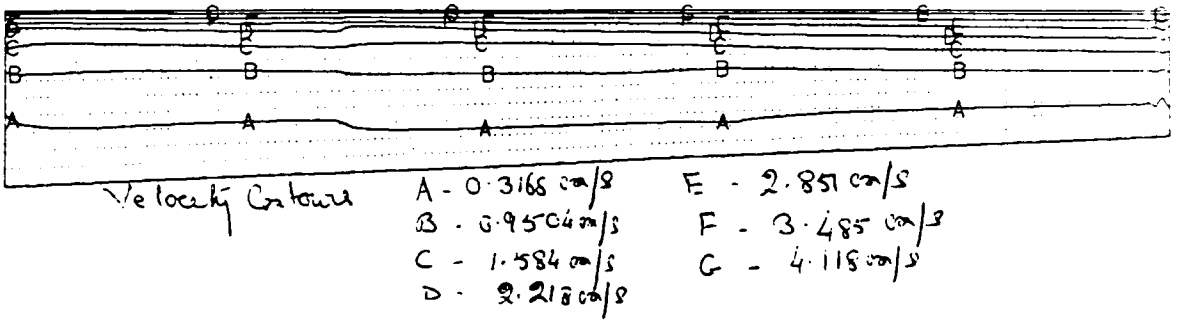

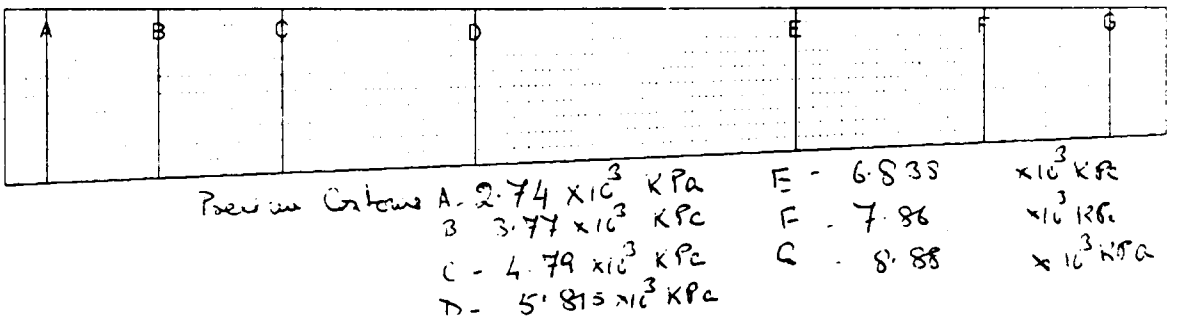

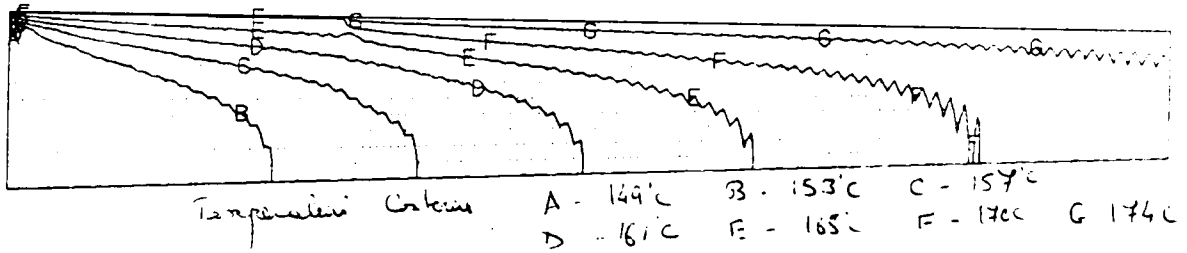

Figure 5. 79. Velcity, Pressure & Temperature Contours for DIDP dry Blend with 1/8 inch die at 35 RPM.

of 1 to 2 gm/min. Changing the barrel temperature or the inlet pressures did not affect the agreement between numerical and experimental flow rates by any significant amount, although the effect of changing the barrel temperature was greater. The pressure predictions at turn 15.75 were not as good as with the larger diameter die and the deviations between the experimental and numerical results were in the range of 2000 Kpa. (300 psi) or about 15 % for DIDP dry blend and a little above 20 % for DHP dry blend. The variation in pressure between repeat runs in the last two zones of the extruder is about a maximum of 860 KPa (125 psi). By varying the inlet pressure by 10 %, it was possible to bring down the variation between numerical and experimental results for DHP dry blend below 20 %. No plot of the velocity variation along the channel depth has been presented as they are similar to Fig. 5.77 and do not show much difference in velocities between the two differently plasticized PVC dry blends. The overall shear rates were above 0.1 1/s and in the range where the temperature and shear rate dependent viscosity can predict the fluid viscosity correctly. At times only in the elements adjacent to the bottom plate, the shear rates fell below this range of 0.1 1/s. The temperature variations along the channel for different turns of the screw are show in Figures 5.80. In the initial turns the temperature variations along the depth are different but the difference diminishes as the materials progress along the screw. The flow domains are longer than the meshes with 1/8 inch diameter die. The longer residence time in the melt zones obliterates the differences in the temperature variation not only between the two materials at the last turn (not shown in the Fig. 5.80) but also reduces the melt temperature between the top and the bottom plate to less than 1 °C. In Fig. 5.81, the velocity streamline, pressure and temperature contours are presented for DIDP dry blend using 1/16 inch diameter die. Because these figures are not to scale, no conclusions can be based on these but the general trends for the quantities are as expected.

The power law model may be inadequate in describing the flow in these cases because of the viscoelastic nature of the melt especially at higher temperatures and pressures obtained with the smaller diameter die and higher barrel temperatures. An estimate can be made as to the effect of the normal stress on the pressure. From the numerical simulation

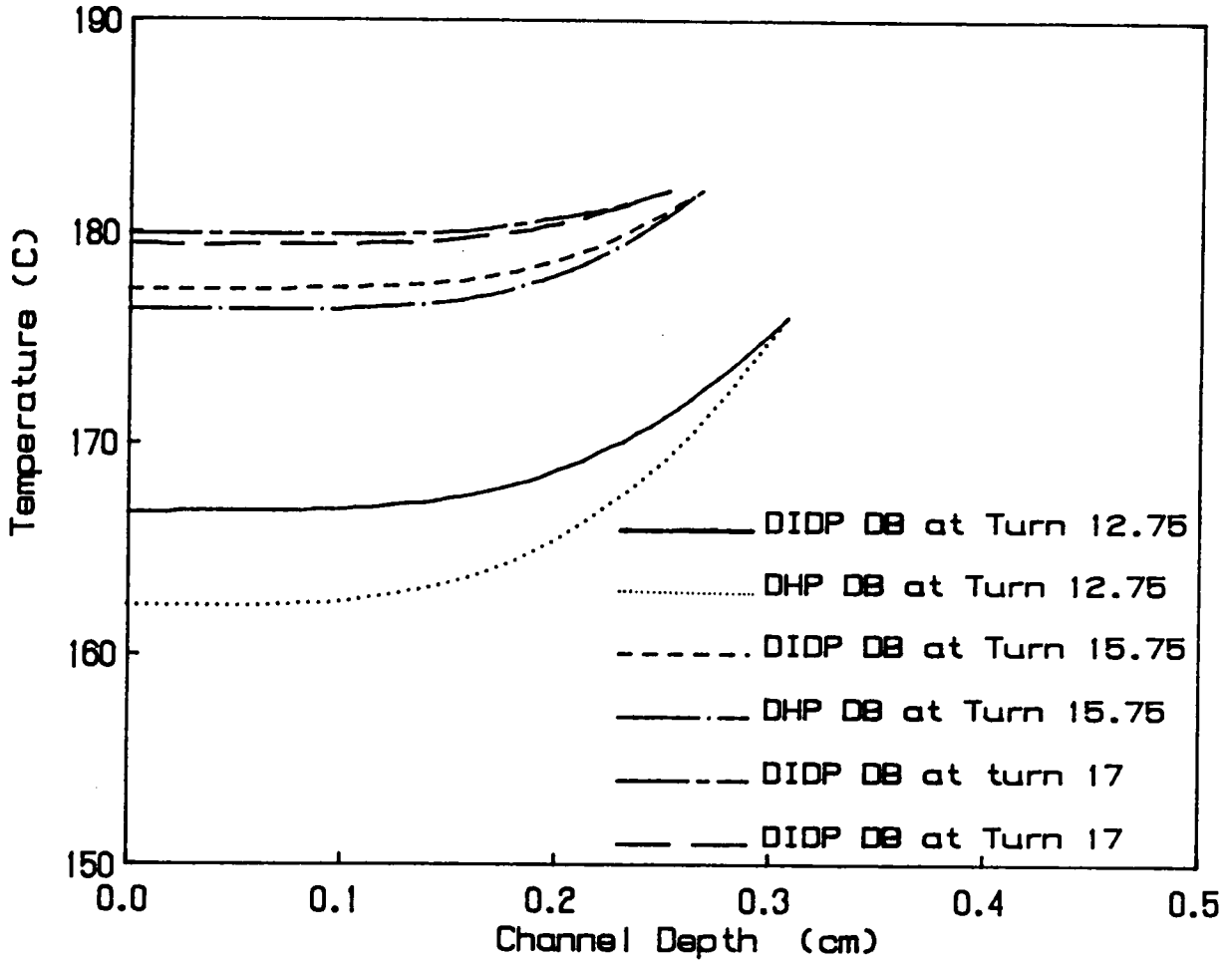

Figure 5. 80. Numerical predictions of Temperature versus Channel Depth at different Screw Turns with 1/16 inch die.

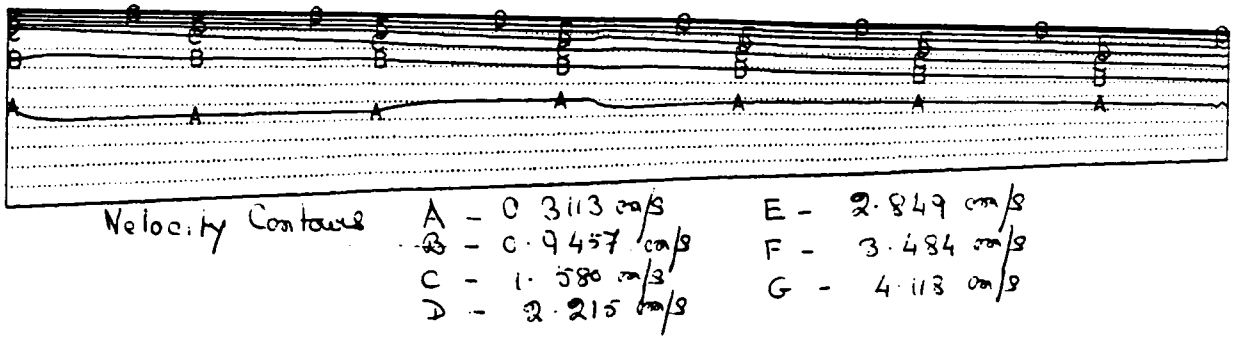

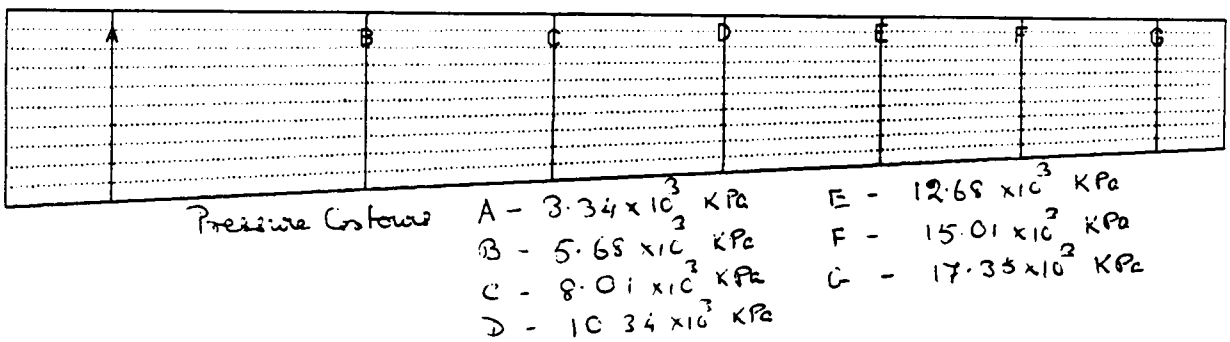

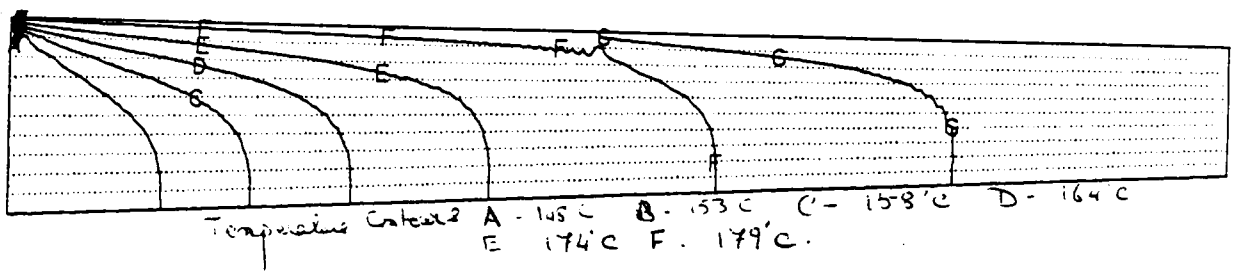

Figure 5. 81. Velocity, Pressure & Temperature Contours for DIDP dry Blend with 1/16 inch die at 35 RPM.

results the average temperature at turn 15.75 for these cases is about 180 °C and the shear rate near the barrel, where the transducer is placed, is approximately 60 1/s. In absence of normal force measurements at 180 °C from steady shear experiments, 2G′ can be approximated as equal to N1 [103]. G′ is the storage modulus from dynamic experiments and N1 is the first normal stress difference from steady shear experiments. No dynamic measurements were performed at 180 °C but if the dynamic data from 170 °C (Table 5.15) is used as an approximation, then the order of magnitude of N1 is around 100 to 200 KPa. This value is inadequate to explain the difference between the numerical and experimental pressures at turn 15.75 for the 1/16 inch diameter die. A different fluid model, with better representation of the viscoelastic behavior, is perhaps required at higher pressures and temperatures.

The results of the numerical simulation of the melt zones with the 1/16 inch diameter die were not as good as the simulation results with the larger die. The flow rate predictions still compare well with the experimental results. Although predicting the correct trend of DIDP dry blend generating higher pressures over the DHP dry blend, the pressure predictions were off the numerical results by 15 to 20 %.

Table 5. 1. Viscosity Shear Rate data of DIDP dry blend

Temperature 190 ° C

Shear Rate (1/s)	Viscosity (Pa.S)
2.51	2678.83
5.02	2129.45
7.52	1758.94
15.05	1328.79
25.08	1084.21
50.16	828.64
77.27	697.00

Temperature 180 ° C

Shear Rate (1/s)	Viscosity (Pa.S)
2.97	6774.18
5.95	4376.54
8.92	3244.66
17.78	2237.40
29.74	1632.67
59.49	1067.28
89.23	863.00

Temperature 170 ° C

Shear Rate (1/s)	Viscosity (Pa.S)
3.30	13881.84
6.61	8508.18
9.91	6669.64
19.83	4144.76
33.04	2917.11
66.09	1803.59
99.13	1353.03

1 Pa.S = 10 Poise

Temperature 160 ° C

Shear Rate (1/s)	Viscosity (Pa.S)
2.19	30824.27
3.65	20954.40
7.29	12754.88
10.94	9573.79
21.87	5884.57
36.45	3996.79
72.90	2320.57
109.36	1707.95

Temperature 150 ° C

Shear Rate (1/s)	Viscosity (Pa.S)
4.27	26365.25
8.53	15250.57
12.80	11075.59
25.60	6500.73
42.67	4217.42
85.35	2486.59
128.02	1721.91

Temperature 140 ° C

Shear Rate (1/s)	Viscosity (Pa.S)
3.93	277705.6
7.86	177243.2
11.78	126686.7
23.57	76709.5
39.28	49949.3
78.56	29445.3
117.83	20407.2

1 Pa.S = 10 Poise

Table 5. 2. Viscosity Shear Rate data of DHP plasticized PVC dry blend

Temperature 190 ° C

Shear Rate (1/s)	Viscosity (Pa.S)
2.45	2050.14
4.91	1550.70
7.36	1409.49
14.72	1070.23
24.54	867.30
49.07	698.48
73.61	604.93

Temperature 180 ° C

Shear Rate (1/s)	Viscosity (Pa.S)
2.68	4610.36
5.37	3116.60
8.05	2428.23
16.11	1693.32
26.85	1390.77
53.69	1009.82
80.54	820.85

Temperature 170 ° C

Shear Rate (1/s)	Viscosity (Pa.S)
3.12	10027.08
6.24	6420.42
9.37	4889.57
18.73	3123.88
31.22	2280.83
62.43	1449.32
93.65	1126.53

1 Pa.S. = 10 Poise

Temperature 160 ° C

Shear Rate (1/s)	Viscosity (Pa.S)
3.47	17089.19
6.94	10546.63
10.42	7942.15
20.83	4825.37
34.72	3445.58
69.44	2071.72
104.16	1502.78

Temperature 150 ° C

Shear Rate (1/s)	Viscosity (Pa.S)
3.43	24254.95
6.87	15476.32
10.30	11879.58
20.60	7287.86
34.33	5142.62
68.65	3054.21
102.98	2173.80

Temperature 140 ° C

Shear Rate (1/s)	Viscosity (Pa.S)
3.58	351093.1
7.16	208596.5
10.73	156231.0
21.47	94237.3
35.78	67036.6
71.56	40921.2
107.33	28474.0

1 Pa.S = 10 Poise

Table 5. 3. Viscosity Shear Rate data of DOP plasticized PVC dry blend

Temperature 190 ° C

Shear Rate (1/s)	Viscosity (Pa.S)
2.51	2647.35
5.03	1869.39
7.54	1567.73
15.08	1246.51
25.14	982.44
50.28	793.23
75.42	637.44

Temperature 180 ° C

Shear Rate (1/s)	Viscosity (Pa.S)
2.79	5712.64
5.58	3937.26
8.38	3155.93
16.75	2048.62
27.92	1715.18
55.84	1140.87
83.77	878.57

Temperature 170 ° C

Shear Rate (1/s)	Viscosity (Pa.S)
3.30	11090.19
6.60	6965.39
9.91	5318.82
19.81	3305.74
33.02	2367.11
66.04	1474.04
99.06	1074.26

1 Pa.S = 10 Poise

Temperature 160 ° C

Shear Rate (1/s)	Viscosity (Pa.S)
3.52	11749.32
7.04	11170.39
10.55	8214.84
21.11	5158.78
35.18	3558.36
70.35	2019.96
105.53	1591.33

Temperature 150 ° C

Shear Rate (1/s)	Viscosity (Pa.S)
3.59	25339.53
7.18	15587.83
10.78	11456.22
21.55	6804.31
35.92	4767.41
71.83	2904.55
107.75	2134.41

1 Pa.S = 10 Poise

Table 5. 4. Viscosity Shear Rate data of DIDP plasticized PVC pellets

Temperature 190 ° C

Shear Rate (1/s)	Viscosity (Pa.S)
2.51	4496.24
5.02	3241.33
7.53	2680.24
15.05	1993.33
25.08	1581.78
50.17	1207.61
75.25	1218.04

Temperature 180 ° C

Shear Rate (1/s)	Viscosity (Pa.S)
2.92	7871.46
5.84	6121.90
8.77	4544.14
17.53	2903.44
29.22	2329.91
58.44	1476.34
87.66	1068.89

Temperature 170 ° C

Shear Rate (1/s)	Viscosity (Pa.S)
3.13	17637.61
6.25	9330.12
9.38	7738.00
18.76	4365.12
31.27	3951.20
62.54	2226.91
93.81	1802.28

1 Pa.S = 10 Poise

Temperature 160 ° C

Shear Rate (1/s)	Viscosity (Pa.S)
3.43	27551.58
6.86	13457.87
10.29	11135.24
20.58	5885.59
34.31	4745.24
68.61	2838.89
102.92	2288.87

Temperature 150 ° C

Shear Rate (1/s)	Viscosity (Pa.S)
4.35	33590.41
8.70	17354.82
13.04	14496.39
26.09	6182.54
43.48	4742.90
86.96	2778.93
130.45	2129.09

1 Pa.S = 10 Poise

Table 5. 5. Viscosity Shear Rate data of DHP plasticized PVC pellets

Temperature 190 ° C

Shear Rate (1/s)	Viscosity (Pa.S)
2.47	2880.95
4.93	2521.96
7.40	2170.60
14.80	1821.70
24.67	1355.58
49.33	1011.10
74.00	841.71

Temperature 180 ° C

Shear Rate (1/s)	Viscosity (Pa.S)
2.74	6192.87
5.47	4231.46
8.21	3042.45
16.42	2346.49
27.37	1711.43
54.73	1098.81
82.10	1095.61

Temperature 170 ° C

Shear Rate (1/s)	Viscosity (Pa.S)
3.14	11616.70
6.29	6600.35
9.43	5714.69
18.86	3187.11
31.43	2553.65
62.85	1567.56
94.28	1227.22
188.56	786.76

1 Pa.S = 10 Poise

Temperature 160 ° C

Shear Rate (1/s)	Viscosity (Pa.S)
3.37	18307.49
6.75	11896.19
10.12	8435.73
20.25	5452.02
33.75	3385.32
67.50	2207.79
101.25	1614.29

Temperature 150 ° C

Shear Rate (1/s)	Viscosity (Pa.S)
3.43	27676.51
6.86	15015.51
10.29	11000.25
20.59	7972.95
34.31	4936.04
68.62	3237.91
102.93	2306.64

1 Pa.S = 10 Poise

Table 5. 6. Viscosity Shear Rate data of DOP plasticized PVC pellets

Temperature 190 ° C

Shear Rate (1/s)	Viscosity (Pa.S)
2.49	3957.45
4.97	3087.99
7.46	2478.80
14.92	1995.31
24.87	1524.96
49.74	1255.62
74.61	1087.67

Temperature 180 ° C

Shear Rate (1/s)	Viscosity (Pa.S)
2.83	6868.57
5.65	5088.76
8.48	3696.01
16.96	2647.45
28.27	1913.44
56.54	1416.47
84.81	1032.74

Temperature 170 ° C

Shear Rate (1/s)	Viscosity (Pa.S)
3.12	13577.98
6.24	9142.53
9.36	6306.41
18.72	4424.02
31.20	2795.67
62.40	1990.18
93.59	1587.83

1 Pa.S = 10 Poise

Temperature 160 ° C

Shear Rate (1/s)	Viscosity (Pa.S)
3.45	21799.05
6.90	10532.12
10.34	9474.67
20.69	5135.53
34.48	4103.62
68.97	2298.45
103.45	1808.71

Temperature 150 ° C

Shear Rate (1/s)	Viscosity (Pa.S)
3.42	29947.13
6.84	19654.04
10.27	14943.75
20.53	9768.88
34.22	6484.95
68.45	3866.22
102.67	2628.36

1 Pa.S = 10 Poise

Table 5. 7. Power law parameters for Plasticized PVC Dry Blends

T = 190 ° C

Material	m (Pa. S^n)	n
DIDP	3932.2	0.602
DOP	3674.2	0.598
DHP	2808.9	0.641

T = 180 ° C

Material	m (Pa. S^n)	n
DIDP	12763.1	0.395
DOP	9979.9	0.456
DHP	7176.4	0.501

T = 170 ° C

Material	m (Pa. S^n)	n
DIDP	31420.8	0.318
DOP	25267.2	0.318
DHP	20757.7	0.357

T = 160 ° C

Material	m (Pa. S^n)	n
DIDP	55146.9	0.264
DOP	44783.1	0.282
DHP	41825.9	0.289

T = 150 ° C

Material	m (Pa. S^n)	n
DIDP	84577.3	0.202
DOP	64605.9	0.272
DHP	60314.1	0.293

10 Poise = 1 Pa.S

Table 5. 8. Power law parameters for Plasticized PVC Pellets

T = 190 ° C

Material	m (Pa. S^n)	n
DIDP	6164.7	0.598
DOP	5553.6	0.616
DHP	4444.4	0.627

T = 180 ° C

Material	m (Pa. S^n)	n
DIDP	16152.2	0.408
DOP	12615.6	0.443
DHP	9965.2	0.477

T = 170 ° C

Material	m (Pa. S^n)	n
DIDP	33452.2	0.349
DOP	28128.4	0.356
DHP	23247.7	0.351

T = 160 ° C

Material	m (Pa. S^n)	n
DIDP	58704.2	0.284
DOP	47784.1	0.288
DHP	42809.7	0.303

T = 150 ° C

Material	m (Pa. S^n)	n
DIDP	106298.4	0.182
DOP	76735.8	0.237
DHP	61924.0	0.294

10 Poise = 1 Pa.S

Table 5. 9. Viscosity comparison of dry-blended PVC

Viscosity Ratio of DIDP Plasticized to DHP Plasticized PVC dry blends

Temperature ° C	Shear Rates 5 1/s	10 1/s	20 1/s	40 1/s
190	1.315	1.280	1.246	1.212
180	1.500	1.393	1.295	1.200
170	1.422	1.384	1.347	1.311
160	1.266	1.245	1.223	1.202
150	1.211	1.137	1.068	1.002

Viscosity Ratio of DIDP Plasticized to DOP Plasticized PVC dry blends

Temperature ° C	Shear Rates 5 1/s	10 1/s	20 1/s	40 1/s
190	1.077	1.080	1.083	1.086
180	1.159	1.111	1.065	1.019
170	1.243	1.244	1.244	1.243
160	1.196	1.181	1.167	1.152
150	1.170	1.114	1.061	1.011

Table 5. 10. Viscosity comparison of pelletized PVC

Viscosity Ratio of DIDP Plasticized to DHP Plasticized PVC pellets

Temperature ° C	Shear Rates 5 1/s	10 1/s	20 1/s	40 1/s
190	1.324	1.297	1.272	1.246
180	1.450	1.383	1.318	1.257
170	1.434	1.432	1.430	1.428
160	1.330	1.313	1.295	1.278
150	1.433	1.326	1.227	1.136

Viscosity Ratio of DIDP Plasticized to DOP Plasticized PVC pellets

Temperature ° C	Shear Rates 5 1/s	10 1/s	20 1/s	40 1/s
190	1.078	1.065	1.052	1.039
180	1.210	1.181	1.153	1.125
170	1.176	1.170	1.165	1.159
160	1.221	1.217	1.214	1.211
150	1.164	1.080	1.002	0.930

Table 5. 11. Viscosity as a function of shear rate and temperature

A) Quadratic regression

DIDP Plasticized PVC dry blend

Below 165 ° C

$$\ln \eta = 19.70559464 - 1.57743827 \ln(\gamma) - 0.0112641 [\ln(\gamma)]^2 - 0.04104788 T + 0.005677892 \ln(\gamma) T$$

Above 165 ° C

$$\ln \eta = 45.47614846 - 3.12212978 \ln(\gamma) - 0.000983486 \ln(\gamma)]^2 - 0.27175089 T + 0.00046539 T^2 + 0.01419457 \ln(\gamma) T$$

DHP dry blend

Below 165 ° C

$$\ln \eta = 18.69321734 - 0.54704777 \ln(\gamma) - 0.01752392 \ln(\gamma)]^2 - 0.03676513 T - 0.000369176 \ln(\gamma) T$$

Above 165 ° C

$$\ln \eta = 47.51430033 - 3.16737007 \ln(\gamma) - 0.0112124 [\ln(\gamma)]^2 - 0.30215025 T + 0.000559484 T^2 + 0.01447588 \ln(\gamma) T$$

B) Arrhenius type dependence of power law parameters

$$\eta = m\dot{\gamma}/(n-1)$$

$$m = M_0 e^{C1/TA}$$

$$n = N_0 e^{C2/TA}$$

DIDP dry blend	M_0	C_1	N_0	C_2
Below 165° C	10	4750	1	-613
Above 165° C	10	4220	4.35×10^{-6}	5210
DHP dry blend				
Below 165° C	10	5620	1.24×10^{-2}	1350
Above 165° C				

η is the viscosity in poise

$\dot{\gamma}$ is the shear rate in s^{-1}

T is temperature in ° C

Table 5. 12. Dynamic Data of DIDP Dry Blend at T = 140°C

ω rad/s	G′ dynes/cm²	G″ dynes/cm²	η^* poise
2.000E-02	1.063E+06	1.492E+05	5.367E+07
3.170E-02	1.179E+06	1.467E+05	3.748E+07
5.024E-02	1.249E+06	1.587E+05	2.507E+07
7.962E-02	1.294E+06	1.551E+05	1.636E+07
1.262E-01	1.351E+06	1.675E+05	1.079E+07
2.000E-01	1.410E+06	1.811E+05	7.110E+06
3.170E-01	1.466E+06	1.992E+05	4.668E+06
5.024E-01	1.545E+06	2.191E+05	3.106E+06
7.962E-01	1.627E+06	2.415E+05	2.066E+06
1.262E+00	1.705E+06	2.626E+05	1.367E+06
2.000E+00	1.817E+06	2.932E+05	9.202E+05
3.170E+00	1.888E+06	2.189E+05	5.996E+05
5.024E+00	2.007E+06	3.800E+05	4.065E+05
7.963E+00	2.107E+06	4.275E+05	2.700E+05
1.262E+01	2.231E+06	4.848E+05	1.809E+05
2.000E+01	2.367E+06	5.477E+05	1.215E+05
3.170E+01	2.509E+06	6.207E+05	8.153E+04
5.024E+01	2.664E+06	7.213E+05	5.493E+04
7.963E+01	2.830E+06	8.417E+05	3.708E+04

1 Pa.S = 10 poise
1 KPa = 10^4 dynes/cm²

Table 5. 13. Dynamic Data of DIDP Dry Blend at T = 150°C

ω rad/s	G′ dynes/cm²	G″ dynes/cm²	η^* poise
2.000E-02	4.2435E+05	9.4355E+04	2.1740E+07
3.170E-02	5.0895E+05	9.9515E+04	1.6365E+07
5.024E-02	5.9525E+05	1.0410E+05	1.2025E+07
7.962E-02	6.3030E+05	1.1305E+05	8.0425E+06
1.262E-01	6.8895E+05	3.3485E+05	5.5635E+06
2.000E-01	7.4420E+05	1.4820E+05	3.7940E+06
3.170E-01	7.9440E+05	1.6720E+05	2.5610E+06
5.024E-01	8.4915E+05	1.8770E+05	1.7315E+06
7.962E-01	9.0170E+05	2.1480E+05	1.1640E+06
1.262E+00	9.5425E+05	2.3975E+05	7.7965E+05
2.000E+00	1.0162E+06	2.7200E+05	5.2595E+05
3.170E+00	1.0945E+06	3.1095E+05	3.5885E+05
5.024E+00	1.1840E+06	3.5515E+05	2.4600E+05
7.963E+00	1.2870E+06	4.0525E+05	1.6950E+05
1.262E+01	1.4035E+06	4.6160E+05	1.1710E+05
2.000E+01	1.5330E+06	5.2600E+05	8.1030E+04
3.170E+01	1.6815E+06	5.9970E+05	5.6315E+04
5.024E+01	1.8475E+06	6.8895E+05	3.9240E+04
7.963E+01	2.0245E+06	8.0065E+05	2.7335E+04

1 Pa.S = 10 poise
1 KPa = 10^4 dynes/cm²

Table 5. 14. Dynamic Data of DIDP Dry Blend at T = 160°C

ω rad/s	G′ dynes/cm²	G″ dynes/cm²	η^* poise
2.000E-02	3.1405E+05	6.4330E+04	1.6030E+07
3.170E-02	3.5050E+05	6.7790E+04	1.1260E+07
5.024E-02	3.8070E+05	7.9540E+04	7.7415E+06
7.962E-02	4.0450E+05	8.7030E+04	5.1960E+06
1.262E-01	4.3090E+05	9.7300E+04	3.5010E+06
2.000E-01	4.6775E+05	1.1125E+05	2.4040E+06
3.170E-01	5.0430E+05	1.2770E+05	1.6410E+06
5.024E-01	5.4735E+05	1.4830E+05	1.1290E+06
7.963E-01	5.9070E+05	1.7020E+05	7.7215E+05
1.262E+00	6.4010E+05	1.9500E+05	5.3020E+05
2.000E+00	6.9570E+05	2.2690E+05	3.6590E+05
3.170E+00	7.5190E+05	2.5210E+05	2.5020E+05
5.024E+00	8.3290E+05	2.9820E+05	1.7610E+05
7.963E+00	9.2185E+05	3.4510E+05	1.2360E+05
1.262E+01	1.0169E+06	3.9625E+05	8.6460E+04
2.000E+01	1.1350E+06	4.5690E+05	6.1185E+04
3.170E+01	1.2745E+06	5.2730E+05	4.3500E+04
5.024E+01	1.4250E+06	6.0780E+05	3.0830E+04
7.963E+01	1.5905E+06	7.0410E+05	2.1840E+04

1 Pa.S = 10 poise
1 KPa = 10^4 dynes/cm²

Table 5. 15. Dynamic Data of DIDP Dry Blend at T = 170°C

ω rad/s	G′ dynes/cm²	G″ dynes/cm²	η^* poise
2.000E-02	7.8405E+04	3.0105E+04	4.2010E+06
3.170E-02	9.8455E+05	3.2710E+04	3.2745E+06
5.024E-02	1.2240E+05	3.7840E+04	2.5500E+06
7.962E-02	1.3415E+05	4.2290E+04	1.7955E+06
1.262E-01	1.4935E+05	5.3605E+04	1.2610E+06
2.000E-01	1.6715E+05	6.4075E+04	9.9515E+05
3.170E-01	1.8655E+05	7.9910E+04	6.4020E+05
5.024E-01	2.1200E+05	9.7080E+04	4.6410E+05
7.963E-01	2.4070E+05	1.1755E+05	3.3635E+05
1.262E+00	2.6140E+05	1.3760E+05	2.3445E+05
2.000E+00	3.0920E+05	1.6430E+05	1.7510E+05
3.170E+00	3.5460E+05	1.9730E+05	1.2800E+05
5.024E+00	4.1415E+05	2.4000E+05	9.5275E+04
7.963E+00	4.8365E+05	2.8725E+05	7.0640E+04
1.262E+01	5.6770E+05	3.4145E+05	5.2490E+04
2.000E+01	6.6090E+05	3.9585E+05	3.8515E+04
3.170E+01	7.7575E+05	4.5635E+05	2.8395E+04
5.024E+01	9.2635E+05	5.4255E+05	2.1365E+04
7.963E+01	1.0930E+06	6.4645E+05	1.5950E+04

1 Pa.S = 10 poise
1 KPa = 10^4 dynes/cm²

Table 5. 16. Dynamic Data of DHP Dry Blend at T = 140°C

ω rad/s	G′ dynes/cm²	G″ dynes/cm²	η^* poise
2.000E-02	8.0245E+05	1.5130E+05	4.0830E+07
3.170E-02	9.3385E+05	1.6235E+05	2.9905E+07
5.024E-02	1.07755E+06	1.5440E+05	2.1605E+07
7.962E-02	1.1560E+06	1.6950E+05	1.4675E+07
1.262E-01	1.2315E+06	1.8010E+05	9.8625E+06
2.000E-01	1.2880E+06	1.9540E+05	6.5125E+06
3.170E-01	1.3405E+06	2.1975E+05	4.2855E+06
5.024E-01	1.4020E+06	2.4740E+05	2.8345E+06
7.962E-01	1.4665E+06	2.7150E+05	1.8730E+06
1.262E+00	1.5430E+06	3.0330E+05	1.2460E+06
2.000E+00	1.6245E+06	3.3905E+05	8.2960E+05
3.170E+00	1.7120E+06	3.8785E+05	5.5375E+05
5.024E+00	1.8315E+06	4.2495E+05	3.7420E+05
7.963E+00	1.9480E+06	4.7545E+05	2.5180E+05
1.262E+01	2.0810E+06	5.3270E+05	1.7020E+05
2.000E+01	2.2235E+06	6.0050E+05	1.1515E+05
3.170E+01	2.3865E+06	6.7785E+05	7.8245E+04
5.024E+01	2.5755E+06	7.8215E+05	5.3565E+04
7.963E+01	2.7965E+06	9.2315E+05	3.6985E+04

1 KPa = 10^4 dynes/cm²
1 Pa.S = 10 Poise

Table 5. 17. Dynamic Data of DHP Dry Blend at T = 150°C

ω rad/s	G′ dynes/cm²	G″ dynes/cm²	η^* poise
2.000E-02	3.5335E+05	8.9965E+04	1.8240E+07
3.170E-02	4.5865E+05	9.0705E+04	1.4745E+07
5.024E-02	4.9795E+05	9.8645E+04	1.01045E+07
7.962E-02	5.4460E+05	1.1270E+05	6.9850E+06
1.262E-01	5.7535E+05	1.3645E+05	4.6855E+06
2.000E-01	6.3085E+05	1.4505E+05	3.2365E+06
3.170E-01	6.7685E+05	1.6275E+05	2.1965E+06
5.024E-01	7.1865E+05	1.8490E+05	1.4770E+06
7.962E-01	7.6655E+05	2.1220E+05	9.9800E+05
1.262E+00	8.2745E+05	2.4235E+05	6.8320E+05
2.000E+00	8.9925E+05	2.7675E+05	4.7045E+05
3.170E+00	9.7640E+05	3.1565E+05	3.2370E+05
5.024E+00	1.0605E+06	3.6000E+05	2.2295E+05
7.963E+00	1.1690E+06	4.1340E+05	1.5580E+05
1.262E+01	1.2930E+06	4.7190E+05	1.0905E+05
2.000E+01	1.4200E+06	5.3535E+05	7.5860E+04
3.170E+01	1.5630E+06	6.0660E+05	5.2880E+04
5.024E+01	1.7315E+06	6.9645E+05	3.7145E+04
7.963E+01	1.9195E+06	8.1780E+05	2.6200E+04

1 KPa = 10^4 dynes/cm²
1 Pa.S = 10 Poise

Table 5. 18. Dynamic Data of DHP Dry Blend at T = 160°C

ω rad/s	G′ dynes/cm²	G″ dynes/cm²	η^* poise
2.000E-02	1.3980E+05	4.3820E+04	7.3240E+06
3.170E-02	1.8230E+05	5.3040E+04	5.9890E+06
5.024E-02	2.2395E+05	5.9100E+04	4.6120E+06
7.962E-02	2.5005E+05	7.1670E+04	3.2670E+06
1.262E-01	2.7515E+05	8.3090E+04	2.2780E+06
2.000E-01	2.9785E+05	9.8875E+04	1.5760E+06
3.170E-01	3.2690E+05	1.1720E+05	1.0960E+06
5.024E-01	3.6425E+05	1.3620E+05	7.7400E+05
7.963E-01	4.0405E+05	1.6260E+05	5.4700E+05
1.262E+00	4.4215E+05	1.8880E+05	3.8100E+05
2.000E+00	4.9180E+05	2.2080E+05	2.6950E+05
3.170E+00	5.6450E+05	2.6330E+05	1.9650E+05
5.024E+00	6.3610E+05	3.0890E+05	1.4080E+05
7.963E+00	7.2390E+05	3.6210E+05	1.0167E+05
1.262E+01	8.2975E+05	4.2290E+05	7.3790E+04
2.000E+01	9.5645E+05	4.9290E+05	5.3500E+04
3.170E+01	1.0807E+06	5.7110E+05	3.9090E+04
5.024E+01	1.2590E+06	6.6140E+05	2.8300E+04
7.963E+01	1.4345E+06	7.6790E+05	2.0430E+04

1 KPa = 10^4 dynes/cm²
1 Pa.S = 10 Poise

Table 5. 19. Dynamic Data of DHP Dry Blend at T = 170°C

ω rad/s	G′ dynes/cm²	G″ dynes/cm²	η^* poise
2.000E-02	6.9400E+04	2.7030E+04	3.7240E+06
3.170E-02	8.8620E+04	3.3330E+04	2.9870E+06
5.024E-02	1.0617E+05	4.0235E+04	2.2620E+06
7.962E-02	1.1480E+05	4.9580E+04	1.6240E+06
1.262E-01	1.3920E+05	6.1270E+04	1.2055E+06
2.000E-01	1.5600E+05	7.4090E+04	8.6345E+05
3.170E-01	1.7475E+05	8.7820E+04	6.1710E+05
5.024E-01	2.0010E+05	1.0725E+05	4.5185E+05
7.963E-01	2.2815E+05	1.2815E+05	3.2860E+05
1.262E+00	2.6275E+05	1.5045E+05	2.3990E+05
2.000E+00	3.1095E+05	1.8535E+05	1.8100E+05
3.170E+00	3.6730E+05	2.3095E+05	1.3690E+05
5.024E+00	4.1835E+05	2.7215E+05	9.9330E+04
7.963E+00	4.9500E+05	3.2715E+05	7.4520E+04
1.262E+01	5.9075E+05	3.8270E+05	5.6170E+04
2.000E+01	7.1000E+05	4.6770E+05	4.2505E+04
3.170E+01	8.4665E+05	5.5165E+05	3.1875E+04
5.024E+01	1.0000E+06	6.3850E+05	2.3630E+04
7.963E+01	1.1690E+06	7.4450E+05	1.7405E+04

1 KPa = 10^4 dynes/cm²
1 Pa.S = 10 Poise

Table 5. 20. Yield stresses of PVC dry blends

DIDP Plasticized PVC dry blend

Temp ° C	130	140	150	160
Yield Stress Pascals	3.0×10^{5}	1.056×10^{5}	4.9×10^{4}	3.05×10^{4}

DHP Plasticized PVC dry blend

Temp ° C	130	140	150	160
Yield Stress Pascals	1.428×10^{5}	7.6024×10^{4}	4.159×10^{4}	1.46×10^{4}

1 Pa = 10 dynes / cm ^{2}.

Table 5. 21. Herschel Bulkley & Bingham Fluid Parameters for the dry blends

DIDP Plasticized PVC Dry Blend

Temp ° C	Yield Stress Pascals	Herschel Bulkley m(Pa.S^n)	n	Bingham μ_0(Pa.S)
140	1.056 x 10 ^{5}	3058.4	0.8861	1128.3
150	4.9 x 10 ^{4}	48019.5	0.2676	1013.9

DHP Plasticized PVC Dry Blend

Temp ° C	Yield Stress Pascals	Herschel Bulkley m(Pa.S^n)	n	Bingham μ_0(Pa.S)
140	8.000 x 10 ^{4}	26814.3	0.4794	1916.7
150	4.159 x 10 ^{4}	27491.7	0.4306	1537.6

1 Pa = 10 dynes / cm ^{2}.
1 Pa.S = 10 Poise

Table 5. 22. Specific Heats of Plasticized PVC Dry Blends

Temperature °C	DIDP Average specific heat cal/gm/°C	DOP Average specific heat cal/gm/°C	DHP Average specific heat cal/gm/°C
70	0.412	0.4097	0.395
75	0.4178	0.4103	0.3975
80	0.418	0.4122	0.3967
85	0.4238	0.4176	0.4012
90	0.4285	0.4214	0.4064
95	0.4353	0.4234	0.4089
100	0.439	0.4285	0.4134
105	0.4433	0.4326	0.4194
110	0.4492	0.4434	0.4280
115	0.4557	0.4468	0.4346
120	0.4603	0.4556	0.4468
125	0.4668	0.4587	0.4503
130	0.4702	0.4675	0.4568
135	0.4749	0.467	0.458
140	0.4839	0.4702	0.4623
145	0.4914	0.4789	0.4673
150	0.4945	0.4834	0.4745
155	0.5004	0.4843	0.4762
160	0.5034	0.4902	0.47786
165	0.5035	0.4953	0.4801
170	0.5052	0.4940	0.4813
175	0.5052	0.4987	0.4837
180	0.5063	0.4972	0.4822
185	0.5053	0.4985	0.4825
190	0.508	0.5023	0.4881
195	0.5109	0.5055	0.4915
200	0.5177	0.5102	0.4972
205	0.521	0.5059	0.4919
210	0.509	0.5038	0.4923
215	0.5066	0.5056	0.4913
220	0.5038	0.5033	0.4917
225	0.5041	0.5030	0.4886

Table 5. 23. Specific Heat of Plasticized PVC pellets

Temperature °C	DIDP Average specific heat cal/gm/°C	DOP Average specific heat cal/gm/°C	DHP Average specific heat cal/gm/°C
70	0.3897	0.3726	0.3685
75	0.399	0.3791	0.3722
80	0.399	0.3717	0.3668
85	0.4007	0.3730	0.3649
90	0.405	0.3770	0.369
95	0.4109	0.3832	0.3733
100	0.4149	0.3858	0.3763
105	0.4206	0.3940	0.3828
110	0.4246	0.3974	0.3865
115	0.4310	0.403	0.39
120	0.4330	0.4088	0.394
125	0.4379	0.4144	0.3967
130	0.4427	0.4156	0.3995
135	0.4468	0.4172	0.3995
140	0.4498	0.4216	0.4017
145	0.4522	0.4237	0.4026
150	0.4551	0.4228	0.4069
155	0.4538	0.4239	0.4037
160	0.455	0.4244	0.4088
165	0.4613	0.4266	0.413
170	0.4657	0.4348	0.4146
175	0.4663	0.4358	0.4159
180	0.4662	0.4379	0.4156
185	0.4646	0.4388	0.4143
190	0.462	0.4409	0.4149
195	0.4571	0.4427	0.4162
200	0.4674	0.445	0.4160
205	0.4724	0.4495	0.4160
210	0.4711	0.4417	0.4
215	0.4719	0.4455	0.4009
220	0.4703	0.4408	0.4019

Table 5. 24. Specific Heats of Plasticized PVC Dry Blend Extrudates

Temperature °C	DIDP Average specific heat cal/gm/°C	DOP Average specific heat cal/gm/°C	DHP Average specific heat cal/gm/°C
80	0.3997	0.4121	0.4050
85	0.3972	0.4149	0.4016
90	0.0135	0.4151	0.4047
95	0.4072	0.4186	0.4097
100	0.4057	0.4187	0.4064
105	0.4083	0.4208	0.4077
110	0.4160	0.4278	0.4152
115	0.4201	0.4299	0.4194
120	0.4236	0.4340	0.4236
125	0.4276	0.4375	0.4262
130	0.4330	0.4395	0.4330
135	0.4348	0.4474	0.4347
140	0.4357	0.4476	0.4355
145	0.4400	0.4513	0.4401
150	0.4457	0.4559	0.4444
155	0.4393	0.4604	0.4448
160	0.4497	0.4558	0.4434
165	0.4509	0.4608	0.4451
170	0.4495	0.4612	0.4481
175	0.4525	0.4653	0.4526
180	0.4559	0.4661	0.4515
185	0.4545	0.4679	0.4607
190	0.4691	0.4688	0.4562
195	0.4608	0.4730	0.4679
200	-	0.4770	0.4607
205	0.4694	0.4811	0.4624

Table 5. 25. Thermal Diffusivities of Dry Blends

DIDP plasticized PVC dry blend Temp ° C	Thermal Diffusivities (cm^2 /s)
68	0.00088
100	0.00075
128	0.00069
145	0.00071
161	0.00062

DHP plasticized PVC dry blend Temp ° C	Thermal Diffusivities (cm^2 /s)
100	0.00076
130	0.00067
147	0.00062
160	0.00060

DOP plasticized PVC blend Temp ° C	Thermal Diffusivities (cm^2 /s)
100	0.00066
125	0.00064
150	0.00062
162	0.000615

Table 5. 26. Friction Coefficient of Dry Blended DIDP

Run number	Tempe-rature	Coefficient of friction	Tempe-rature	Coefficient of friction
1	25	0.3110	40	0.3950
	50	0.4567	60	0.4756
	70	0.4724	80	0.4373
	90	0.4123	100	0.4123
2	20	0.3571	35	0.3417
	40	0.4510	50	0.4337
	60	0.4510	70	0.4260
	80	0.3948	90	0.3879
	100	0.4313		
3	20	0.3050	30	0.3113
	40	0.3678	50	0.3860
	60	0.3860	70	0.4169
	80	0.4244	90	0.4047
	100	0.4102	110	0.3969
4	20	0.3028	40	0.3124
	50	0.3350	60	0.4005
	70	0.4605	80	0.4813
	90	0.46552	100	0.4605
	110	0.44743	120	0.4198
	130	0.3725	140	0.3503

$f(\text{friction coeff.}) = 0.2250227 + 0.00500264\ T - 0.000029375\ T^2$

T is in degrees centigrade

Table 5. 27. Friction Coefficient of Dry Blended DHP

Run number	Tempe-rature	Coefficient of friction	Tempe-rature	Coefficient of friction
1	25	0.2756	40	0.3572
	51	0.38	60	0.4162
	71	0.4212	80	0.4395
	88	0.462	98	0.4506
	108	0.4992	122	0.4513
2	20	0.4028	40	0.4623
	100	0.4781	110	0.4212
3	21	0.2982	40	0.3147
	50	0.3439	59	0.3594
	71	0.4316	79	0.4086
	90	0.4304	101	0.492
	111	0.4898	118	0.4155
	127	0.4033	134	0.3917
4	20	0.3478	34	0.4046
	42	0.4483	50	0.4504
	100	0.454	110	0.4151
	119	0.3842		
5	21	0.3013	30	0.3145
	40	0.337	50	0.3932
	59	0.4546	71	0.4618
	79	0.4254	91	0.4542
	100	0.4645	111	0.3954
6	20	0.2529	40	0.3632
	50	0.4493	59	0.4493
	71	0.4665	80	0.4444
	91	0.4607	102	0.4311
	112	0.4219	121	0.4269

f(friction coeff.) = $0.2170075 + 0.005181198\ T - 0.00002870\ T^2$
T is in degrees centigrade

Table 5. 28. Results of Extruder Runs

Material : Dry blended PVC containing 40 % of plasticizer

Barrel diameter : 2.54 cm. L/D = 20:1
Screw Compression 2:1 Die diameter 0.3175 cm.(1/8 inch)

Zone temperature settings

Zone 1	146°C	Zone 3	176°C
Zone 2	170°C	Zone 4	179°C

Materials	RPM	Flow Rate gm/min	Amps	P1 KPa	P2 KPa	P3 KPa	P4 KPa
DIDP dry blend							
	15	21.43	1.7	-	2102	4827	6206
	25	34.90	2.0	-	-	6122	8881
	35	50.11	2.0	-	2413	6723	9398
DHP dry blend							
	15	20.13	1.3	-	-	2241	4571
	25	33.54	1.6	-	-	3103	5950
	35	47.88	1.9	-	-	4178	7212
DOP dry blend							
	15	19.00	1.5	-	483	4054	6895
	25	32.84	1.8	-	552	4744	8101
	35	42.97	1.8	-	-	4227	8274

1 KPa = 10^4 dynes/cm^2.

Table 5. 29. Results of Extruder Runs

Material : Dry blended PVC containing 40 % of plasticizer

Barrel diameter : 2.54 cm. L/D = 20:1
Screw Compression 2:1 Die diameter 0.3175 cm.(1/8 inch)

Zone temperature settings

Zone 1	146°C	Zone 3	176°C
Zone 2	170°C	Zone 4	179°C

Materials	RPM	Flow Rate gm/min	Amps	P1 KPa	P2 KPa	P3 KPa	P4 KPa
DIDP dry blend							
	15	21.42	1.8	-	-	5460	6805
	25	33.76	1.95	-	-	6998	9115
	35	50.53	2.25	-	-	7812	9708
DHP dry blend							
	15	19.18	1.7	-	-	2144	4992
	25	33.11	1.8	-	-	3213	6619
	35	46.77	1.8	-	-	3537	6723
DOP dry blend							
	15	18.85	1.6	-	-	4606	6840
	25	31.00	1.75	-	-	5467	8798
	35	40.98	1.8	-	-	5047	8798

1 KPa = 10^4 dynes/cm^2.

Table 5. 30. Results of Extruder Runs

Material : Dry blended PVC containing 40 % of plasticizer

Barrel diameter : 2.54 cm. L/D = 20:1
Screw Compression 2:1 Die diameter 0.3175 cm. (1/8 inch)

Zone temperature settings

Zone 1	152°C	Zone 3	182°C
Zone 2	176°C	Zone 4	185°C

Materials	RPM	Flow Rate gm/min	Amps	P1 KPa	P2 KPa	P3 KPa	P4 KPa
DIDP dry blend							
	35	49.54	1.95	-	1896	6137	8701
	45	64.66	2.0	-	1896	6295	9026
DHP dry blend							
	35	45.44	1.55	-	-	1706	5585
	45	57.54	1.70	-	-	1706	6068
DOP dry blend							
	35	41.90	1.55	-	-	2020	5909
	45	53.31	1.50	-	-	2330	6074

1 KPa = 10^4 dynes/cm^2.

Table 5. 31. Results of Extruder Runs

Material : Dry blended PVC containing 40 % of plasticizer

Barrel diameter : 2.54 cm. L/D = 20:1
Screw Compression 2:1 Die diameter 0.3175 cm. (1/8 inch)

Zone temperature settings

Zone 1	152°C	Zone 3	182°C
Zone 2	176°C	Zone 4	185°C

Materials	RPM	Flow Rate gm/min	Amps	P1 KPa	P2 KPa	P3 KPa	P4 KPa
DIDP dry blend							
	35	48.92	1.80	-	-	5571	8619
	45	62.03	1.85	-	-	5461	8950
DHP dry blend							
	35	46.60	1.50	-	-	1813	5420
	45	58.73	1.60	-	-	1917	5909
DOP dry blend							
	35	43.19	1.45	-	-	1400	5089
	45	54.64	1.50	-	-	1551	5744

1 KPa = 10^4 dynes/cm^2.

Table 5. 32. Results of Extruder Runs

Material : Pelletized PVC containing 40 % of plasticizer

Barrel diameter : 2.54 cm. L/D = 20:1
Screw Compression 2:1 Die diameter 0.3175 cm. (1/8 inch)

Zone temperature settings

Zone 1	146°C	Zone 3	176°C
Zone 2	170°C	Zone 4	179°C

Materials	RPM	Flow Rate gm/min	Amps	P1 KPa	P2 KPa	P3 KPa	P4 KPa
DIDP pellets							
	25	36.06	2.1	159	2041	6523	9039
	35	50.89	2.4	324	2406	6888	9570
	45	59.66	2.3	-	-	4137	9598
DHP pellets							
	25	33.98	1.75	103	290	3254	6846
	35	46.63	1.95	110	310	3530	7371
	45	60.78	2.15	-	-	3082	7964
DOP pellets							
	25	31.79	1.70	96	241	1827	6240
	35	40.52	1.85	-	-	1572	6833
	45	53.87	1.90	-	-	2075	7185

1 KPa = 10^4 dynes/cm^2.

Table 5. 33. Results of Extruder Runs

Material : Pelletized PVC containing 40 % of plasticizer

Barrel diameter : 2.54 cm. L/D = 20:1
Screw Compression 2:1 Die diameter 0.3175 cm. (1/8 inch)

Zone temperature settings

Zone 1	146°C	Zone 3	176°C
Zone 2	170°C	Zone 4	179°C

Materials	RPM	Flow Rate gm/min	Amps	P1 KPa	P2 KPa	P3 KPa	P4 KPa
DIDP pellets							
	25	36.69	2.2	255	2303	6357	9770
	35	50.59	2.5	517	3144	7054	10652
	45	58.53	2.3	-	-	3261	8668
DHP pellets							
	25	31.86	1.70	103	283	2524	6488
	35	44.73	1.90	103	310	2062	7536
	45	59.59	2.10	-	-	2999	7343
DOP pellets							
	25	30.49	1.70	96	221	1827	6302
	35	40.08	1.85	96	365	1689	6833
	45	53.29	1.90	-	-	2020	7881

1 KPa = 10^4 dynes/cm^2.

Table 5. 34. Results of Extruder Runs

Material : Dry blended PVC containing 40 % of plasticizer

Barrel diameter : 2.54 cm. L/D = 20:1
Screw Compression 2:1 Die diameter 0.1588 cm. (1/16 inch)

Zone temperature settings

Zone 1	152°C	Zone 3	182°C
Zone 2	176°C	Zone 4	185°C

Materials	RPM	Flow Rate gm/min	Amps	P1 KPa	P2 KPa	P3 KPa	P4 KPa
DIDP dry blend							
	35	45.43	2.5	2220	9156	13942	18547
	45	55.40	2.5	1744	7364	13183	18637
DHP dry blend							
	35	42.50	2.4	2324	7867	12466	15741
	45	58.30	2.7	-	-	13962	18189
DOP dry blend							
	35	40.50	2.3	1882	7433	13369	16320

1 KPa = 10^4 dynes/cm^2.

Table 5. 35. Results of Extruder Runs

Material : Dry blended PVC containing 40 % of plasticizer

Barrel diameter : 2.54 cm. L/D = 20:1
Screw Compression 2:1 Die diameter 0.1588 cm. (1/16 inch)

Zone temperature settings

Zone 1	152°C	Zone 3	182°C
Zone 2	176°C	Zone 4	185°C

Materials	RPM	Flow Rate gm/min	Amps	P1 KPa	P2 KPa	P3 KPa	P4 KPa
DIDP dry blend							
	35	47.39	2.6	4757	10991	15024	18816
	45	55.96	2.7	2723	7260	13755	18623
DHP dry blend							
	35	44.09	2.3	2709	6468	13404	15321
	45	57.77	2.5	-	-	13094	17196
DOP dry blend							
	35	40.79	2.2	1889	6840	12301	17623

1 KPa = 10^4 dynes/cm^2.

Table 5. 36. Results of Extruder Runs

Material : Pelletized PVC containing 40 % of plasticizer

Barrel diameter : 2.54 cm. L/D = 20:1
Screw Compression 2:1 Die diameter 0.1588 cm. (1/16 inch)

Zone temperature settings

Zone 1	152°C	Zone 3	182°C
Zone 2	176°C	Zone 4	185°C

Materials	RPM	Flow Rate gm/min	Amps	P1 KPa	P2 KPa	P3 KPa	P4 KPa
DIDP pellets							
	25	37.74	2.7	9267	13528	18003	20098
	35	52.54	3.0	9639	14404	19092	20733
DHP pellets							
	25	30.83	2.20	1303	9487	12335	16589
	35	43.03	2.45	834	9929	13245	18065
DOP pellets							
	25	30.60	2.35	1379	5516	10529	14686
	35	42.55	2.35	2089	6295	11122	15617

1 KPa = 10^4 dynes/cm^2.

Table 5. 37. Results of Extruder Runs

Material : Pelletized PVC containing 40 % of plasticizer

Barrel diameter : 2.54 cm. L/D = 20:1
Screw Compression 2:1 Die diameter 0.1588 cm. (1/16 inch)

Zone temperature settings

Zone 1 152°C Zone 3 182°C
Zone 2 176°C Zone 4 185°C

Materials	RPM	Flow Rate gm/min	Amps	P1 KPa	P2 KPa	P3 KPa	P4 KPa
DIDP pellets							
	25	35.51	2.6	8742	14328	18417	21815
	35	49.12	2.65	8329	14486	18857	22733
DHP pellets							
	25	29.00	1.90	4137	9425	13211	16879
	35	47.84	2.10	4447	10287	14783	18734
DOP pellets							
	25	31.06	2.30	882	5005	10756	15051
	35	41.36	2.20	-	2732	10205	15183

1 KPa = 10^4 dynes/cm^2.

Table 5. 38. Results of Extruder Runs

Material : Pelletized PVC containing 40 % of plasticizer

Barrel diameter : 2.54 cm. L/D = 20:1
Screw Compression 2:1 Die diameter 0.1588 cm. (1/16 inch)

Zone temperature settings

Zone 1	152°C	Zone 3	182°C
Zone 2	176°C	Zone 4	185°C

Materials	RPM	Flow Rate gm/min	Amps	P1 KPa	P2 KPa	P3 KPa	P4 KPa
DIDP pellets							
	15	18.69	2.3	-	6729	11659	16058
	45	53.23	3.0	-	6936	14610	20947
DHP pellets							
	15	16.92	1.6	-	-	8030	12562
	45	55.33	2.65	-	5530	12487	18334
DOP dry blend							
	15	15.99	1.55	-	1551	6330	11204
	45	49.60	2.40	-	2840	11108	17892

1 KPa = 10^4 dynes/cm^2.

Table 5. 39. Results of Extruder Runs

Material : Pelletized PVC containing 40 % of plasticizer

Barrel diameter : 2.54 cm. L/D = 20:1
Screw Compression 2:1 Die diameter 0.1588 cm. (1/16 inch)

Zone temperature settings

Zone 1	152°C	Zone 3	182°C
Zone 2	176°C	Zone 4	185°C

Materials	RPM	Flow Rate gm/min	Amps	P1 KPa	P2 KPa	P3 KPa	P4 KPa
DIDP pellets							
	15	18.98	2.45	-	5612	10508	14838
	45	51.65	3.0	-	6137	13624	20416
DHP pellets							
	15	16.94	1.75	-	-	7302	11783
	45	56.73	2.75	-	5743	12245	17893
DOP dry blend							
	15	16.20	1.65	-	1551	5923	10687
	45	48.75	2.30	-	2689	10218	16720

1 KPa = 10^4 dynes/cm^2.

Table 5. 40. Results of Dry Extruder Runs

Material : DIDP dry blend

Screw speed : 15 rpm

Barrel Temperature °C	End Pressure KPa	Flow Rate gm/min
78	0 - 3303	2.309
89	3303 - 5943	18.360
99	2144 - 4454	18.28
115	1648 - 3303	19.16
130	2144 - 3792	19.53

Table 5. 41. Results of Dry Extruder Runs

Material : DIDP dry blend

Screw speed : 25 rpm

Barrel Temperature °C	End Pressure KPa	Flow Rate gm/min
95	2448 - 5481	6.94
107	4895 - 7729	23.42
110	4206 - 6552	28.79
115	4012 - 6171	27.83
124	4799 - 6412	25.67
135	4599 - 6027	26.00

Table 5. 42. Results of Dry Extruder Runs

Material : DIDP dry blend

Screw speed : 35 rpm

Barrel Temperature °C	End Pressure KPa	Flow Rate gm/min
105	6895 - 10136	42.25
114	4695 - 8356	35.00
122	2820 - 5847	34.77
129	1827 - 5537	38.37
135	1800 - 5315	38.78

Table 5. 43. Density of Extrudates from Dry Extruder Runs

Material : DIDP dry blend

Speed(rpm)	Barrel Temp.(C)	Density (gm/cc)
25	106	0.32
	110	0.47
	115	0.85
	124	1.16
35	105	0.33
	114	0.59
	122	1.16

Table 5. 44. Comparisons of Tempertaure Predictions from Fidap and Finite difference methods for Power Law fluid from Ref. [98].

Power Law Index = 0.50

ψ Dimensionless Dist.	θ Bav Dimensionless Avg. Temp.(Fidap)	θ Bav Dimensionless Avg. Temp.(Ref. 98)
0.6	0.185	0.18
0.8	0.119	0.11

Power Law Index = 0.25

ψ Dimensionless Dist.	θ Bav Dimensionless Avg. Temp.(Fidap)	θ Bav Dimensionless Avg. Temp.(Ref. 98)
0.6	0.211	0.19
0.8	0.127	0.12

Table 5. 45. Testing of HB Model

Ratio of Yield Stress to Wall Stress	Deviation between Analytical & Numerical Flow Rate Predictions
0.4	0.1 %
0.7	0.8%
0.8	2.0%
0.9	3.5%

Ratio of Yield Stress to Wall Stress = 0.8

Power Law Index 'n'	Deviation between Analytical & Numerical Flow Rate Predictions
0.8861	0.2%
0.7	4.7%
0.5	7.9%

Ratio of Yield Stress to Wall Stress = 0.7

Power Law Index 'n'	Deviation between Analytical & Numerical Flow Rate Predictions
0.8861	0.8%
0.7	1.7%
0.5	3.9%

Table 5. 46. Fitting of Finite Difference Solids Conveying Model for a Tapered Channel to the Experimental Data from Dry Extruder Runs

SPEED (rpm)	FLOW RATE gm/min	NIPD Factor
15	18.50	.1716 - .1767
25	36.00	.1737 - .1787
35	38.40	.1768 - .1876

NIPD Factor - Non-Istropic Pressure Distribution factor

Table 5. 47. 2-D Modeling of Solids Conveying in Tapered Extruder Channel using HB model

Screw Speed RPM	Pl - Po dynes/sq.cm	Flow Rate cu.cm/min
15	Drag	45.0182
	3.02E7	40.8737
	3.78E7	39.8608
	5.00E7	38.3057
25	Drag	74.8199
	5.7E7	66.8308
	6.0E7	65.1557
	6.36E7	65.9791
35	Drag	104.5878
	5.8E7	96.2302
	6.5E7	95.2948
	7.1E7	94.4630
	8.5E7	92.5897
	10.1	90.4675

Table 5. 48. 3-D Solids Conveying Model in Tapered Extruder Channels using HB Models (includes cross channel flow)

Pl-Po dynes/sq.cm	2 D Flow rate cu.cm/min	3 D Flow rate cu.cm/min
15 RPM		
3.0E7	40.8737	35.2457
3.78E7	39.8608	35.1408
25 RPM		
5.7E7	66.8308	62.553
6.36E7	65.9791	62.70
35 RPM		
8.5E7	92.5897	90.5664
6.5E7	95.2948	90.8340

Table 5. 49. Approximate Density Values Required to Match 3-D Numerical Simulation Results and Experimental Results of Dry Extruder ru

Speed (rpm)	Density (gm/cc)
15	0.525
25	0.415
35	0.423

Table 5. 50. Comparison of Numerical and Experimental Results for DIDP Dry Blend usin 1/8 inch Diameter die.

A) Experimental Conditions

Barrel Temp. 1 = 170 C — Barrel Temp. 2 = 176 C

Inlet Pressure = 2.17 x 10^3 KPa. — Exit Pressure = 9.39 x 10^3 KPa.

Flow Rate (Num.) gm/min	Flow Rate (Expt.) gm/min	Press. at Turn15.75 (Num.) KPa.	Press. at Turn15.75 (Expt.) KPa.
51.20	50.11	6.43 x 10^3	6.72 x 10^3

B) Higher Barrel Temperature than Experimental Conditions

Barrel Temp. 1 = 172 C — Barrel Temp. 2 = 176 C

Inlet Pressure = 2.17 x 10^3 KPa. — Exit Pressure = 9.39 x 10^3 KPa.

Flow Rate (Num.) gm/min	Flow Rate (Expt.) gm/min	Press. at Turn15.75 (Num.) KPa.	Press. at Turn15.75 (Expt.) KPa.
48.88	50.11	5.73 x 10^3	6.72 x 10^3

C) 10 % Lower Inlet Pressure than Experimental Conditions

Barrel Temp. 1 = 170 C — Barrel Temp. 2 = 176 C

Inlet Pressure = 1.95 x 10^3 KPa. — Exit Pressure = 9.39 x 10^3 KPa.

Flow Rate (Num.) gm/min	Flow Rate (Expt.) gm/min	Press. at Turn15.75 (Num.) KPa.	Press. at Turn15.75 (Expt.) KPa.
50.89	50.11	6.31 x 10^3	6.72 x 10^3

Table 5. 51. Comparison of Numerical and Experimental Results for DHP Dry Blend usin 1/8 inch Diameter die.

A) Experimental Conditions

Barrel Temp. 1 = 170 C — Barrel Temp. 2 = 176 C

Inlet Pressure = 1.724×10^3 KPa. — Exit Pressure = 7.212×10^3 KPa.

Flow Rate (Num.) gm/min	Flow Rate (Expt.) gm/min	Press. at Turn15.75 (Num.) KPa.	Press. at Turn15.75 (Expt.) KPa.
49.09	47.88	3.88×10^3	4.18×10^3

B) Higher Barrel Temperature than Experimental Conditions

Barrel Temp. 1 = 172 C — Barrel Temp. 2 = 176 C

Inlet Pressure = 1.724×10^3 KPa. — Exit Pressure = 7.212×10^3 KPa.

Flow Rate (Num.) gm/min	Flow Rate (Expt.) gm/min	Press. at Turn15.75 (Num.) KPa.	Press. at Turn15.75 (Expt.) KPa.
47.426	47.88	3.53×10^3	4.18×10^3

C) 10 % Lower Inlet Pressure than Experimental Conditions

Barrel Temp. 1 = 170 C — Barrel Temp. 2 = 176 C

Inlet Pressure = 1.552×10^3 KPa. — Exit Pressure = 7.212×10^3 KPa.

Flow Rate (Num.) gm/min	Flow Rate (Expt.) gm/min	Press. at Turn15.75 (Num.) KPa.	Press. at Turn15.75 (Expt.) KPa.
48.798	47.88	3.77×10^3	4.18×10^3

Table 5. 52. Comparison of Numerical and Experimental Results for DIDP Dry Blend usin 1/16 inch Diameter die.

A) Experimental Conditions

Barrel Temp. 1 = 176 C — Barrel Temp. 2 = 182 C

Inlet Pressure = 2.1 x 10^3 KPa. — Exit Pressure = 18.55 x 10^3 KPa.

Flow Rate (Num.) gm/min	Flow Rate (Expt.) gm/min	Press. at Turn15.75 (Num.) KPa.	Press. at Turn15.75 (Expt.) KPa.
42.53	45.43	1.18 x 10^4	1.39 x 10^4

B) Lower Barrel Temperature than Experimental Conditions

Barrel Temp. 1 = 174 C — Barrel Temp. 2 = 180 C

Inlet Pressure = 2.1 x 10^3 KPa. — Exit Pressure = 18.55 x 10^3 KPa.

Flow Rate (Num.) gm/min	Flow Rate (Expt.) gm/min	Press. at Turn15.75 (Num.) KPa.	Press. at Turn15.75 (Expt.) KPa.
44.34	45.43	1.20 x 10^4	1.39 x 10^4

C) 10 % Higher Inlet Pressure than Experimental Conditions

Barrel Temp. 1 = 176 C — Barrel Temp. 2 = 182 C

Inlet Pressure = 2.31 x 10^3 KPa. — Exit Pressure = 18.55 x 10^3 KPa.

Flow Rate (Num.) gm/min	Flow Rate (Expt.) gm/min	Press. at Turn15.75 (Num.) KPa.	Press. at Turn15.75 (Expt.) KPa.
42.73	45.43	1.19 x 10^4	1.39 x 10^4

D) 20 % Lower Inlet Pressure than Experimental Conditions

Barrel Temp. 1 = 176 C — Barrel Temp. 2 = 182 C

Inlet Pressure = 1.68 x 10^3 KPa. — Exit Pressure = 18.55 x 10^3 KPa.

Flow Rate (Num.) gm/min	Flow Rate (Expt.) gm/min	Press. at Turn15.75 (Num.) KPa.	Press. at Turn15.75 (Expt.) KPa.
42.13	45.43	1.17 x 10^4	1.39 x 10^4

Table 5. 53. Comparison of Numerical and Experimental Results for DHP Dry Blend usin 1/16 inch Diameter die.

A) Experimental Conditions

Barrel Temp. 1 = 176 C — Barrel Temp. 2 = 182 C

Inlet Pressure = 3.248×10^3 KPa. — Exit Pressure = 15.74×10^3 KPa.

Flow Rate (Num.) gm/min	Flow Rate (Expt.) gm/min	Press. at Turn15.75 (Num.) KPa.	Press. at Turn15.75 (Expt.) KPa.
43.99	42.50	0.843×10^4	1.246×10^4

B) Lower Barrel Temperature than Experimental Conditions

Barrel Temp. 1 = 174 C — Barrel Temp. 2 = 180 C

Inlet Pressure = 3.248×10^3 KPa. — Exit Pressure = 15.74×10^3 KPa.

Flow Rate (Num.) gm/min	Flow Rate (Expt.) gm/min	Press. at Turn15.75 (Num.) KPa.	Press. at Turn15.75 (Expt.) KPa.
45.52	42.50	1.04×10^4	1.246×10^4

C) 10 % Higher Inlet Pressure than Experimental Conditions

Barrel Temp. 1 = 176 C — Barrel Temp. 2 = 182 C

Inlet Pressure = 2.31×10^3 KPa. — Exit Pressure = 18.55×10^3 KPa.

Flow Rate (Num.) gm/min	Flow Rate (Expt.) gm/min	Press. at Turn15.75 (Num.) KPa.	Press. at Turn15.75 (Expt.) KPa.
43.60	42.50	1.02×10^4	1.246×10^4

D) 20 % Lower Inlet Pressure than Experimental Conditions

Barrel Temp. 1 = 176 C — Barrel Temp. 2 = 182 C

Inlet Pressure = 2.60×10^3 KPa. — Exit Pressure = 15.74×10^3 KPa.

Flow Rate (Num.) gm/min	Flow Rate (Expt.) gm/min	Press. at Turn15.75 (Num.) KPa.	Press. at Turn15.75 (Expt.) KPa.
43.22	42.50	1.01×10^4	1.248×10^4

6.0 CONCLUSIONS AND RECOMMENDATIONS

In Chapter 5, the results and discussions of the experimental and numerical work on the effect of plasticizers on extrusion of PVC were presented. The conclusions about the experimental and numerical work will be made in section 6.1 and 6.2, respectively. Following the conclusions, recommendations will be made for further work in this area in section 6.3.

6.1 Conclusions : Experimental Study

The experimental goals of this work have been divided into two categories. In the first category, the effects of plasticizers on physical properties that can affect extrusion have been studied. In the second category, the differences in extrusion characteristics and melting mechanisms owing to the plasticizer type were observed and attempts were made to correlate these differences to the differences in the physical properties. Conclusions regarding physical properties have been made in statements 1 to 6 and those regarding the extrusion studies in statements 7 to 11.

1) The plasticizer type affects the viscosity of the plasticized PVC dry blends and pellets. The viscosity difference between the DIDP and the DHP dry blends was significantly different between 160 and 190 ° C. The DIDP dry blend has higher viscosity than the DOP dry blend but the difference is less distinctive than the difference in viscosity between the DIDP and the DHP dry blends. The difference in viscosity was higher at lower shear rates but diminished at higher shear rates. Following the same trends as the dry blends, the DIDP pellets have higher viscosities than the other two plasticized PVC pellets.

2) Plasticized PVC displays dual valued flow energetics. The compaction tests for the dry blends and the pellets did not produce any difference in density owing to plasticizer type. However the tests provided insight into the change in flow mechanism for PVC plasticized dry blends from a particulate to a melt-like flow at about 165 ° C brought about by fusion between particles. The change in flow mechanism necessitates using different expressions for viscosity above and below 165 °C during numerical simulation. The temperature, where the change in flow mechanism occurs for plasticized PVC, is depressed by about 20 ° C from that of rigid PVC but the critical temperature does not seem to be influenced by the choice of plasticizers or the shear rates.

3) The DIDP and the DHP dry blends exhibit definite yield stress behavior below 150 ° C and the behavior becomes more prominent at lower temperatures. The DIDP dry blend displayed higher yield stress than the DHP dry blend and the yield stress decreased with temperature. The Herschel Bulkley model fit the capillary rheometer data quite well at 140 and 150 ° C and the Herschel Bulkley model was used to model the solids conveying zone.

4) The DSC scans of both rigid and plasticized PVC dry blends and pellets show no large endothermic transitions until about 200 °C that can be associated with melting of crystallites. The scans indicated a gradual change from the solid to the melt like state, which was governed by the fusion or interdiffusion of the amorphous chains between the PVC particles. The specific heat of the plasticized dry blends and the pellets are not very sensitive to the plasticizer type. The shear and thermal histories affected the values of the specific heat. The specific heat - temperature curves changed their slopes for the dry blends and the pellets at

about 165 ° C, a temperature at which the change in flow mechanism takes place for plasticized PVC at 40 % plasticizer loading.

5) There is no observable difference between the measured values of thermal diffusivities of plasticized dry blends above 100 ° C.

6) The scatter in the friction coefficient data does not permit any definite conclusions regarding the effect of the plasticizer type but a definite trend is observed for the PVC mixes that were tested. The friction coefficients rise with temperature and then remain constant over a 20 or 25 °C temperature range before they start to drop as the materials become softer at higher temperatures.

7) The plasticizer type introduces a definite difference in the extrusion characteristics of plasticized PVC in a single screw extruder. The DIDP dry blend gave rise to higher pressures and generated higher amperages than the DHP dry blend and also the DOP dry blends. But the differences in the extrusion characteristics between the DIDP and DOP dry blends at lower speeds were less pronounced. For the plasticized PVC pellets, the difference in the extrusion characteristics between the DIDP plasticized materials and the other two pellets were significant at all the screw speeds. The effect of plasticizer on the flow rates is not very distinct but overall the DIDP plasticized mixes, with a few exceptions, registered higher flow rates.

8) The differences in the pressure build-ups have been linked to the differences in the viscosities. The higher viscosity materials gave rise to higher pressures but the magnitude of the viscosity differences could not be related to the magnitude of the differences in pressure build-ups.

9) The plasticized PVC mixes which give rise to higher pressures, fuse earlier and over a smaller distance in the extruder. The correlation between higher pressure build-up and earlier fusion was universal for all the materials. Although no definite conclusions could be drawn, it seems likely that higher pressures generated by the more viscous materials pushed back the site where fusion was initiated.

10) The fusion studies of the PVC microstructure by SEM show that DIDP plasticized dry blends fuse earlier and these studies also demonstrate how the large 100 μm particles fused

to a homogeneous structureless mass. The fusion or the interdiffusion between the particles obliterated the original particle boundaries to the extent that no individual particles of approximately 1 μm or larger were distinguishable. Also in the later turns of the screw, the crystallites appear to be more homogeneously distributed in the DIDP dry blend than in the DHP dry blend.

11) At low barrel temperatures, not high enough to initiate fusion, the solids conveying seems to be dominated by the drag induced by the rotating screw. The fact that the flow rates are not influenced by changes in the barrel temperature indicate that for a temperature range between 90 and 135 ° C, isothermal properties could possibly be used to model the solids conveying zone.

6.2 *Conclusions : Numerical Study*

The final objective of this study was to numerically simulate the solids conveying zone as a fluid with yield stress and to predict the difference in extrusion characteristics in the melt zones between the two different dry blends based on difference in their properties. The differences in properties were owing to the difference in the plasticizer type. As only shear flow exists in the extruder channel, the viscosity models were chosen to to predict only this kind of behavior. No provisions for incorporation of viscoelastic response was possible because of the inability of Fidap to handle any other constitutive equation other than GNF. Although initially it was planned to do both solids and melt zones modeling in 3-D, the melt zone modeling had to be done in 2-D because of the constraint on the memory and computation time involving large 3-D problems. Conclusions regarding modeling of different viscosity empiricisms as well as simulation results in the two zones are given below.

1) The temperature and shear dependent power law viscosity and Herschel Bulkley viscosity have been successfully modeled. The two temperature dependent viscosity expressions, above and below a critical transition temperature in the flow phenomenon, were able to predict flow rates for simple shear flows for shear rates and temperatures in the range experienced in the extruder. The 2-D HB modeling gave much better predictions than the previous models and was effective in predicting flow rates over a wide range of flow conditions and fluid property variations.

2) The solids conveying zone has been modeled as a HB fluid but a certain parameter (density) needs to be modified to match the numerical and experimental results. For a material whose compaction conditions change as it moves in the flow domain, the use of average density for the HB fluid seems to be a rational assumption; but some more work need to be done with other materials before the model can be claimed as truly successful. The ease and repeatability of measuring fluid properties (used in the model) in comparison to friction measurements makes the proposed solids conveying model an attractive one.

3) The numerical predictions with the 1/8 inch diameter die are found to be in excellent agreement with the experimental results. Both the pressure and flow rates predictions for different dry blends are in good agreement and the difference in extrusion performance were predicted based on the viscosity difference owing to the plasticizer type. The GNF model with shear rate and temperature dependent viscosity proved to be adequate in describing the flow in the extruder with the 1/8 inch diameter die.

4) The numerical predictions with the 1/16 inch diameter die are in good agreement with the experimental flow rates but not for the experimentally observed pressures. The trends of the pressure predictions were in the right direction but the absolute values were off by 15 to 20 %. This discrepancy probably calls for modeling of the flow by a viscoelastic model.

6.3 *Recommendations*

Although most questions have been answered with regard to the objectives of this research, there are a lot of areas where improvements can be made and some unanswered questions are still to be addressed. The recommendations for future work are as follows.

1) The effect of plasticizers on progression of fusion in the extruder can be studied by transmission electron microscopy. This will possibly help one to observe more clearly the distribution of crystallites as a function of plasticizer type in the extruder channel.

2) Flow birefrigence measurement data from other researchers can be used to evaluate the stress field in shear flow at shear rates existing in the extruder. Different plasticizers might affect the stress field differently and these experimental data have helped in comprehending the viscoelastic response of plasticized PVC. Correlations between these experiments and the ones presented in this thesis might lead to better fluid models with diferent constitutive equations. It may provide the answers to why the modeling which proved to be adequate in simulating the melt zones with the larger diameter die was not good enough for simulating the melt zones with a smaller diameter die. In the latter case the pressures were much higher and temperatures were slightly higher.

3)The solids conveying model needs to be extended to more polymers that display yield stress behavior to see whether their solids conveying rates can be predicted by treating them as a fluid with yield stress. Also the non-isothermal solids conveying model based on the same principles should be investigated so that the whole extruder can be modeled as one flow domain.

4) The viscoelastic response of the plasticized PVC mixes needs to be incorporated in the fluid model to see whether they are able to predict better pressures at higher temperatures and flow rates. Also the effect of incorporating viscous dissipation in the energy equation needs to be explored.

5) 3-D modeling of the melt zones needs to be accomplished. It is possible to break down the flow domain into 2 or 3 different sections and use velocity and temperature between the sections as a continuity constraint. This process will prove to be tedious but will circumvent the problems of large memory and computation time.

Appendix A. APPENDIX A - EXISTING SOLIDS CONVEYING MODEL

The procedure and the equations needed for calculating the pressure rise for a fixed flow rate in the solids conveying zone for a tapered channel are presented here. The equations for the solids conveying zone in a straight channel were originally developed by Darnel and Mol [79] and were later modified for the tapered channel by Tadmor et al. [54]. Also factors, which take into account the variations of normal forces on the barrel and screw surfaces, were incorporated in the later model.

The flow rate in the solids conveying zone is expressed in terms of the solids conveying angle, ϕ, which is the angle between the direction of the force exerted by the moving plate on the solids and the direction of motion of the moving plate. The angle ϕ and the angle θ_B, which is the angle at which the barrel is dragged across the screw channel, are shown in Fig. 2.26. The angle ϕ is calculated from force and torque balance performed over a down channel increment of the solid plug. In the straight channel, the value of ϕ is constant in the entire solids conveying zone as the geometry of the channel and the components of the force and torque balances remain do not change along the channel length. For tapered channel, additional forces need to be included in the force and torque balances as they can significantly

alter the solids conveying capacities. For tapered channels, lubrication approximation is assumed; i.e. changes in the down channel direction takes place slowly so the equations derived for the straight channel can be applied locally for the tapered channel. The calculations have to be performed over small axial increments because in case of large increments the changes in the values of the additional forces (arising out of the tapered channel geometry) could be large and this might lead to errors.

Other factors have to be taken into account when calculating ϕ and pressure rise. The bulk density changes as the material gets more compacted and this can affect the values of ϕ as the material moves down the screw channel. The assumption that the compressed solids behave as a continuous media and have contacts with the barrel and all the screw surfaces might not be necessarily true. For any surface, the frictional forces and the normal forces are related through the friction coefficient, μ The normal stresses on the barrel and screw surfaces have different values but are proportional to the pressure in the down channel direction. If P is the isotropic down channel pressure, then $P_i = K_i P$ where P_i are the effective pressures on the barrel and screw surfaces and K_i are the proportionality constants between P and P_i. K_is will be referred to as the non-isotropic pressure distribution factors or NIPD factors.

At each increment, ϕ is calculated from the following relations:

$$\tan\phi = \frac{Qs\ \tan\theta_B}{\Pi^2\rho NHDb(DS - H)\tan\theta_B\left(\frac{\overline{w}}{\overline{w}+e}\right) - Qs} \qquad \text{(A.1)}$$

Qs - mass flow rate

N - screw speed

H - variable channel depth

Db - diameter of the barrel

$\overline{w}$ - average channel width

e - flight width

θ_B - helix angle

ϕ - solids conveying angle

ρ - is the density

Density can either be assumed to be constant or expressed as a function of pressure as follows:

$$\frac{\rho_\infty - \rho}{\rho_\infty - \rho_0} = e^{-cP} \qquad (A.2)$$

ρ_∞ - final density

ρ_0 - initial density

P - pressure

C - constant

The helix angle is assumed to be constant and is calculated from the extruder geometry by using the following expression :

$$\theta_B = \tan^{-1}\left(\frac{L}{\pi Db}\right) \qquad (A.3)$$

θ B - helix angle

L - axial distance of one full turn of the screw

Db - diameter of the barrel

Knowing the values of ϕ for each differential down channel increment, a torque and a force balance on the differential element is performed to obtain the pressure P_2 at the exit of the element (element length = Zb2 - Zb1) is calculated using the following relation:

$$P_2 = P_1 \exp \int_{Zb1}^{Zb2} \frac{B_1 - A_1 K}{A_2 K + B_2} dZ \qquad (A.4)$$

P_1 - initial pressure

P_2 - final pressure

A_1 = f_1(screw geometry, ϕ, θ_B, f_s , f_b, NIPD)

A_2 = f_2(screw geometry)

B_1 = f_3(screw geometry, ϕ, θ_B, f_s , f_b, NIPD)

B_2 = f_4(screw geometry)

$K = f_s$(screw geometry, f_s)

where the known values of friction coefficients are

f_s - friction coefficient on the screw surfaces

f_b - friction coefficient on the barrel surface

The total length of the channel Z (= Zb2 - Zb1) for an extruder length, I, is given by

$$Z = \frac{I}{\sin \theta_B}$$

Z - length of screw channel (A.5)

θ_B - helix angle

The process is repeated at small increments from the start to the end of the solids conveying zone of length Z and the final value of P_2 is obtained.

For a fixed flow rate, different variables can be changed to numerically predict different exit pressures. The ratio of friction coefficients on the barrel and screw surfaces can be varied to change the exit pressure. Also, the NIPD values can be changed to alter the values of the exit pressures. A finite difference program was written to calculate the exit pressure at the end of the solids conveying zone for a given mass flow rate of the material. There were provisions to change the NIPD values and the ratio of the friction coefficients to vary the exit pressure.

REFERENCES

1. E.Yorkgitis, Ph.D Dissertation, VPI&SU, Blacksburg, (1986).

2. B.Ranby, Pure and Appl. Chem., 53, p-509, (1981).

3. C.L. Sieglaff, Pure & Appl. Chem, 53, p-509, (1981).

4. J. Lyngaae-Jorgensen, Pure & Appl. Chem, 53, p-533, (1981).

5. M. W. Allsopp, Pure 7 Appl. Chem, 53, p-449, (1981).

6. Krzewki and Sieglaff, Polm. Engg. & Sci., p-1174, (1978).

7. J. W. Summers, J. of Vinyl Tech, 3(2), p-107, (1981).

8. R. Khanna, SPE J., 29, p-48, (1973).

9. J. K. Sears & J. R. Derby, The technology of Plasticizers, John Wiley and Sons, NY.,(1982).

10. J. Aklonis & W. J. Macknight, Introduction to Polymer Viscoelasticity, John Wiley & Sons, NY., (1982).

11. G. Pezzin, Pure and Applied Chemistry, 26, p. 241 (1971).

12. C. J. Singleton, T. Stephenson, J. Isner & P. H. Geil, B 14 (1), p-29, (1977)."

13. A. R. Berens & V. L. Folt, Polm. Eng. & Sci., 8, p-5, Jan, (1968).

14. A. R. Berens & V. L. Folt, Polm. Eng. & Sci., 9, p-27,Jan, (1969).

15. R. J. Krzewki & E. A. Collins, J. of Macromol. Sci(Phy)., B20(4), p-443, (1981).

16. E. B. Rabinovitch, SPE Tech Papers, 27, p-403, (1981).

17. T. Hattori, K. Tanaka & M. Matsuo, Polm. Eng. & Sci. 12(3), p-199, (1972).

18. J. W. Summers, E. B. Rabinovitch & P. C. Booth, J. of Vinyl Tech., 8(1), p-2 (1986).

19. J. Rosenthal, J. of Vinyl Tech., 5(3), p-104, (1983).

20. D. Smith, J. of Vinyl Tech., 5(3), p-132, (1983).

21. S. H. Hookanson, D. L. Smith & J. L. Irvine, SPE Tech Papers, 31, p-1021, (1985).

22. D. L. Smith, S. H. Hookanson & J. L. Irvine, SPE Tech Papers, 31, p-1018, (1985)."

23. J. Simonik, J. Juroz, J. Chytilek & J. Drexler, SPE Tech Papers, 27, p-560, (1981).

24. C. L. Sieglaff, Polm. Eng. & Sci., 9(2), (1969).

25. E. A. Collins & A. P. Metzger, Polm. Eng. & Sci., 10(2), p-57, (1970).

26. E. A. Collins & A. P. Metzger, Polm. Eng. & Sci., 11(6), (1971).

27. E. A. Collins & C. A. Daniels, Polm. Eng. & Sci., 14(5), (1974).

28. G. Pezzin & G. Ajroldi & C. Garbuglio, Rheological Acta, 8, p-304, (1969)."

29. H. Munstedt, J. of Macromol. Sci(Phy), B14(2), p-195, (1977).

30. C. L. Sieglaff, SPE Transactions, p-129, (1964).

31. P. L. Shah, SPE Journal, 27, p-49, (1971).

32. M. Tse, Polm. Eng. & Sci., 21(15), p-1037, (1981).

33. G. A. Adam, N. Al-Jabari & K. Yakob, Polm-Plast. Technol. Eng., 24(2 & 3), p-129, (1985).

34. I. K. Park, J. of Vinyl Tech., 3(3), (1981).

35. A. Rudin, Polm. Eng. & Sci., 10(2), p-94, (1970).

36. E. A. Collins, Pure & Appl. Chem., 49, p-581, (1977).

37. M. T. Payne & J. A. Cannon, J. of Vinyl Tech., 4(3), (1982).

38. P. A. Schwab & J. A. Wingrave, J. of Macromol. Sci(Phy)., B20(3), p-429, (1981).

39. D. H. Paul, SPE Technical Papers, 27, p-413, (1981).

40. L. A. Utracki, J. of Polymer Sci., 12, p-563, (1974).

41. L. A. Utracki, Polm. Eng. & Sci., 14, p-28, (1974).

42. I. K. Park & D. W. Riley, J. of Vinyl Tech., 2(3), p-160, (1980).

43. L. A. Utracki, SPE Technical Papers, 32, p-1252, (1986).

44. R. J. Krzewki & E. A. Collins, J. of Vinyl Tech., 3(2), p-116, (1981).

45. P. L. Shah, SPE Technical Papers, 27, p-43, (1981).

46. P. L. Shah, Polm. Eng. & Sci, 14(11), p-773, (1974).

47. J. E. Hartitz, Polm. Eng. & Sci, 14(5), p-392, (1974).

48. Z. Tadmor & C. Gogos, Principles of Polymer Processing, John Wiley & Sons, N.Y., (1979).

49. Z. Tadmor & I. Klein, Engineering Principles of Plasticating Extrusion, Robert E. Krieger Publishing Company, (1978).

50. B. H. Maddock, SPE Technical Papers, 15 p. 383 (1959).

51. Z. Tadmor, I. J. Duvdevani & I. Klein, Polm. Eng. 7 Sci., July (1967).

52. G. M. Gale, Plastics 7 Polymer, p-183, June(1970).

53. V. P. Klenk, Rheological Acta, 7, p-75, (1968).

54. E. Broyer & Z. Tadmor, Polm. Eng. & Sci., 12(1), p-12, (1972).

55. Z. Tadmor & E. Broyer, Polm. Eng. & Sci., 12(5), p-378, (1972).

56. Z. Tadmor, Polm. Eng. & Sci., p-185, July (1966).

57. D. Marshall & I. Klein, Polm. Eng. & Sci., p-191, July (1966).

58. I. Klein & D. Marshall, Polm. Eng. 7 Sci., p-198, July (1966).

59. R. C. Donovan, Polm. Eng. & Sci., 11(3), p-247, (1971).

60. R. C. Donovan, Polm. Eng. & Sci., 11(6), p-484, (1971).

61. I. Klein & Z. Tadmor, Polm. Eng. & Sci., 9(1), p-11, (1969).

62. E. Agur & J. Vlachopoulos, Polm. Eng. & Sci., 22(17), p-1984, (1982).

63. E. Zavadsky & J. Karnis, Rheological Acta, 24, p-556, (1985).

64. M. Viriyayuthakorn & B. Kassahun SPE Technical Papers, 30, p-81, (1984).

65. F. Kulas & N. Thorshaug, J. of Appl. Polm. Sci., 23, p-1781, (1979).

66. T. E. Fahey, J. of Macromol. Sci(Phy), B20(3), p-415, (1981).

67. J. A. Cannon, D. E. Emge & M. T. Payne, J. of Vinyl Tech., 2(4), (1980).

68. J. A. Summers, E. B. Rabinovitch & J. G. Quisenberry, SPE Technical Papers, 30, p-869, (1984).

69. A. S. Pazur, J. of Vinyl Tech., 5(3), p-126, (1983).

70. L. Wagner, Ph.D. dissertation, Chemical Engineering, V.P.I. & S.U., (1986).

71. H. Fukase, T. Kunio, S. Shinya & A. Nomura, Polm. Eng. & Sci., 22(9), (1982).

72. P. H. Geil, J. of Macromol. Sci(Phy)., A11(8), p-1461, (1977).

73. P. G. Faulkner, J. of Macromol. Sci(Phy)., B11(2), p-251, (1979).

74. P. L. Soni, P. H. Geil & E. A. Collins, J. of Macromol. Sci(Phy)., B20(4), p-479, (1981).

75. J. T. Lindt, Polymer Engineering Science, 16, p-284 (1976).

76. P. H. Geil, Macromol. Sci.-Chem., A11(7), p-1271 (1977).

77. C. Rauwendaal, Polymer Extrusion, Hanser Publication, Munich, (1986).

78. R. J. Krzewki & E. A. Collins, J. Macro. Sci. (Phy), B20 (4), p-465, (1981).

79. W. H. Darnel & E. A. Mol, SPE J. 12, p-20, (1956).

80. K. Schneider, Kunststoffe, July, p-97, (1969).

81. E. B. Bagley, J. of Appl. Phys., 28, p-624, (1957).

82. K. Weisenberg as cited by B. Rabinowitsch, Z. Physik-Chemie, A-145 1, (1929)

83. Carl Reed, Ph.D Dissertation, VPI&SU, Blacksburg, (1989).

84. J.N. Reddy, An Introduction To The Finite Element Method, McGraw Hill, (1984)

85. Fidap Manuals, Fluids Dynamics Int. Inc., Evanston, Revision 3 and 4 (1986-1989).

86. M. Keentok, Rheol. Acta, 21, p-325, (1982).

87. S. Onogi & T. Matsumoto, Polymer Engineering Reviews, Vol.I No 1, p-45, (1981).

88. L. A. Utracki, J. of Vinyl. Tech., 7(4), p-150, (1985).

89. T. C. Papanastasiou, Trans. from Chemical Engg. Dept., Univ. of Mich., Ann Arbor.

90. J.D. Ferry, Viscoelastic Properties of Polymers, John Wiley & Sons, Inc..

91. SAS Mamuals

92. Math Library, IMSL Software Systems, Houston, Ver. 1.0, (1987).

93. N. S. Eiss & G. S. Vincent, presented at ASLE Annual Meeting, (1981).

94. N. S. Eiss & K. A. Smyth, J. of Lubrication Tech. (Trans. of ASME), 103, p-266 (1981).

95. N. Q. Dzuy & D. V. Boger, J. of Rheol., 27(4), p-321, (1983).

96. M. A. Buckingham, L. D. Bensten, J. Makosey, G. R. Angell & D. P. Hasselman, Trans. J. Br. Ceram. Soc., 82, p-18, (1983).

97. R. B. Bird, G. C. Dai & B. J. Yarusso, I (1), 'Rheology of Viscoplastic Materials', Chem. Eng. Dept. & Rheol. Rsch. Center, Univ. of Wisconsin, Madison, (1983).

98. R. J. Soto & V. L. Shah, Appl. Sci. Rsch., 32, p-73, (1976).

99. G. Forrest and W. L. Wilkinson, J. of Heat & Mass. Trans., 16, p-2377, (1973).

100. I. P. Grinchik & A. Kh. Kim, J. of Eng. Phys. (Engl. Trans.), 23, p-336, (1972).

101. R. M. Griffith, Ind. Eng. Chem. Fund., 1, p-189, (1962) as cited in Reference in [49].

102. R. E. Colwell & K. R. Nicholls, Ind. Eng. Chem. J., 51, p-841, (1959) as cited in reference [49].

103. R. B. Bird, R. C. Armstrong & O. Hassager, p-51, Dynamics of Polymeric Liquids, Vol. 1, John Wiley & Sons, (1987).

104. S. Middleman, Fundamentals of Polymer Processing, (1980).

105. W. H. Suckow, P. Hrycak & R. G. Grisley, Polm. Eng. Sci., 11 (5), p-401, (1971).

106. J. Vlachopoulos & C. K. Keung, AIChE J., 18 (6), p-1272, (1972).

The vita has been removed from the scanned document